

Sheffield Hallam University

Development of Optical Biosensors Based on Metal Nanostructures for Pollution (Mycotoxins) Detection

AL-RUBAYE, Ali Ghanim Gatea

Available from the Sheffield Hallam University Research Archive (SHURA) at:

<http://shura.shu.ac.uk/24704/>

A Sheffield Hallam University thesis

This thesis is protected by copyright which belongs to the author.

The content must not be changed in any way or sold commercially in any format or medium without the formal permission of the author.

When referring to this work, full bibliographic details including the author, title, awarding institution and date of the thesis must be given.

Please visit <http://shura.shu.ac.uk/24704/> and <http://shura.shu.ac.uk/information.html> for further details about copyright and re-use permissions.

**Development of Optical Biosensors Based on Metal
Nanostructures for Pollution (Mycotoxins) Detection**

Ali Ghanim Gatea Al Rubaye

A thesis submitted in partial fulfilment of the requirements of
Sheffield Hallam University
for the degree of Doctor of Philosophy

March 2019

DECLARATION

I hereby declare that this thesis submitted for the degree of PhD is the result of my own research and that this thesis has not been submitted for higher degree to any other university or institution.

Ali Ghanim Gatea Al Rubaye

DEDICATION

To my parents, my wife and my children

ABSTRACT

This work aims to develop optical biosensors for detection of the bio-toxins, particularly mycotoxins. The main detection technology chosen is a combination of a localized surface plasmon resonance (LSPR) transducer with direct immunoassay with specific bio-receptors antibodies or aptamers immobilized on the gold surface. The LSPR platform is based on gold nano-islands produced by thermal annealing of thin gold films deposited on glass. Thermal annealing was substituted with much quicker and more efficient microwave annealing in later stages of the project. The gold nano-structures produced were analyzed with scanning electron microscopy (SEM), atomic force microscopy (AFM), X-ray diffraction (XRD), optical absorption spectroscopy, and spectroscopic ellipsometry. The method of total internal reflection ellipsometry (TIRE) was chosen for LSPR bio-sensing because of its superior sensitivity as compared to conventional UV-vis absorption spectroscopy. The TIRE spectroscopic measurements were performed using the experimental set-up developed on the basis of J.A. Woollam M2000 spectroscopic instrument. The sensitivity of LSPR measurements is however limited by a finite evanescent field decay length in gold nano-islands which is typically in the range of tens of nanometres. In order to achieve the best results, the bio-receptors must be small and placed as close to the gold surface as possible. In our case the problem was solved using either halved antibodies or aptamers immobilized covalently on the surface of gold. A series of bio-sensing experiments to detect mycotoxins, i. e. aflatoxin B1, M1, zearalenone, and ochratoxin A, went successfully and resulted in the detection of the above mycotoxins in concentrations down to 0.01ng/mL. In this work we attempted, for the first time, the TIRE detection of Aflatoxin B1, M1 and ochratoxin A (OTA) in an assay with a specific aptamer. We compared the results obtained for the detection of mycotoxins using bio-receptors of different dimensions: large-size whole antibodies electrostatically immobilized on the surface of gold nano-islands, and small-size split antibodies or specific aptamers immobilised via thiol (SH) groups. For small-size receptors, the low detection limit (LDL) was 0.01ng/ml which is one order of magnitude lower than for whole antibodies. The results obtained demonstrate the advantages of using small bio-receptors in LSPR bio-sensing. The minimal detected concentration OTA was 0.01ng/ml, which is a remarkable result for direct aptamer assay format. The mycotoxin/aptamer binding kinetics were analysed using dynamic TIRE measurements and yielded an association constant K_A in the range of 10^7 Mol^{-1} which confirmed the high specificity of aptamer. An attempt to make gold nanostructures for SERS biosensing using nanosphere lithography was successful.

ACKNOWLEDGEMENT

I would like to express my appreciation and acknowledgements to my director of study Professor Alexei Nabok, without his support and guidance, this work would not have been possible. His patience, motivation, interest, and massive knowledge have helped me throughout my PhD.

I would also like to thank my second supervisor, Prof. Tom Smith and third supervisor Dr Anna Tsargorodska, for their assistance and support.

Great thanks for our collaborations to Prof. Jean-Louis Marty and Dr. Gaelle Catanante from Perpignan University and, Dr. Ezster Takacs from Agro-Environmental Research Institute for their contribution to this research.

Special thanks to my parents, my wife, my children, and my siblings, for their support, patience and understanding throughout the course of my studies.

I would also like to acknowledge my financial sponsor, the Ministry of Higher Education and Scientific Research in Iraq and Basra Technical Institute, Southern Technical University, Environmental Pollution Research unit.

I gratefully acknowledge the Iraqi Cultural Attaché in London for their support during my PhD research.

Finally, I would like to thank my colleagues and friends for making life interesting during many hours underground in the laboratory, especially, Burak Yahya Kadem, Maytham Al-Shanawa, Hisham Abu-Ali and Ali Madlool Al-jawdah. Special thanks are also due to all MERI staff and technicians who were always of assistance.

LIST OF ABBREVIATIONS

Ab	Antibody
AFM	Atomic force microscopy
AFT B1	Aflatoxin B1
AFT M1	Aflatoxin M1
DMSO	Dimethyl sulfoxide
DTT	Dithio threitol
Fab	Fragment antigen-binding
Fc region	Fragment crystallizable
HV	Hypervariable
IgG	Immunoglobulin
LDL	Low detection limit
LSPR	Localized surface plasmon resonance
n	Refractive index
NP	Nanoparticles
OTA	Ochratoxin A
PAH	Poly (allylamine hydrochloride)
PBS	Phosphate buffer solution
PSN	Polystyrene nanosphere
PSS	Poly (styrene sulfonate) sodium salt
RIS	Refractive index sensitivity

RIU	Refractive index unity
SDS-PAGA	Sodium dodecyl sulphate-polyacrylamide gel electrophoresis
SE	Spectroscopic Ellipsometry
SEM	Scanning electron microscopy
SH	Thiol group
SPR	Surface plasmon resonance
TIRE	Total internal reflection ellipsometry
THF	Tetrahydrofuran
Ttb-H ₂ P _c	Tetratertbutyl metal free phthalocyanine
Trisma buffer	Poly (3, 4-ethylenedioxythiophene)
XRD	X-ray diffraction
ZEN	Zearalenone

LIST OF PUBLICATIONS OF THE CANDIDATE

Journal publications:

1. **Al-Rubaye**, A. G., Nabok, A., & Tsargorodska, A. (2017). LSPR Biosensor Based on Nanostructured Gold Films: Detection of Mycotoxins. *Procedia Technology*, 27, 131-132.
2. **Al-Rubaye**, A. G., Nabok, A., & Tsargorodska, A. (2017). Spectroscopic ellipsometry study of gold nanostructures for LSPR bio-sensing applications. *Sensing and Bio-Sensing Research*, 12, 30-35.
3. **Al-Rubaye**, A., Nabok, A., Abu-Ali, H., Szekacs, A., & Takacs, E. (2017, October). LSPR/TIRE bio-sensing platform for detection of low molecular weight toxins. In *SENSORS, 2017 IEEE* (pp. 1-3). IEEE.
4. **Al Rubaye**, A., Nabok, A., Catanante, G., Marty, J. L., Takacs, E., & Szekacs, A. (2018). Detection of ochratoxin A in aptamer assay using total internal reflection ellipsometry. *Sensors and Actuators B: Chemical*, 263, 248-251.
5. **Ali Ghanim Al-Rubaye**, A., Nabok, A., Catanante, G., Marty, J. L., Takács, E., & Székács, A. (2018). Label-Free Optical Detection of Mycotoxins Using Specific Aptamers Immobilized on Gold Nanostructures. *Toxins*, 10(7), 291.
- 6- Nabok, A., **Al-Rubaye**, A. G., Al-Jawdah, A. M., Tsargorodska, A., Marty, J. L., Catanante, G. & Takacs, E. (2019). Novel optical biosensing technologies for detection of mycotoxins. *Optics & Laser Technology*, 109, 212-221.

Conference publications:

1. **Ali Al-Rubaye**, A. Nabok, A. Tsargorodska, Spectroscopic ellipsometry characterization of nano-structured gold films for LSPR biosensing, *Advanced Vibrational Spectroscopy for Biomedical Applications: Faraday Discussion*, 21–23 March, Cambridge, UK; 2016.
2. Alexei Nabok, **Ali Ghanim Al-Rubae**, Anna Tsargorodska, Detection of mycotoxins using optical immunosensor based on LSPR phenomenon in nano-structured gold films,

13th European Conference on Optical Chemical and Biosensors (EUROPT(R)ODE XIII), Graz, Austria, March 20-23, 2016.

3. **Ali Al-Rubaye**, Alexei Nabok, Gaelle Catanante, Jean-Louis Marty, Label-free detection of aflatoxins B1 and M1 in aptamer assay using spectroscopic ellipsometry, XXII Transfrontier Meeting on Sensors and Biosensors, Montpellier, France, 21-22 Sep. 2017.

4. Eszter Takàcs, **Ali Al-Rubaye**, Alexei Nabok, Gaelle Catanante, Andràs Szèkàcs, Jean-Louis Marty, Detection of Ochratoxin A in Direct Immunoassay with Specific Aptamers Using Total Internal Reflection Ellipsometry, XXI Transfrontier Meeting on Sensors and Biosensors, Barcelona, Spain, 29 Sep. 2016.

5. **A.G. Al-Rubaye**, A. Nabok, A. Tsargorodska, LSPR biosensor based on nanostructured gold films: detection of mycotoxins. 26th Anniversary world Congress on Biosensors, Gothenburg, Sweden; 2016.

6. **A.G. Al-Rubaye**, A. Nabok, A. Tsargorodska, T. Smith, Optical bio-sensor for mycotoxins based on LSPR phenomenon in nano-structured gold films, *MERI Research Symposium proceedings*, 2017.

7. **Ali Al Rubaye**, Alexei Nabok, Gaelle Catanante, Jean-Louis Marty, Ezster Takacs, Andras Szekacs, optical biosensors detection of mycotoxins using aptamer-based gold nanostructures, Nanotech Middle East -Conference and Exhibition 4-6 December, Dubai, 2017.

8. **Ali Al Rubaye**, Alexei Naboka, Gaelle Catananteb, Jean-Louis Martyb, Ezster Takacsc, Andras Szekacsc, Detection of ochratoxin A in aptamer assay using total internal reflection ellipsometry, Nano Medicine international conference and exhibition 23-25 October 2018, Venice, Italy, 2018.

Posters:

1. **A.G. Al-Rubaye**, A. Nabok, A. Tsargorodska, Characterization of Metal-nanostructure gold film for Localized Surface Plasmon Resonance (LSPR) biosensing. MERI symposium, Winter poster event, 17th December 2015, Sheffeild Hallam University; 2015.

2. A. Nabok, A. Tsargorodska, **A. Al-Rubaye**, I. Rubinstein, A. Vaskevich, Nanostructured gold films for LSPR biosensing, European Conference on Organised Films (ECOF) 14, 29 June 2015 – 2 July 2015, Italy;2015.
3. **A.G. Al-Rubaye**, A. Nabok, A. Tsargorodska, Ellipsometric and morphological study of nanostructured gold films for LSPR sensing applications. MERI research symposium, 17th & 18th May 2016, Sheffield Hallam University; 2016.
4. **Ali Al Rubaye**, Alexei Nabok, Gaelle Catanante, Jean-Louis Marty, Ezster Takacs, Andras Szekacs, Detection of ochratoxin A in aptamer assay using total internal reflection ellipsometry5th International Conference on Bio-Sensing Technology 7 - 10 May 2017 | Riva del Garda (on Lake Garda), Italy.
5. **A. Al-Rubaye**, A. Nabok, G. Catanante, J-L. Marty, E. Takacs, A. Szekacs, Detection of mycotoxins using a combination of LSPR and TIRE methods: the effect of bio-receptor dimensions. EUROPT(R)ODE conference 25-28 March 2018, Napoli, Italy;2018.
6. **Ali Al-Rubaye**, Alexei Nabok, Anna Tsargorodska, Formation of gold nanostructures for LSPR and SERS Biosensing by microwave annealing, MERI-BMRC winter poster event 14th, 2018.
7. Cansu Ozkaya, Hisham Abu-Ali, **Ali Al Rubaye**, Alexei Nabok, electrochemical Aptasensor for detection of Dopamine, MERI-BMRC winter poster event 14th, 2018.

Contents

DECLARATION	I
DEDICATION	II
ABSTRACT	III
ACKNOWLEDGEMENT	IV
LIST OF ABBREVIATIONS	V
LIST OF PUBLICATIONS OF THE CANDIDATE	VII
LIST OF FIGURES	XIV
LIST OF TABLES	XXI
Chapter 1: Introduction	1
1.1 General background and motivation for research	1
1.1.1 Motivation for research	6
1.1.2 Mycotoxins and their detection	7
1.1.3 Optical biosensors technologies (SPR, TIRE, LSPR).....	10
1.1.3.1 Surface Plasmon Resonance (SPR) sensors	11
1.1.3.2 Total Internal Reflection ellipsometry TIRE.....	12
1.1.3.3 Localized surface plasmons Resonance (LSPR)	12
1.1.4 Bio-receptors (antibodies and aptamers)	13
1.2 Aims and objectives	14
Reference list	16
Chapter 2: Literature review	19
Chapter overview	19
2.1 Optical bio-sensing technologies	20
2.1.1 Optical biosensors based on evanescent field	20
2.1.2 Surface plasmon resonance (SPR)	22
2.1.3 Ellipsometry	24
2.1.4 Total Internal Reflection Ellipsometry (TIRE)	29
2.1.4.1 TIRE data fitting.....	32
2.1.4.2 TIRE kinetic analysis	33
2.1.5 Localized Surface Plasmon Resonance (LSPR)	35

2.1.6 Raman spectroscopy	39
2.1.7 Surface Enhanced Raman Spectroscopy	40
2.2 Metal nanostructures.....	44
2.2.1 Formation of nano-islands by de-wetting	46
2.3 Biosensing receptors (general classification).....	49
2.3.1 Immobilization of bio-receptors	52
2.3.2 Antibodies and their immobilization.....	53
2.3.2.1 Production of antibodies	55
2.3.2.2 Antigen – antibody reaction	56
2.3.2.3 Immobilization of antibodies	57
2.3.3 Split Antibodies and their immobilization	60
2.3.4 Aptamers	61
2.3.4.1 Aptamer structure.....	63
2.3.4.2 Aptamer production	65
2.3.4.3 Aptamer immobilization	66
Reference list	68
Chapter 3: Experimental details (Methodology)	81
3.1 Samples preparation	81
3.1.1 Thermal evaporation of metals	82
3.1.2 Annealing of metals	83
3.2 Immobilization of bio-receptors on Au surface.....	84
3.2.1 Immobilization of whole antibodies	84
3.2.2 Immobilization of split antibodies	85
3.2.3 Immobilization of aptamers	86
3.3 Characterization techniques	87
3.3.1 UV-visible absorption spectroscopy	87
3.3.2 Spectroscopic ellipsometry	90
3.3.3 Raman spectroscopy	92
3.3.4 X-ray diffraction (XRD).....	93
3.3.5 Scanning electron microscopy (SEM)	95
3.3.6 Atomic Force Microscopy (AFM)	98
Reference list	102

Chapter 4: Characterization of gold nanostructures and development of LSPR/TIRE method for biosensing	104
4.1 Introduction	104
4.2 Fabrication and characterization of gold nano-islands.....	105
4.2.1 SEM and AFM study.....	105
4.3 Optical study	113
4.3.1 UV-vis spectroscopy	113
4.3.2 Spectroscopic ellipsometry	114
4.4 Comparison between thermal and microwave annealing.....	118
4.4.1 XRD study of gold nanostructures	120
4.4.2 UV-vis absorption spectroscopy.....	121
4.5 Evaluation of refractive index sensitivity (RIS)	123
4.6 Limitations of LSPR.....	128
Summary	134
Reference list.....	135
Chapter 5: Detection of mycotoxins using antibodies.....	136
5.1 Introduction	136
5.2 Aflatoxin detection using TIRE method: Preliminary results using whole antibodies as bio-receptors.....	137
5.3 Electrophoresis study	140
5.4 Detection of aflatoxin B1 and Zearalenone using small size of bio-receptors: split antibodies	141
Summary	144
Reference list.....	145
Chapter 6: Small size bio-receptors: Aptamers for the detection of mycotoxins	146
6.1 Introduction	146
6.2 Results and discussion.....	147
6.2.1 OTA detection using 25 nm continuous Au film.....	147
6.2.1.1 Sample preparation and immobilization of aptamers	147
6.2.1.2 TIRE measurements	148
6.2.1.3 OTA-aptamer binding kinetics	152
6.2.2 Detection of AFT B1 and M1 using aptamers immobilized on 5 nm nano-structured Au film	153
6.2.2.1 Samples preparation	153

6.2.2.2 Aptamers for AFT B1 and M1	154
6.2.2.3 Immobilization of aptamers on gold	156
6.2.2.4 TIRE experimental of detection AFTB1 and M1	156
6.2.2.5 Study of Aflatoxin-Aptamer Binding Kinetics.....	160
Summary	163
Reference list.....	165
Chapter 7: Development of nano-structured Au platform for SERS biosensing	166
7.1 Introduction	166
7.2 Formation of Au nano-structures using nano-sphere lithography.....	166
7.3 Characterization of Au nano-structures produced by nano-sphere lithography.....	170
7.4 SERS measurements of gold-nano-structures.....	172
Summary	174
Reference list.....	176
Chapter 8: Conclusion and Future work	177
8.1 Conclusion	177
8.2 Future work	181

LIST OF FIGURES

Figure 1.1. Principles of optical biosensor.....	3
Figure 1.2. Blood glucose monitor.....	4
Figure 1.3. Pregnancy test device.....	4
Figure 1.4. U.S. Biosensors Market Size, By Application, 2012 - 2024 (USD Million).....	5
Figure 1.5. Global Biosensors Market, by End-use (USD Million).....	5
Figure 2.1. Light transmission, reflection, and total internal reflection.....	20
Figure 2.2. Formation of the evanescent wave between two media, when coupling of light through prism at total internal reflection conditions occurs	21
Figure 2.3. SPR set-up configuration by Otto (Otto, 1968) (a) and Kretschmann (Kretschmann, 1971) (b).....	23
Figure 2.4. Typical Surface Plasmon Resonance spectra (Byun, 2010).....	24
Figure 2.5. The changes in polarization of light reflected from the surface.....	25
Figure 2.6. Optical model for an ambient/thin film/substrate structure (J A Woollam Co. Inc, 2001).....	27
Figure 2.7. The schematic of rotating analyzer spectroscopic ellipsometry.....	29
Figure 2.8. Typical TIRE spectra of Ψ and Δ for 25nm thick Au film deposited on glass (Nabok et al., 2011).....	31
Figure 2.9. Evaluation of the adsorption (k_a) and desorption (k_d) rates.....	34
Figure 2.10. Schematic diagram illustrating localized surface plasmon resonance.....	35
Figure 2.11. LSPR sensitivity to refractive index of the ambient.....	37
Figure 2.12. Energy-level of the states involved in Raman spectra.....	40

Figure 2.13. Electromagnetic field simulation for (a) a triangular nanoparticle (700 nm), (b) a dimer of spherical nanoparticles (520 nm), (Hao and Schatz, 2004).....	42
Figure 2.14. Fabrication processes: bottom-up and top-down.....	44
Figure 2.15. Classification of nanomaterials depending on the dimension	45
Figure 2.16. Classification of plasmonic nanostructures and the corresponding electron microscopy images (Examples of such shapes are nano-islands, nanorods, nanowires nano-spheres, and nano-stars) (Yu et al., 1979; Wu et al., 2010; Chen et al., 2010; Liu and searson, 2006; Yu et al., 1997; Huang et al., 2006).....	46
Figure 2.17. Solid-state dewetting of thin metal film.....	47
Figure 2.18. Stages of dewetting for Au film: hole initiation (1), hole growth (2), interconnected islands (3), isolated islands (4), island coarsening (5), and particles (6).....	47
Figure 2.19. Gold nano-island formation by dewetting after high temperature thermal annealing.....	48
Figure 2.20. Different types of bioreceptors (Nicu and Leïchl��, 2008).....	50
Figure 2.21. Classification of immobilization methods for bio- receptors.....	52
Figure 2.22. Antibody structure (IgG).....	54
Figure 2.23. Classes of antibodies	54
Figure 2.24. The Camel Heavy – Chain antibody and Nanobody.	55
Figure 2.25. Antibodies production.....	56
Figure 2.26. Forces involved in antigen-antibody binding (Abbas and Lichtman, 2005)....	57
Figure 2.27. Orientation of antibodies, random, upside, down effect on binding antigens (Chen et al. 2014).	58
Figure 2.28. Immobilization methods of antibody on the gold surface.....	59

Figure 2.29. Split antibody into two fragments using 2-Mercaptoethylamine and immobilization of half antibodies on gold surface via their native thiol group (Karyakin et al., 2000).....	60
Figure 2.30. Comparison in size between an aptamer and an antibody (Lee et al., 2008).....	63
Figure 2.31. Examples of aptamer shapes (a) Pseudoknot (b) G-quadruple (c) stem loop / bulge (d) Hairpin.....	64
Figure 2.32. A scheme for the Systematic Evolution of Ligands by Exponential enrichment process (SELEX).	65
Figure 2.33. Immobilization of aptamer on gold surface via thiol group.....	67
Figure 3.1. (a) Edwards thermal evaporator (b) schematic illustration showing the evaporation process.....	83
Figure 3.2. Microwave unit (a); (b) Microwave Kiln, inset show the glass slide coated with 5 nm gold annealed in microwave.....	83
Figure 3.3. Electrostatically immobilization of whole antibodies via cations poly allylamine hydrochloride (PAH) and protein A.	85
Figure 3.4. The scheme of immobilization of split antibodies on the gold surface via native thiol group.....	86
Figure 3.5. Aptamer immobilized on gold surface.....	87
Figure 3.6. (a) UV-visible Carry 50 spectrophotometer; and (b) schematic diagram of UV-visible spectroscopy.....	88
Figure 3.7. Lambert-Beer law for the light travelling through the sample with a thickness (x).....	89
Figure 3.8. (a) J.A. Woollam M2000 Ellipsometer and (b) an illustration of the changes in the polarised light after reflected from the surface.	91
Figure 3.9. Raman spectroscopy unit.....	92
Figure 3.10. The components of Raman spectroscopy.....	93

Figure 3.11. (a) XRD instrument and (b) The outline of a diffracted ray utilising X-ray diffraction.....	95
Figure 3.12. (a) FEI-nova nanosem 200 Scanning Electron Microscope (SEM) device (b) schematic diagram of SEM.....	96
Figure3.13. Secondary electrons and backscattered electrons (b) interaction between electron beam and sample producing (a)	97
Figure 3.14. (a) Nano Scope IIIa Multimode 8 SPM system components (b) Block diagram of atomic-force microscope (AFM).....	99
Figure 3.15. Van der Waals force against distance.....	100
Figure 4.1. AFM images of nanostructured Au films with different nominal thickness...	106
Figure 4.2. SEM images of Au nanostructured films with different nominal thickness prepared by thermal evaporation and annealing 2 hours at 480°C.	107
Figure 4.3. Distribution of equivalent diameters of Au island films of different nominal thicknesses: (a) 5nm, (b) 6nm, (C) 8 and (d)10 nm.....	110
Figure 4.4. (a) AFM image of Cr 3nm/5nm gold nanostructure (b) histogram of height distribution of gold nano-islands	112
Figure 4.5. The dependence of Au islands diameter Vs initial film thickness obtained by AFM data particle analysis.....	112
Figure 4.6. UV-vis absorption spectra of Au thin films of different thicknesses before (dotted lines) and after (solid lines) (a) thermal annealing, (b) Microwave annealing.....	114
Figure 4.7. Spectroscopic ellipsometry spectra of a series of gold nano-structures made from different nominal films thicknesses:(a) ψ spectra; (b) Δ spectra.....	115
Figure 4.8. Dispersion characteristics of n (a) and k (b) obtained by ellipsometry data fitting Inset shows the dependence of the position of LSPR peak on the actual gold film thickness.....	118
Figure 4.9. SEM images and their analysis for gold films: annealed using microwave (a) and oven(b).....	119

Figure 4.10. XRD pattern of Au 10 nm film annealed in microwave.....	120
Figure 4.11. (a) UV-vis spectra of 10nm Au film before and after annealing (b) position of LSPR is gradually shifted to high wavelengths.....	122
Figure 4.12. spectroscopic ellipsometry spectra (ψ and Δ) of 5nm Au film annealing using microwave	123
Figure 4.13. Cell designed to measurement different solution using external ellipsometry.....	124
Figure 4.14. Dependencies of LSPR band position vs. refractive index obtained from (a) absorption spectra and (b) ellipsometry measurements (our samples Au 4,5,6,8 and 10nm) (c) absorption spectra and (d) ellipsometry measurements (samples from our collaborates au 5,7.5 and 10nm).....	126
Figure 4.15. Spectroscopic ellipsometry Psi spectra of Cr/Au nanostructures different thicknesses (4, 5, 6, 8 and 10nm) deposition of PAH – PSS layers, inset shows saturation of deposition of PAH and PSS layers and SEM and AFM images of gold thin film.....	131
Figure 4.16. Dependence of the position of LSPR band vs the number of PAH/PSS layers deposited (a) Au of our samples (b) Au from collaborates.....	133
Figure 5.1. TIRE spectra Ψ (a) and Δ (b) for Au nano-structures of different nominal thicknesses.....	138
Figure 5.2. The series of TIRE Δ spectra corresponding to deposition of layers of PAH, antibodies, and aflatoxin B1 on nanostructured Au film of 5 nm of nominal thickness annealed at higher temperature 550 °C for 10 h.....	139
Figure 5.3. The series of TIRE Δ spectra corresponding to deposition of layers of PAH, antibodies, and aflatoxin B1 on continuous Au film of 25 nm deposited on glass slide and 3nm Cr as intermediate layers.....	139
Figure 5.4. SDS – PAG electrophoresis of antibodies before and after splitting.....	140
Figure 5.5. Ellipsometric Δ spectra recorded after binding of aflatoxin B1 molecules of different concentrations to split antibodies immobilized on 5nm nano-Au layer.....	142

Figure 5.6. The spectral shift of Δ vs the concentration of aflatoxin B1.....	143
Figure 5.4. TIRE spectra of zearalenone 0.1- 0.01 ng/ml on split antibodies.....	144
Figure 6.1. TIRE spectra recorded on aptamer layer (1), and after binding OTA of 0.01ng/ml (2), 1ng/ml (3), and 10ng/ml (4).....	149
Figure 6.2. Dependence of the thickness increment of the aptamer layer vs OTA concentration.....	150
Figure 6.3. TIRE spectra of aptamer layer show no shift after injecting pure PBS buffer solution with no ochratoxin A into the cell.....	151
Figure 6.4. Figure 6.4. Typical time dependence of Δ during binding of OTA of 1ng/ml to aptamers (a); evaluation of K_A (b).....	153
Figure 6.5. The sequence of steps of samples preparation and immobilization of aptamer on gold nanostructures.....	154
Figure 6.6. A series of TIRE Δ spectra recorded upon binding of AFT B1 (a) and AFT M1 (b) to respective specific aptamers	158
Figure 6.7. Dependences of the aptamer layer thickness vs concentration of AFT B1 (a) and AFT M1 (b).....	159
Figure 6.8. Typical time dependences of Δ at 600 nm during binding of AFT B1 of different concentrations (a) 0.1 ng/ml, (b)1ng/ml, (c)10ng/ml and (d)100ng/mL to specific aptamer (e) $1/\tau$ against AFT B1 concentration.....	162
Figure 7.1. Deposition of close-packed spheres by slow lifting method.....	167
Figure 7.2. Deposition of polystyrène nano-spheres monolayer on glass slide by slow lifting method.....	168
Figure 7.3. Formation of gold nanostructure by nanosphere lithography.....	169
Figure 7.4. SEM images of closely -packed monolayer of polystyrene nanosphere coated by gold (a) and gold-nanostructures obtained after removing polystyrene sphere (b).....	171

Figure 7.5. AEM image of closely -packed monolayer of polystyrene nanosphere coated by gold.....171

Figure 7.6. UV-Visible absorption spectra of gold layer before and after remove polystyrene nano-spheres.....172

Figure 7.7. Raman spectra of ttb-H₂P_c deposited on 25nm thick continuous Au film (pink curve) and Au nanostructures formed by nanosphere lithography.....173

Figure 7.8. Raman spectra of ttb-H₂P_c deposited on 25nm thick continuous Au film (pink curve) and Au nanostructures formed by nanosphere lithography.....174

LIST OF TABLES

Table 1.1. Types of mycotoxins, fungal sources and their chemical structures.....	9
Table 2.1. Four layers model for TIRE data fitting (Nabok and Tsargorodska, 2008).....	32
Table 4.1. AFM image analysis of gold nano-structures made from Cr 3 nm and Au films of different nominal thickness annealed at 480°C for 2 hours.....	111
Table 4.2. AFM image analysis of gold nano-structures made of different thickness annealed at 550C for 10 hours.....	111
Table 4.3. The results of ellipsometry data fitting.....	117
Table 4.4. XRD data of the size of Au nan -crystals evaluated by XRD analysis.....	121
Table 4.5. Evaluation of refractive index sensitivity using UV. Visible absorption and spectroscopic ellipsometry the sample prepared in our laboratory the gold layer coated on typical glass slide on Cr 3nm as intermediate layer to improve adhesion of gold on glass surface annealed at 480 °C for 2 hours.....	127
Table 4.6. Evaluation of refractive index sensitivity using UV. Visible absorption and spectroscopic ellipsometry the samples from our collaboration the just gold coated on cover slide without Cr intermediate layer and using different annealing condition for 10 hours at 550 °C (samples from collaborates)	128

Chapter 1: Introduction

1.1 General background and motivation for research

Innovative analytical devices featuring precision, sensitivity, specificity, speed, and usability continue to be developed to meet the increasing demand for legislative actions on the monitoring of a growing number of pollutants. To detect different environmental contaminants, quantitative analysis of water samples is generally performed using traditional analytical methods such as chromatography and mass spectroscopy. Although accurate and sensitive, these methods require sophisticated and expensive instrumentation, expert personnel for their operation, multistep and complicated sample preparation. These methods are also labour intensive and time consuming, and it is difficult to achieve on-site, real-time, and monitoring of contaminants (Bellan, 2011).

To meet these requirements, researchers have been striving to develop robust, cost-effective, automated devices for rapid and sensitive analysis of environmental pollutants in water. Biosensors combining advances in biochemistry, biology, nanotechnology, physics, and electronics, can meet the requirements of risk assessment, management approaches and environmental legislation because of their unique characteristics such as speed, sensitivity, specificity, ease-of-use, and real-time remote monitoring capability (Rogers, 2006).

The development of biosensors for mycotoxins has risen sharply in the last decade with a large number of different biosensing technologies been used which were extensively reviewed in (Van et al., 2003; Pohanka and Kuca, 2007; Ying et al., 2012; Vidal et al., 2013). According to a review in optical biosensing of mycotoxins (Ying et al., 2012), the

traditional SPR method allowed the detection of OTA down to 1.5ng/ml in concentrations, while the use of LSPR in functionalized gold nanoparticles reduced LDL substantially down to 0.04 ng/ml. The SPR LDLs for AFT B1 and ZON are, respectively, 0.2 ng/ml and 0.3ng/ml. Electrochemical detection of mycotoxins reviewed in (Vidal et al., 2013) appeared to be more sensitive, for example LDL of 0.5 ng/ml for OTA detection was achieved with impedance spectroscopy; the use of aptamers in electrochemical detection of mycotoxins allowed decreasing LDL to 0.03–0.8 ng/ml for OTA.

This work reviews our recent progress in the development of novel optical methods of detection of mycotoxins in direct assay with either specific antibodies or aptamers. The main method in this work was based on the total internal reflection ellipsometry (TIRE) combined with LSPR transducers based on gold nano-structures produced by annealing of thin gold films. LSPR method which is more sensitive method, represent a new and simpler technology than other techniques.

A biosensor is an analytical device that integrates a biological sensing element (e.g., an antibody or aptamer) with a physical transducer (e.g., optical, mass, or electrochemical), whereby the interaction between the target and the bio-recognition molecules is translated into a measurable electrical signal (Rogers, 2006). The modern concept of a biosensor was developed by Leland C. Clark Jr. in 1962. (Turner et al., 1987). As shown in Figure 1.1. optical biosensors that exploit the phenomena of light absorption, fluorescence, luminescence, reflectance. Optical biosensors can be powerful alternatives to conventional analytical techniques; they provide rapid, highly sensitive, real-time, and fast monitoring without any time-consuming sample concentration and/or prior sample pre-treatment steps. Therefore, optical biosensors have great potential application in the areas of environmental

monitoring, food safety, drug development, biomedical research, and diagnostics (Borisov and Wolfbeis, 2008; Fan et al., 2008).

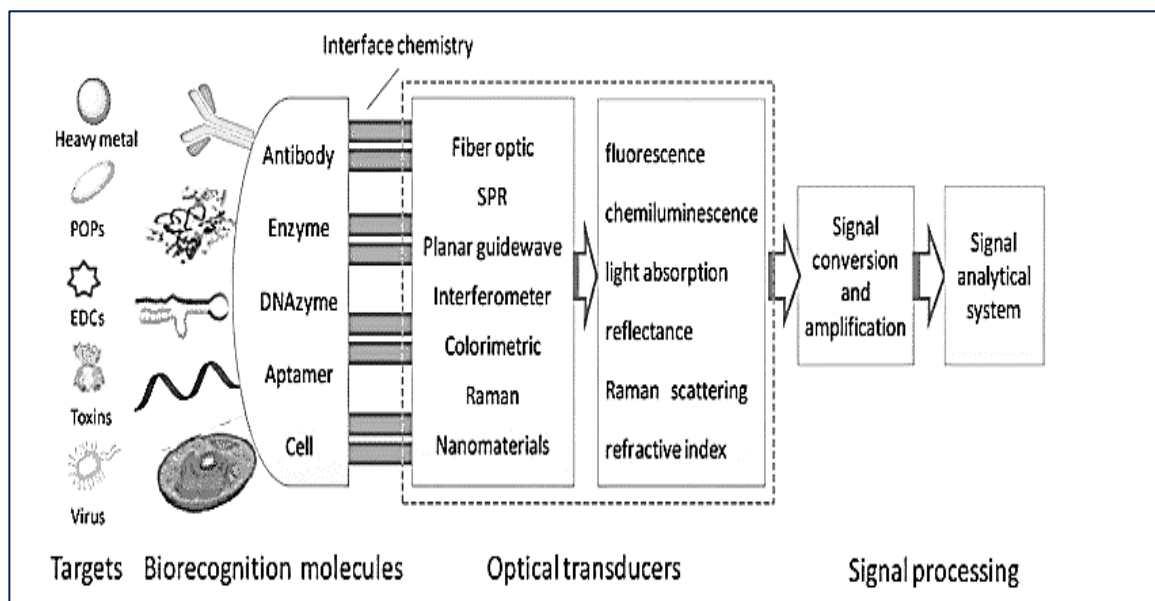


Figure 1.1. Principles of optical biosensor

Biosensor usage can be seen in the areas of health care, for example, blood glucose monitoring, there are devices which measure the concentration of glucose within a person's blood often referred to as blood, sugar (see figure 1.2). Blood glucose monitors measure the amount of sugar in a sample of blood using a complex electro-chemical process involving the enzyme Glucose Oxidase and some electrochemically active chemicals such as ferrocene. The products of glucose decomposition influence the current and the concentration of blood sugar can be measured (Han et al., 2002).



Figure 1.2. Blood glucose monitor

The pregnancy test is an easy and most reliable test that looks for the presence of the hormone known as human chorionic gonadotropin (hCG) which is produced by the placenta and can be found in a woman's system as soon as implantation of a fertilized egg occurred. The urine sample is collected on the test strip of a home pregnancy test, it then diffuses across the strip and comes into contact with a test line which contains antibodies for the (hCG) labelled with a dye molecule. That reaction creates a colour strip indicating pregnancy as shown in Figure 1.3 (Bhalla et al., 2016).

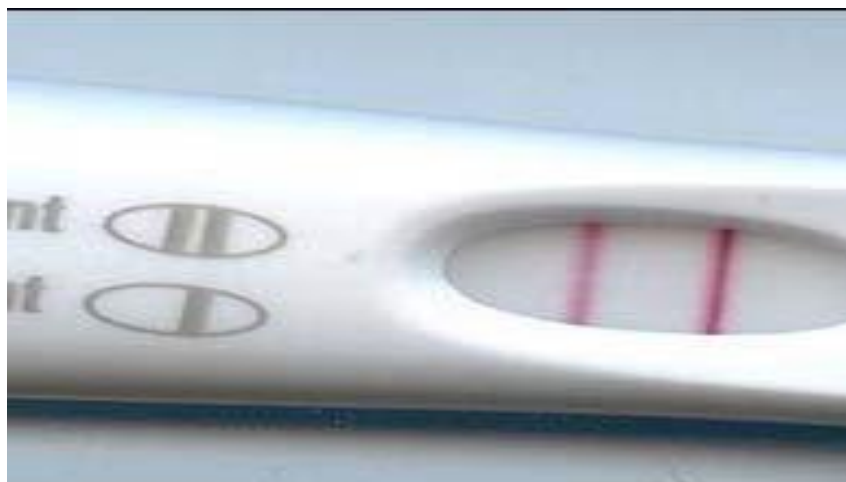


Figure 1.3. Pregnancy test device

The biosensors market size was 14.8 billion USD in 2015 with an 8% CAGR (compound annual growth rate) estimation from 2016 to 2024 (see Figure 1.4 and 1.5).

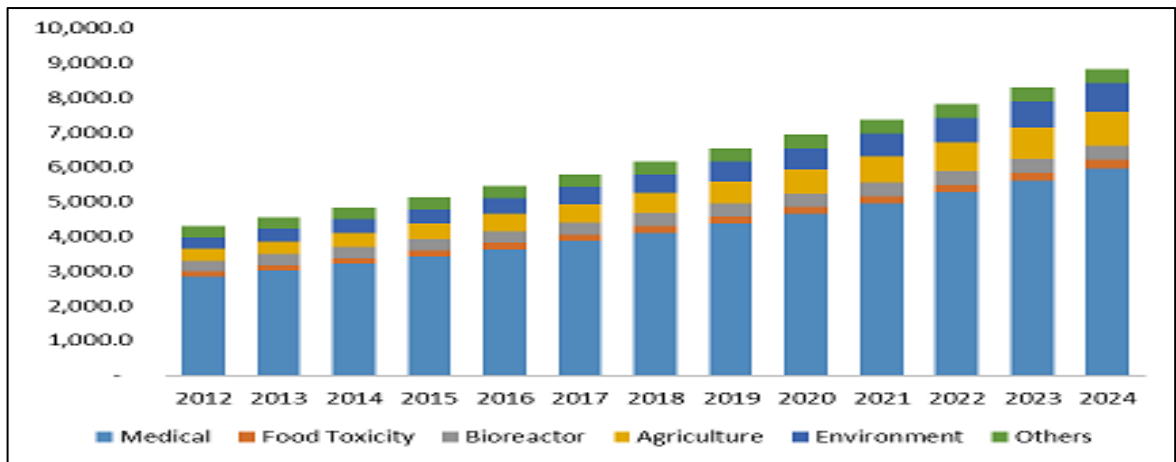


Figure 1.4. U.S. Biosensors Market Size, by Application, over the period 2012 - 2024 (USD Million)

Rapid technological advancements, growing popularity of point of care diagnostics, expanded applications of biosensors in the field of medical science and rising diabetic population base are some of the pivotal factors driving the global biosensors market size in the forecast period. The biosensors market size is predominantly influenced by rising demand for disposable, cost-efficient, and user-friendly devices (Alocilja and Radke, 2003).

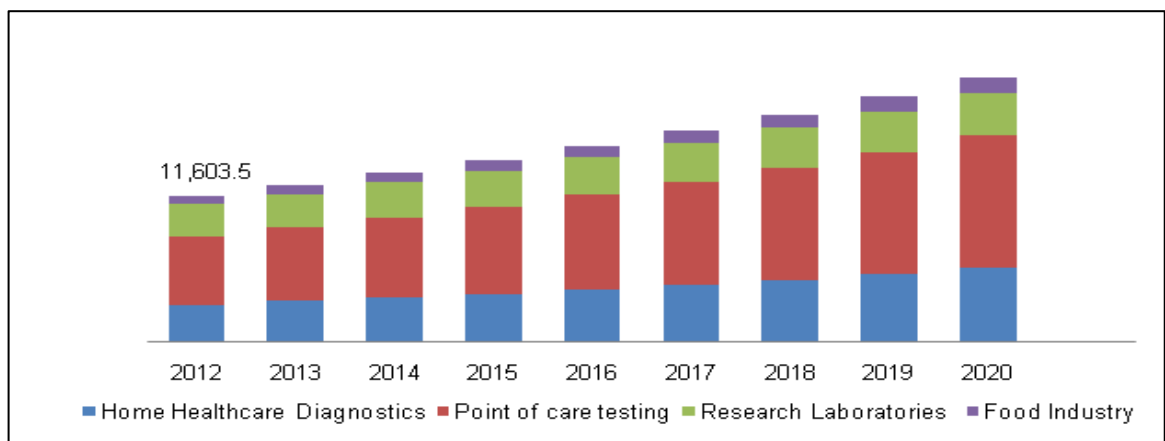


Figure 1.5. Global Biosensors Market, by End-users (USD Million)

In Figure 1.5 the point of care testing segment was the most revenue generating segment in 2012-2020. The development of biosensors has initiated a revolution in the rapidly evolving point of care testing which provides real-time health monitoring, and thus, have the potential to improve patient care. Key applications analysed include food toxicity detection, agriculture, industrial process control, environment, medical applications and others. Rapid advances in biosensor technology have been mostly stimulated by the healthcare sector, in particular, by demands in blood glucose monitoring. Electrochemical biosensors were the largest technology segment of the biosensors market in 2013 to 2020 because of ease of miniaturization, robustness, low detection limits, accuracy of analysis.

Optical biosensors are expected to witness a healthy growth during the forecast period because of their use in the environmental monitoring and early warning fields.

1.1.1 Motivation for research

The motivation of this study is mainly driven by the importance of the detection of toxins, either naturally produced or human-made, which is currently one of the main problems in analytical sciences. A particular interest is on the detection of mycotoxins, products of metabolism of numerous fungi species which can grow on inappropriately stored agriculture products (grains, nuts, coffee beans, spices, fruits, etc.) and associated food. Mycotoxins are well-known by their toxicity, carcinogenic and endocrine disrupting properties which resulted in strict legislations on their content in food and feed, typically in ppb concentration range. In addition to traditional analytical methods for toxin detection, the development of low cost, portable, though highly sensitive bio-sensors suitable for in-field a point-of-care diagnostics is in great demand nowadays. Our research is dedicated to development of novel optical bio-sensing technologies for the detection of mycotoxins exploiting novel optical transducing techniques, such as total internal reflection

ellipsometry (TIRE), and localized surface plasmon resonance (LSPR). It would be of special interest to develop novel optical biosensors based on LSPR biosensing, in order to open the door to applications of biosensors for rapid and highly accurate detection of pollutants in environmental samples..

1.1.2 Mycotoxins and their detection

Mycotoxins are products of metabolism of numerous fungi species which can grow on different agriculture products, such as grains (corn, maize, rice, etc.), nuts, spices, coffee and cocoa beans, dried fruits, etc., at elevated temperatures and high humidity (Pohanka et al., 2007). Therefore, mycotoxins appeared to be quite common contaminants in the above agriculture products and associated food and animal feed (Peraica, et al., 1999). Furthermore, the presence of mycotoxins in animal feed causes their wider distribution in food chain, for example in poultries, meet, and milk (Bhat et al., 2009). Mycotoxins gained great deal of attention in the last 10–15 years because of their negative impact on human and animal health; many mycotoxins are toxic, carcinogenic, and endocrine disruptive agents. The examples of three mycotoxins which were actually the subjects of study in this work are given in Table 1.1:

Aflatoxins B1 and M1 (AFT B1 & M1) (Dorner, 2004) are produced by *Aspergillus flavus* and *A. parasiticus* species grown on grains and cereals (maize, rice, wheat, etc.), spices (chilli and black pepper, coriander, turmeric, ginger), and tree nuts (almond, pistachio, walnut, coconut, brazil nut). Aflatoxin B1 is one of the most carcinogenic substances known. AFT M1 being a 4-hydroxylated metabolite of AFT B1 is found in cow and sheep milk and milk products.

Ochratoxin A (OTA) (Bayman and Baker, 2006) produced by *Aspergillus ochraceus*, *A. carbonarius*, and *Penicillium verrucosum* is one of the most abundant contaminants in grain and pork products, coffee, dried grapes, also in wine and beer (Mateo et al., 2007). OTA is carcinogenic and neurotoxic for humans, and immunotoxic for animals.

Zearalenone (ZEN) (Desjardins and Proctor, 2007). is produced by *Fusarium* or *Giberella* species grown on crops (maize, barley, oats, wheat, rice, also bread) is a potent oestrogen metabolite causing infertility in swine and poultry.

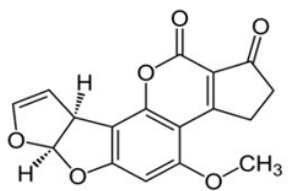
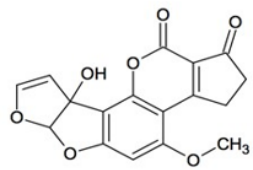
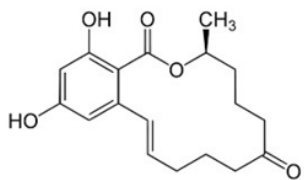
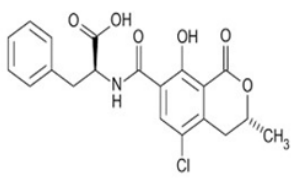
The danger of mycotoxins is well-recognised worldwide, and recent legislations set quite strict limits for mycotoxins' content in food and feed. The allowed dosage is slightly varied depending on the type of agriculture products, foods, and feeds. The lowest limits for mycotoxins in ppb (part per billion) and even below (0.05 ppb for baby food) are established in EU, with similar standards in China and Japan, while US legislation is more lenient (Worldwide Mycotoxin Regulations, 2016).

Table 1.1 summarises the sources of fungal species and chemical structures of mycotoxins selected for this study. One of common characteristics of the selected mycotoxins is their low molecular weight, which makes their detection even more difficult.

One of the conventional methods for the detection of mycotoxins is thin layer chromatography (TLC) which is a chromatography technique used to separate non-volatile mixtures (Harry and Christopher, 1989). It is performed on a sheet of glass, plastic, or aluminum foil, which is coated with a thin layer of adsorbent material, usually silica gel, aluminum oxide, or cellulose and has been used to determine aflatoxins in various food in particular nuts such as pistachios. The measurements using this technique provide a limit of detection (LOD) ranging from 0.1 µg/kg to 0.7 µg/kg for Aflatoxin B 1

(Stroka et al., 2000). High performance liquid Chromatography (HPLC) is a common technique in analytical chemistry used to separate, identify, and quantify each component in a mixture.

Table 1.1 Types of mycotoxins, fungal sources and their chemical structures

Types of mycotoxins	Commodities	Fungal source	Molecular weight g/mol	Chemical structures
Aflatoxin B1	Maize, pistachio, wheat	<i>Aspergillus flavus parasiticus</i> species	312.2798	
Aflatoxin M1	Milk	<i>Aspergillus</i> Species	328.276	
Zearalenone	maize, barley, wheat	<i>Fusarium (Gibberella)</i> species	318.364	
Ochratoxin A	coffee, wine grapes	<i>Aspergillus ochraceus</i> , <i>Aspergillus carbonarius</i> , and <i>Penicillium verrucosum</i>	403.81	

It relies on pumps to pass a pressurized liquid solvent containing the sample mixture through a column filled with a solid adsorbent material, where each component in the sample interacts slightly differently with the adsorbent material, causing different flow rates

for the different components and leading to the separation of the components as they flow out of the column (Gerber et al., 2004). HPLC method has been selected for the detection of aflatoxin B I and ochratoxin A produced in bee pollen with detection limits of 0.49 $\mu\text{g}/\text{kg}$ and 0.20 $\mu\text{g}/\text{kg}$ respectively (Garcia-Villanova et al., 2004).

Traditional chromatographic methods have the disadvantages of being expensive and time-consuming, associated with steps taken for sample clean up, pre-concentration, and require trained personnel. Although most validated detection methods are chromatographic, alternative detection means based on biosensing principles are more promising for example the ELISA kits are one of the most widely used biosensing methods (Maragos, 2002). Typically, 96-well plates can be purchased. The limit of detection reached by commercial methods based on ELISA or affinity chromatography is similar. For example, aflatoxins were detected with limit of detection (LOD) slightly above 2 ppb (Zheng et al., 2005). Optical biosensors can be considered as possible devices for mycotoxins analysis (Rasooly and Herold, 2006).

1.1.3 Optical biosensors technologies (SPR, TIRE, LSPR)

Optical biosensors are devices combining an optical transducer with a sensing biochemical component capable of detection of analyte molecules using one of specific biological reactions, such as immune binding. Finding suitable bio-receptors for particular pollutants is an important part of the work which can be achieved using specific antibodies. A range of antibodies specific to particular mycotoxins are either commercially available or could be provided by specialized research institution. A novel approach in immune-sensing based on using artificial receptors such as aptamers or peptides has been developed, and it will be attempted in this project.

There are many types of optical transducers used in optical bio-sensing with surface plasmon resonance (SPR) being the most common and widely used method. Recent advances in nanotechnology brought to practice some new methods which explore novel physical phenomena of localized surface plasmon resonance (LSPR) and surface enhanced Raman scattering (SERS) in metal nanostructures. Such nanostructures can be fabricated by different methods starting with gold-nanoparticles and nanorods, down to nanopatterned metal structures made by deposition of metals through layers of polymeric or inorganic spheres (microsphere lithography), interference lithography as well as irregular metal islands formed by annealing of thin evaporated metal layers. Some of these technologies in combination with the optical methods of UV-vis absorption spectroscopy, spectroscopic ellipsometry, and Raman spectroscopy are explored in this research.

1.1.3.1 Surface Plasmon Resonance (SPR) sensors

The SPR biosensor technology allows the real-time detection and monitoring of biomolecular binding events. The SPR instrumentation was first introduced in 1990, by Pharmacia AB, Uppsala, Sweden (Kooyman et al., 2008). This technology is widely used nowadays, due to its high sensitivity and speed of analysis. In a SPR experiment, one interacting molecule (ligand) is bound to the biosensor surface (the transducer) while the other (analyte) is delivered to the surface in a continuous flow through a microfluidic system. The technology requires no labeling of biomolecules and can provide quantitative information on kinetic parameters (association and dissociation rate constants) and measurements of active concentrations (Malmquist, 1999). SPR technology is used to characterize molecular interactions involving small molecules, proteins, polysaccharides, lipids and nucleic acids, when studying epitope mapping, molecular assembly, ligand fishing and small molecule screening (Karlsson, 2004; Pattnaik, 2005).

1.1.3.2 Total Internal Reflection ellipsometry TIRE

A relatively novel method of total internal reflection ellipsometry (TIRE) combines the advantages of the accuracy of the spectroscopic ellipsometry instrumentation with the experimental conveniences of Krestchmann SPR geometry. Although theoretically the TIRE method was known a long time ago (Azzam and Bashara, 1992), its experimental realization has been achieved relatively recently (Westphal and Bornmann, 2002). This idea was successfully implemented and developed further by the Nabok research group (Nabok et al., 2005). The modelling showed that Δ is about 10 times more sensitive than ψ to small changes in thickness and refractive index of adsorbed layers (Nabok and Tsargorodskaya, 2008).

1.1.3.3 Localized surface plasmons Resonance (LSPR)

Localized surface plasmons (LSPs) are collective oscillations of the conducting electrons in resonance with incident electromagnetic field which occur in metal nanoparticles (NP). The oscillating electric field of the incident radiation induces the oscillation of free surface electrons (plasmons) at a unique resonance frequency matching plasmon oscillations within the NP. Excitation of LSPs results in a number of interesting phenomena: strong light scattering, intense surface plasmon absorption bands, and the enhancement of the local electromagnetic field in the vicinity of the particle. These unique properties have been found to be useful in different applications, such as biological markers and stains for various microscopies, nanoscale optics and photonics, LSPR, SERS, and chemical and biological sensor applications. LSPR is typically used in combination with UV-vis

absorption spectroscopy for the detection of large molecules, e.g. proteins. In this work we tried to utilize LSPR for detection of small mycotoxin molecules.

1.1.4 Bio-receptors (antibodies and aptamers)

The most common bio-receptors are antibodies which can be produced against particular targets, in our case mycotoxins. Bio-sensors based on the use of antibodies, usually called immunosensors, are the most common in optical biosensing. Antibodies are typically immobilized on the surface of optical transducers (metal films, optic fibers, nano particles, etc.) using well-developed immobilization routes including covalent binding, electrostatic binding, encapsulation into a polymer matrix, etc. Although, the strongest and thus the most stable covalent binding is commonly used in majority of optical immunosensors.

A simple splitting of IgG-based antibody by cutting di-sulphide bonds between two heavy chains through the treatment with 2-mercaptoethylamine has resulted in two half-antibodies with thiol groups available for subsequent covalent binding on the surface of gold (Karyakin, 2000). According to this study, the other di-sulphide bonds as well as Fab-fragments in IgG are not affected. The half antibodies for aflatoxin B1 were used in the current work; the immobilization protocol was similar to that described in (Karyakin, 2000). Another possibility resulting in even smaller bio-receptors lies in the use of so-called nano-bodies which are just the variable fragments VL or VH of IgG-based antibodies (Ahmad et al., 2013) or variable fragments of camelid antibodies (Huand et al., 2010).

Another type of bio-receptors commonly used these days instead of antibodies are aptamers. Aptamers are synthetic oligonucleotide or peptide molecules that reproduce a similar function to antibodies i.e. specific binding of particular target molecules. Aptamers are typically based on RNA or DNA oligonucleotides of particular sequence

complementary to that of target molecules (Ellington and Szostak,1990); they are assembled from a vast pool of amino acids using the SELEX (systematic evolution of ligands by exponential enrichment) procedure. Aptamers have a number of advantages over traditional antibodies which include better stability, much simpler and more ethical synthesis (without the use of immunization of small animals) and, not least, the lower price. The popularity of using aptamers as bio-receptors has rocketed in the last decade, and nowadays aptamers are commercially produced by specification for a wide range of targets. The presence of a thiol group at one end of aptamer allowed simple immobilization of aptamers on gold; the other end of the aptamer could be either label-free or may contain functional groups, i.e. redox groups or luminophores. The aptamers change their conformation upon binding the target molecules. Aptamers labeled with redox groups were successfully used for electrochemical detection of OTA and other mycotoxins (Rhouati et al., 2013).

1.2 Aims and objectives

The main aims of this research are:

- The fabrication of gold nano-structures and their characterization using SEM, XRD, AFM, UV-vis absorption spectroscopy and spectroscopic ellipsometry.
- The development of optical biosensors based on the LSPR phenomenon in nano-structured gold films suitable for the detection of low molecular weight bio-analytes such as mycotoxins.

To achieve these aims the following objectives were identified:

- To develop the technology of fabrication of gold nanostructures by annealing thin gold films.
- To establish a correlation between the structure and morphology of gold-nanostructures with their optical properties, mainly LSPR and surface enhanced Raman spectroscopy (SERS).
- To develop a novel optical biosensing technology which combines gold nanostructures possessing LSPR effect with highly sensitive detection method of TIRE.
- To optimize the parameters of gold nano-structures to improve the sensitivity of LSPR/TIRE method.
- To improve the sensitivity of LSPR/TIRE detection using small size bio-receptors, such as half-antibodies or aptamers.
- To attempt the use of SERS effect in gold nanostructure for detection of mycotoxins.

Reference list

- Ahmad, M. Z., Akhter, S., Rahman, Z., Akhter, S., Anwar, M., Mallik, N., & Ahmad, F. J. (2013). Nanometric gold in cancer nanotechnology: current status and future prospect. *Journal of Pharmacy and Pharmacology*, 65(5), 634-651.
- Alocilja, E. C., & Radke, S. M. (2003). Market analysis of biosensors for food safety. *Biosensors and Bioelectronics*, 18(5-6), 841-846.
- Azzam, R.M.A., Bashara, N.M., Ellipsometry and Polarized Light, North-Holland Amsterdam, 1992.
- Bayman, P. Baker, J.L. Ochratoxins: a global perspective, *Mycopathologia* 162 (3) (2006) 215–223.
- Bellan, L.M.; Wu, D.; Langer, R.S. (2011). Current trends in nanobiosensor technology. *WIREs Nanomed. Nanobiotech*, 3, 229–246.
- Bhalla, N., Jolly, P., Formisano, N., & Estrela, P. (2016). Introduction to biosensors. *Essays in biochemistry*, 60(1), 1-8.
- Bhat, R. Rai, R.V. Karim, A.A. (2009). Mycotoxins in food and feed: present status and future concerns, *Comprehensive Reviews in Food Science and Food Safety*, Wiley Online Library, Borisov, S.M.; Wolfbeis, O.S. Optical biosensors. *Chem. Rev.* 2008, 108, 423–461.
- Desjardins, A. E., & Proctor, R. H. (2007). Molecular biology of Fusarium mycotoxins. *International journal of food microbiology*, 119(1-2), 47-50.
- Dorner, J. W. (2004). Biological control of aflatoxin contamination of crops. *Journal of Toxicology: Toxin Reviews*, 23(2-3), 425-450.
- Ellington, A.D. Szostak, J.W. In vitro selection of RNA that binds specific ligands, *Nature* 346. (1990). 818–822. Fan, X.; White, I.M.; Shopova, S.I.; Zhu, H.; Suter, J.D.; Sun, Y. Sensitive optical biosensors for unlabeled targets: A review. *Anal. Chim. Acta* 2008, 620, 8–26.
- Garcia-Villanova, R. J., Cordon, C., González Paramás, A. M., Aparicio, P., & Garcia Rosales, M. E. (2004). Simultaneous immunoaffinity column cleanup and HPLC analysis of aflatoxins and ochratoxin A in Spanish bee pollen. *Journal of agricultural and food chemistry*, 52(24), 7235-7239.
- Gerber, F.; Krummen, M.; Potgeter, H.; Roth, A.; Siffrin, C.; Spöndlin, C. (2004). "Practical aspects of fast reversed-phase high-performance liquid chromatography using 3µm particle packed columns and monolithic columns in pharmaceutical development and production working under current good manufacturing practice". *Journal of Chromatography A*.
- Han, I. S., Bae, Y. H., & Magda, J. J. (2002). *U.S. Patent No. 6,475,750*. Washington, DC: U.S. Patent and Trademark Office.

- Harry W. Lewis & Christopher J. Moody (13 Jun 1989). *Experimental Organic Chemistry: Principles and Practice* (Illustrated ed.). WileyBlackwell. pp. 159–173.
- Huang, L., Muyldermans, S., & Saerens, D. (2010). Nanobodies: proficient tools in diagnostics. *Expert review of molecular diagnostics*, 10(6), 777-785.
- Karlsson, R. (2004). SPR for molecular interaction analysis: a review of emerging application areas. *Journal of Molecular Recognition* 2004, 17, 151-161.
- Karyakin, A. A., Presnova, G. V., Rubtsova, M. Y., & Egorov, A. M. (2000). Oriented immobilization of antibodies onto the gold surfaces via their native thiol groups. *Analytical chemistry*, 72(16), 3805-3811.
- Kooyman, R. P., Corn, R. M., Wark, A., Lee, H. J., Gedig, E., Engbers, G., ... & Chinowsky, T. (2008). *Handbook of surface plasmon resonance*. Royal Society of Chemistry.
- Malmquist, M. (1999). BIACORE: an affinity biosensor system for characterization of biomolecular interactions. *Biochemical Society Transactions*, 27, 335-340.
- Mateo, R., Medina, Á., Mateo, E. M., Mateo, F., & Jiménez, M. (2007). An overview of ochratoxin A in beer and wine. *International journal of food microbiology*, 119(1-2), 79-83.
- Nabok, A. V., Tsargorodskaya, A., Hassan, A. K., & Starodub, N. F. (2005). Total internal reflection ellipsometry and SPR detection of low molecular weight environmental toxins. *Applied Surface Science*, 246(4), 381-386.
- Nabok, A., & Tsargorodskaya, A. (2008). The method of total internal reflection ellipsometry for thin film characterisation and sensing. *Thin Solid Films*, 516(24), 8993-9001.
- Nabok, A., Tsargorodskaya, A., Holloway, A., Starodub, N. F., & Demchenko, A. (2007). Specific binding of large aggregates of amphiphilic molecules to the respective antibodies. *Langmuir*, 23(16), 8485-8490.
- Pattnaik, P. (2005). Surface plasmon resonance - Applications in understanding receptor-ligand interaction. *Applied Biochemistry and Biotechnology* 2005, 126, 79-92.
- Peraica, M. Radic, B. Lucic, A. Pavlovic, M. (1999). Toxic effects of mycotoxins in humans, *Bull. World Health Organ.* 77 (9) 754–766.
- Perumal, V., & Hashim, U. (2014). Advances in biosensors: Principle, architecture and applications. *Journal of applied biomedicine*, 12(1), 1-15.
- Pohanka, M., Jun, D., & Kuca, K. (2007). Mycotoxin assays using biosensor technology: A review. *Drug and chemical toxicology*, 30(3), 253-261.
- Rhouati, A., Yang, C., Hayat, A., & Marty, J. L. (2013). Aptamers: A promising tool for ochratoxin A detection in food analysis. *Toxins*, 5(11), 1988-2008.

Rogers, K.R. (2006). Recent advances in biosensor techniques for environmental monitoring. *Anal. Chim. Acta*, 568, 222–231.

Stroka, J., Van Otterdijk, R., & Anklam, E. (2000). Immunoaffinity column clean-up prior to thin-layer chromatography for the determination of aflatoxins in various food matrices. *Journal of Chromatography A*, 904(2), 251- 256.

Turner, A., Karube, I., & Wilson, G. S. (1987). *Biosensors: fundamentals and applications*. Oxford university press.

Westphal, P., & Bornmann, A. (2002). Biomolecular detection by surface plasmon enhanced ellipsometry. *Sensors and Actuators B: Chemical*, 84(2-3), 278-282.

Van der Gaag, B., Spath, S., Dietrich, H., Stigter, E., Boonzaaijer, G., van Osenbruggen, T., & Koopal, K. (2003). Biosensors and multiple mycotoxin analysis. *Food Control*, 14(4), 251-254.

Vidal, J. C., Bonel, L., Ezquerro, A., Hernández, S., Bertolín, J. R., Cubel, C., & Castillo, J. R. (2013). Electrochemical affinity biosensors for detection of mycotoxins: A review. *Biosensors and Bioelectronics*, 49, 146-158.

Ying Li, Xia Liu, Zhao Lin, Recent developments and applications of surface plasmon resonance biosensors for the detection of mycotoxins in foodstuffs, *Food Chem.* 132 (3) (2012) 1549–1554.

Chapter 2: Literature review

Chapter overview

This chapter provides an extensive analysis of the literature related to the current PhD project and gives an overview of several optical bio-sensing technologies and bio-receptors. It starts with one of the most common bio-sensing technique of surface plasmon resonance (SPR), then describes the method of total internal reflection ellipsometry (TIRE) which is a combination of SPR and ellipsometry. The TIRE method appeared to be much more sensitive than SPR and thus suitable for the detection of small molecules of mycotoxin. Other emerging techniques are localized surface plasmon resonance (LSPR) and surface enhanced Raman scattering (SERS). LSPR biosensors have gained increasing interest in recent years as relatively simple and low-cost method for biological and chemical sensing. TIRE method was also chosen for LSPR bio-sensing because of its superior sensitivity as compared to conventional UV-vis absorption spectroscopy. Surface Enhanced Raman Scattering (SERS), a method capable of detection of single molecules of analyte (Haynes et al., 2005) and highly important for sensing application, and is also discussed here. Furthermore, a general description of bio-receptors and their immobilization on gold surface was given. Finally, the fabrication of metal nanostructures, and gold nano-islands in particular, are reviewed with the emphasis on their application in mycotoxins detection.

2.1 Optical bio-sensing technologies

2.1.1 Optical biosensors based on evanescent field

An evanescent wave is an oscillating electric or magnetic field which does not propagate as an electromagnetic wave but whose energy is spatially concentrated in the vicinity of the source (oscillating charges and currents) (Thio, 2006). An evanescent wave is a nearfield standing wave exhibiting exponential decay with distance. Evanescent waves are always associated with matter and are most intense within one-third wavelength from any acoustic, optical, or electromagnetic transducer; optical evanescent waves are commonly found during total internal reflection.

The evanescent field is associated with the electric field disseminated along the interface between two materials under the conditions of total internal reflection (Marston, 2002), as shown in Figure 2.1.

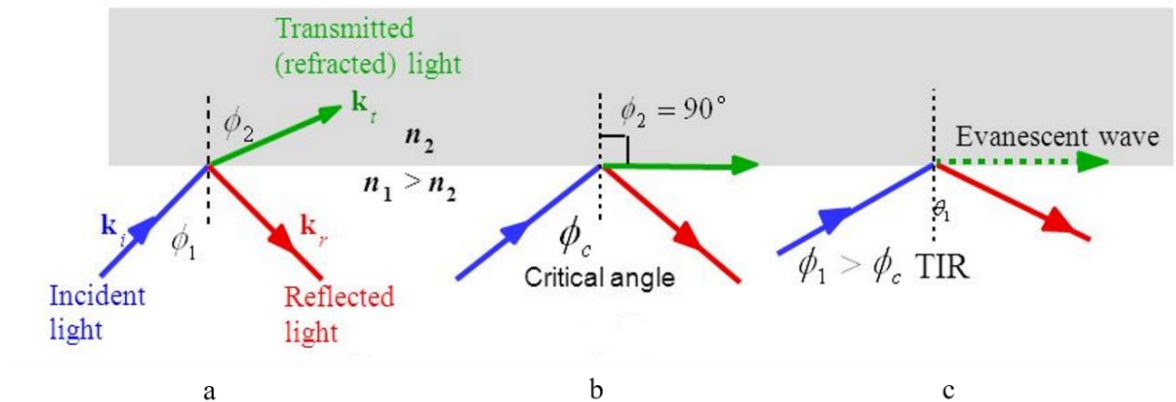


Figure 2.1: Light transmission, reflection, and total internal reflection

Depending on the incidence angle with respect to ϕ_c which is determined by the ratio of refractive indices of two media, the wave may be transmitted (refracted) when $\phi_I < \phi_c$ (a), critical conditions for total internal reflection are achieved when $\phi_I = \phi_c$ (b) or totally reflected when $\phi_I > \phi_c$ (c).

The optical methods that are based on the evanescent field phenomenon joined with the thin film nanotechnology opens the doors for some new opportunities in bio-sensing. Optical methods can be label-free and suitable for express in-situ and in-field analysis. Very often optical evanescent field sensors use thin metal film as the transducing elements. Typically, parameters identified by this method are the intensity or phase shift of the reflected light. Evanescent field methods are compatible with the thin film nanotechnology that can place few molecular layers on a surface.

The amplitude of the evanescent electric field decays exponentially in the direction perpendicular to the interface as shown in Figure 2.2. This phenomenon is fully expended in biosensing methods such as SPR. The examples of optical biosensing methods based on evanescent field are SPR, optical fibres, planar waveguides, Mach-Zehnder (MZ) interferometers, and ring-resonators (Leung et al., 2007; Hutchinson, 1995; Lading et al., 2002

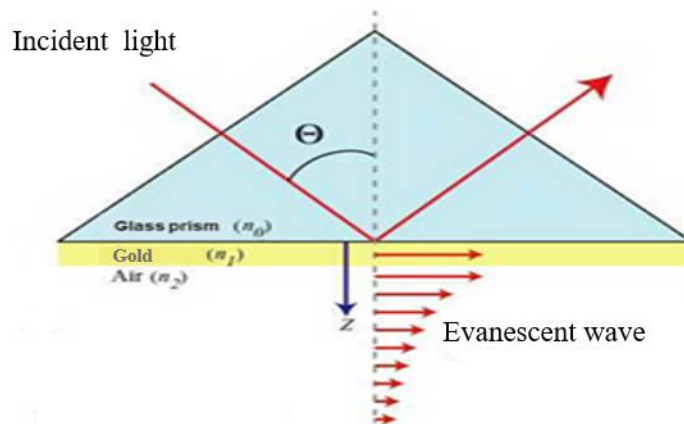


Figure 2.2. Formation of the evanescent wave between two media, when coupling of light through prism at total internal reflection conditions occurs

2.1.2 Surface plasmon resonance (SPR)

The idea of surface plasmon resonance lies in the interaction of the incident electromagnetic wave with the surface plasmons. A p-polarized light beam (usually from a low-power HeNe laser) enters the prism with its bottom surface coated with a thin film (in the range of 40 to 50 nm) of highly conductive metal, such as gold or silver. Alternatively, the metal film can be deposited on a glass slide, which is then brought into optical contact with the prism via the index matching fluid (oil immersion). If the internal incident angle is larger than the total internal reflection angle, the reflected light intensity reaches its maximum. While the evanescent wave perpendicular the surface However, if the k-vector (or frequency) of the evanescent field matches the frequency of plasmon oscillations in thin metal film, the energy will be transferred to plasmons, and the reflected light intensity will be reduced. Such condition is often referred to as the surface plasmon resonance. Surface plasmon resonance can be observed by measuring the intensity of reflected light during scanning the beam over a range of angles of incidence, and thus changing the x-component (in the plane of a sample) of k-vector. The SPR method has found numerous applications as a film characterization technique capable of measuring refractive index (n) and extinction coefficient (k) with an accuracy ranging from 10^{-4} to 10^{-5} , and the thickness (d) with an accuracy of 10^{-2} nm (Nabok, A., and Tsargorodskaya, 2008). Because of the high sensitivity towards n , k and d , as well as convenient geometry of measurements, which does not involve light propagation through the tested medium, SPR has become very popular in chemical and biosensing applications. The most common designs of SPR sensor based on a prism coupler in attenuated total reflection (ATR) mode were developed by Otto, (1968) and Krestchmann, (1971) (see Figure 2.3). Between the two, the Krestchmann

geometry setup was found to be more appropriate and convenient for bio-sensing applications.

The light in the Kretschmann setup is totally reflected at the interface between a prism and the examined medium. A thin metal film of 20-40 nanometres in thickness does not have a significant effect on the conditions of total internal reflection. However, it plays a vital role in the event when the energy of incident light matches the energy of plasmon oscillations in metal (Otto, 1968). Such situation known as surface plasmon resonance appeared experimentally as a dip in the reflected light intensity on typical SPR graph (either spectrum or angle-dependence) in Figure 2.4.

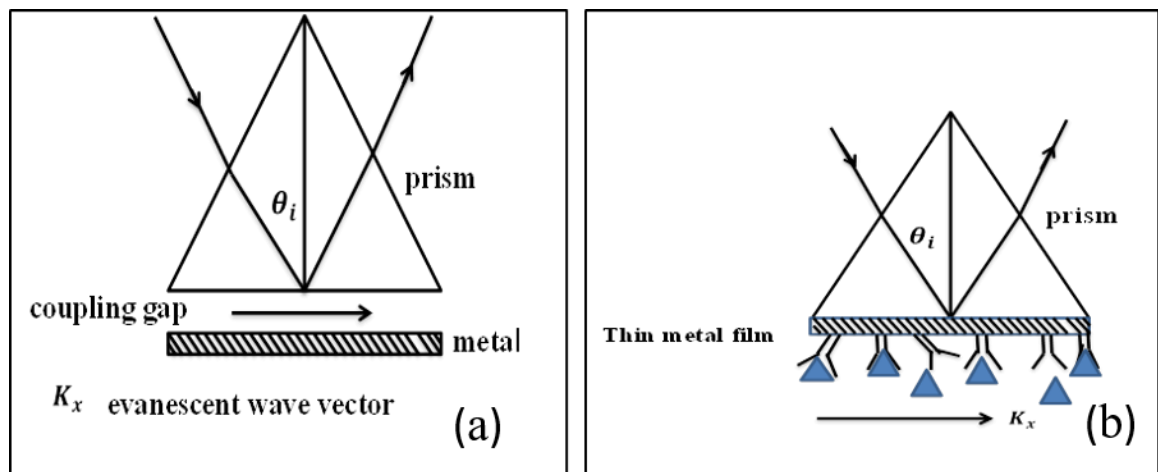


Figure 2.3. SPR set-up configuration by Otto (Otto, 1968) (a) and Kretschmann (Kretschmann,1971) (b)

The position of the SPR minimum depends on the refractive index of a medium, therefore the presence of an adsorbed molecular layer on the surface of the metal film causes the shift of SPR spectrum, which constitute the main principle of SPR sensing. Figure 2.4 shows typical SPR spectra: one corresponding to the surface of bare gold and the other one shifted to higher angles or wavelengths corresponding to the layer adsorbed on the surface of gold. Any alteration in this adsorbed layer that is caused, for instance, by immune binding can be

registered as an additional shift of the SPR minimum. For example, the value of a spectral shift depends on the thickness and optical parameters of the adsorbed layer such as the refractive index (n), extinction coefficient (k) and thickness (d). These parameters can be obtained by fitting the SPR curve to Fresnel's theory using one of the least-square minimization techniques.

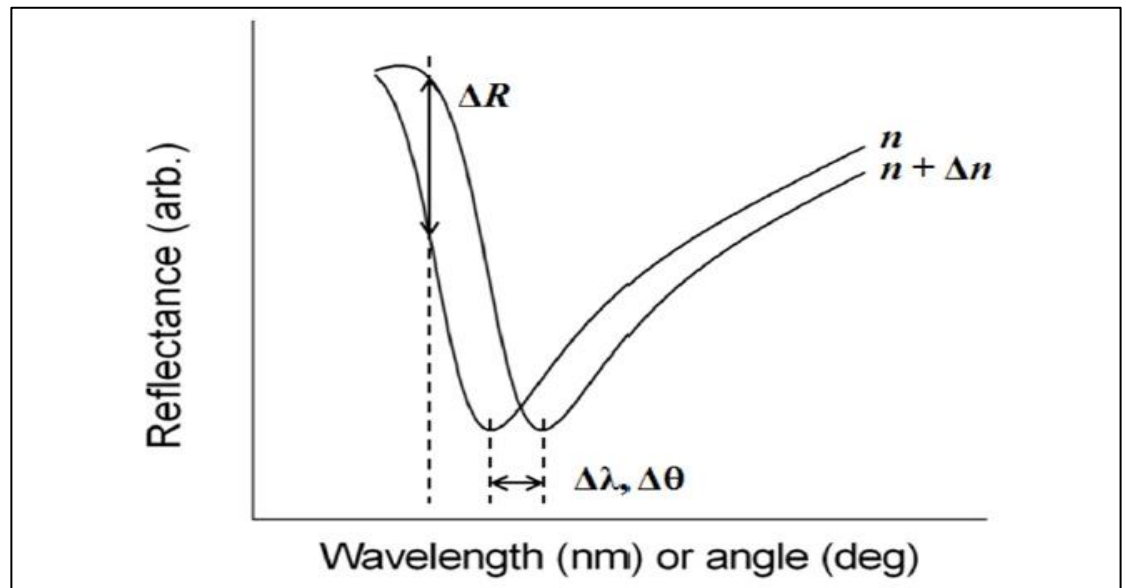


Figure 2.4. Typical Surface Plasmon Resonance spectra (Byun, 2010)

2.1.3 Ellipsometry

Ellipsometry is a non-destructive optical method used to determine the optical properties of materials. The idea of ellipsometry lies in the measurements of changes of polarized light upon its reflection from a sample. As light reflects from a sample surface the state of polarized light changes from linear to elliptical, as shown as example in Figure 2.5.

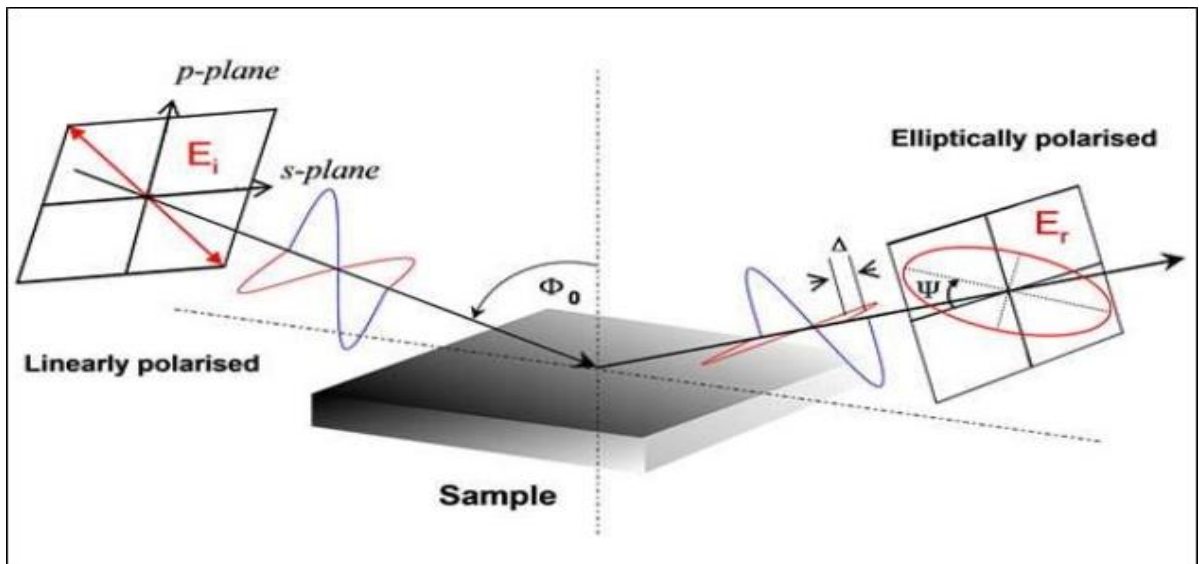


Figure 2.5. The changes in polarization of light reflected from the surface

Ellipsometry techniques do not measure directly the optical properties of the material but the angles of (Ψ) and (Δ), which are related to the ratio (ρ) of complex reflection coefficients r_p and r_s for electric vectors, p (parallel) and s (normal) to the plane of incidence via the main ellipsometry equation (Arwin et al., 2004):

$$\rho = \frac{r_p}{r_s} = \tan(\Psi) \exp(i\Delta) \quad (2.1)$$

In eq. 2.1, Ψ represents the amplitude ratio of p and s components of polarized light while Δ is the phase difference between p and s components.

$$\tan\Psi = \frac{|r_p|}{|r_s|}, \quad \Delta = \delta_p - \delta_s \quad (2.2)$$

In the case of reflection / transmission at the interface between two media with respective indices N_0 and N_1 , the reflection and transmission coefficients are described by Fresnel's formula (Fujiwara, 2007):

$$r_s = \left(\frac{E_{0r}}{E_{0i}} \right)_s = \frac{n_i \cos \theta_i - n_t \cos \theta_t}{n_i \cos \theta_i + n_t \cos \theta_t} \quad r_p = \left(\frac{E_{0r}}{E_{0i}} \right)_p = \frac{n_t \cos \theta_i - n_i \cos \theta_t}{n_i \cos \theta_t + n_t \cos \theta_i} \quad (2.3)$$

$$t_s = \left(\frac{E_{0t}}{E_{0i}} \right)_s = \frac{2 n_i \cos \theta_i}{n_i \cos \theta_i + n_t \cos \theta_t} \quad t_p = \left(\frac{E_{0t}}{E_{0i}} \right)_p = \frac{2 n_i \cos \theta_i}{n_i \cos \theta_t + n_t \cos \theta_i} \quad (2.4)$$

Substitution of r_p and r_s in equation (2.3), their values from (2.4) and Snell's Law, $N_0 \sin \theta_0 = N_1 \sin \theta_1$, yields:

$$N_1 = N_0 \tan \theta_0 \left[1 - \frac{4\rho}{(1+\rho^2)} \sin^2 \theta_0 \right]^{1/2} \quad (2.5)$$

For the three layer system, consisting of a substrate, films and ambient (Figure 2.6), the total reflectance can be calculated as:

$$R = r_{01} + t_{01} t_{10} r_{12} e^{-i2\beta} + t_{01} t_{10} r_{10} r_{12} e^{-i4\beta} + \dots \quad (2.6)$$

Where r_{01} , r_{12} , t_{01} and t_{10} are Fresnel reflection and transmission coefficients at the 0/1, 1/0 and 1/2 interfaces respectively and β is the phase thickness of the film: (Fujiwara, 2007)

$$\beta = 2\pi \left(\frac{d_1}{\lambda} \right) N_1 \cos \theta_1 = 2\pi \left(\frac{d_1}{\lambda} \right) (N_1^2 - N_0^2 \sin^2 \theta_0)^{1/2} \quad (2.7)$$

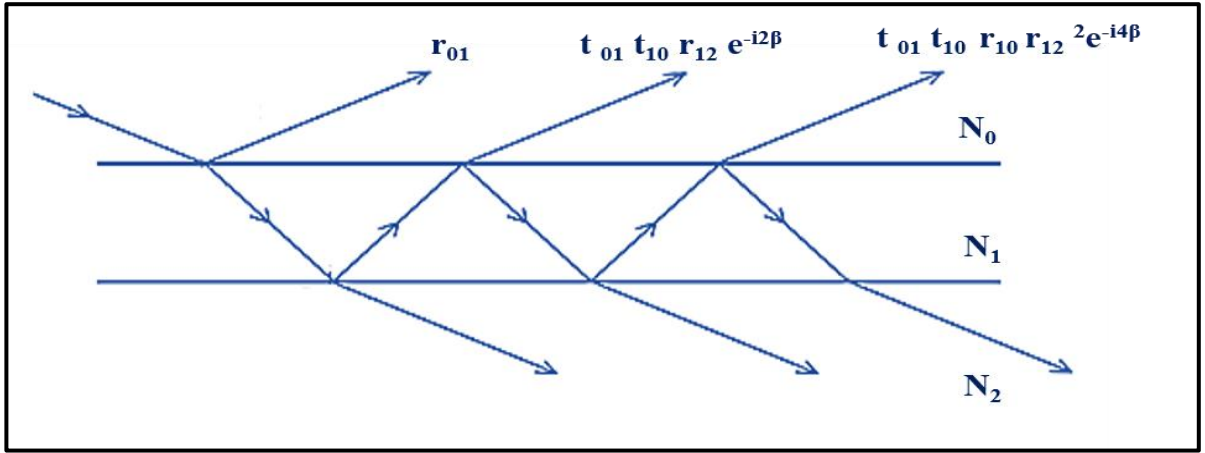


Figure 2.6. Optical model for an ambient/thin film/substrate structure (J A Woollam Co. Inc, 2001)

The summation of equation (2.6) for the p and s reflectance components is given by;

$$R_p = \frac{r_{01p} + r_{12p} e^{-i2\beta}}{1 + r_{01p} r_{12p} e^{-i2\beta}} \quad \text{and} \quad R_s = \frac{r_{01s} + r_{12s} e^{-i2\beta}}{1 + r_{01s} r_{12ps} e^{-i2\beta}} \quad (2.8)$$

The main ellipsometric equation shows the dependence ψ and Δ on a number of parameters of the system through Fresnel's formula:

$$\tan\Psi e^{i\Delta} = \rho(N_0, N_1, N_2, d_1, \theta_0, \lambda) \quad (2.9)$$

Solving the main ellipsometric equation is quite a difficult task. Two approaches are typically used, namely, forward and reverse ellipsometry problems. In the forward ellipsometry problem, the values of Ψ and Δ can be found from known parameters $N_0, N_1, N_2, d_1, \theta_0, \lambda$ by solving Fresnel equations analytically, which is a rather straightforward procedure. Solving the reverse ellipsometric problem, i.e. finding the parameters of the reflective system such as refractive index (N_1) and thickness (d_1) of the

film from the experimental values of Ψ_{exp} and Δ_{exp} is much more complex. It can be tackled using some of the least square techniques which involve solving a forward problem (Fresnel equation) several times and finding the theoretical values (Ψ_{the} and Δ_{the}) and subsequent minimizations of the error function.

The approach is based on finding the minimum mean square error (MSE) between the experimental values of Ψ_i^{exp} and Δ_i^{exp} and theoretical (modelled) ones Ψ_i^{mod} and Δ_i^{mod} as given, for example in (Woollam,2009);

$$MSE = \frac{1}{2N - M} \sum_{i=1}^N \left[\left(\frac{\Psi_i^{mod} - \Psi_i^{exp}}{\sigma_{\Psi,i}^{exp}} \right)^2 + \left(\frac{\Delta_i^{mod} - \Delta_i^{exp}}{\sigma_{\Delta,i}^{exp}} \right)^2 \right] = \frac{1}{2N - M} \chi^2 \quad (2.10)$$

A smaller MSE implies a better fit. MSE is weighted by the error bars of each measurement, so noisy data are weighted less.

There are several types of ellipsometry instrumentation developed within the last four or five decades ranging from simple fixed angle, single wavelength null-ellipsometers to modern spectroscopic ellipsometric instruments. Spectroscopic ellipsometers can be split into two major categories: instruments that use rotating optical elements (analyzer or compensator) and instruments that use a photo elastic modulator. The J. A. Woollam M2000 spectroscopic ellipsometric instrument (which was used in this work) exploits the principle of a rotating compensator and consists of a wide spectral range light source (370 – 1680 nm), monochromator polarizer, rotating compensator, analyzer and a CCD array photodetector, as shown in Figure 2.7.

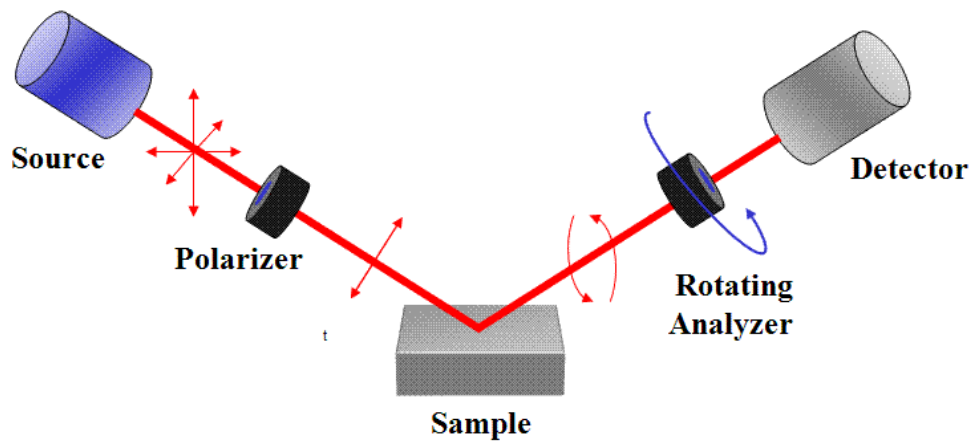


Figure 2.7. The schematic of rotating analyzer spectroscopic ellipsometry

The method of ellipsometry is not very popular in sensing because the light beam travels through the medium which does affect the measurements (Nabok et al, 2011).

The construction of a measurement cell is quite a complex engineering task which involves the optical windows that are not changing polarisation of light; usually ellipsometry cells are quite large in volume and thus not suitable for biosensing.

2.1.4 Total Internal Reflection Ellipsometry (TIRE)

The method of total internal reflection ellipsometry (TIRE) was developed in the last decade as a combination of spectroscopic ellipsometry and Kretschmann type of surface plasmon resonance (SPR). TIRE was established as a highly sensitive analytical tool in biosensing, particularly attractive for detection of low molecular weight analytes such as mycotoxins (Nabok and Tsargorodskaya, 2008). While the traditional surface plasmon resonance technique is struggling to detect low molecular weight analytes (in the range of few hundred of atomic units) (Nabok et al., 2007), the TIRE method is capable of solving such problem (Kim et al., 1989 ; Poksinski and Arwin, 2004; Arwin et al., 2004; Westphal and Bornmann 2002; Nabok et al., 2005,2004). The TIRE method theoretically have been

known for long time (Bashara, 1992) but was implemented experimentally only recently (Westphal, and Bornmann, 2002; Arwin, Poksinski and Johansen, 2004). Westphal (Westphal and Bornmann, 2002) was the first who introduced the notion of using ellipsometry in the internal reflection mode. It was first proved empirically when the prism was utilized to couple the light beam to a thin metal film; it thus connected the SPR phenomenon with the ellipsometric principle of detection. The upsurge in the sensitivity was attained and the method was initially referred to as the Surface Plasmon Enhanced Ellipsometry. Arwin (Poksinski and Arwin, 2004) explained the theory of TIRE method and introduced the present name of total internal reflection ellipsometry (TIRE). Nabok and his group developed the TIRE in more detail, they found that the sensitivity of TIRE is 10 times higher than traditional SPR method (Nabok and Tsargorodska, 2008). A combination of LSPR and TIRE (which is discussed in detail later) appeared to be much more sensitive and thus suitable for detection of small molecules such as mycotoxins. This method was chosen later for LSPR bio- spectroscopy to detect mycotoxins. TIRE is a highly sensitive method for analyzing and monitoring adsorption and desorption of biological molecules on thin metal films as well as for detection of small toxin molecules such as mycotoxins (Aflatoxin B1, Aflatoxin M1, Ochratoxin A, Zearalenone, with their molecular weights being (312.28, 328.276, 403.81 and 318.364 g/mol respectively) (Nabok et al., 2007).

The main advantage of TIRE is the use of two ellipsometric parameters Ψ and Δ , which are related, respectively, to the ratio of amplitudes and phase shift of p- and s- components of polarized light ($\tan \Psi = A_p / A_s$, $\Delta = \varphi_p - \varphi_s$) as compared to SPR dealing only with the amplitude of p- polarized light. As one can see from Figure 2.8., the spectrum of Ψ resembles typical SPR curve with the minimum at about 800 nm corresponding to plasmon

resonance, while the spectrum of Δ exhibits a sharp drop of phase near the resonance. The ellipsometry data modelling showed that the parameter Δ is about 10 times more sensitive to changes in the film thickness and refractive index as compared to Ψ (Nabok and Tsargorodska, 2008). In other words, the method of TIRE appeared to be 10 times more sensitive than conventional SPR. Moreover, there are several other advantages of TIRE, for example: a label-free detection, a possibility of real-time dynamic study, low cost, easy to-use, non-destructive, rapid, highly sensitive and saving biochemical analysis (Arwin and Johansen, 2004; Liu et al., 2015).

TIRE method is therefore found to be more suitable for the registration of low molecular weight toxins, such as mycotoxin (Nabok et al., 2008). The high sensitivity of TIRE for thin layers opens up a pathway to analyse in detail the structure of thin protein layers (Arwin, Poksinski, & Johansen, 2004).

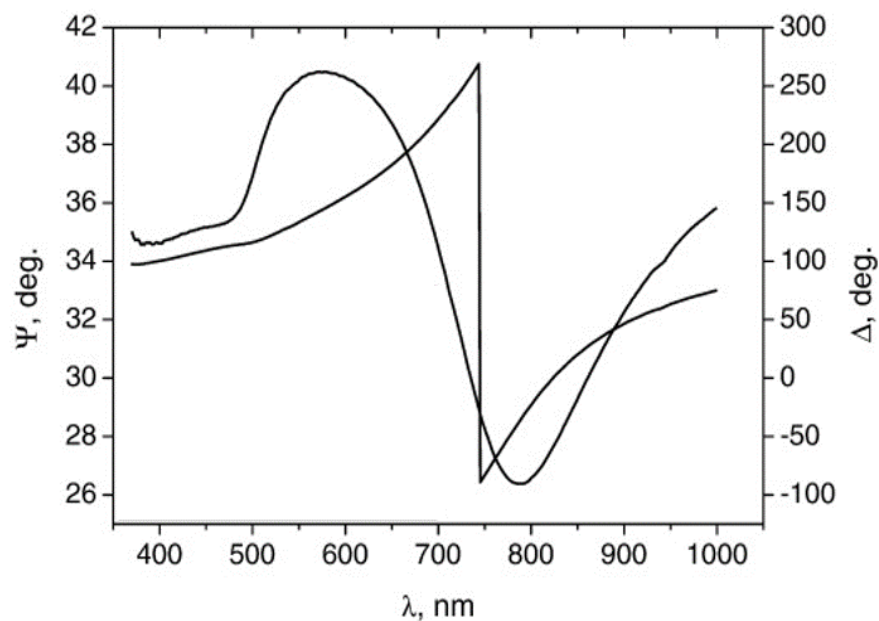


Figure 2.8. Typical TIRE spectra of Ψ and Δ for 25nm thick Au film deposited on glass (Nabok et al., 2011)

2.1.4.1 TIRE data fitting

For fitting of TIRE experimental data, we use WVASE32® software (J.A. Woollam), and the model consisting of four-layer was applied. The following example in Table 2.1 shows the upside-down model in which the light from a glass medium enters the gold film with adsorbed molecular layer in contact with water - based buffer.

Table 2.1. Four layers model for TIRE data fitting (Nabok and Tsargorodska, 2008)

Number	Name of layer	Parameters
3	Glass slide BK7	n, k dispersions from WVASE32 software library ($n^* = 1.515, k^* = 0$ at 633nm)
2	Cr/Au layer	Thickness (d) in the range of 25-30nm ($n=0.359\pm 0.078; k=2.857\pm 0.114, d=29.8\pm 2.6$ nm at 633nm)
1	Cauchy layer	Cauchy model $A_n^* = 1.396, B_n^* = 0.01; C_n^* = 0, k = 0$ at 633nm
0	Buffer solution	n, k dispersion from WVASE32 library - $n^* = 1.3326; k^* = 0$ at 633nm)

In the above model, parameters indicated with (*) were fixed during data fitting. A Cauchy dispersion function was used for fitting of biomaterial layers and adsorbed molecules.

The optical dispersion characteristics for BK7 glass layer number (3) and buffer solution (0) were taken from the J. A. Woollam material library and were always fixed.

The characteristic values of n and k for glass and water are given in Table 2.1 at the wavelengths of 633 nm (corresponding to HeNe laser). The effective values of thickness (d) and $n(\lambda)$ and $k(\lambda)$ dispersions for Cr/Au layer were found earlier by fitting TIRE data for a bare gold surface. TIRE measurements were always performed on the bare gold surface before deposition of molecular layers. Then the obtained values of thickness (d),

and dispersion functions for n and k were kept fixed in further TIRE fittings on this sample after deposition of molecular layers. For organic layers deposited on the sensing surface, the Cauchy dispersion function was used: (Nabok et al., 2008).

$$n(\lambda) = A + \frac{B}{\lambda^2} + \frac{C}{\lambda^4} + \dots, \quad (2.11)$$

During fitting, the parameters of A_n , B_n and C_n were fixed at 1.396, 0.01, and 0, respectively, giving the value for n of about 1.42 at $\lambda=633\text{nm}$, which is typical for organic materials. A zero value for coefficient ($k = 0$) was used since all molecular layers were considered to be optically transparent in the spectral range used (370 –1000 nm). The only variable parameter was the thickness (d). The shift of TIRE spectra is therefore related to changes in the film thickness.

2.1.4.2 TIRE kinetic analysis

Adsorption kinetics analysis was well described in the literature, for example (Nabok et al., 2008, 2007; Liu et al., 2003). The measurements of dynamic spectra of Ψ and Δ , caused by binding mycotoxins to bioreceptors were used in this work. The obtained time dependencies of ψ or Δ at fixed wavelength were used for the evaluation of the rates of adsorption (k_a) and desorption (k_d) and their ratios, known as the association constant (K_A) and the affinity constant (K_D).

Following the Langmuir theory, the adsorption of molecules to the binding site of concentration N on the gold surface is described by the following differential equation:

$$\frac{dn}{dt} = Ck_a (N - n) - k_d n, \quad (2.12)$$

where n is concentration of adsorbed analyte molecules, and N is the concentration of binding sites on the surface, C is the concentration of analyte in the sample, $N-n$ is the concentration of available binding sites on the surface. The solution of this differential equation for the concentration of analyte molecules (n) adsorbed on the surface is given as

$$n = N \frac{k_a C}{k_a C + k_d} [1 - \exp(-t/\tau)] \quad (2.13)$$

where k_a and k_d are the rates of adsorption and desorption, and τ is the time constant given as

$$\tau = \frac{1}{k_a C + k_d} \quad (2.14)$$

The values of τ for each concentration of analytes were found by fitting experimental kinetic of ψ or Δ . Then the dependence of $\frac{1}{\tau}$ against the concentration is plotted as $\frac{1}{\tau} = k_a C + k_d$. The adsorption (k_a) and desorption (k_d) rates were evaluated from the gradient and intercept, respectively of the line in Figure 2.9.

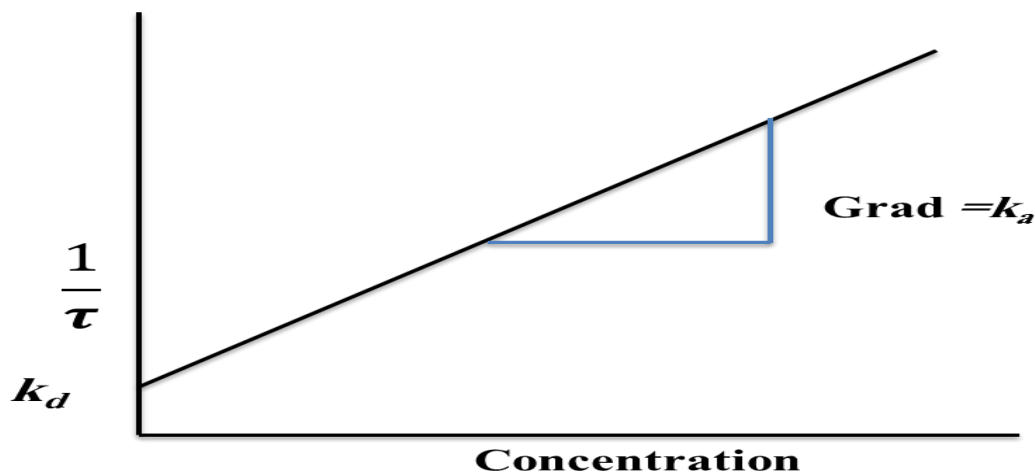


Figure 2.9. Evaluation of the adsorption (k_a) and desorption (k_d) rates

Then the association constant K_A is found as the ratio of k_a and k_d .

$$K_A = \frac{k_a}{k_d} \quad (2.15)$$

And the affinity constant is

$$K_D = \frac{1}{K_A} = \frac{k_d}{k_a} \quad (2.16)$$

The typical values of $K_A \approx 10^6$ - 10^7 mol⁻¹ were found for mycotoxins binding to their specific antibodies (Nabok et al., 2011).

2.1.5 Localized Surface Plasmon Resonance (LSPR)

The phenomenon of localized surface plasmon resonance (LSPR) is related to interaction of external electromagnetic waves (e.g. light) with localized surface plasmons, e.g. oscillations of free electrons confined into small volumes comparable with the wavelength of light as schematically illustrated in Figure 2.10.

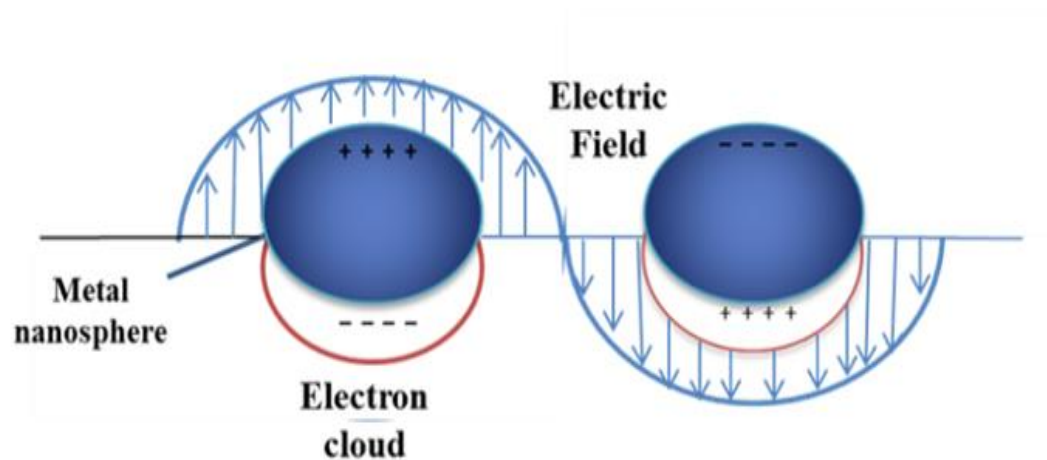


Figure 2.10. Schematic diagram illustrating localized surface plasmon resonance

LSPR is typically observed in metal nano-structures, for example in nanoparticles, as an absorption band in the visible spectral range. The phenomenon of LSPR has been described theoretically by Mie more than a century ago (well before the quantum mechanics was established) as a light scattering on conductive (metal) spherical particles of dimensions comparable with the wavelength of light. This effect known as Mie scattering (Mie, 1908) is described by the following dispersion characteristic of light absorption:

$$\sigma_{ext} = \frac{9V\varepsilon_m^{3/2}}{c} \frac{\omega\varepsilon''(\omega)}{[\varepsilon'(\omega) + 2\varepsilon_m]^2 + \varepsilon''(\omega)^2}, \quad (2.17)$$

where σ_{ext} is the extinction cross-section, $\varepsilon'(\omega)$ and $\varepsilon''(\omega)$ are dispersions of the real and imaginary parts of dielectric permittivity of metal, respectively, ε_m is the dielectric permittivity of the medium, and V is the particle volume. The extinction maximum (resonance) is achieved when $\varepsilon'(\omega) = -2\varepsilon_m$ (ε' is negative for metals). Therefore, the position of LSPR band depends on the medium refractive index. The latter fact actually constitutes the main principle of LSPR biosensing; small changes in the refractive index due to molecular adsorption cause the “red” spectral shift of the LSPR band as shown in Figure 2.11.

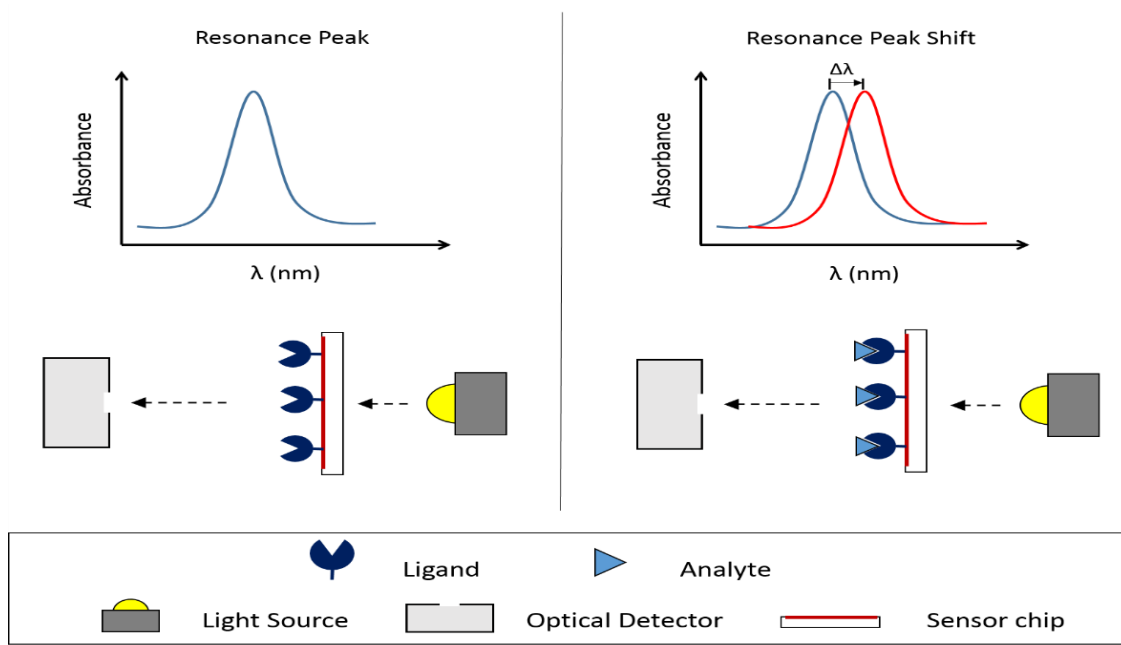


Figure 2.11. LSPR sensitivity to refractive index of the ambient

Interest in LSPR has grown dramatically recently due to its possible applications in biosensing and was also stimulated by fast evolvement of nanotechnology which is now capable of producing different types of metal nanostructures. For a while, LSPR was only observed in metal nano-particles (Raschke et al., 2003; McFarland and Van Duyne 2003), then many other types of LSPR nanostructures such as nano-rods (Gabudean et al., 2011; Zang et al., 2014), nano-islands (Lahav et al., 2004; Karakouz et al., 2008), and nano-holes (Brolo et al., 2004; Sepúlveda et al., 2009), appeared in recent years. Such nanostructures could be mono- or poly-dispersed in terms of their dimensions, they could be random or ordered. The ordered nanostructures can be produced using different types of nano-lithography, i.e. electron beam lithography (Abu Hatab et al., 2008), interference lithography (Tsargorodska et al., 2014), and nano-sphere lithography (Haynes and Van Duyne, 2001). Noble metals such as gold and silver are commonly used for the formation of nano-structures; aluminum and copper were also used. Although Ag nano-structures

have the best LSPR characteristics, e.g. the sharp plasmon resonance (McFarland and Van Duyne, 2003), gold nano-structures are the most popular due to the chemical inertness of gold and well-developed thiol-chemistry of immobilization of proteins on gold surface (Sepúlveda et al., 2009; Tsargorodska et al., 2014). The theory of LSPR has been developed further using the concept of quantum confinement of surface plasmons in different metal nano-structures of different dimensions and shapes, and now appeared as a new subject of quantum plasmonic (Townsend and Bryant, 2012; Petryayeva and Krull, 2011). The appearance of multiple LSPR peaks can be explained by quantization of plasmons in different directions (Petryayeva and Krull, 2011).

The applications of LSPR in bio-sensing have become very attractive recently mainly because of potential extremely high sensitivity of LSPR biosensors (Sepúlveda et al., 2009; Petryayeva and Krull, 2011; Hutter and Fendler, 2004). The term “single molecule detection” has become associated with LSPR biosensors. Another attraction is deceptively simple instrumentation for LSPR biosensing; a simple UV-vis spectrometer with the cuvette filled with gold nanoparticles functionalized with specific antibodies can be capable of detection of the analytes of interest. In reality, the sensitivity of such LSPR biosensors is rather poor. Although, the adsorption of a single protein molecule on a metal nanoparticle may indeed cause a substantial shift of the LSPR band, in reality the light beam of few square millimeters probes millions of such particles, and the resulted spectral shift may be unnoticeable.

As a result such simple LSPR bio-sensors are capable of detection of large protein molecules in ppm concentration range (Kedem et al., 2014) and the detection of small molecules is only possible in competitive or sandwich immunoassay formats (Kedem et al., 2014). True single molecule detection was achieved only recently using extremely fast

camera capable of capturing the light scattered by a single metal nano-rods passing through microfluidic channels (Armstrong and Zijstra, 2018); these experiments are quite unique and require expensive optical equipment.

2.1.6 Raman spectroscopy

The effect of inelastic light scattering was experimentally demonstrated for the first time in 1928 by the Indian scientist C.V. Raman (Singh, 2002) after it had already been predicted by Smekal (Vandenabeele, 2010). At the time, Sir Raman used filtered sunlight, and he needed several hours of irradiation to be able to record the spectrum of a large volume of a pure liquid. Spectra were recorded on photographic plates. Nowadays, due to instrumental improvements, in particular the development of powerful lasers, it is possible to record the spectrum of a micrometer-sized sample in a couple of seconds. Raman spectroscopy is able to reveal the molecular composition of a sample at the micrometer scale in a non-destructive way allowing scientists to extract new information from their valued samples. Increased speed of analysis and data processing has also allowed sample mapping, which can provide knowledge on the spatial distribution of the molecules in the sample, a result that is difficult to obtain with other analytical techniques (Vandenabeele, 2010). Raman spectroscopy is commonly used in chemistry to provide a fingerprint, by which molecules can be identified.

Rayleigh (ordinary) scattering occurs when the photon is absorbed to a higher virtual state and is instantly scattered (emitted) elastically back to the initial level. The photons emitted by Stokes-Raman scattering usually have a lower energy and frequency than that of the photons absorbed, and these photons are inelastically scattered transferring some of their energy to the molecule. The reverse situation is also possible; the photons emitted have a

higher energy (and frequency) than the photons absorbed. This is called anti-Stokes-Raman scattering, but it is not likely to occur at room temperature as electrons prefer to be in the ground state (Rostron et al., 2016; Bumbrah and Sharma, 2016) Figure 2.12.

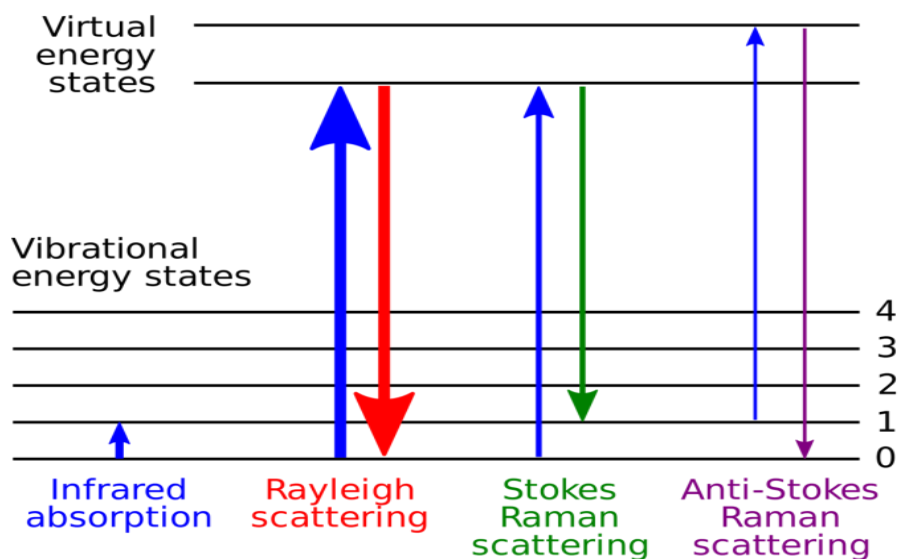


Figure 2.12. Energy-level of the states involved in Raman spectra

In Raman scattering only one in every 30 million photons are inelastically scattered, and the photon transfers some of its energy to the molecule. Therefore, conventional Raman spectroscopy has a poor signal to noise ratio and thus not very common in sensing applications.

2.1.7 Surface Enhanced Raman Spectroscopy

SERS technique allows for more sensitive molecular identification. Recently, SERS has been widely used as a signal transduction mechanism in biological and chemical sensing. For example, it was used in analysis of pesticides (Weißenbacher et al., 1997), nuclear waste (Bao et al., 2003) and glucose detection (Shafer-Peltier et al., 2003). SERS has been

applied to identify bacteria (Jarvis and Goodacre, 2004) and immunoassay test (Mulvaney et al., 2003; Cao and Mirkin, 2002). Modern SERS instrumentation makes the technique practical for trace analysis in clinics (Young et al., 2004). Since the SERS discovery 28 years ago, this technique has progressed from studies of model systems, such as pyridine on a roughened silver electrode, to state-of-the art surface science and real-world sensor applications. In the last decade, the development in nanofabrication methods, spectroscopic instrumentation and novel detection platform has generated widespread interest in the use of SERS, which is now considered a robust analytical tool.

The mechanism of SERS enhancement was a subject of intensive research recently since the discovery of the phenomenon. The enhancement of the Raman peaks is associated with two main mechanisms, e.g. chemical, and electromagnetic enhancements. The chemical mechanism is manifested through the chemical absorption of molecules to the noble metal which allows electrons from the molecule interacting with electrons in metal. These mechanisms lead to about 100 times enhancement of the signals (Chang, 2013). The electromagnetic mechanism is a wavelength-dependent effect which is closely related to the (LSPR) phenomenon, where collective oscillations of conduction electrons might occur in metal nano-structures having sharp edges and tips which can enhance the incident electric field intensity by 10^2 - 10^5 times (Schatz and Van Duyne, 2002). With both of these mechanisms present SERS enhancement factor can reach 10^7 . LSPR phenomenon has two crucial consequences: (i) selective absorption (scattering) at the resonant wavelength of electromagnetic radiation and (ii) generation of large electromagnetic fields at the surface roughness features (Figures 2.13 a and b).

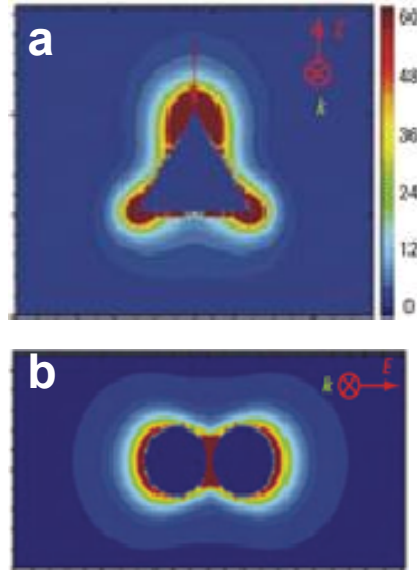


Figure 2.13. Electromagnetic field simulation for (a) a triangular nanoparticle (700 nm), (b) a dimer of spherical nanoparticles (520 nm), (Hao and Schatz, 2004)

Extensive theoretical modeling has been performed to provide insight into electromagnetic enhancement by noble-metal nanoparticles (Schatz, 2001; Jensen et al., 1999). A simple example of an isolated metallic sphere interacting with the incident electromagnetic field has been used to derive the formula for electric field enhancement:

$$E^2 \approx E_0 \left| \frac{\epsilon_m - \epsilon^1}{\epsilon^1 + 2\epsilon_m} \right|^2 \quad (2.18)$$

in which E is the electric field magnitude at the surface of the sphere, E_0 is the incident field magnitude, ϵ^1 is the wavelength-dependent dielectric constant of the metal composing the sphere, and ϵ_m is the dielectric constant of the local environment around the sphere (Schatz and Van Duyne, 2002). This relation reveals that when $\epsilon_m = -2\epsilon^1$, which can be achieved for silver and gold at certain wavelengths in the visible and near-IR, the magnitude of the electric field at the surface of the sphere becomes very large.

When researchers achieved the milestone of detecting a single molecule with SERS, they raised further questions about the enhancement mechanism. The Nie and his groups (Nie and Emory, 1997) achieved single-molecule detection independently and with different experimental conditions. The Nie study included a correlated topographical and optical characterization of separated silver nanoparticles doped with Rhodamine 6G (R6G) molecules. They hypothesized that only 1 of every 100–1000 nanoparticles are “optically hot” and that only 1 of every 10,000 surface sites on a “hot” particle has efficient enhancement (Nie and Emory, 1997). Accordingly, the single-molecule enhancement is 10^6 – 10^7 larger than the population-averaged enhancement. The Kneipp research group, on the other hand, probed small (100–150 nm) silver colloid aggregates doped with crystal violet molecules. The large (10^{14}) single-molecule enhancement is hypothetically attributed to large electromagnetic fields generated by fractal-pattern clusters of silver colloid nanoparticles (Kneipp et al., 1997). Since these two pioneering experiments, SERS has been used to detect single molecules of biologically significant compounds, such as haemoglobin (Xu et al., 1999). Although the entire SERS community is excited by the recent development of single-molecule SERS, a new controversy surrounds the huge enhancement factors. Current hypothesis of the single-molecule enhancement mechanism states that SERS substrates have a small number of “hot spots”, which are thought to occur at the junctions between two nanoparticles (Kleinman et al., 2013).

The method of SERS due to the amplification of Raman signal has become one of the most used techniques in the study of adsorbed molecules. In the case of SERS the adsorbed molecules are both under the influence of the electric field radiation as under the plasmonic field. The Raman Stokes lines of the molecule are also close to the frequency of the excitation radiation, they will also be in resonance with the surface plasmon.

2.2 Metal nanostructures

Metal nanostructures have high surface areas and unique physical-chemical properties that can be easily tuned, making them ideal candidates for developing biosensing devices (Vaskevich et al., 2007; Daniel and Astruc, 2004; karakouz et al., 2009)

There are various ways to obtain nanostructures by either top-down or bottom-up approaches (Figure 2.14). Top down approaches involve various lithography and etching processes, which offer precision in the location and morphologies of the nanostructures but suffer from high processing cost. On the other hand, bottom up approaches are simpler and lower in processing cost but suffer from lack of precision in location. (Vidotti et al., 2011).

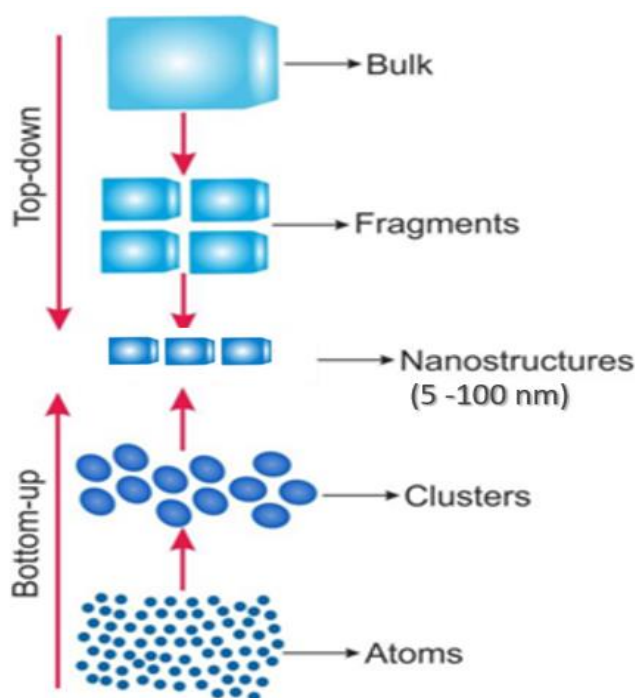


Figure 2.14. Fabrication processes: bottom-up and top-down

Bottom-up synthesis for nanoparticle arrays is usually categorized into gas (vapor) phase fabrication and liquid phase fabrication. Gas phase fabrication, such as pyrolysis or inert gas condensation, involves evaporation, gas-solid surface reaction (nucleation), and grain

growth (Bae et al., 2008; Karakouz et al., 2009). Liquid phase fabrication, such as solvothermal reaction, sol-gel, or micellar structured media, involves liquid-surface reaction, nucleation and grain growth (Kelsall and Geoghegan, 2005).

Depending on the dimension in which the size effect on the resultant property becomes apparent, the nanomaterials can be classified as:

1- Zero-dimensional (quantum dots) in which the movement of electrons is confined in all three dimensions.

2- One-dimensional (quantum wires) in which the electrons can only move freely in the X-direction.

3- Two-dimensional (thin films) in which case the free electrons can move in the X-Y plane, typically materials belonging to this group are nanostructures.

4- Three-dimensional nanostructured material built of nanoparticles as building blocks in which the free electrons can move in the X, Y and Z directions. Considering the three dimensions, we can classify each system by the number of dimensions that are not in the nanometric range Figure 2.15 (Pokropivny and Skorokhod, 2007).

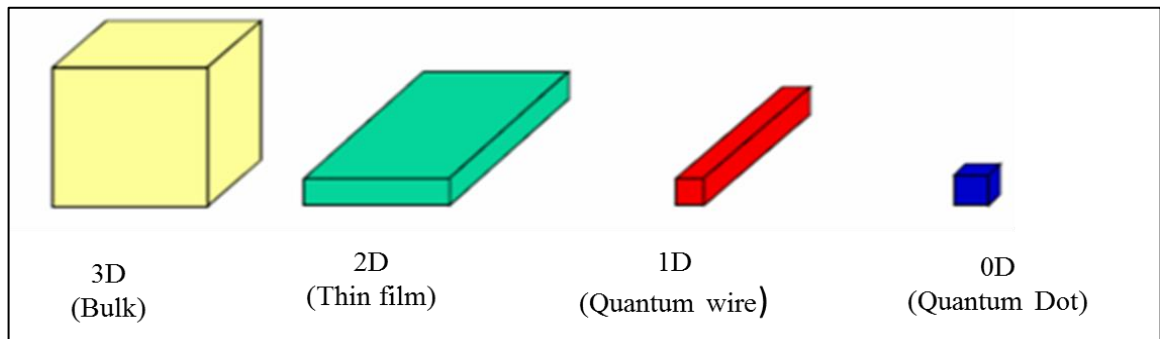


Figure 2.15. Classification of nanomaterials depending on the dimension

Examples of gold nanostructures depending on fabrication methods are shown in Figure 2.16.

Interference lithography and colloidal lithography techniques are employed to provide regular pattern arrays of fine features such as regular nanostructure.

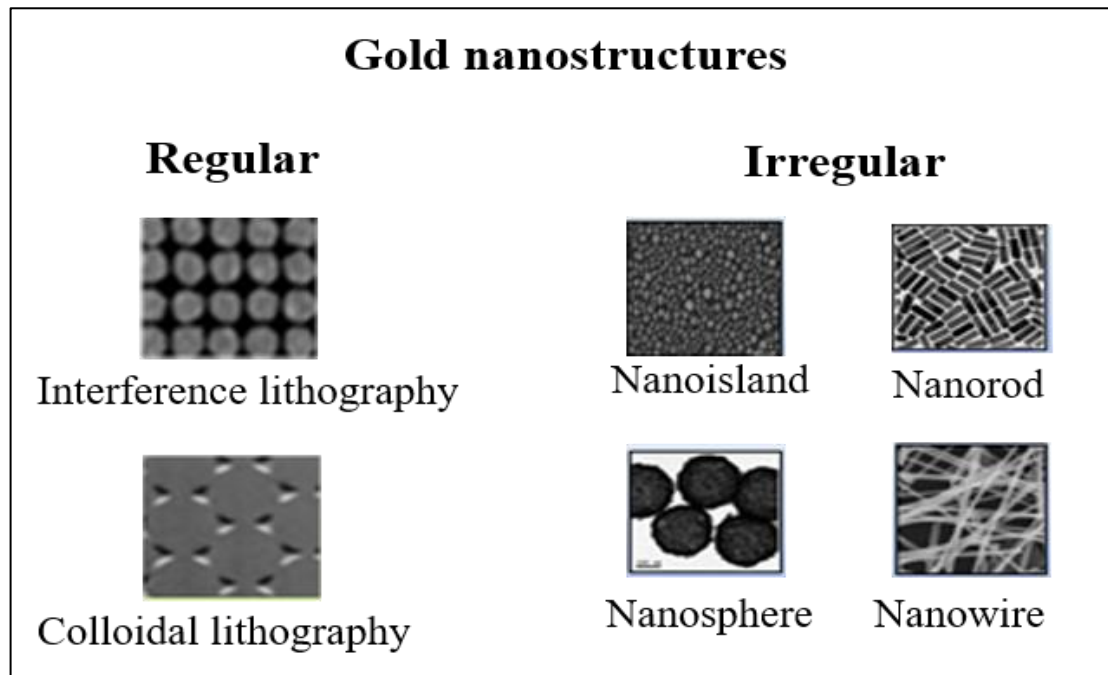


Figure 2.16. Classification of plasmonic nanostructures and the corresponding electron microscopy images (Examples of such shapes are nano-islands, nano-rods, and nano-spheres, and nanowires) (Yu et al., 1979; Wu et al., 2010; Chen et al., 2010; Liu and searson, 2006; Yu et al., 1997; Huang et al., 2006)

2.2.1 Formation of nano-islands by de-wetting

In the bottom-up approach, one of the simplest methods for the formation of metal nano-islands is the dewetting process. This process is applicable to almost all materials including polymers and metals. Dewetting occurs via diffusion to minimize surface energy and

interface energy between the film and substrate and can occur even in the solid state at temperatures below the melting point of the metal (Wang and Schaaf, 2013).

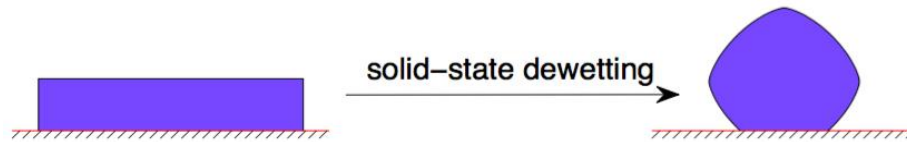


Figure 2.17 Solid-state dewetting of thin metal film

Solid-state dewetting is generally carried out by annealing thin film of metal in the furnace at temperatures below melting point (Figure 2.17) (Tian et al., 2013). The process of dewetting of gold can generally be divided into six stages, as follows: hole initiation, hole growth, interconnected islands, isolated islands, island coarsening, and particles (Figure 2.18) (Esterine et al., 2015).

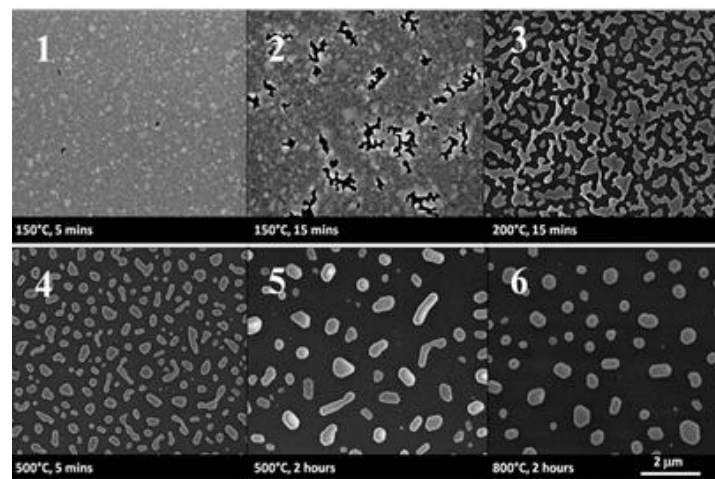


Figure 2.18. Stages of dewetting for Au film: hole initiation (1), hole growth (2), interconnected islands (3), isolated islands (4), island coarsening (5), and particles (6)

Depending on the intended applications, solid-state dewetting can be a more suitable approach than liquid-state dewetting to produce nanoparticles. For example, for magnetic application, solid-state dewetting is preferred because it enables the formation of

magnetically hard single crystal nanoparticles such as cobalt (Co) and cobalt platinum (CoPt) structure (Oh et al., 2009; Karakouz et al., 2008).

Gold nano-islands can be fabricated by using successive thin films evaporation and thermal dewetting Figure 2.19, thin Au films thermally evaporated on a glass substrate in series and then thermally annealed in a box furnace (Kang et al., 2017).

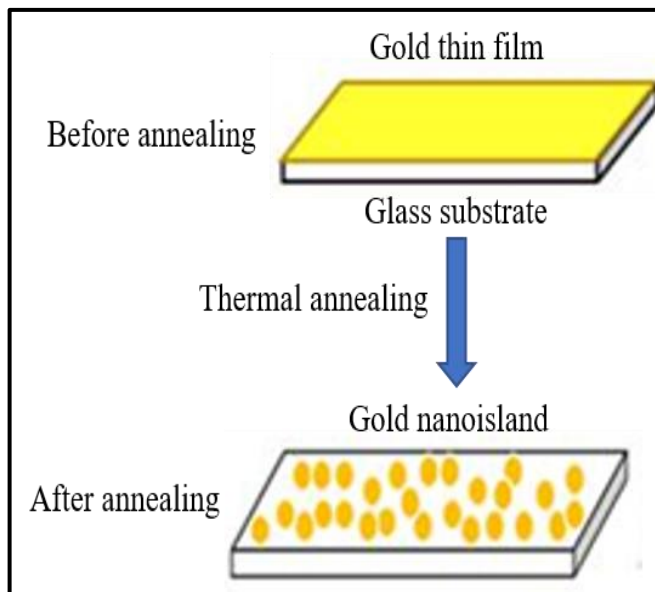


Figure 2.19. Gold nano-island formation by dewetting after high temperature thermal annealing

Au films onto glass substrates followed by annealing at ≥ 550 °C. Annealing induces percolation and formation of large, well-separated islands, partially embedded in the glass thermal embedding of gold nano-island in the glass at high temperature provides stable plasmonic transducers suitable for LSPR sensing applications (Karakouz et al., 2011), annealing of the films at temperatures close to or higher than the softening temperature of the glass substrate induces morphological transformation to discrete Au islands and gradual embedding of the formed islands in the glass surface (Karakouz et al., 2013).

This is one of the easiest methods of making gold nano-structures, annealing of thin gold films which results in the formation of gold nano-islands due to de-wetting processes (Tesler et al., 2013). Thin films are generally metastable in the as-deposited state and will dewet or agglomerate to form arrays of islands when heated.

This process occurs well below the melting temperature of the solid material, for example melting temperature of gold is 1,406 °C and that of glass falls between 1,427 and 1,538 °C; typical annealing temperatures are around 500 °C for duration of 1–2 h. In order to improve the adhesion of gold on glass a thin (2–3 nm) layer of Cr has to be evaporated first. Alternatively, the annealing at slightly high temperatures (550 °C) and longer time (up to 10 h) can be used, resulting in stable gold nano-islands embedded into a glass matrix (Karakouz et al., 2008).

2.3 Biosensing receptors (general classification)

The bioreceptor is a biomolecule which recognize the target analyte, while the transducer converts the event to some kinds of measurable signal. The unique idea of a biosensor is a combination of the bioreceptors and transducers in one device. As shown in Figure 2.20 (Nicu and Leichlé, 2008) the bioreceptors can be classified into five different groups, e. g. enzymes, antibodies, DNA (or RNA) receptors, cells or bacteria, and biomimetic receptors.

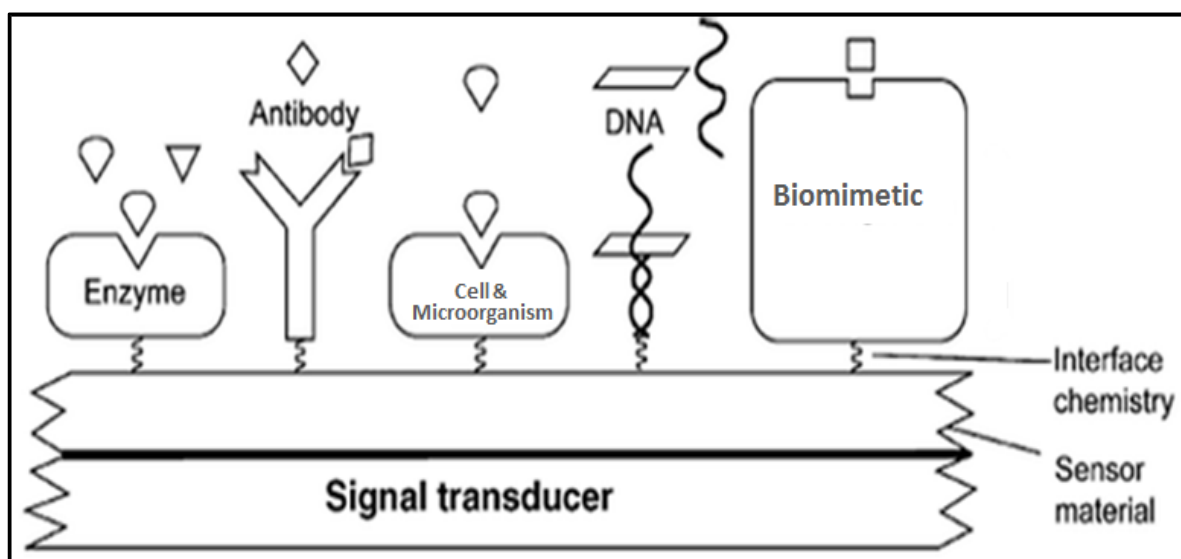


Figure 2.20. Different types of bio-receptors (Nicu and Leïchl , 2008)

The specificity of a biosensor comes from the specificity of the bioreceptor used (Perumal and Hashim, 2014). The five different receptors can be described as follows:

1. Enzyme is a type of protein that is synthesized inside a cell from amino acids according to the coding written in the DNA. Enzymes work as a catalyst for the biochemical reactions in the cell. Due to its specific three-dimensional structure, an enzyme can only accommodate a particular molecule called the substratum. Enzymes help to accelerate the chemical decomposition of the substratum by reducing the activation energy needed for this reaction, which makes it ideal for bioreceptors. Enzyme selective binding sites accept only one substratum, and cause its decomposition on few products, which can be easily detected by the transducer (Pita et al., 2008; Ansari and Husain, 2012). The most common transducing technique is electrochemical, so the majority of enzyme sensors are electrochemical. Enzymes are typically very fragile and strongly dependent of the environmental conditions, e.g. pH, temperature, buffer composition, etc.

2. Antibodies are Y-shaped proteins which are produced by the immune system to identify and to get rid of foreign substances (also called antigens). As bioreceptors, antibodies can

detect antigens which stick to the antibodies' binding sites in the lock - key interaction. Antibodies are highly specific and can bind only particular target analyte (antigen) (Conroy et al., 2009). Optical sensors (such as SPR) are very common in immunosensing.

3. DNA is biomolecule essential to all forms of life. The genetic makeup of every living thing, DNA and RNA are molecules composed of only four nucleotides. The unique sequence of the nucleotides not only provides genetic variation but also act as a terrific bioreceptors because each DNA (or RNA) strand is unique and can bind only to a complementary strand. (Tombelli et al., 2005; Sassolas et al., 2008; Sassolas et al., 2007). Another possibility is to use DNA or RNA oligonucleotides called aptamers to accommodate specific target molecules.

4. Cells are the smallest units of life. In the last decade there has been a significant increase in the use of whole-cells as bioreceptors to detect toxicity of the environment. The combination of this approach with the concept of sensor arrays has resulted in the development of whole-cell biosensor arrays (Melamed et al., 2011). Microorganisms such as bacteria and cell organelles are also used here because they react to pollution in an apparent manner (Fang, 2006; Wang et al., 2005). Whole cell biosensors appear as excellent alternatives to conventional chemical sensing methods. Cells are easy to cultivate and manipulate, thus the use of whole cells (mainly bacteria, yeasts and algae) as sensing elements in electrochemical biosensors has found applications in water quality monitoring (Lagarde and Jaffrezic, 2011).

5. Biomimetic receptors are artificial bioreceptors created by synthetic biology. Biomimetic often implies either genetically engineered bioreceptors molecules, artificial membranes, or molecular imprinted polymers (MIP). The latter technique is based on creating holes or

pockets in polymers that can bind specifically the target analytes (Hussain et al., 2013; Sansone et al., 2010; Sarikaya et al., 2003).

2.3.1 Immobilization of bio-receptors

The critical and important step in the design and fabrication of biosensors is the utilization of a reliable strategy for the immobilization of bioreceptors on the transducer surface.

Since the current research in optical biosensors involved mostly gold surfaces, the immobilization on gold will be described. Bioreceptors can be immobilized on the surface of gold through entrapment, physical absorption, crosslinking methods, covalent binding, or a combination thereof. Depending on the selected technique, the method of immobilization can be reversible or irreversible (Tavakoli and Tang, 2017; Hoa et al., 2009). Bioreceptors can be attached or immobilized to the transducer surface in two main ways: covalent and non-covalent binding, as shown in Figure 2.21 (Cosnier, 1999).

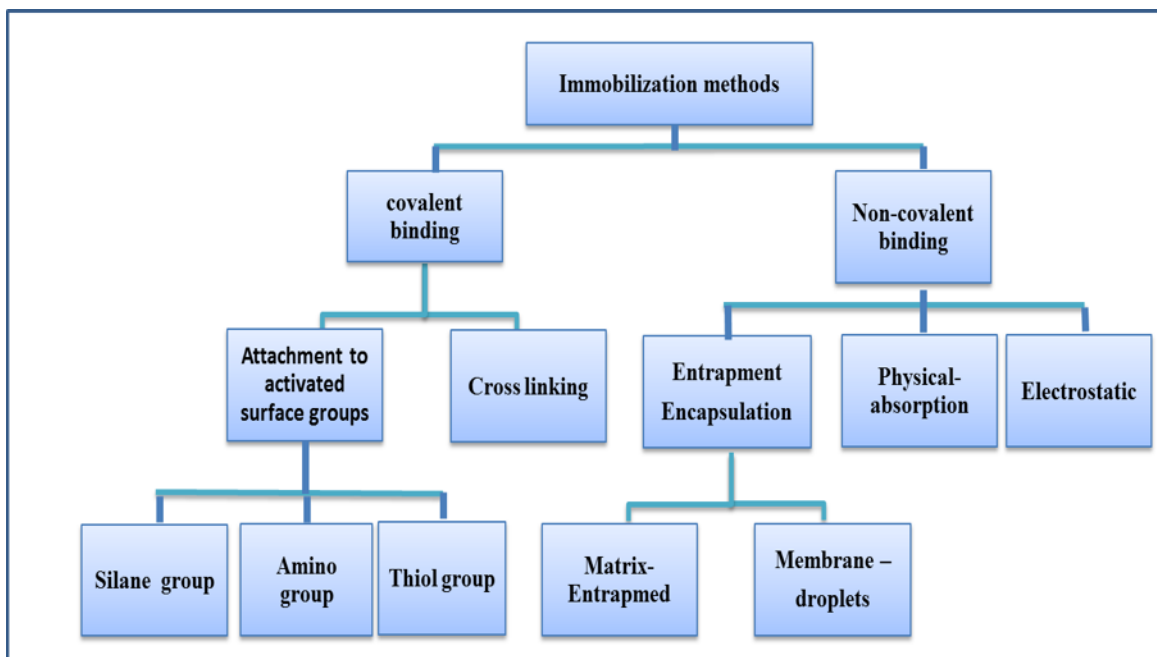


Figure 2.21. Classification of immobilization methods for bio- receptors

2.3.2 Antibodies and their immobilization

There are five classes of immunoglobulin antibodies which differ by their constant domain structure and the immune function (see Figure 2.22).

The five subclasses of antibodies are:

1. Immunoglobulin A (IgA), which is found in high concentrations in the mucous membranes, particularly those lining the respiratory passages and gastrointestinal tract, as well as in saliva and tears.
2. Immunoglobulin G (IgG), the most abundant type of antibody, is found in all body fluids and protects against bacterial and viral infections.
3. Immunoglobulin M (IgM), which is found mainly in the blood and lymph fluid, is the first antibody to be made by the body to fight a new infection.
4. Immunoglobulin E (IgE), which is associated mainly with allergic reactions (when the immune system overreacts to environmental antigens such as pollen or pet dander). It is found in the lungs, skin, and mucous membranes.
5. Immunoglobulin D (IgD), which exists in small amounts in the blood, is the least understood antibody.

Immunoglobulins types IgM and IgG are the most commonly used in immunosensors (Casali and Schettino, 1996).

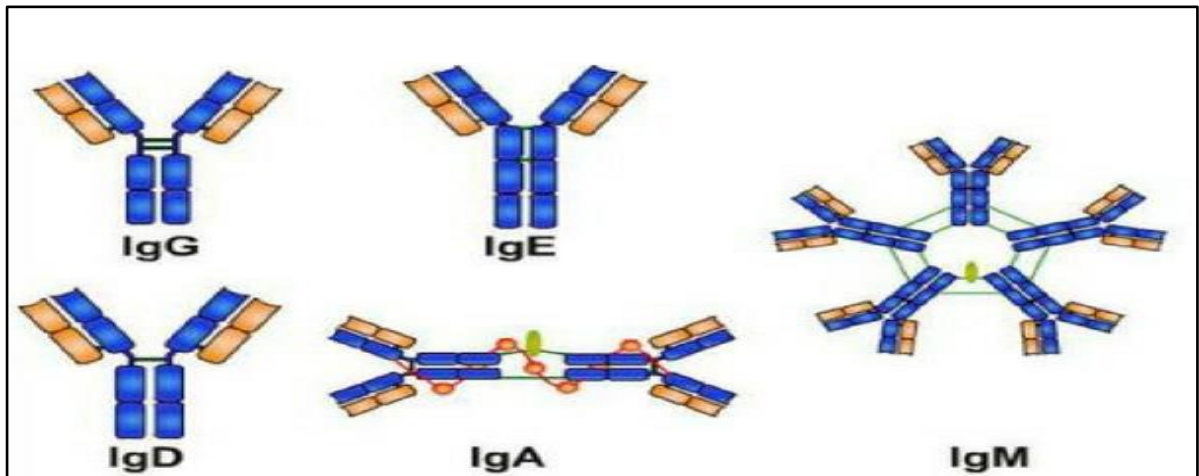


Figure 2.22. Classes of antibodies

As shown in Figure 2.23 antibody structure can be divided into two parts, the top part of Y (variable domain V) that has the ability to bind antigen, and the trunk part (constant domain C) (Rodriguez et al., 2015).

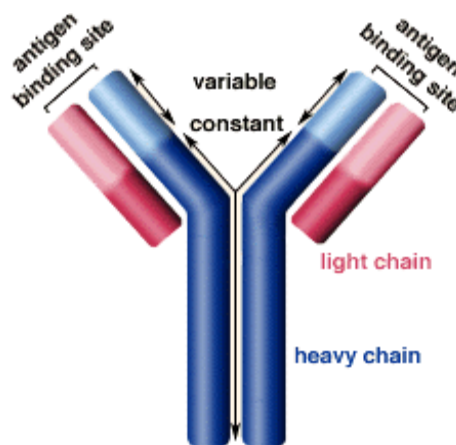


Figure 2.23. Antibody structure (IgG)

Amino acid sequence in the tips of the "Y" is unique for each antibody. The variable region, V contains from 110 to 130 amino acids which determine the specificity of the antibody for a particular antigen. The variable region of the structure includes the ends of the light and heavy chain sequences.

There are other types of antibodies, for example Camelids antibodies. The Camelidae antibody consists of light chains in which the single N-terminal domain is fully capable of antigen binding (Figure 2.24). These single-domain antibody fragments (VHH) (or nanobody) are the antigen binding fragments of the heavy chain antibodies. Nanobodies could be just the variable fragments VL or VH of IgG-based antibodies (Ahmed et al., 2012) or variable fragments of camelid antibodies (Huang et al., 2010), as shown in Figure 2.24. The antigen binding regions (variable domains) are highlighted in yellow and green. Nanobodies are small (15kDa) as compared to the conventional antibody (left) and to the camel antibody (middle). Nanobodies can be directly immobilized on the surface of transducer; they could be particularly useful for LSPR biosensing.

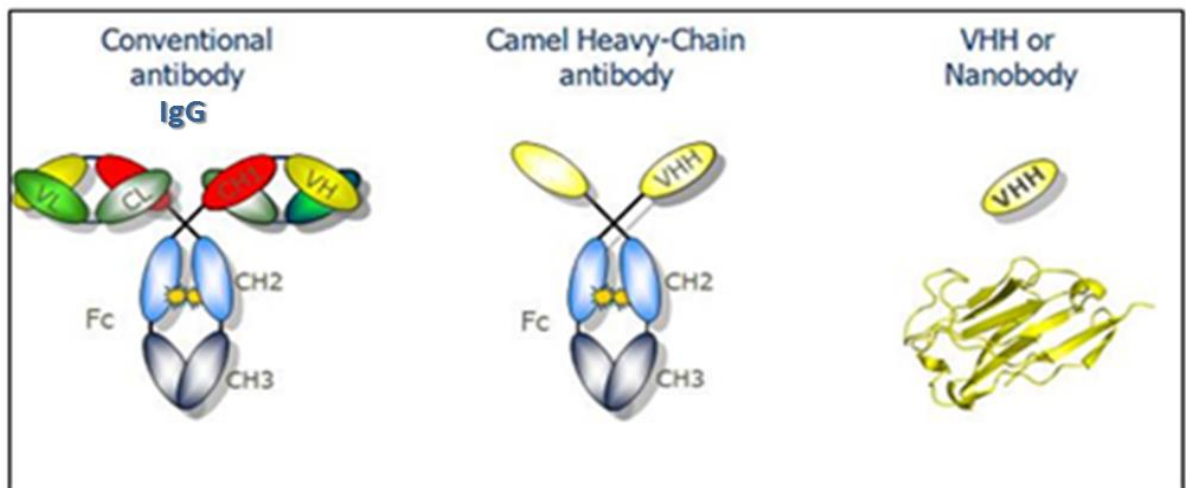


Figure 2.24. The Camel Heavy – Chain antibody and Nanobody

2.3.2.1 Production of antibodies

There are two types of antibodies depending on their production method, i.e. polyclonal and monoclonal antibodies. Monoclonal antibodies are identical because they are produced by one type of immune cell, all clones of a single parent cell (Spadiut et al., 2014). Polyclonal antibodies are derived from different cell lines. They may slightly differ in amino acid sequence. Monoclonal antibodies are a single type of antibody that are identical and are

directed against a specific antigen or antigenic determinant (see Figure 2.24) (Vijayasankaran et al., 2010). Monoclonal antibodies are generated by immunizing laboratory animals with a target antigen. B cells and myeloma cells are fused and then selected in hypoxanthine-aminopterin-thymidine (HAT) medium. Finally, hybridoma cells producing the desired antibodies are screened as shown in (Figure 2.25) (Saeed et al., 2017). Polyclonal antibodies are extracted from the blood serum and contain mixed population of types of antibodies (Kimura et al., 1991; Huang, 2012; Fisher, 2011; Lizak, 2011).

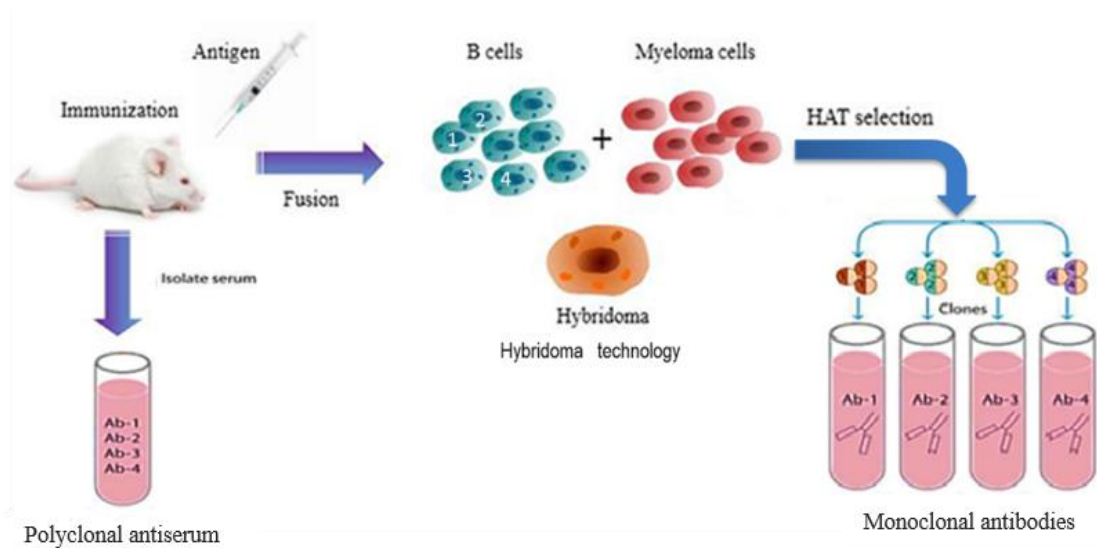


Figure 2.25. Antibodies production

2.3.2.2 Antigen – antibody reaction

Antibody to antigen bonding is a result of multiple reversible intermolecular connections. The non-covalent bonds are weaker than covalent bonds. However, these bonds in large number have strong total binding energy. The force of interaction between the antigen and antibody is called as antibody affinity. The types of non-covalent bonds involved in the

antigen antibody interaction are: hydrophobic interaction, hydrogen bonding, electrostatic forces and Van der Waals forces (Figure 2.25) (Fernandes et al., 2011; DeLisi, 2013).

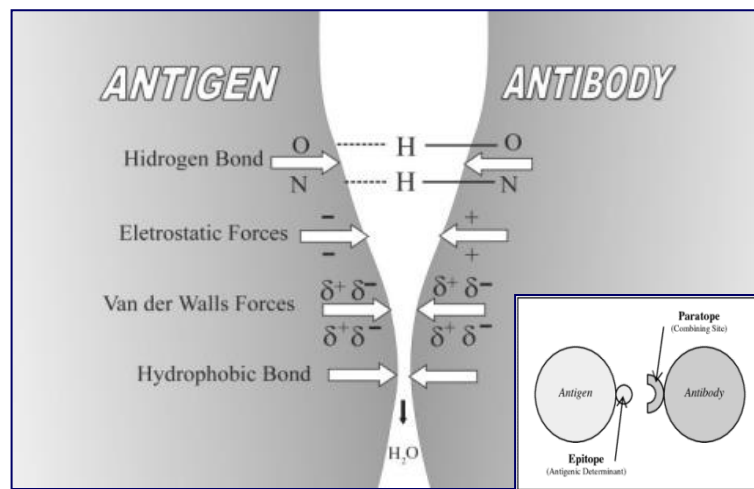


Figure 2.26. Forces involved in antigen-antibody binding (Abbas and Lichtman, 2005)

The van der Waals and Hydrophobic interaction forces in antigen-antibody binding occurs when the antigens and antibodies are close to each other, while hydrogen bonding and electrostatic interactions appear at larger distances (see Figure 2.26). The inset in Figure 2.26 illustrates interaction of antigenic determinant (epitope) and antigen combining site (paratope) on the antibody.

2.3.2.3 Immobilization of antibodies

One of the most important aspects of the biosensor development is immobilization of bioreceptors on the traducer surface. The ideal orientation of the immobilized antibody is when Fc fragments are facing the medium, sometimes referred to as “end-on”. However, randomly immobilized antibodies may have various surface orientations also referred to as “head-on,” “side-on,” and “lying-on” as shown in Figure 2.27 (Chen et al., 2014; Welch et al., 2017).

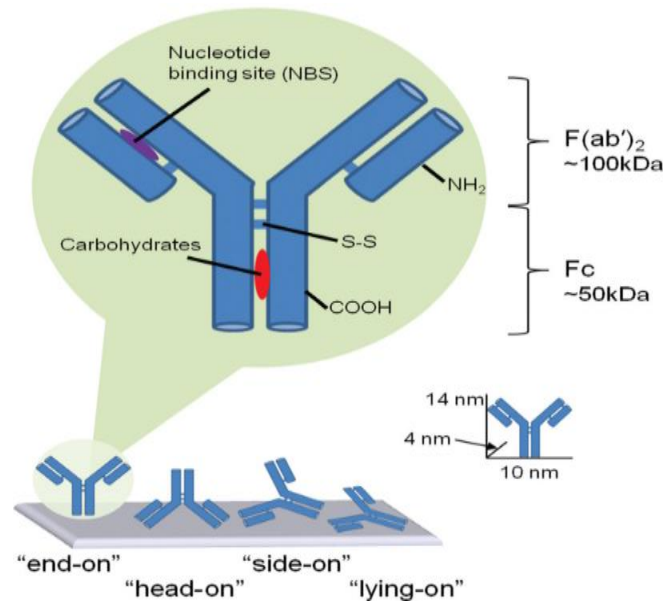


Figure 2.27. Orientation of antibodies, random, upside, down effect on binding antigens
(Chen et al. 2014)

Immunosensor action is directly relied on the immobilization matrix used, the density and orientation of the antibodies on the transducer surfaces. Many strategies can be used for immobilization of the recognition elements directly on the gold surface, as illustrated by Figure 2.28 (Kong and Hu, 2012). These include covalent bonding via amine or thiol groups, or cross linking, for example using glutaraldehyde. Antibodies could be embedded (entrapped) in solid or liquid matrix; the latter is often called hydrogel. This immobilization approach is getting very common nowadays. Electrostatic binding established in our research group has been successfully used in various biosensing applications.

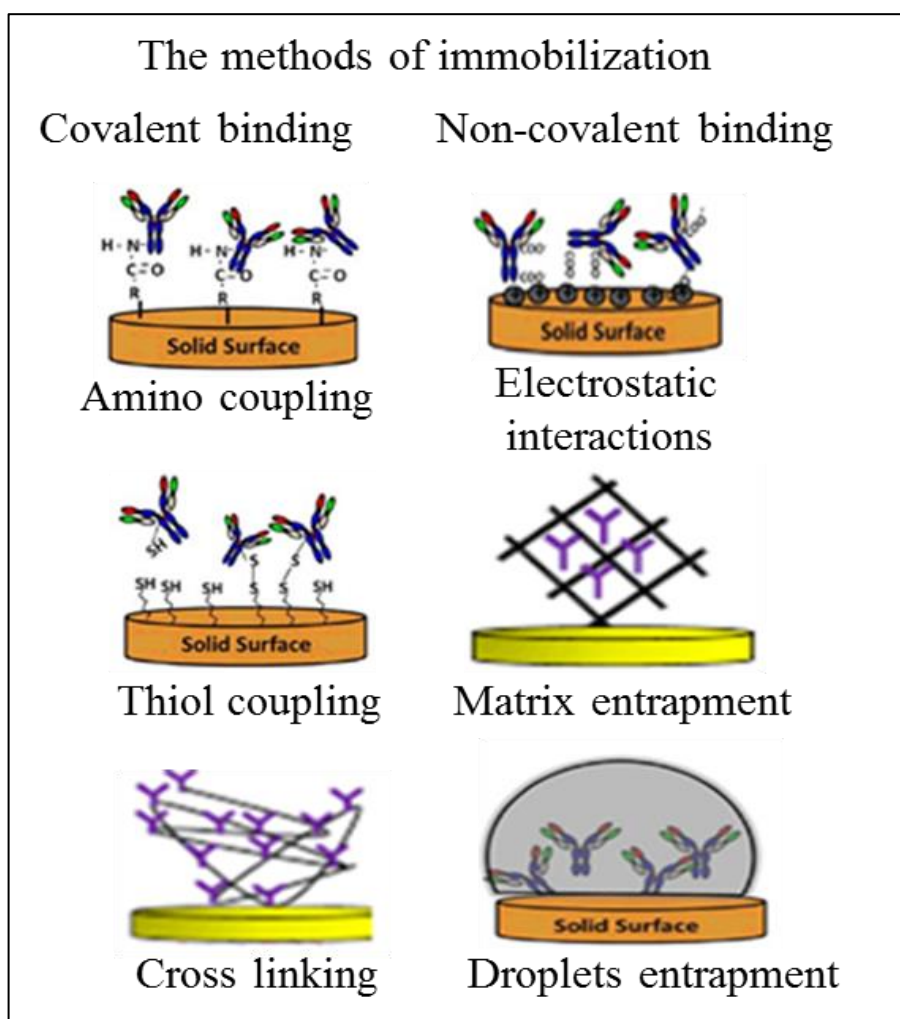


Figure 2.28. Immobilization methods of antibody on the gold surface

It is important to choose a method of immobilization that will not change the chemical nature or reactive groups in the active sites of the antibodies (Kong and Hu, 2012).

In order to use the antibodies in bio-sensing, they have to be immobilized on the transducer surface, (e.g. gold surface which was used in this work). Electrostatic binding of antibodies to the surface is one of the methods of immobilization which can be achieved using intermediate layers of polyelectrolytes. Polyelectrolytes provide a natural environment for proteins and allow biomolecules to retain their functions for a significantly extensive period of time. The most common polyelectrolytes are typically polycations - poly allylamine hydrochloride (PAH) and poly stearyl sulfonate salt (PSS) (Yoo et al., 1997).

2.3.3 Split Antibodies and their immobilization

Immunoglobulin IgG can be split into two half-IgG fragments without destruction of the binding site of the antibody (Karyakin et al., 2000). It is possible to split two heavy chains by reducing immunoglobulin with 2-mercaptoethylamine and to obtain the two “half-immunoglobulin” fragments (Figure 2.29) (Hermanson et al., 1992). The procedure is expected to not affect the binding site of the antibody, which is formed by the coupling of heavy and light chains.

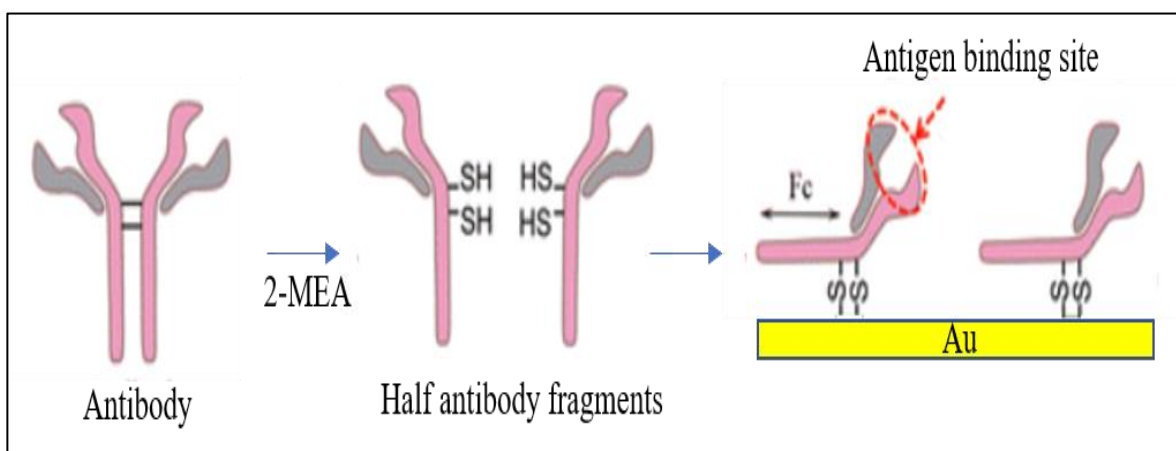


Figure 2.29. Split of antibody into two fragments using 2-Mercaptoethylamine and immobilization of half antibodies on gold surface via their native thiol group (Karyakin et al., 2000)

In general, the known strategies for immobilization of biomolecules onto the gold surfaces are based on the strong attachment of thiol functional groups (SH or SS) to Au. The antibodies are usually linked to gold substrates using a bifunctional reagent with the thiol group on one side (Mirsky and Riepl, 1997). The immobilization of half-antibodies uses the native sulfide group of immunoglobulin (IgG) liberated after splitting the whole antibody. The immobilization of half-IgG fragments on the gold surface is shown schematically in (Figure 2.28) (Karyakin et al., 2000; Liu and May, 2012).

2.3.4 Aptamers

Aptamers are oligonucleotides, such as ribonucleic acid (RNA) or single-strand deoxyribonucleic acid (ssDNA) or peptide molecules that can bind to their targets with high affinity and specificity due to their specific three-dimensional structures. Especially, RNA and ssDNA aptamers can differ from each other in sequence and folding pattern, although they bind to the same target. The term “aptamer” is derived from the Latin word “aptus” meaning “to fit” and the Greek term “meros” meaning a part or region (Jayasena, 1999). Recently, aptamers have attracted the attention of scientists, because they not only have all of the advantages of antibodies, but also have unique merits, such as thermal stability, simple regeneration procedure, low cost, and can be used in numerous applications (Klussmann, 2004). The concept of joining nucleic acids with proteins began to emerge in the 1980s from research on human immunodeficiency virus (HIV) and adenovirus (Minunni, 2004). It indicated that these viruses encode a number of small structured RNAs that bind to viral or cellular proteins with high affinity and specificity (Klussmann, 2004). Due to the development of Systematic evolution of ligands by exponential enrichment protocol (SELEX), which is now a basic technique for the isolation of aptamers, many aptamers could be directly selected in vitro against various targets, from small biomolecules to proteins and even cells (Han, 2010). Aptamers have been studied in numerous investigations concerning their use as a diagnostic and therapeutic tool and biosensing probe, and in the development of new drugs and drug delivery systems. Developed aptamers have been studied primarily for applications as diagnostic or therapeutic tools. (Bunka and Stockley, 2006). Aptamers are widely known as a substitute for antibodies, because of several advantages described below (Han, 2010):

1. High stability of aptamers: It is well known that proteins are easily denatured and lose their tertiary structure at high temperatures, while oligonucleotides are more thermally stable at room temperature and maintain their structures over repeated cycles of denaturation/renaturation. Hence, the greatest advantage of oligonucleotide-based aptamers over protein-based antibodies is their stability at high temperatures. Aptamers recover their native conformation and can bind to targets after re-annealing, whereas antibodies easily undergo irreversible denaturation. Thus, aptamers can be used under a wide range of assay conditions (Mascini, 2008).

2. Relative simplicity of production of aptamers (synthesis or modification): The identification and production of monoclonal antibodies are laborious and very expensive processes involving screening of a large number of colonies. Additionally, the clinical commercial success of antibodies has led to the need for very large-scale production in mammalian cell culture (Birch and Racher, 2006). Moreover, immunoassays are required to confirm the activity of the antibodies in each new batch, because the performance of the same antibody tends to differ depending on the batch. In contrast the aptamers, once selected, can be synthesized in large quantities with great accuracy and reproducibility. These chemical processes are more cost effective than the production of antibodies. Furthermore, aptamers can be easily modified by various chemical reactions to increase their stability and nuclease resistance (Ferreira and Missailidis, 2007; Jayasena, 1999).

3. Low immunogenicity of aptamers: Aptamers usually seem to be low-immunogenic and low-toxic molecules, because nucleic acids are not typically recognized by the human immune system as foreign agents. However, antibodies are significantly immunogenic, which precludes repeat dosing (Ireson et al., 2006; Tombelli et al., 2005).

4. Aptamers are about ten times smaller than antibodies as shown in Figure 2.30 giving them better access to tissues and cells (Lee et al., 2008), which also makes them suitable for LSPR biosensing.

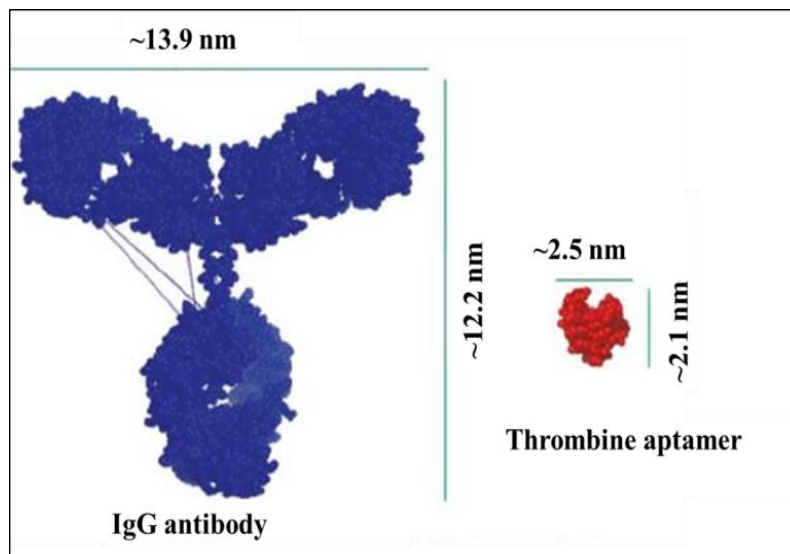


Figure 2.30. Comparison in size between an aptamer and an antibody (Lee et al., 2008)

Based on the numerous advantages described above, aptamers are considered to be an alternative to antibodies in many biological applications (Song, 2012; Rhouati et al., 2013).

2.3.4.1 Aptamer structure

Most of the aptamer structures are the result of intra-molecular base pairing that create loops or bulges; typical peptide structures are shown in Figure 2.31.

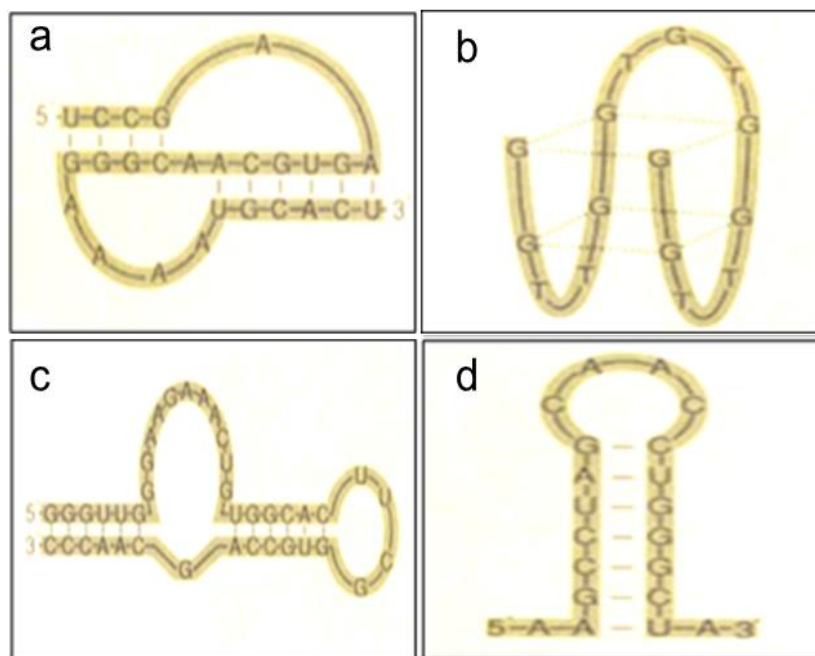


Figure 2.31. Examples of aptamer shapes (a) pseudoknot (b) G-quadruple (c) stem loop / bulge (d) Hairpin.

According to base pair, cytosine (C) always pairs with guanine (G), and adenine (A) with thymine (T) in DNA or uracil (U) in RNA, the aptamer structures can be arranged as follows: A pseudoknot (Figure 2.31a) is a nucleic acid secondary structure of aptamer containing at least two stem-loop structures in which half of one stem is intercalated between the two halves of another stem. G- quadruple (Figure 2.31b) is the structure formed in nucleic acids by sequences that are rich in guanine. Single stranded subsequence bounded by base pairs are called loop, a loop at the end of a stem is called a Hairpin loops (Figure 2.31d) occur when two regions have the same strand. Simple substructures consisting of a single stem and loop are called Stem loop (Figure 2.31c) a unit consisting of two nucleobases bound contact to each other by hydrogen bonds (Hong et al., 2001).

2.3.4.2 Aptamer production

A random library of nucleic acids is incubated together with a target molecule. First, the non-bound nucleic acids are separated from those bound to a target. Then the linked chains of bound nucleic acids are separated from the target and amplified by PCR (polymerase chain reaction) and used in the binding of next cycles. From 6 to 12 sequential cycles are performed for every target; and the last enhanced library is cloned and sequenced see Figure 2.32 (Mallikaratchy et al., 2009).

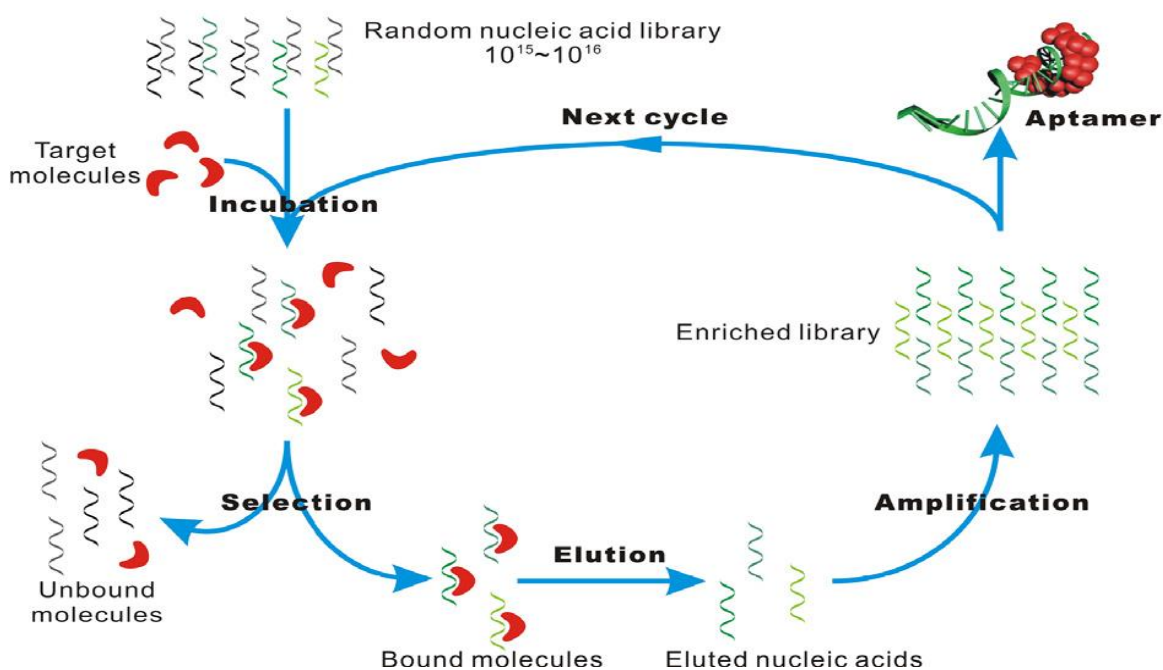


Figure 2.32. A scheme for the Systematic Evolution of Ligands by Exponential enrichment process (SELEX)

Aptamers have several applications in biomedical diagnostic; they can be particularly useful in biomedical diagnosis for the development of disease biomarkers. A diagnostic-based aptamer kit was developed for detection of mycotoxins and aflatoxins in particular

(Penner, 2012; Goud et al., 2016). Aptagen (biotechnology company) developed an interesting technology known as the aptamer-beacon (Apta-beacon) which can be utilized for quick biomarker development. Apta-beacon is potentially great as a point-of-care system applied for the improved treatment of patients (Tuleuova et al., 2010), developed a biosensor for the rapid and simple detection of aflatoxin B1; it led to the advance of several aptasensors for AFB1 analysis in food. The aptamer assay displayed an extensive dynamic range from 0.1 to 10 ng/mL (Shim, 2014). This technique is used as a molecular identification probe for the detection of AFB1. The detection method is based on chemiluminescence competitive assay utilizing hemin G quadruplex horseradish peroxidase-like DNAzyme (HRP-DNAzyme) connected to AFB1 aptamer. The assay permitted the detection of AFB1 in spiked corn samples with LOD = 0.35 nM (Goud et al., 2016; Cruz-Aguado et al. and Penner, 2008; Kim et al., 2007).

2.3.4.3 Aptamer immobilization

The aptamers immobilized on metal surfaces of sensors were reported as early as 1998 (Potyrailo et al., 1998), while immobilization on gold was first reported in 2002 (Liss et al., 2002). Aptamer can be immobilized on a clean gold surface by immersion in buffer solution of thiol-terminated aptamer, the thiol group is typically attached to the (5') terminus of the aptamer (Figure 2.33) (Love et al., 2005). There are various methods for the immobilization of aptamers (C5-SH) on different substrates. In most cases, covalent linking to surfaces is preferred over physisorption. Several different approaches for the immobilization of aptamers can be used depending on the chemical composition of the surface, the subject of availability of suitable aptamer linkers, and the chemistry of attachment (O'Sullivan, 2002). An important goal for aptamer immobilization is to maintain

the binding affinity and selectivity that the aptamer displays in solution. This is usually achieved by covalently tethering the aptamer to a surface-bound linker. For example, the SPR and electrochemical methods require the aptamer to be tethered within close proximity to metallic surfaces in order to induce analytical signals (Balamurugan et al., 2006). Furthermore, immobilization allows the construction of sensor array, either exclusively used aptamers or in combination with antibodies or other receptors for parallel detection of several targets simultaneously (Ikebukuro et al., 2005).

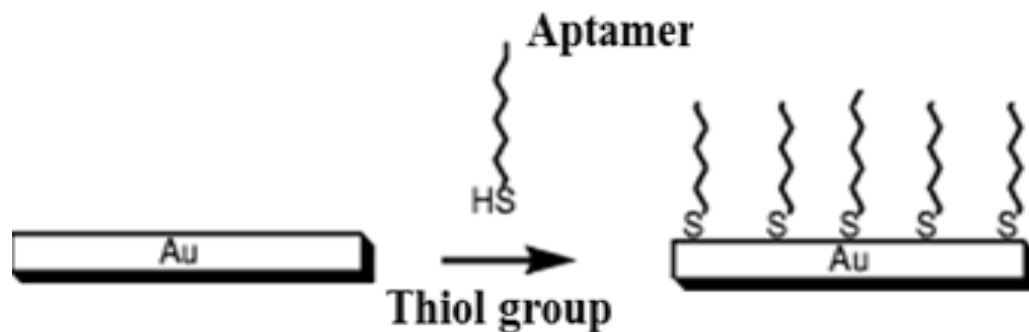


Figure 2.33. Immobilization of aptamers on gold surface via thiol group

Reference list

Abbas, A. K., & Lichtman, A. H. (2005). Introduction to immunology. *Cellular and molecular immunology*, 5th ed. Elsevier Saunders, Philadelphia, 1-40.

Abu Hatab, N.A., Oran, J.M., Sepaniak, M.J. (2008). Surface-enhanced Raman spectroscopy substrates created via electron beam lithography and nanotransfer printing, *ACS Nano*, 2 (2), 377–385.

Ahmad, M.Z., Akhter, S., Rahman, Z., Akhter, S., Anwar, M., Mallik, N., Ahmad, F.J. (2012). Nanometric gold in cancer nanotechnology: current status and future prospects, *J. Pharmacy and Pharmacology*, Wiley Online Librar.

Al-Ammar, R., Nabok, A., Hashim, A., & Smith, T. (2013). Optical detection of microcystin produced by cyanobacteria. In *Journal of Physics: Conference Series* (Vol. 450, No. 1, p. 012006). IOP Publishing.

Ansari, S.A.; Husain, Q. (2012), Potential applications of enzymes immobilized on/in nano materials: A review. *Biotechnol. Adv*, 30, 512–523.

Arwin, H., Poksinski, M., & Johansen, K. (2004). Total internal reflection ellipsometry: principles and applications. *Applied optics*, 43(15), 3028-3036.

Armstrong, R.E., Zijstra, P. (2018). Single protein plasmonic sensors using DNA aptamers, XIV Conference on Optical Chemical Sensors and Biosensors, Europt(r)ode XIV, March 25-28, Naples, Italy, OC14.

Azzam, R.M. A. (1992) and Bashara, N.M., Ellipsometry and polarized light, North Holland, Amsterdam.

Azzam, R.M.A. and BasharaN.M. (1978), Ellipsometry and Polarized, *Surface Technology*,7 (3)269.

Balamurugan, S., Obubuafo, A., Soper, S. A., McCarley, R. L., & Spivak, D. A. (2006). Designing highly specific biosensing surfaces using aptamer monolayers on gold. *Langmuir*, 22(14), 6446-6453.

Baldrich, E., Acero, J. L., Reekmans, G., Laureyn, W., & O'Sullivan, C. K. (2005). Displacement enzyme linked aptamer assay. *Analytical chemistry*, 77(15), 4774-4784.

Bae, C., Kim, S., Ahn, B., Kim, J., Sung, M. M., & Shin, H. (2008). Template-directed gas-phase fabrication of oxide nanotubes. *Journal of Materials Chemistry*, 18(12), 1362-1367.

- Bao, L., Mahurin, S. M., Haire, R. G., & Dai, S. (2003). Silver-doped sol–gel film as a surface-enhanced Raman scattering substrate for detection of uranyl and neptunyl ions. *Analytical chemistry*, 75(23), 6614-6620.
- Basnar, B., Elnathan, R., & Willner, I. (2006). Following aptamer–thrombin binding by force measurements. *Analytical chemistry*, 78(11), 3638-3642.
- Birch, J.R.; Racher, A.J. (2006). Antibody production. *Adv. Drug Deliv. Rev*, 58, 671–685.
- Brolo, A.G., Gordon, R., Leathem, B., Kavanagh, K.L. (2004), Surface plasmon sensor based on the enhanced light transmission through arrays of nanoholes in gold films, *Langmuir*, 20 (12), 4813–4815.
- Bunka, D.H.; Stockley, P.G. Aptamers come of age—At last. *Nat. Rev. Microbiol* (2006), 4, 588–596.
- Bumrah, G. S., & Sharma, R. M. (2016). Raman spectroscopy—Basic principle, instrumentation and selected applications for the characterization of drugs of abuse. *Egyptian Journal of Forensic Sciences*, 6(3), 209-215.
- Byun, K. M. (2010). Development of nanostructured plasmonic substrates for enhanced optical biosensing. *Journal of the Optical Society of Korea*, 14(2), 65-76.
- Cao, Y. C., Jin, R., & Mirkin, C. A. (2002). Nanoparticles with Raman spectroscopic fingerprints for DNA and RNA detection. *Science*, 297(5586), 1536-1540.
- Chang, R. (Ed.). (2013). *Surface enhanced Raman scattering*. Springer Science & Business Media.
- Chen, H., Liu, F., Qi, F., Koh, K., & Wang, K. (2014). Fabrication of calix [4] arene derivative monolayers to control orientation of antibody immobilization. *International journal of molecular sciences*, 15(4), 5496-5507.
- Chen, J., Yang, M., Zhang, Q., Cho, E. C., Cogley, C. M., Kim, C., ... & Xia, Y. (2010). Gold nanocages: a novel class of multifunctional nanomaterials for theranostic applications. *Advanced functional materials*, 20(21), 3684-3694.
- Conroy, P.J.; Hearty, S.; Leonard, P.; O’Kennedy, R.J. (2009). Antibody production, design and use for biosensor-based applications. *Semin. Cell Dev. Biol.*, 20, 10–26.
- Cosnier, S. (1999). Biomolecule immobilization on electrode surfaces by entrapment or attachment to electrochemically polymerized films. A review. *Biosensors and Bioelectronics*, 14(5), 443-456.
- DeLisi, C. (2013). Antigen antibody interactions (Vol. 8). *Springer Science & Business Media*. Fang, Y. Label-free cell-based assays with optical biosensors in drug discovery. *Assay Drug Dev. Technol.*, 4, 583–595.

Daniel, M. C., & Astruc, D. (2004). Gold nanoparticles: assembly, supramolecular chemistry, quantum-size-related properties, and applications toward biology, catalysis, and nanotechnology. *Chemical reviews*, 104(1), 293-346.

Doron-Mor, I.; Barkay, Z.; Filip-Granit, N.; Vaskevich, A.; Rubinstein, I. (2004). Ultrathin gold island films on silanized glass. Morphology and optical properties. *Chem. Mater.*, 16 (18), 3476–3483.

Duwez, A. S. (2004). Exploiting electron spectroscopies to probe the structure and organization of self-assembled monolayers: a review. *Journal of Electron Spectroscopy and Related Phenomena*, 134(2-3), 97-138.

Esterina, R., Liu, X. M., Adeyeye, A. O., Ross, C. A., & Choi, W. K. (2015). Solid-state dewetting of magnetic binary multilayer thin films. *Journal of Applied Physics*, 118(14), 144902.

Famulok, M.; Hartig, J.S.; Mayer, G. (2006). Functional aptamers and aptazymes in biotechnology, diagnostics, and therapy. *Chem. Rev.* 2007, 107, 3715–3743. Fang, Y. Label-free cell-based assays with optical biosensors in drug discovery. *Assay Drug Dev. Technol.*, 4, 583–595.

Ferreira, C.S.; Missailidis, S. (2007). Aptamer-based therapeutics and their potential in radiopharmaceutical design. *Braz. Arch. Biol. Technol.*, 50, 63–76.

Fernandes, H. P., Cesar, C. L., & Barjas-Castro, M. D. L. (2011). Electrical properties of the red blood cell membrane and immunohematological investigation. *Revista brasileira de hematologia e hemoterapia*, 33(4), 297-301.

Fujiwara, H. (2007). Spectroscopic ellipsometry: principles and applications. John Wiley & Sons.

Gabudean, A.M., Biro, D., Astilean, S. (2011), Localized surface plasmon resonance (LSPR) and surface-enhanced Raman scattering (SERS) studies of 4-aminothiophenol adsorption on gold nanorods, *Journal of Molecular Structure*, 993 (1–3), 420-424.

Geoghegan Kelsall, R., Hamley, I. W., & Geoghegan, M. (Eds.). (2005). *Nanoscale science and technology*. John Wiley & Sons.

Ghanim Al-Rubaye, A., Nabok, A., Catanante, G., Marty, J. L., Takács, E., & Székács, A. (2018). Label-Free Optical Detection of Mycotoxins Using Specific Aptamers Immobilized on Gold Nanostructures. *Toxins*, 10(7), 291.

Goud, K.Y., Catanante, G., Hayat, A., Satyanarayana, M., Gobi, K.V. and Marty, J.L., (2016). Disposable and portable electrochemical aptasensor for label free detection of aflatoxin B1 in alcoholic beverages. *Sensors and Actuators B: Chemical*, 235, pp.466-473.

Cruz-Aguado, J.A. and Penner, G. (2008), Determination of ochratoxin A with a DNA aptamer, *Journal of agricultural and food chemistry*, 56(22) 10456-10461.

- Han, K.; Liang, Z.; Zhou, N. Design strategies for aptamer-based biosensors. *Sensors* 2010, *10*, 4541–4557.
- Hao, E., & Schatz, G. C. (2004). Electromagnetic fields around silver nanoparticles and dimers. *The Journal of chemical physics*, *120*(1), 357-366.
- Haynes, C.L., Van Duyne R.P. (2001), Nanosphere Lithography: A Versatile Nanofabrication Tool for Studies of Size-Dependent Nanoparticle Optics, *J. Phys. Chem. B*, *105* (24), 5599–5611.
- Haynes, C. L., McFarland, A. D., & Van Duyne, R. P. (2005). Surface-enhanced Raman spectroscopy.338-A.
- Herne, T. M., & Tarlov, M. J. (1997). Characterization of DNA probes immobilized on gold surfaces. *Journal of the American Chemical Society*, *119*(38), 8916-8920.
- Hermanson, G. T., Mallia, A. K., & Smith, P. K. (1992). *Immobilized affinity ligand techniques*. Academic Press.
- Hoa, X. D., Kirk, A. G., & Tabrizian, M. (2009). Enhanced SPR response from patterned immobilization of surface bioreceptors on nano-gratings. *Biosensors and Bioelectronics*, *24*(10), 3043-3048.
- Huang, C. C., Huang, Y. F., Cao, Z., Tan, W., & Chang, H. T. (2005). Aptamer-modified gold nanoparticles for colorimetric determination of platelet-derived growth factors and their receptors. *Analytical chemistry*, *77*(17), 5735-5741.
- Huang, L., Muyldermans, S., Saerens D. (2010), Nanobodies: proficient tools in diagnostics, *Expert Review of Molecular Diagnostics*, *10*(6), 777-785.
- Huang C.J. (2012) Industrial production of recombinant therapeutics in *Escherichia coli* and its recent advancements. *J. Ind. Microbiol. Biotechnol.*, *39*:383–399.
- Huang, C. J., Chiu, P. H., Wang, Y. H., Chen, W. R., & Meen, T. H. (2006). Synthesis of the gold nanocubes by electrochemical technique. *Journal of The Electrochemical Society*, *153*(8), D129-D133.
- Hussain, M., Wackerlig, J., & Lieberzeit, P. A. (2013). Biomimetic strategies for sensing biological species. *Biosensors*, *3*(1), 89-107.
- Hutchinson, A. M. (1995). Evanescent wave biosensors. *Molecular biotechnology*, *3*(1), 47-54. Hutter, E., Fendler, J.H. (2004), Exploitation of localized surface plasmon resonance, *Advanced Materials*, *16*(19), 1685-1706.
- Ikebukuro, K., Kiyohara, C., & Sode, K. (2005). Novel electrochemical sensor system for protein using the aptamers in sandwich manner. *Biosensors and Bioelectronics*, *20*(10), 2168-2172.

Ireson, C.R.; Kelland, L.R. (2006) Discovery and development of anticancer aptamers. *Mol. Cancer Ther*, 5, 2957–2962.

J A Woollam Co. Inc, Guide to using WVASE32, Software for Spectroscopic Ellipsometry Data Acquisition and Analysis. New York: Wex Tech Systems Inc., 2001.

Jarvis, R. M., Brooker, A., & Goodacre, R. (2004). Surface-enhanced Raman spectroscopy for bacterial discrimination utilizing a scanning electron microscope with a Raman spectroscopy interface. *Analytical Chemistry*, 76(17), 5198-5202.

Jensen, T., Kelly, L., Lazarides, A., & Schatz, G. C. (1999). Electrodynamics of noble metal nanoparticles and nanoparticle clusters. *Journal of Cluster Science*, 10(2), 295-317.

Karakouz, T., Maoz, B. M., Lando, G., Vaskevich, A., & Rubinstein, I. (2011). Stabilization of gold nanoparticle films on glass by thermal embedding. *ACS applied materials & interfaces*, 3(4), 978-987.

Karakouz, T., Tesler, A.B, Bendikov, T.A., Vaskevich, A., Rubinstein, I. (2008), Highly stable localized plasmon transducers obtained by thermal embedding of gold island films on glass, *Advanced Materials*, 20, 3893-3899.

Karakouz, T.; Holder, D.; Goomanovsky, M.; Vaskevich, A.; Rubinstein, I. (2009) Morphology and refractive index sensitivity of gold island films. *Chem. Mater.*, 21 (24), 5875–5885.

Karakouz, T., Tesler, A. B., Sannomiya, T., Feldman, Y., Vaskevich, A., & Rubinstein, I. (2013). Mechanism of morphology transformation during annealing of nanostructured gold films on glass. *Physical Chemistry Chemical Physics*, 15(13), 4656-4665.

Karyakin, A. A., Presnova, G. V., Rubtsova, M. Y., & Egorov, A. M. (2000). Oriented immobilization of antibodies onto the gold surfaces via their native thiol groups. *Analytical chemistry*, 72(16), 3805-3811.

Kedem, O., Vaskevich A., Rubinstein, I. (2014), Critical issues in localized plasmon sensing, *J. Phys. Chem. C*, 118 (16), 8227–8244.

Kedem, O.; Tesler, A. B.; Vaskevich, A.; Rubinstein, I. (2011) Sensitivity and optimization of localized surface plasmon resonance transducers. *ACS Nano*, 5 (2), 748–760.

Kelsall, R., Hamley, I. W., & Geoghegan, M. (Eds.). (2005). *Nanoscale science and technology*. John Wiley & Sons.

Kim, M. W., Peiffer, D. G., Chen, W., Hsiung, H., Rasing, T., & Shen, Y. R. (1989). Polymer concentration profile near a liquid-solid interface: evanescent wave ellipsometry study. *Macromolecules*, 22(6), 2682-2685.

Kim, Y.S., Jung, H.S., Matsuura, T., Lee, H.Y., Kawai, T. and Gu, M.B. (2007), Electrochemical detection of 17 β -estradiol using DNA aptamer immobilized gold electrode chip, *Biosensors and Bioelectronics*, 22(11) pp.2525-2531.

Kimura, T., Ishikawa, N. and Shinkai, K. (1991), Differences in IgG and IgE antibody responses to a low-molecular compound in inbred strains of mice. *Arerugi, Allergy*, 40(3 Pt 1), pp.248-255.

Kleinman, S. L., Frontiera, R. R., Henry, A. I., Dieringer, J. A., & Van Duyne, R. P. (2013). Creating, characterizing, and controlling chemistry with SERS hot spots. *Physical Chemistry Chemical Physics*, 15(1), 21-36.

Klussmann, S. (Ed.). (2006). *The aptamer handbook: functional oligonucleotides and their applications*. John Wiley & Sons.

Kneipp, K., Wang, Y., Kneipp, H., Perelman, L. T., Itzkan, I., Dasari, R. R., & Feld, M. S. (1997). Single molecule detection using surface-enhanced Raman scattering (SERS). *Physical review letters*, 78(9), 1667.

Kneipp, K. , H., Kartha, V. B., Manoharan, R., Deinum, G., Itzkan, I., & Feld, M. S. (1998). Detection and identification of a single DNA base molecule using surface-enhanced Raman scattering (SERS). *Physical Review E*, 57(6), R6281.

Kong, F., & Hu, Y. F. (2012). Biomolecule immobilization techniques for bioactive paper fabrication. *Analytical and bioanalytical chemistry*, 403(1), 7-13.

Krestchmann.E. (1971), "Determination of Optical Constants of Metals by Excitation of Surface Plasmons," *Zeitschrift Fur Physik*, vol. 241 pp. 313.

Lading, L., Nielsen, L. B., & Sevel, T. (2002). Comparing biosensors. In *SENSORS, 2002 IEEE* (Vol. 1, pp. 229-232). IEEE.

Lagarde, F., & Jaffrezic-Renault, N. (2011). Cell-based electrochemical biosensors for water quality assessment. *Analytical and Bioanalytical Chemistry*, 400(4), 947.

Lahav, M., Vaskevich, A., Rubinstein, I. (2004), Biological sensing using transmission surface plasmon resonance spectroscopy, *Langmuir*, 20 (18), 7365–7367.

Lee, J. O., So, H. M., Jeon, E. K., Chang, H., Won, K., & Kim, Y. H. (2008). Aptamers as molecular recognition elements for electrical nanobiosensors. *Analytical and bioanalytical chemistry*, 390(4), 1023-1032.

Leung, A., Shankar, P. M., & Mutharasan, R. (2007). A review of fiber-optic biosensors. *Sensors and Actuators B: Chemical*, 125(2), 688-703.

Liss, M., Petersen, B., Wolf, H., & Prohaska, E. (2002). An aptamer-based quartz crystal protein biosensor. *Analytical Chemistry*, 74(17), 4488-4495.

- Liu, H., & May, K. (2012). Disulfide bond structures of IgG molecules: structural variations, chemical modifications and possible impacts to stability and biological function. In *MABs* (Vol. 4, No. 1, pp. 17-23). Taylor & Francis.
- Liu, X., Wei, J., Song, D., Zhang, Z., Zhang, H., & Luo, G. (2003). Determination of affinities and antigenic epitopes of bovine cardiac troponin I (cTnI) with monoclonal antibodies by surface plasmon resonance biosensor. *Analytical biochemistry*, *314*(2), 301-309.
- Liu, W., Niu, Y., Viana, A. S., Correia, J. P., & Jin, G. (2016). Potential Modulation on Total Internal Reflection Ellipsometry. *Analytical chemistry*, *88*(6), 3211-3217.
- Liu, Z., & Searson, P. C. (2006). Single nanoporous gold nanowire sensors. *The Journal of Physical Chemistry B*, *110*(9), 4318-4322.
- Lizak C. (2011). N-Linked glycosylation of antibody fragments in Escherichia coli. *Bioconjug. Chem*, *22*:488–496.
- Love, J. C., Estroff, L. A., Kriebel, J. K., Nuzzo, R. G., & Whitesides, G. M. (2005). Self-assembled monolayers of thiolates on metals as a form of nanotechnology. *Chemical reviews*, *105*(4), 1103-1170.
- Mallikaratchy, P., Liu, H., Huang, Y. F., Wang, H., Lopez-Colon, D., & Tan, W. (2009). Using aptamers evolved from cell-SELEX to engineer a molecular delivery platform. *Chemical Communications*, (21), 3056-3058.
- Marston, P.L. (2002). Scattering of acoustic evanescent waves by circular cylinders: Partial wave series solution. *The Journal of the Acoustical Society of America*, *111*(5) pp. 2378-2378.
- Mascini, M. (2008). Aptamers and their applications. *Anal. Bioanal. Chem*, *390*, 987–988.
- Mayer, K.M., Hafner, J.H. (2011), Localized surface plasmon resonance sensors, *Chemical Reviews*, ACS, *111*, 3828-3857.
- McFarland, A. D., Van Duyne, R. P. (2003), Single silver nanoparticles as real-time optical sensors with zeptomole sensitivity. *Nano Lett.* *3*, 1057–1062.
- Melamed, S., Ceriotti, L., Weigel, W., Rossi, F., Colpo, P., & Belkin, S. (2011). A printed nanolitre-scale bacterial sensor array. *Lab on a Chip*, *11*(1), 139-146.
- Mie, G. (1908). Beiträge zur Optik trüber Medien, speziell kolloidaler Metallösungen, *Annalen der Physik*, *25* (3) 377-445,
- Miller, M. M., & Lazarides, A. A. (2005). Sensitivity of metal nanoparticle surface plasmon resonance to the dielectric environment. *The Journal of Physical Chemistry B*, *109*(46), 21556-21565.

Mirsky, V. M., Riepl, M., & Wolfbeis, O. S. (1997). Capacitive monitoring of protein immobilization and antigen–antibody reactions on monomolecular alkythiol films on gold electrodes. *Biosensors and Bioelectronics*, 12(9-10), 977-989.

Mitsui, K., Handa, Y., & Kajikawa, K. (2004). Optical fiber affinity biosensor based on localized surface plasmon resonance. *Applied Physics Letters*, 85(18), 4231-4233.

Mittal, S.; Kaur, H.; Gautam, N.; Mantha, A.K. (2017) Biosensors for breast cancer diagnosis: A review of bioreceptors, biotransducers and signal amplification strategies. *Biosens. Bioelectron.*, 88, 217–231.

Minunni, M., Tombelli, S., Gullotto, A., Luzi, E., & Mascini, M. (2004). Development of biosensors with aptamers as bio-recognition element: the case of HIV-1 Tat protein. *Biosensors and Bioelectronics*, 20(6), 1149-1156.

Mulvaney, S. P., Musick, M. D., Keating, C. D., & Natan, M. J. (2003). Glass-coated, analyte-tagged nanoparticles: a new tagging system based on detection with surface-enhanced Raman scattering. *Langmuir*, 19(11), 4784-4790.

Nabok, A. V., Tsargorodskaya, A., Hassan, A. K., & Starodub, N. F. (2005). Total internal reflection ellipsometry and SPR detection of low molecular weight environmental toxins. *Applied Surface Science*, 246(4), 381-386.

Nabok, A., & Tsargorodskaya, A. (2008). The method of total internal reflection ellipsometry for thin film characterisation and sensing. *Thin Solid Films*, 516(24), 8993-9001.

Nabok, A. (2005). *Organic and Inorganic Nanostructures* (Artech House Memos and Sensors Library). Artech House Publishers Hardcover: 286 pages.

Nabok, A., & Tsargorodskaya, A. (2008). The method of total internal reflection ellipsometry for thin film characterisation and sensing. *Thin Solid Films*, 516(24), 8993-9001.

Nabok, A., Tsargorodskaya, A., Holloway, A., Starodub, N. F., & Demchenko, A. (2007). Specific binding of large aggregates of amphiphilic molecules to the respective antibodies. *Langmuir*, 23(16), 8485-8490.

Nabok, A., Tsargorodskaya, A., Mustafa, M. K., Szekacs, I., Starodub, N. F., & Szekacs, A. (2011). Detection of low molecular weight toxins using an optical phase method of ellipsometry. *Sensors and Actuators B: Chemical*, 154(2), 232-237.

Nabok, A. V., Mustafa, M. K., Tsargorodskaya, A., & Starodub, N. F. (2011). Detection of aflatoxin B1 with a label-free ellipsometry immunosensor. *BioNanoScience*, 1(1-2), 38-45.

- Nie, S., & Emory, S. R. (1997). Probing single molecules and single nanoparticles by surface-enhanced Raman scattering. *science*, 275(5303), 1102-1106.
- Nicu, L.; Leïchlé, T. (2008) Biosensors and tools for surface functionalization from the macro-to the nanoscale: The way forward. *J. Appl. Phys.*, 104, 12.
- Oh, Y. J., Ross, C. A., Jung, Y. S., Wang, Y., & Thompson, C. V. (2009). Cobalt Nanoparticle Arrays made by Templated Solid-State Dewetting. *Small*, 5(7), 860-865.
- O'Sullivan, C. K. (2002). Aptasensors—the future of biosensing. *Analytical and bioanalytical chemistry*, 372(1), 44-48.
- Otto, A. (1968). "Excitation of nonradiative surface plasma waves in silver by the method of frustrated total reflection," *Z. Phys.*, vol. 216 pp. 398-410.
- Pelaez, M., Falaras, P., Likodimos, V., Kontos, A. G., Armah, A., O'shea, K., & Dionysiou, D. D. (2010). Synthesis, structural characterization and evaluation of sol–gel-based NF-TiO₂ films with visible light-photoactivation for the removal of microcystin-LR. *Applied Catalysis B: Environmental*, 99(3-4), 378-387.
- Paleček, E., Tkáč, J., Bartošík, M., Bertók, T., Ostatná, V., & Paleček, J. (2015). Electrochemistry of nonconjugated proteins and glycoproteins. Toward sensors for biomedicine and glycomics. *Chemical reviews*, 115(5), 2045-2108).
- Petryayeva, E., Krull, U.J. (2011), Localized surface plasmon resonance: nanostructures, bioassays and biosensing – A review, *Analytica Chimica Acta*, 706, 8-24.
- Penner G. (2012), Commercialization of an aptamer-based diagnostic test, *IVD Technol*, 18(4) 31-37.
- Perumal, V., & Hashim, U. (2014). Advances in biosensors: Principle, architecture and applications. *Journal of applied biomedicine*, 12(1), 1-15.
- Pita, M.; Minko, S.; Katz, E. (2008) Enzyme-based logic systems and their applications for novel multi-signal-responsive materials. *J. Mater. Sci.*, 20, 457–462.
- Pokropivny, V. V., & Skorokhod, V. V. (2007). Classification of nanostructures by dimensionality and concept of surface forms engineering in nanomaterial science. *Materials Science and Engineering: C*, 27(5-8), 990-993.
- Poksinski, M., & Arwin, H. (2004). Protein monolayers monitored by internal reflection ellipsometry. *Thin solid films*, 455, 716-721. Potyrailo, R. A., Conrad, R. C., Ellington, A. D., & Hieftje, G. M. (1998). Adapting selected nucleic acid ligands (aptamers) to biosensors. *Analytical Chemistry*, 70(16), 3419-3425.
- Raschke, G. Kowarik, S. Franz, T., Sönnichsen C., Klar, T.A., Feldmann, J., Nicht, A., Kürzinger, K. (2003), Biomolecular Recognition Based on Single Gold Nanoparticle Light Scattering, *Nano Letters*, 3 (7), 935–938.

- Rhouati, A., Yang, C., Hayat, A. and Marty, J.L. (2013). Aptamers: A promising tool for ochratoxin A detection in food analysis. *Toxins*, 5(11), pp.1988-2008.
- Rodriguez, B.A., Trindade, E.K., Cabral, D.G., Soares, E.C., Menezes, C.E., Ferreira, D.C., Mendes, R.K. and Dutra, R.F. (2015). Nanomaterials for Advancing the Health Immunosensor.
- Rostron, P., Gaber, S., and Gaber, D. (2016). Raman spectroscopy, review. *laser*, 21, 24.
- Roy, D., & Fendler, J. (2004). Reflection and absorption techniques for optical characterization of chemically assembled nanomaterials. *Advanced Materials*, 16(6), 479-508.
- Saeed, A. F., Wang, R., Ling, S., & Wang, S. (2017). Antibody engineering for pursuing a healthier future. *Frontiers in microbiology*, 8, 495.
- Sai, V. V. R., Kundu, T., Deshmukh, C., Titus, S., Kumar, P., & Mukherji, S. (2010). Label-free fiber optic biosensor based on evanescent wave absorbance at 280 nm. *Sensors and Actuators B: Chemical*, 143(2), 724-730.
- Sansone, F.; Baldini, L.; Casnati, A.; Ungaro, R. Calixarenes (2010) From biomimetic receptors to multivalent ligands for biomolecular recognition. *New J. Chem.*2010, 34, 2715–2728.
- Sarikaya, M.; Tamerler, C.; Jen, A.K.Y.; Schulten, K.; Baneyx, F. (2003) Molecular biomimetics: Nanotechnology through biology. *Nat. Mater.*, 2, 577–585.
- Sassolas, A.; Leca-Bouvier, B.D.; Blum, L.J. (2008) DNA biosensors and microarrays. *Chem. Rev.*, 108, 109–139.
- Schatz, G. C.; Van Duyne, R. P. (2002) In *Handbook of Vibrational Spectroscopy*; Chalmers, J. M., Griffiths, P. R., Eds.; John Wiley & Sons: New York, Vol. 1, pp 759–774.
- Schatz, G. C. (2003). Electrodynamics of nonspherical noble metal nanoparticles and nanoparticle aggregates. *Journal of Molecular Structure: THEOCHEM*, 573(1-3), 73-80.
- Sepúlveda, B., Angelomé, P.C., Lechuga, L.M., Liz-Marzán, L.M. (2009), LSPR-based nanobiosensors, *Nano Today*, 4(3), 244-251.
- Shim, W.B., Mun, H., Joung, H.A., Ofori, J.A., Chung, D.H. and Kim, M.G. (2014), Chemiluminescence competitive aptamer assay for the detection of aflatoxin B1 in corn samples, *Food Control*, 36(1) pp.30-35.
- Song, K. M., Lee, S., and Ban, C. (2012). Aptamers and their biological applications. *Sensors*, 12(1), 612-631.

Spadiut, O., Capone, S., Krainer, F., Glieder, A., & Herwig, C. (2014). Microbials for the production of monoclonal antibodies and antibody fragments. *Trends in biotechnology*, 32(1), 54-60.

Singh, R. (2002). CV Raman and the Discovery of the Raman Effect. *Physics in Perspective*, 4(4), 399-420

Starodub, N. F., Nabok, A. V., Starodub, V. M., Ray, A. K., & Hassan, A. K. (2001). Immobilization of biocomponents for immune optical sensors. *Ukrains' kyi biokhimichnyi zhurnal (1999)*, 73(4), 55-64.

Tame, M.S., McEnery, K.R., Özdemir, Ş.K., Lee, J., Maier, S.A., Kim, M.S. (2013). Quantum plasmonics, *Nature Physics*, 9, 329–340.

Tavakoli, J., & Tang, Y. (2017). Hydrogel based sensors for biomedical applications: An updated review. *Polymers*, 9(8), 364. Toward a glucose biosensor based on surface-enhanced Raman scattering. *Journal of the American Chemical Society*, 125(2), 588-593.

Tesler, A. B., Maoz, B. M., Feldman, Y., Vaskevich, A., & Rubinstein, I. (2013). Solid-state thermal dewetting of just-percolated gold films evaporated on glass: development of the morphology and optical properties. *The Journal of Physical Chemistry C*, 117(21), 11337-11346.

Thio, T. (2006). A Bright Future for Subwavelength Light Sources, *American Scientist*, vol. 94 pp. 40-47.

Thompson, C. V. Solid-state dewetting of thin films. *Annu. Rev. Mater. Res.* (2012). 42, 399–434.

Tombelli, S.; Minunni, M.; Mascini, M. (2005). Analytical applications of aptamers. *Biosens. Bioelectron.*, 20, 2424–2434.

Townsend, E., Bryant, G.W. (2012). Plasmonic properties of metallic nanoparticles: The effect of size quantization, *Nano Letters*, 12, 429-434.

Tsargorodska, A., El Zubir, O., Darroch, B., Cartron, M. L., Basova, T., Hunter, C. N., Nabok, A., Leggett, G. J. (2014). Fast, simple, combinatorial routes to the fabrication of reusable, plasmonically active gold nanostructures by interferometric lithography of self-assembled monolayers, *ACS Nano*, 8 (8), 7858–7869.

Tuleuova, N., Jones, C.N., Yan, J., Ramanculov, E., Yokobayashi, Y. and Revzin, A. (2010). Development of an aptamer beacon for detection of interferon-gamma, *Analytical chemistry*, 82(5) pp.1851-1857.

Vaskevich, A.; Rubinstein, I. (2012). Localized surface plasmon resonance (LSPR) transducers based on random evaporated gold island films: Properties and sensing

applications. In *Nanoplasmonic Sensors*; Dmitriev, A., Ed.; Springer Publishing: New York, pp 333–368.

Vandenabeele, P. (2010). Raman spectroscopy, *Analytical and Bioanalytical Chemistry*, 397, 2629-2630.

Vijayasankaran, Li, F., N., A., Shen, Kiss, R., and Amanullah, A. Cell culture processes for monoclonal antibody production. *mAbs* .(2010). 2: 466–477. *CrossRef| PubMed| Web of Science® Times Cited*, 66.

Wang, P.; Wu, C.; Cai, H.; Hu, N.; Zhou, J. (2005). Wang, P. Cell-based biosensors and its application in biomedicine. *Sens. Actuator B* 2005, 108, 576–584.

Weißbacher, N., Lendl, B., Frank, J., Wanzenböck, H. D., Mizaikoff, B., & Kellner, R. (1997). Continuous surface enhanced Raman spectroscopy for the detection of trace organic pollutants in aqueous systems. *Journal of molecular structure*, 410, 539-542.

Welch, N. G., Scoble, J. A., Muir, B. W., & Pigram, P. J. (2017). Orientation and characterization of immobilized antibodies for improved immunoassays. *Biointerphases*, 12(2), 02D301.

Westphal, P. and Bornmann, A. (2002). bioelcular detection by surface Plasmon enhanced ellipsometry, sensors and actuators, b: chemical, 84 ,278-282.

Yaseen, M. T., Chen, M., & Chang, Y. C. (2014). Partially embedded gold nano-islands in a glass substrate for SERS applications. *RSC Advances*, 4(98), 55247-55251.

Wang, D., & Schaaf, P. (2013). Solid-state dewetting for fabrication of metallic nanoparticles and influences of nanostructured substrates and dealloying. *physica status solidi (a)*, 210(8), 1544-1551.

Woollam, J. (2009). Software for: Spectroscopic ellipsometry, data acquisition and analysis. Technical Report, JA Woollam, 2009 Google Scholar.

Wu, H. L., Kuo, C. H., & Huang, M. H. (2010). Seed-mediated synthesis of gold nanocrystals with systematic shape evolution from cubic to trisoctahedral and rhombic dodecahedral structures. *Langmuir*, 26(14), 12307-12313.

Xiao, Y., Piorek, B. D., Plaxco, K. W., & Heeger, A. J. (2005). A reagentless signal-on architecture for electronic, aptamer-based sensors via target-induced strand displacement. *Journal of the American Chemical Society*, 127(51), 17990-17991.

Xu, D., Xu, D., Yu, X., Liu, Z., He, W., & Ma, Z. (2005). Label-free electrochemical detection for aptamer-based array electrodes. *Analytical Chemistry*, 77(16), 5107-5113.

Xu, H., Bjerneld, E. J., Käll, M., & Börjesson, L. (1999). Spectroscopy of single hemoglobin molecules by surface enhanced Raman scattering. *Physical review letters*, 83(21), 4357.

Yoo, D., Wu, A., Lee, J. and Rubner, M.F. (1997). New electro-active self-assembled multilayer thin films based on alternately adsorbed layers of polyelectrolytes and functional dye molecules, *Synthetic Metals*, 85(1) pp.1425-1426.

Young, M. A., Stuart, D. A., Lyandres, O., Glucksberg, M. R., & Van Duyne, R. P. (2004). Surface-enhanced Raman spectroscopy with a laser pointer light source and miniature spectrometer. *Canadian journal of chemistry*, 82(10), 1435-1441.

Yu, Y. Y., Chang, S. S., Lee, C. L., & Wang, C. C. (1997). Gold nanorods: electrochemical synthesis and optical properties. *The Journal of Physical Chemistry B*, 101(34), 6661-6664.

Zhang, Z., Chen, Z., Qu, C., Chen, L. (2014). Highly sensitive visual detection of copper ions based on the shape-dependent LSPR spectroscopy of gold nanorods, *Langmuir*, 30(12), 3625–3630.

Chapter 3: Experimental details (Methodology)

3.1 Samples preparation

Gold nano-structures were prepared by evaporation of gold (purchased from Agar Scientific) in 10^{-6} Torr vacuum using Edwards 360 unit onto standard microscopic glass slides (from Sigma-Aldrich) cut into three pieces prior metal deposition. The glass surface was cleaned from organic contaminants by immersion in freshly prepared piranha solution* (1:3 hydrogen peroxide, 30%: sulfuric acid, 95-98%) for 1 hours followed by extensive rinsing with water using. The cleaned glass substrates were stored in ethanol until use. Before gold deposition, the slides were dried under a nitrogen gas stream. A 2 nm thick layer of chromium was deposited first to improve adhesion of gold. Thin gold films of different nominal thicknesses (4, 5, 6, 8, and 10 nm) were deposited and then annealed at 480 °C for 2 hours following the procedure described in (Tesler et al., 2013). Some of the samples were prepared by annealing of 5nm thick gold films evaporated on glass (with no chromium under layer) at higher temperature of 550 °C for 10 hours following the procedures described in (Karakuse et al., 2008) which resulted in gold nano- islands partially imbedded in glass. Later in the project, we started using microwave annealing for 13 minutes with similar outcome as thermal annealing.

*Piranha solution is very dangerous, in addition to being a corrosive liquid and strong oxidizer.

3.1.1 Thermal evaporation of metals

Evaporation process occurs in vacuum, where gases are almost completely removed before the evaporation begins. Therefore, particles can travel straight to the deposition target avoiding collision with the background vapor. Hot objects inside the evaporation chamber, such as heating filaments, creates an unwanted vapor that limits the quality of the vacuum. Generally, other unwanted gases may react with evaporated material. For example, if chromium is deposited in the presence of oxygen, it will form chromium oxide. They also reduce the amount of vapor that reaches the substrate, which makes the thickness difficult to control (Mahana,2000). Shown Edwards E 306 A Figure 3.1(a). The metal source to be evaporated, typically gold and chromium, is placed in a suitable filament or crucible, through which a large current is passed. The metal melts, and evaporates onto the target substrate above the source, producing a film. The thickness of the metal film is monitored in-situ using a quartz crystal thickness monitor (QCM). Even though the turret can accommodate up to four different materials, and changed via manual rotation, the most common practice was to evaporate two material (Au and Cr) during one pump-down cycle. The major components of the Edwards E306A Thermal Evaporator a diffusion pump supported by a rotary pumping system, Chamber, an electrical system, and Bell-jar vacuum chamber (see Figure 3.1 b).

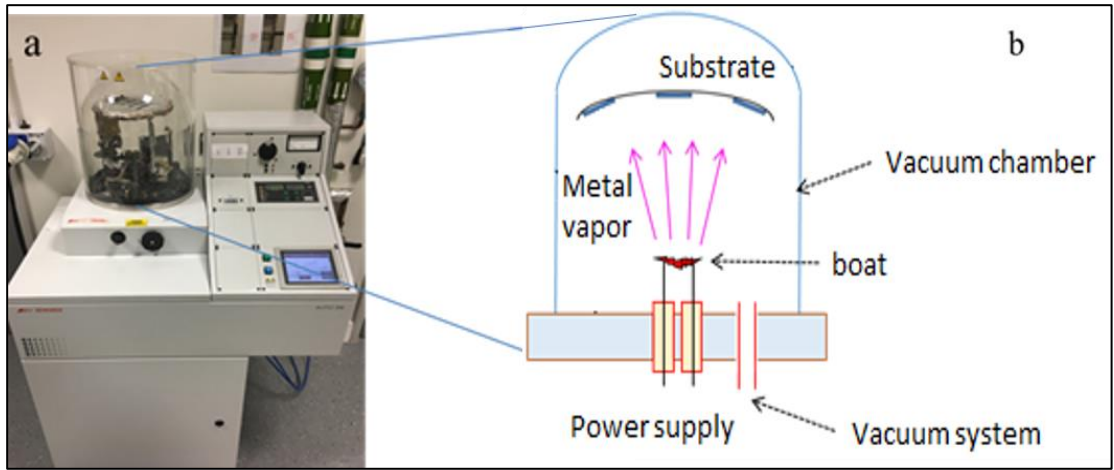


Figure 3.1 (a) Edwards thermal evaporator (b) schematic illustration showing the evaporation process

3.1.2 Annealing of metals

After evaporation the metal samples were placed in a glass Petri dish and annealed either in the oven (Ney Vulcan 3-550) at temperature of 550 °C or 480 °C for 10 and 2 hours respectively or in microwave for 10-13 minutes Figure 3.2. The annealing of thin gold films at high temperatures close to the glass transition temperature of the substrate leads to embedding gold nano-island into glass (Karakouz et al., 2008, Karakouz et al., 2009, Tesleret et al., 2011).



Figure 3.2 Microwave unit (a); (b) Microwave Kiln, inset show the glass slide coated with 5 nm gold annealed in microwave

Annealing at high temperatures enhances not only the surface diffusion but also the recrystallization rate, allowing the formation of well-separated islands from relatively thick Au films. In the present work high-temperature annealing of evaporated Au films of variable nominal thicknesses (4, 5, 6, 8 and 10 nm) was exploited for tuning the LSPR band in a visible wavelength range.

3.2 Immobilization of bio-receptors on Au surface

3.2.1 Immobilization of whole antibodies

Monoclonal antibodies specific to aflatoxin B1 were electrostatically attached to the glass surface via a polycation layer of poly (allylamine hydrochloride) (PAH 1mg/ml in water). An intermediate layer of protein A molecules having a binding site to the second domain of the IgG type antibodies was used to orient antibodies with their Fab fragments towards the solution as one can see in Figure 3.3.

The immobilisation of antibodies (Ab) (1/1000) was carried out in the TIRE cell by consecutive injections of solutions of PAH, protein A 0.02 mg/ml in 35mM Tris –HCL or PBS, and Ab into the cell. Then, the immune reaction between Ab and aflatoxin B1 (AFB1) was studied by performing a series of injections of solutions containing different concentrations of AFB1 (starting from the smallest concentration). The incubation time of 15 min was typically used in all adsorption and binding stages; the cell was rinsed after each adsorption step by purging Trizma/HCl or PBS buffer solution pH 7.5 (10 times the cell volume) through the cell. Furthermore de-ionized water was used for rinsing the cell after adsorption of PAH. (Nabok et al., 2005; Nabok et al., 2009; Starodub et al., 2001). All chemicals were purchases from (Sigma Aldrich).

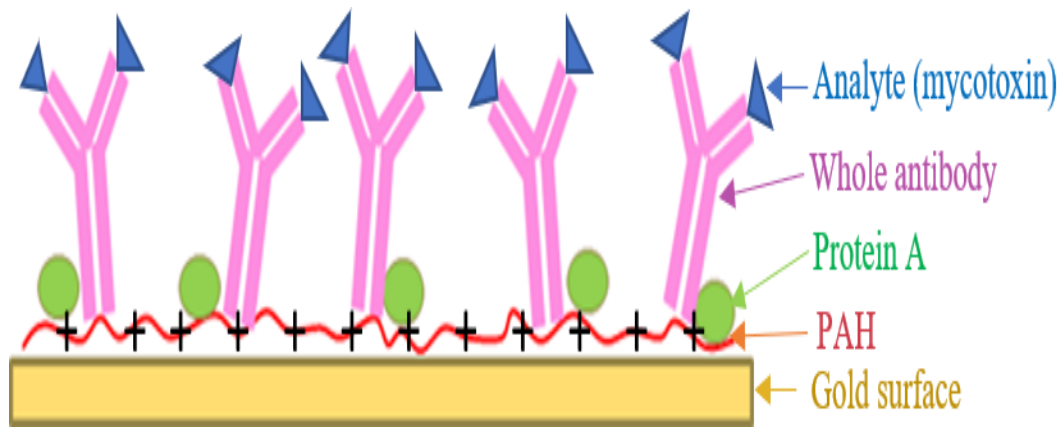


Figure 3.3. Electrostatically immobilization of whole antibodies via cations poly allylamine hydrochloride (PAH) and protein A

The diagram in Figure 3.3 shows that the PAH layer have positive charge to immobilize antibody electrostatically with gold surface and by using protein A to orient Ab towards the solution.

3.2.2 Immobilization of split antibodies

In this work we used the technology of splitting antibodies by the S-S bridge in the main domain using 2-mercaptoethylamine with subsequent immobilization of halved antibodies on the surface of gold via native thiol groups (Karyakin et al.,2008) as shown in Fig. 3.4 As a result the sensitive Fab-fragments appeared to be much closer to the surface.

Intact IgG was dissolved in 0.1 M phosphate buffer (pH 6.0), then 12 mg of 2-Mercaptoethylamine (MEA) was added to the antibody solution and incubated at 37 °C for 1.5 h. For long-term storage, the solution of half-IgG fragments was mixed with an equal amount of glycerol and kept at -20 °C. Under such conditions, the half- IgG fragments were completely stable for several months. The solution containing fragments of antibodies was diluted with 0.01 M PBS (pH 7.4).

The solution containing split antibodies was injected into a TIRE cell with the incubation time of 10min. Dynamic spectra were recorded during the binding reaction, while single spectroscopic scans were recorded in a standard PBS (100mM, pH 7) after completion of each binding step.

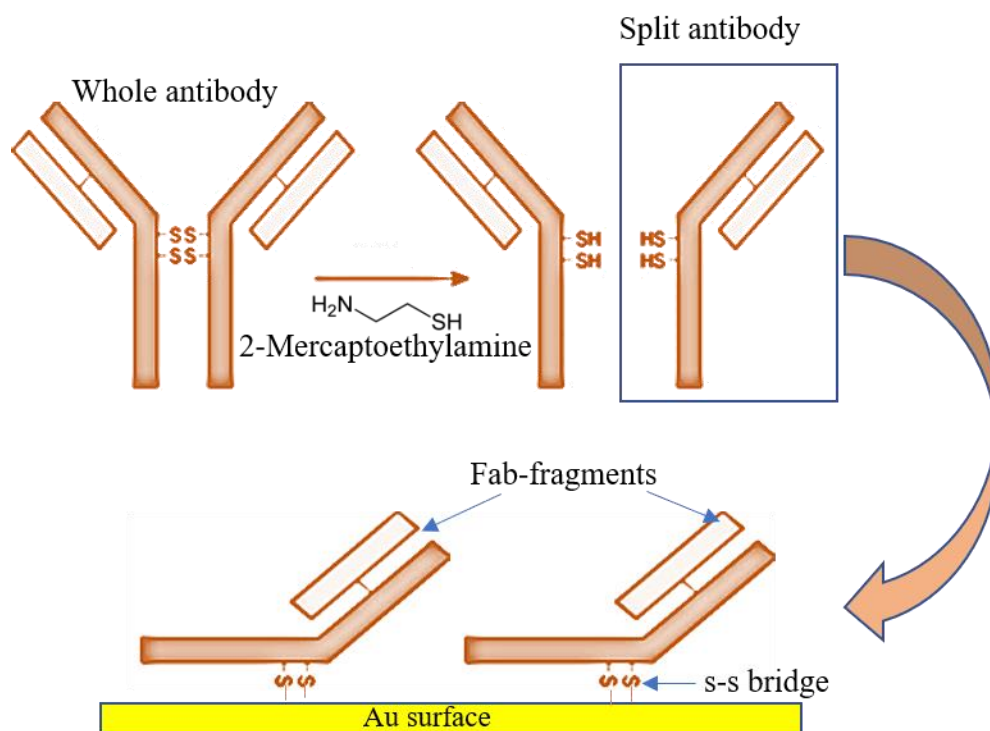


Figure 3.4. The scheme of immobilization of split antibodies on the gold surface via native thiol group

3.2.3 Immobilization of aptamers

A 100 μ M aptamer solution in water was made in 2mM of 1,4-Dithiothreitol diluted in 100mM HEPES buffer (pH 7.4) containing 2mM of MgCl₂; the latter was used to protect aptamers from self-coiling (Rhouati et al., 2013). Before immobilization, the liquid aptamer samples were activated by quick (5 min) heating up to 90 °C followed by 5 min cooling to 4 °C using thermo-cycling PCR unit. Immobilization was carried out by casting aptamer

solution onto gold coated slides as shown in Figure 3.5 the immobilization time was 4 h at room temperature in moist atmosphere. The unreacted oligonucleotide was removed from the gold slides by several rinsing stages with HEPES/MgCl₂ buffer. The immobilized aptamers are prone to self-coiling. In order to prevent that and keep aptamers active, the gold coated glass slides with immobilized aptamers were kept in HEPES/ MgCl₂ buffer. The samples with immobilized aptamers were quite stable and keep their functionality for a few weeks. Interestingly, the old samples with immobilized aptamers could be reactivated by thermocycling in PCR machine.

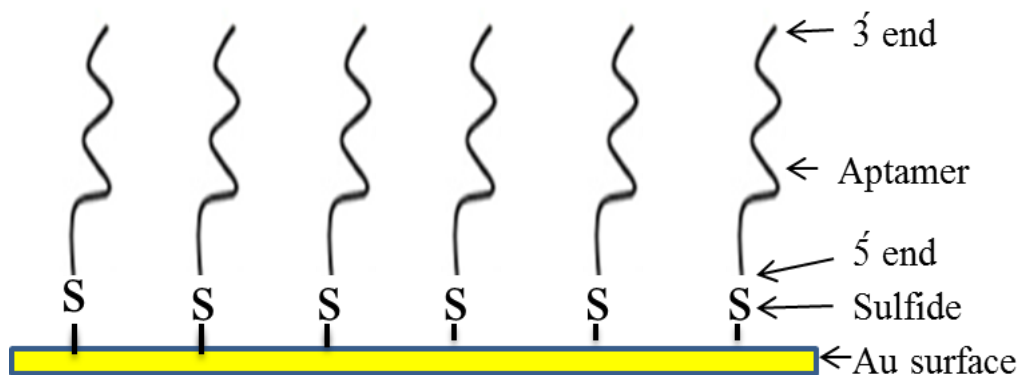


Figure 3.5. Aptamer immobilized on gold surface

3.3 Characterization techniques

The analytical methods used for structural and optical characterization of gold nanostructures are described in this chapter.

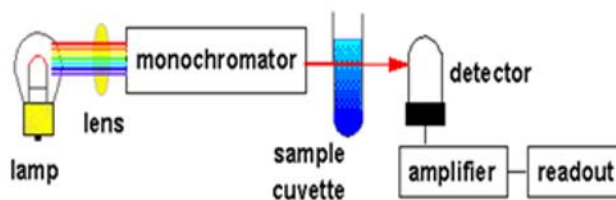
3.3.1 UV-visible absorption spectroscopy

The UV-Visible absorption spectra have been recorded with Varian Carry 50 UV-visible spectrophotometer (shown in Figure 3.6 (a). This spectrophotometer is designed around four fundamental parts: (i) the light source, (ii) monochromator (iii) the sample holder (iv)

the detection system, which makes up the optical section as shown in Figure 3.6(b). Most commercial spectrophotometers cover the spectral range between 190 to 1100 nm and are used to investigate the absorption and transmittance spectra of the studied samples. The UV-Visible spectral region is divided into three sub-regions termed as near UV (185-400 nm), visible (400-700 nm) and near infrared (700-1100 nm). The absorption or attenuation can occur when light passes through a thin film or a translucent liquid sample (Schnabel, 2007).



(a)



(b)

Figure 3.6 (a) UV-visible Carry 50 spectrophotometer; and (b) schematic diagram of UV-visible spectroscopy

All the samples have been measured using clean glass as substrate as well as using quartz cuvette shown in Figure 3.7 for the measurements of liquids of different refractive indices to evaluate refractive index sensitivity (RIS). The reference sample (e.g. glass slide) is measured first in order to obtain the baseline, followed by the measurements of samples of gold films deposited on glass.

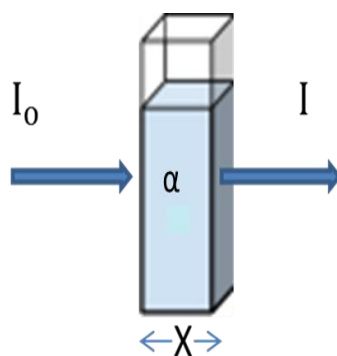


Figure 3.7. Lambert-Beer law for the light travelling through the sample with a thickness (x)

The absorption of light could be expressed in the following formula which is well-known as Lambert-Beer equation (Ingle and Crouch, 1988).

$$I = I_0 e^{-\alpha x} \quad (3.1)$$

where α absorption coefficient and x thickness. As one can see from Figure 3.7, the transmittance (T) is defined as the ratio of the intensity of light exited from sample (I) to the initial intensity (I_0) entering the sample as given by the following equation:

$$T\% = \frac{I}{I_0} \quad (3.2)$$

The absorbance (Abs) can be derived as:

$$\text{Abs} = \log \frac{I_0}{I} \approx \frac{\alpha x}{2.3} \quad (3.3)$$

Therefore, absorption coefficient can be found from Abs value as:

$$\alpha = \frac{2.3 \text{ Abs}}{x} \quad (3.4)$$

UV/Vis spectroscopy is routinely used in analytical chemistry for the quantitative determination of different analytes, such as transition metal ions, highly conjugated organic

compounds, and biological macromolecules. Spectroscopic analysis is commonly carried out in solutions, but solids such as thin gold film in this research also be studied.

According to the Beer-Lambert Law the absorbance is proportional to the concentration of the substance in solution and as a result UV-visible spectroscopy can also be used to measure the concentration of a sample. UV-visible spectrophotometer has been used in the current study to determine the position of the LSPR peak of thin gold film.

3.3.2 Spectroscopic ellipsometry

A commercial M2000 J. A. Woollam Spectroscopic Ellipsometer shown in Figure 3.8 (a) operating in the spectral range of 370–800 nm has been used in the current study to determine thickness (d), refractive index (n) and extinction coefficient (k) of thin film materials. Later in the project, the instrument was upgraded and the spectral range was extended to 1680 nm. The resulted data are represented by two ellipsometry parameters ψ and Δ , related, respectively, to the amplitude ratio and phase shift between the p - and s - components of polarised light (Azzam and Bashara, 1992; Jellison, 1993) as shown in Figure 3.8 (b). In order to determine the thickness of films as well as its optical constants, data fitting is performed on the measured ψ and Δ spectra by solving Fresnel equations many times for different values of refractive index (n) and film thickness (d) and subsequently minimizing the error function of the experimental and theoretical (calculated) values of ψ and Δ using one of least square techniques. The ellipsometry principles and data fitting were explained in detail early in chapter 2.

Commercial WVASE32 and complete EASE software by J.A. Woollam Co. Inc., were used for this task. Data processing requires building an optical model, which corresponds to the sample under investigation. Dielectric functions of some layers (namely: BK7 glass,

gold, water-based buffer) are known and can be selected from the software library (J A Woollam Co. Inc, 2000). Ellipsometry data fitting requires a great deal of experience, and the outcomes depend on the selection of a physically adequate model as well as the choice of initial parameters, fitting routine, limiting the range of variable parameters. In order to achieve reliable results, the fitting procedure needs to be repeated several times (preferably from different initial conditions) until consistent values of thickness (d), refractive index (n) and extinction coefficient (k) are achieved.

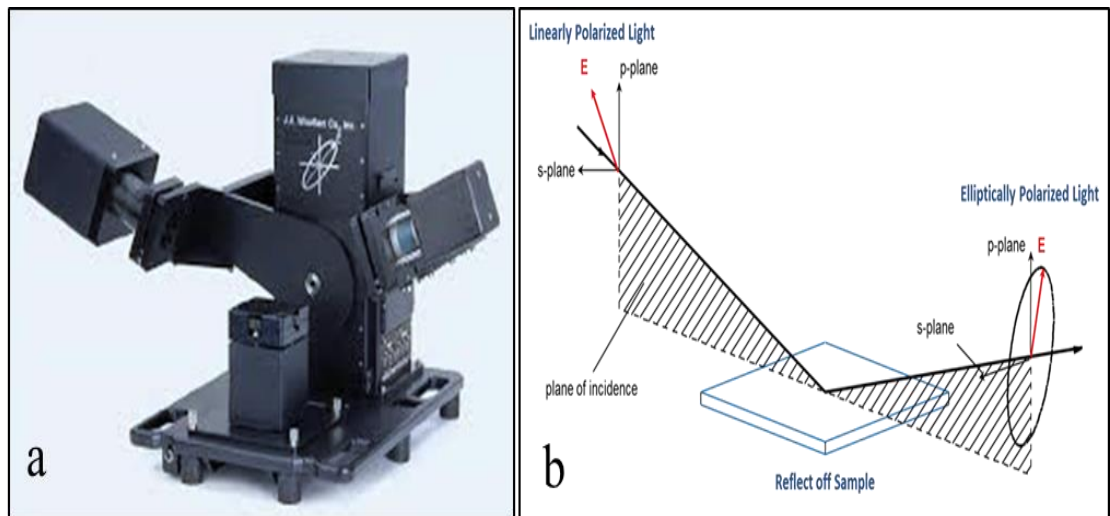


Figure 3.8. (a) J.A. Woollam M2000 Ellipsometer and (b) an illustration of the changes in the polarised light after reflected from the surface

Ellipsometry is primarily used to determine film thickness and optical constants. However, it is also applied to characterize composition, crystallinity, roughness, and other material properties associated with a change in optical response.

3.3.3 Raman spectroscopy

Raman spectroscopy was performed using Raman microscope (Thermo Fisher Scientific DXR2 Raman Microscope) shown in Figure 3.9.



Figure 3.9 Raman spectroscopy unit

The sample is illuminated with a monochromatic laser beam (532 wavelengths), which interacts with the samples' molecules and causes light scattering constituting Raman spectra (Vandenabeele, 2010). Instrumentation for modern Raman spectroscopy consists of three components: an excitation source, a sampling apparatus, and a detector as illustrated schematically in Figure 3.10. Lasers are typically used as a light source because of high intensity and monochromatic nature of light, but not all lasers are suitable for Raman spectroscopy.

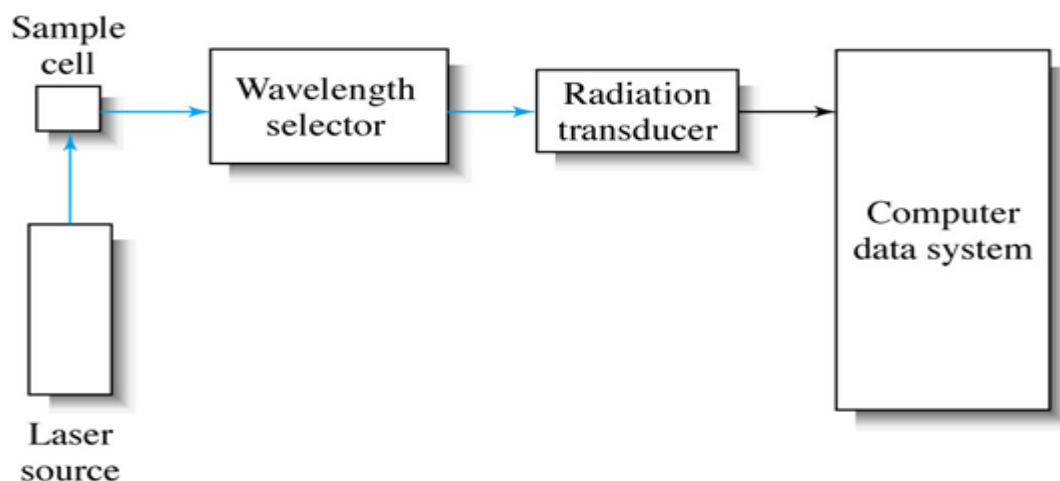


Figure 3.10 The components of Raman spectroscopy

Because the intensity of Raman scattering varies as the fourth power of the frequency, argon and krypton lasers that emit in blue and green region of the spectrum have an advantage over the other sources (Bumbrah et al., 2016). There is also red laser at 630 nm (Le Ru and Etchegoin, 2008). Because the intensity of Raman scattering is usually quite low, surface enhanced Raman scattering was used in our work, where single spectra was used in the current research.

3.3.4 X-ray diffraction (XRD)

The X-ray based analytical methods covers several phenomena based on the scattering, emissions and absorption properties of X-radiation. The most commonly used X-ray technique are X-ray diffraction (XRD), Energy Dispersive X-ray spectroscopy (EDX) and X-ray fluorescence (XRF) spectroscopy. These techniques are used to provide information about the crystal structure and chemical composition and physical properties of materials.

In the current study, XRD has been used to study the structure of thin gold films to analyse their use for bio-sensing application. XRD is a non-destructive technique, which is used to

determine the crystallographic structure, phase and crystallite size of materials. In XRD analysis, the crystalline sample is exposed to the monochromatic radiation (X-ray) generated by cathode ray tube. The incident ray interacts with the sample and produces constructive interference between diffracted rays when conditions satisfy Bragg's law. The Bragg's law states that the constructive interference occurs when the path difference between two interfering waves is equal to the whole number (n) of the wavelength (λ). The Bragg's law is given by the following equation (Cherry and Duxbury, 2009).

$$n\lambda = 2d \sin(\theta) \quad (3.5)$$

where d is the inter-atomic distance (lattice spacing) and θ is the angle between the incident beam and scattering plane. The XRD characteristics generated in the XRD analysis provides useful information about the crystal phases presented in the sample.

Multipurpose X'Pert Philips X-ray diffractometer (MPD), Figure 3.11 (a and b), with Cu-K α X-ray source of the wavelength 1.54 Å and with source voltage and current of 40 kV and 40 mA respectively was used to measure the X-ray diffraction patterns of thin gold films deposited on glass slides. The structure parameters of studied active layers are evaluated by fitting the maximum peaks at 2θ with one Gaussian to estimate the full width at half maximum (FWHM) the d-spacing as well as the peak position with the intensity height. The grain size (D) of the nanocrystalline films was calculated using Scherer equation where β is the FWHM at 2θ (Monshi et al., 2012).

$$D = \frac{0.94 \lambda}{\beta \cos(\theta)} \quad (3.6)$$

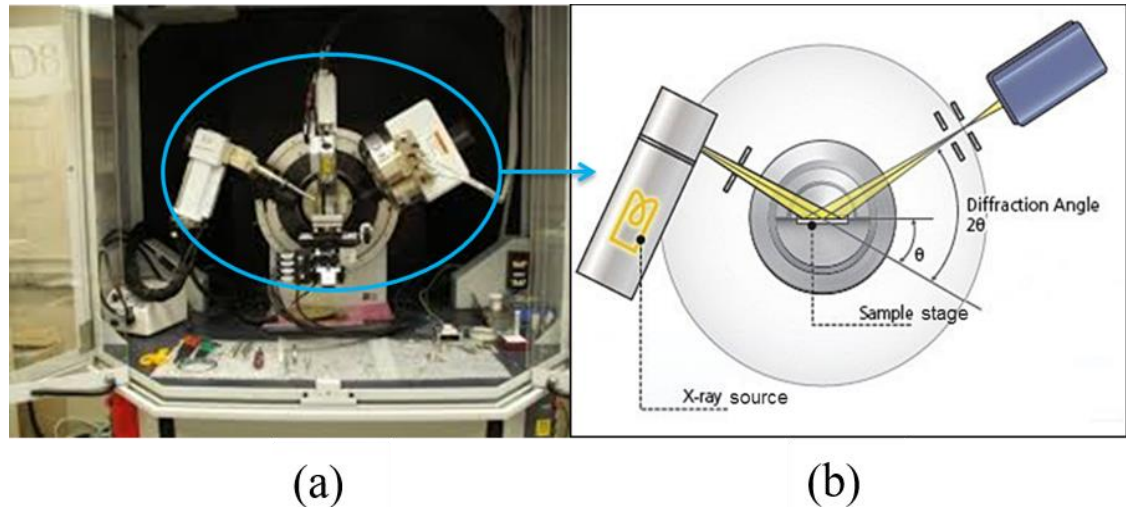


Figure 3.11 (a) XRD instrument and (b) The outline of a diffracted ray utilising X-ray diffraction

XRD used to determine crystallographic structure and to help determining grain size of a crystalline materials. XRD can also be used for the identification of crystalline species in a material.

3.3.5 Scanning electron microscopy (SEM)

Scanning electron microscopy was performed using a FEI-Nova NanoSEM 200 instrument shown in Figure 3.12 (a). The scheme of SEM operation in Figure 3.12 (b) consists of electron gun as an electron source, two condenser lenses, scanning coils, which facilitates the deflection of the electron beam in x and y directions, an objective lens, and detectors for backscattered and secondary electrons.

Electron microscopy is one of the traditional and well-established methods in surface science. SEM operates under vacuum, with a high energy electron beam (typically from 2 to 25kV) focused into a spot down to several tens of nanometers in diameter (Keyse, 1998).

Because of the short wavelength of the electrons used (for example, electrons with the energy of 10^4 eV have wavelength λ_e equal to 0.12 nm) the resolution of SEM is limited by the beam diameter and image distortions, introduced by the focusing system; Modern SEMs are capable of capturing images with nm resolution. In a SEM experiment, the sample is placed in a chamber, which is pumped down to about 10^{-7} mbar. The electron gun, which is usually made of a tungsten filament, heats up to about 2400°C where it starts emitting electrons. These electrons are accelerated along the column by high voltage applied to anodes. A complex electromagnetic system provides both the formation of the electron beam and its scanning over the samples surface. Reflected and scattered electrons are collected by detector to present an image of the specimen (Egerton, 2005).

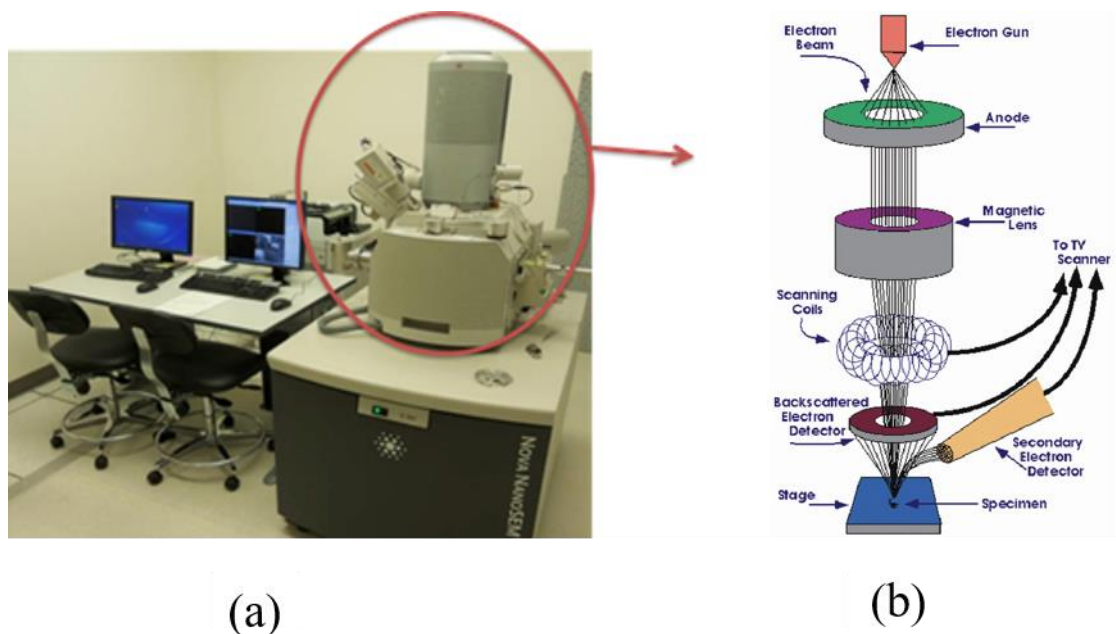


Figure 3.12 (a) FEI-nova NanoSEM 200 Scanning Electron Microscope (SEM) device (b) schematic diagram of SEM

Two imaging modes are available in SEM: secondary electron imaging (SEI) and backscattered electron imaging (BEI) as shown in Figure 3.13(a). In the former, low energy secondary electrons (typically < 50 eV) emitted from the interaction between the incident beam of high energy electrons with the atoms of the sample via inelastic collisions are detected and used to build an image of the surface topography of the sample (see Figure 3.13(b)). Due to the relatively low energies of these secondary electrons, only those from the surface (a very thin layer of tens of nanometres) are able to emerge from the sample. In the case of BEI, the image is derived from scattered or reflected electrons from elastic collisions of the high energy electron beam with the nuclei of the atoms at high angles approaching 180° . The yield of backscattered electrons is a function of atomic number. Heavier elements, i.e. those with a higher atomic number, reflect a greater proportion of electrons and therefore appear brighter, and lighter elements with a low atomic number reflect a lower proportion of electrons and appear darker. The contrast indicates the average atomic number of the elements present within the microstructure and is indicative of the varying elemental compositions (Seiler, 1983), to the surface (10 nm deep at maximum) because of the relatively low energy (50 eV) of secondary electrons.

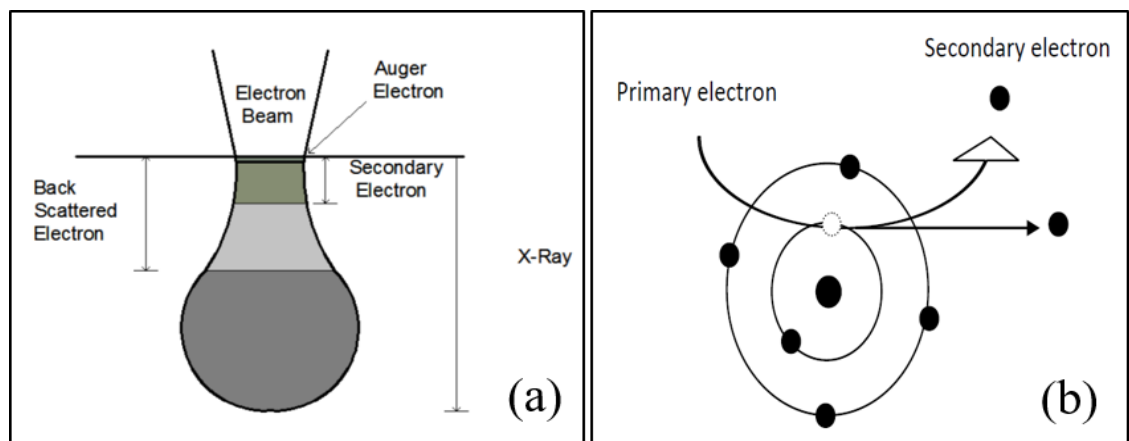


Figure 3.13. Secondary electrons and backscattered electrons (a), and interaction between electron beam and sample producing (b) (Goldstein et al., 2017)

Scanning Electron Microscopy (SEM) is used to determine surface topography, morphology, composition and to estimate dimensions of materials in nanoscale. SEM can be used in a variety of industrial, commercial, and research application in particular

3.3.6 Atomic Force Microscopy (AFM)

AFM was invented in 1986 by Binnig et al. (Binnig et al., 1986). Like all other scanning probe microscopes, AFM utilises a sharp probe moving over the surface of a sample in a raster scan (Puchner and Gaub, 2009). The AFM instrument used in this study is NanoScope IIIa Multimode 8 AFM shown in Figure 3.14(a); the microscope itself rests on an anti-vibration platform, which can be spring suspended on a tripod to reduce the noise. Further the NanoScope IIIa Multimode 8 instrument gives the opportunity to take images of the sample surface with nanometer resolution and to determine their characteristics, such as surface roughness, height and lateral size distributions. Changes in the tip-sample interaction are monitored using an optical cantilever detection system, where a laser beam is reflected back from the cantilever and collected by a position sensitive detector consisting of two closely spaced photodiodes connected to a differential amplifier Figure 3.14 (b).

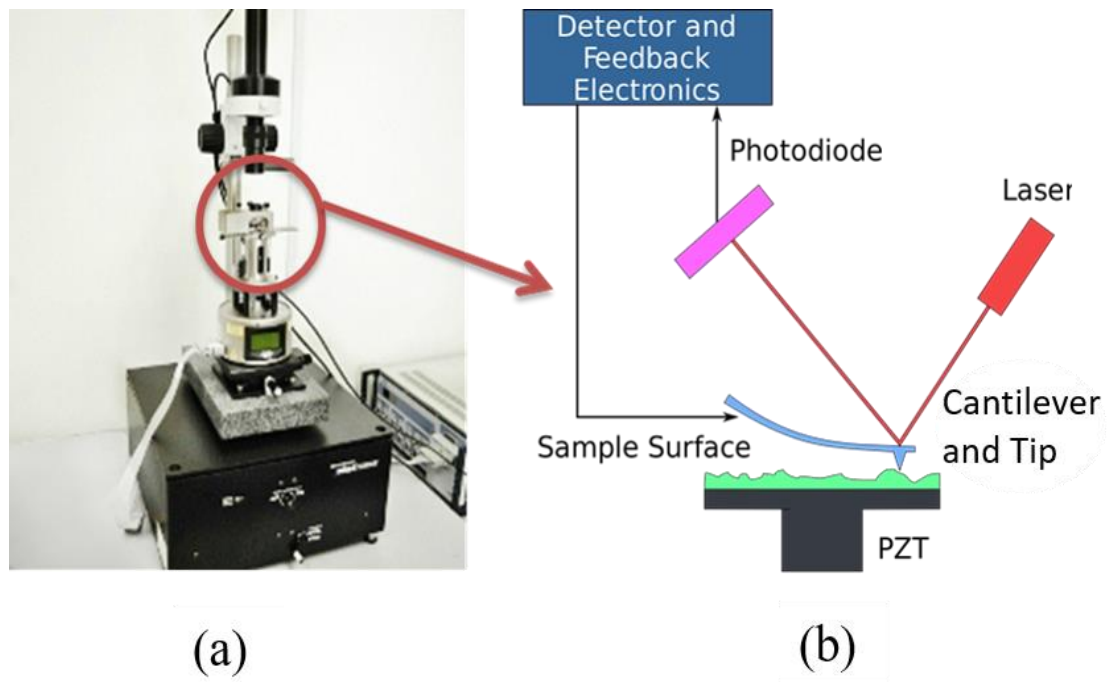


Figure 3.14. (a) NanoScope IIIa Multimode 8 SPM system components (b) Block diagram of atomic-force microscope (AFM)

Three different primary imaging modes are possible depending to the distance (d) between the sample surface and the tip: contact mode (when $d < 0.5$ nm), non-contact mode (0.5 nm $< d < 10$), and tapping mode ($d \sim 0.5$ - 2 nm), as shown in Figure 3.15. In the contact mode, the tip is brought into close contact with the sample surface, the deflection of the cantilever caused by this force is registered with a photodetector, the signal is compared to the predefined value of deflection (force), and the DC feedback system generates a certain voltage applied to the Z-part of the piezo-ceramic to keep the value of deflection (force) constant. This DC voltage measures the surface roughness. The vertical resolution of the AFM contact mode is in the range of 10^{-2} nm, while the lateral resolution could reach the value of less than 1 nm, depending mostly on the tip radius (De Stefanis and Tomlinson, 2001). The disadvantage of the contact mode is that it could damage both the sample and the tip; the tip could leave scratches in the surface of

soft materials, and the tip could be broken on hard rough surfaces (Cappella, and Dietler, 1999). In non-contact mode, the separation of the tip from the sample surface is large distance, that the interaction between the tip and the sample surface is small and mostly in the range of the damping forces in ambient conditions. Therefore, the non-contact mode is appropriate for fast sweep measurements. In tapping mode, the cantilever oscillates, and the tip slightly taps the surface during scanning. Thus, the surface is less damaged than in the case of contact mode while the lateral forces are eliminated. The feedback loop maintains constant oscillation amplitude by maintaining a constant tip-sample interaction during the scan (Schmitz et al., 1997).

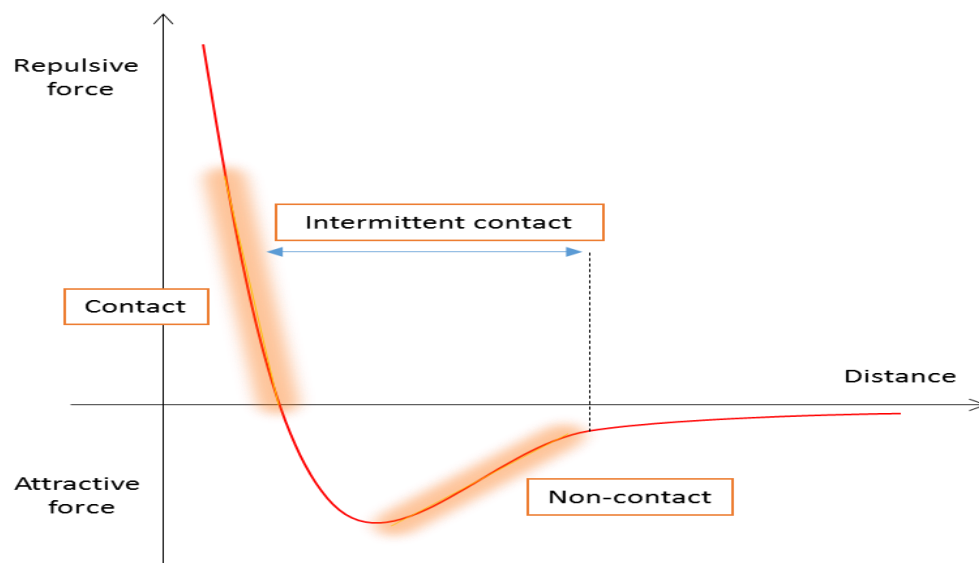


Figure 3.15. Van der Waals force against distance

On the other hand, tapping mode tends to be more applicable to general imaging in air, particularly for soft surfaces, as the resolution is similar to or even better than contact mode, while the forces applied to the sample is lower. In fact, the only disadvantage of

tapping mode is that the scan speed is slightly slower than in contact mode and the AFM operation is a bit more complex (Tsargorodska, 2007). In this work we used non-contact mode to scan our samples.

For the AFM image analysis, software provided with this system (NanoScope An analysis 1.50) has been used to analyse the cross-section, roughness, particle size, etc., and creates virtual 2D and 3D images of the sample surface.

Atomic force microscopy (AFM) is applied in nanotechnology applications where for instance, imaging of polymers and lateral dimensions of nanostructures can be obtained.

Reference list

- Azzam, R.M. A. and Bashara, N.M. (1992). Ellipsometry and polarized light, North Holland, Amsterdam.
- Binnig, G., Quate, C.F. and Gerber, C. (1986). Atomic force microscope, *Physical review letters*, 56(9), p.930.
- Bumbrah, G. S., & Sharma, R. M. (2016). Raman spectroscopy–Basic principle, instrumentation and selected applications for the characterization of drugs of abuse. *Egyptian Journal of Forensic Sciences*, 6(3), 209-215.
- Cappella, B. and Dietler, G. (1999). Force-distance curves by atomic force microscopy, *Surface science reports*, 34(1), pp.1-104.
- Cherry, P., & Duxbury, A. (Eds.). (2009). Practical radiotherapy: Physics and equipment. John Wiley & Sons.
- De Stefanis, A., & Tomlinson, A. A. (2001). Scanning Probe Microscopies: From Surface Structure to Nano-scale Engineering. Trans Tech Publications.
- Egerton, R. F. (2005). Physical principles of electron microscopy: an introduction to TEM, SEM, and AEM. Springer Science & Business Media.
- Goldstein, J. I., Newbury, D. E., Michael, J. R., Ritchie, N. W., Scott, J. H. J., & Joy, D. C. (2017). *Scanning electron microscopy and X-ray microanalysis*. Springer.
- Ingle Jr, J. D., & Crouch, S. R. (1988). Spectrochemical analysis J A Woollam Co. Inc, Guide to using WVASE32, Software for Spectroscopic Ellipsometry Data Acquisition and Analysis. New York: Wex Tech Systems Inc., 2001.
- Jellison Jr, G. E. (1993). Data analysis for spectroscopic ellipsometry. *Thin Solid Films*, 234(1-2), 416-422.
- Karakouz, T., Holder, D., Goomanovsky, M., Vaskevich, A., & Rubinstein, I. (2009). Morphology and refractive index sensitivity of gold island films. *Chemistry of Materials*, 21(24), 5875-5885.
- Karakouz, T., Tesler, A. B., Bendikov, T. A., Vaskevich, A., & Rubinstein, I. (2008). Highly stable localized plasmon transducers obtained by thermal embedding of gold island films on glass. *Advanced Materials*, 20(20), 3893-3899.
- Karyakin, A. A., Presnova, G. V., Rubtsova, M. Y., & Egorov, A. M. (2000). Oriented immobilization of antibodies onto the gold surfaces via their native thiol groups. *Analytical chemistry*, 72(16), 3805-3811.
- Keyse, R.J. (1998). Introduction to scanning transmission electron microscopy. *BIOS Scientific Publishers in association with the Royal Microscopical Society*.
- Le Ru, E., & Etchegoin, P. (2008). Principles of Surface-Enhanced Raman Spectroscopy: and related plasmonic effects. Elsevier.

- Mahan, J. E. (2000). Physical vapor deposition of thin films. *Physical Vapor Deposition of Thin Films*, by John E. Mahan, pp. 336. ISBN 0-471-33001-9. Wiley-VCH, January 2000., 336.
- Monshi, A., Foroughi, M. R., & Monshi, M. R. (2012). Modified Scherrer equation to estimate more accurately nano-crystallite size using XRD. *World Journal of Nano Science and Engineering*, 2(03), 154.
- Nabok, A., Tsargorodskaya, A., Mustafa, M. K., Székács, A., Székács, I., & Starodub, N. F. (2009). Detection of low molecular weight toxins using optical phase detection techniques. *Procedia Chemistry*, 1(1), 1491-1494.
- Puchner, E. M., & Gaub, H. E. (2009). Force and function: probing proteins with AFM-based force spectroscopy. *Current opinion in structural biology*, 19(5), 605-614.
- Rhouati, A., Yang, C., Hayat, A., & Marty, J. L. (2013). Aptamers: A promising tool for ochratoxin A detection in food analysis. *Toxins*, 5(11), 1988-2008.
- Schmitz, I., Schreiner, M., Friedbacher, G., & Grasserbauer, M. (1997). Tapping-mode AFM in comparison to contact-mode AFM as a tool for in situ investigations of surface reactions with reference to glass corrosion. *Analytical chemistry*, 69(6), 1012-1018.
- Schnabel, W. (2007). *Polymers and Light: Fundamentals and Technical Applications*, Wiley-VCH, Weinheim.
- Seiler, H. (1983). Secondary electron emission in the scanning electron microscope. *Journal of Applied Physics*, 54(11), R1-R18.
- Starodub, N. F., Nabok, A. V., Starodub, V. M., Ray, A. K., & Hassan, A. K. (2001). Immobilization of biocomponents for immune optical sensors. *Ukrains'kyi biokhimichnyi zhurnal* (1999), 73(4), 55-64.
- Tesler, A. B., Maoz, B. M., Feldman, Y., Vaskevich, A., & Rubinstein, I. (2013). Solid-state thermal dewetting of just-percolated gold films evaporated on glass: development of the morphology and optical properties. *The Journal of Physical Chemistry C*, 117(21), 11337-11346.
- Tesler, A. B., Chuntunov, L., Karakouz, T., Bendikov, T. A., Haran, G., Vaskevich, A., & Rubinstein, I. (2011). Tunable localized plasmon transducers prepared by thermal dewetting of percolated evaporated gold films. *The Journal of Physical Chemistry C*, 115(50), 24642-24652.
- Tsargorodska, A., & Sheffield Hallam University. (2007). *Research and Development in Optical Biosensors for Determination of Toxic Environment Pollutants*.
- Vandenabeele, P. (2010). Raman spectroscopy, *Analytical and Bioanalytical Chemistry*. (397)2629-2630.

Chapter 4: Characterization of gold nanostructures and development of LSPR/TIRE method for biosensing

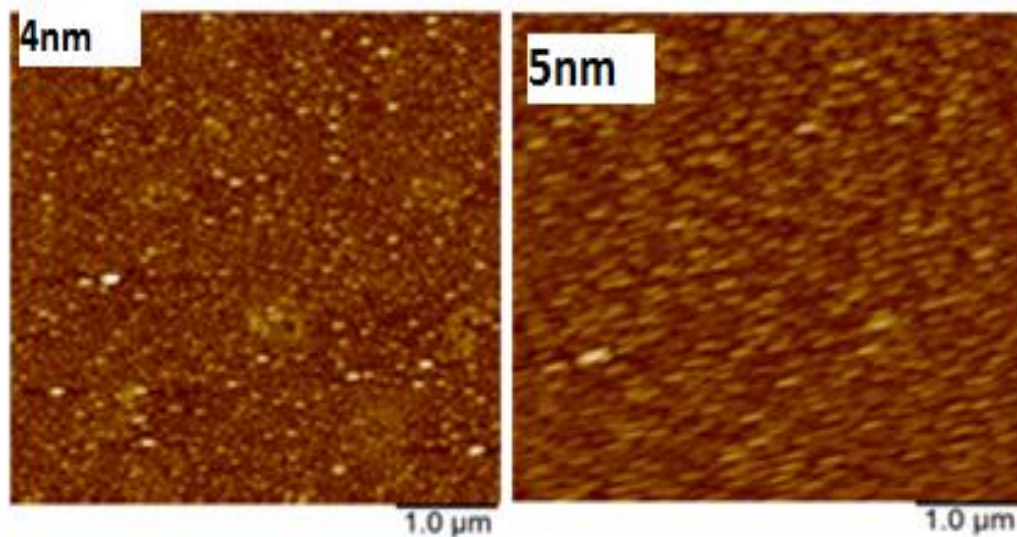
4.1 Introduction

This chapter describes the development of optical biosensing method based on the LSPR phenomenon in nano-structured gold films suitable for detection of mycotoxins. A simple technology of annealing thin gold films was utilized for the formation of gold nano-islands exhibiting the LSPR effect. The morphology of gold nano-structures produced was studied with SEM and AFM while their optical properties were analysed with UV-vis absorption spectroscopy and spectroscopic ellipsometry (SE). A blue spectral shift of LSPR band caused by changes in the refractive index of medium constitutes the main principle of LSPR sensing. The refractive index sensitivity of Uv. visible absorption and (SE) were evaluated and compared. It appeared that spectroscopic ellipsometry (SE) is more sensitive, therefore the method of total internal reflection ellipsometry was chosen for further biosensing experiments. However, our initial attempt of using LSPR/TIRE combination for detection of aflatoxin B1 in direct immunoassay with specific antibodies electrostatically immobilized on the surface of Au nano-islands were not successful. The LDL was 2 orders of magnitude lower than that in our traditional TIRE biosensing using continuous 25nm thick Au layers (Nabok et al., 2011a). That lead to furthermore detailed study of LSPR limitation caused by short evanescent field decay length of gold nanostructures.

4.2 Fabrication and characterization of gold nano-islands.

4.2.1 SEM and AFM study

The samples of nanostructured gold produced were characterized with SEM (FEI-Nova, NanoSEM 200) and AFM (Nanoscope IIIa). As shown in AFM and SEM images in Figure 4.1 and Figure 4.2 respectively of the samples of Cr/Au thin gold films of different nominal thicknesses annealed at 480 °C for 2 hours formed well-defined Au nano-islands. Scanning Electron Microscopy images of Au island films of different nominal thicknesses, prepared as described in methodology section 3.2, are presented in Figure 4.2.



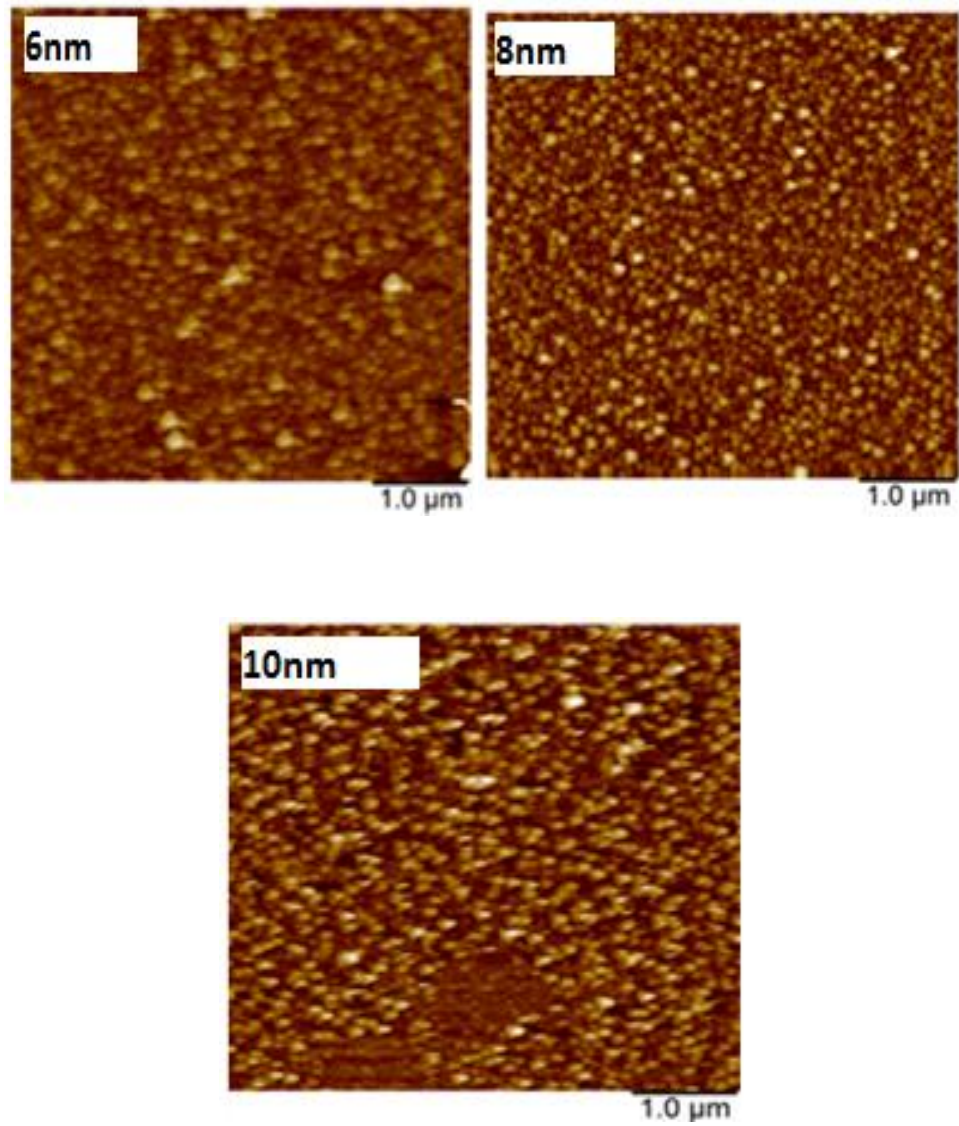


Figure 4.1 AFM images of nano-structured Au films with different nominal thickness

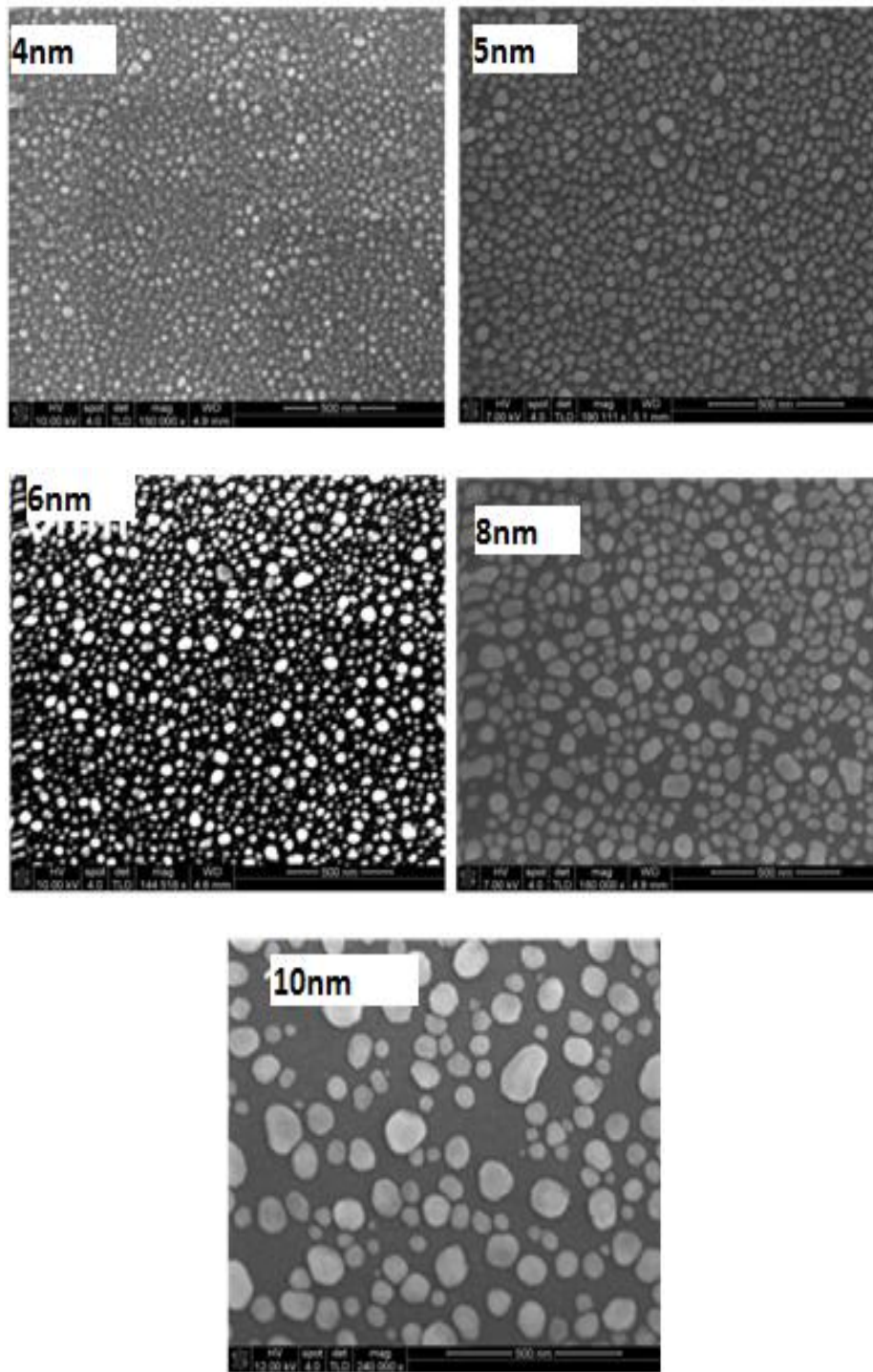
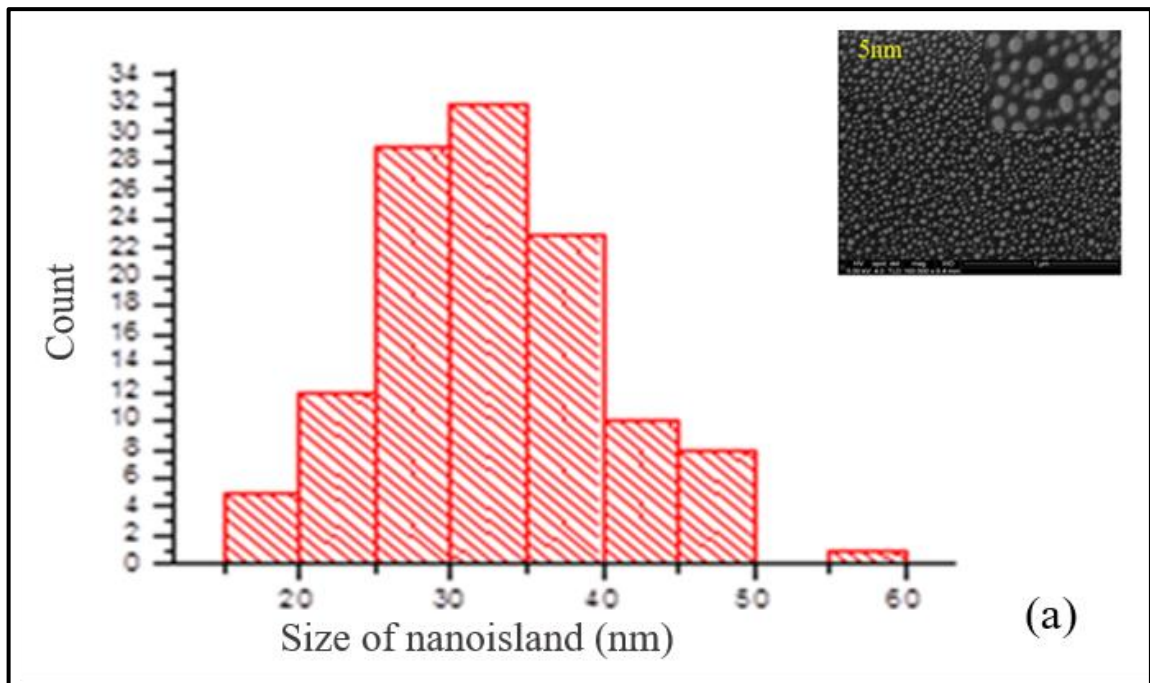
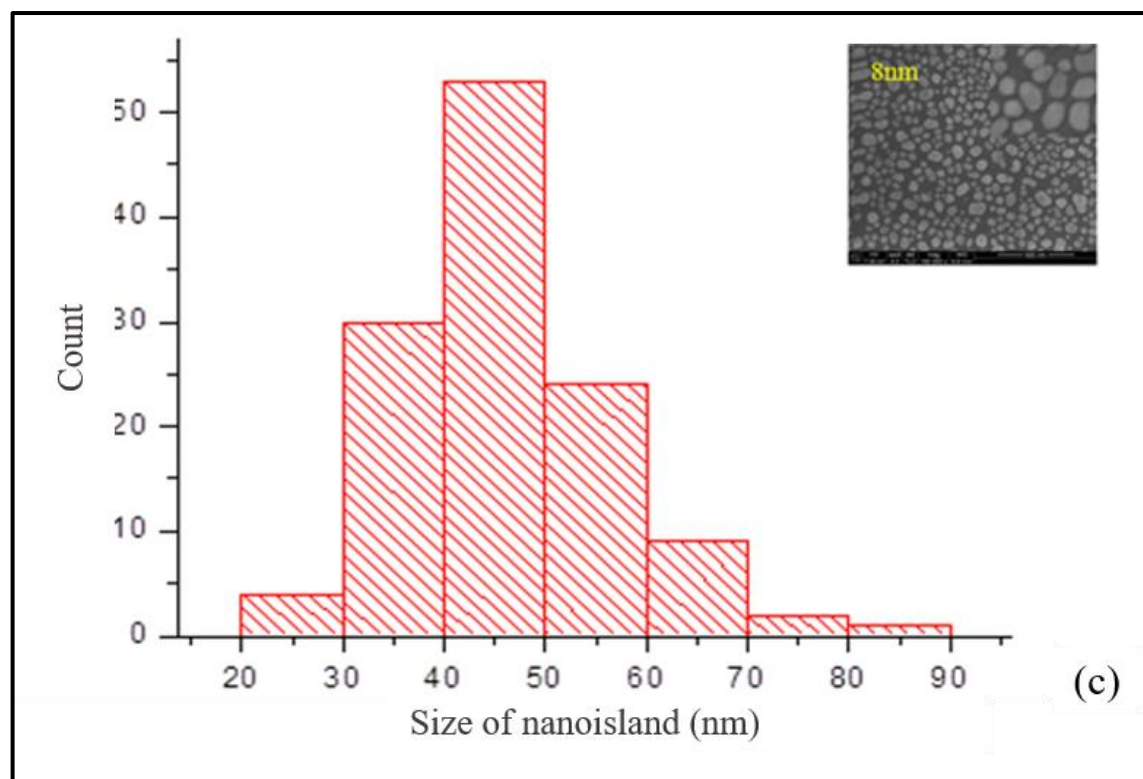
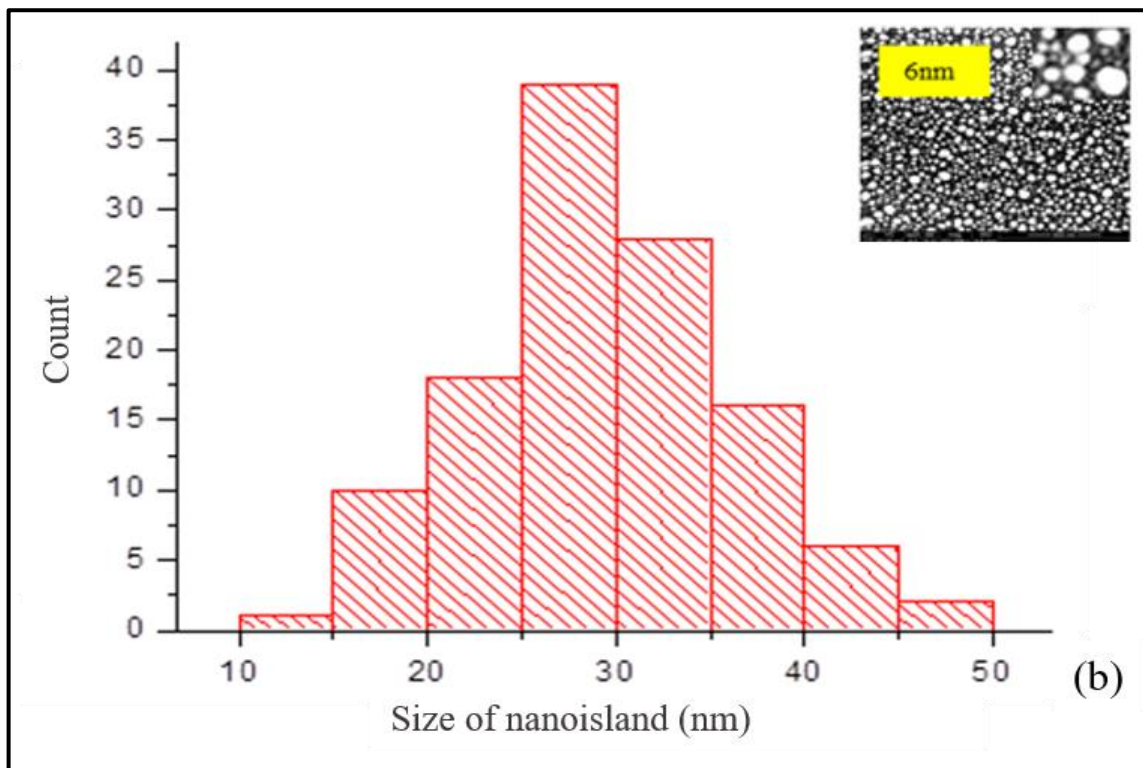


Figure 4.2 SEM images of Au nano-structured films with different nominal thickness prepared by thermal evaporation and annealing for 2 hours at 480°C (scale of SEM images is 500nm)

The distribution of equivalent diameter as shown in Figure 4.3 (a, b, c and d) calculated from average size of the nano-islands, shows a continuous increase in the average island dimensions with increase of nominal thickness.

Variation of the average island size influences the refractive index sensitivity and plasmon decay length of the island films, which determine the analytical volume and sensitivity of the LSPR transducers.





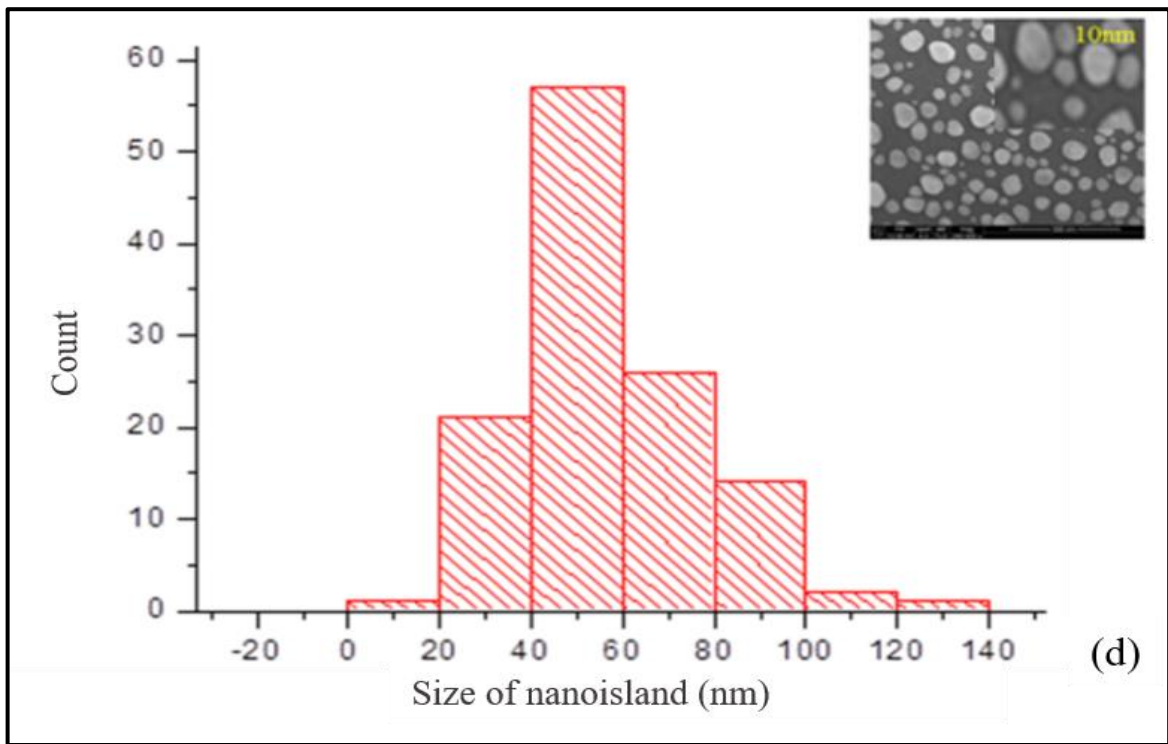


Figure 4.3. Distribution of equivalent diameters of Au/Cr island films of different nominal thicknesses: (a) 5nm, (b) 6nm, (C) 8 and (d)10 nm

Improved adhesion of the Au islands to the glass substrate was achieved using a high annealing temperature of 550 °C close to the temperature of softening of glass and longer annealing time (10 hours) (Au without Cr underlayer).

Au nano-islands formed at higher temperatures are larger than those annealed at lower temperature and shorter time (Karakouz et al., 2008b). Furthermore, they are partially embedded into the glass matrix as was shown by Tesler et al., 2013 which may provide better stability of nano-structured gold films in biosensing experiments (Karakouz et al., 2008a).

The analysis of AFM images for all samples studied given in Table 4.1 showed gradual increase in both the average diameter and average thickness of gold nano-islands with the increase in the nominal thickness of Au films.

Table 4.1 AFM image analysis of gold nano-structures made from Cr of 3 nm and Au films of different nominal thickness annealed at 480 °C for 2 hours.

Nominal Au film thickness	5 nm	6 nm	8 nm	10 nm
Island height (nm)	12.2 ± 2.3	9.6 ± 2.5	13.9 ± 2.4	34.1 ± 6.6
Island diameter (nm)	35.0 ± 12.0	71.7 ± 12.6	68.2 ± 10.7	90.9 ± 25.0

Table 4.2 AFM image analysis of gold nano-structures made of different thickness annealed at 550C for 10 hours.

Nominal Au film thickness	5 nm	6 nm	8 nm	10 nm
Island height (nm)	12.2 ± 1.26	12.27 ± 1.3	13.9 ± 1.4	19.45 ± 1.9
Island diameter (nm)	56.15 ± 5.6	79.3 ± 7.9	92.98 ± 9.3	126 ± 12.6

As an example, Figure 4.4a shows AFM image of Au film of 5nm nano-island and Figure 4.4b the histogram of height distribution obtained by analysis of that AFM image.

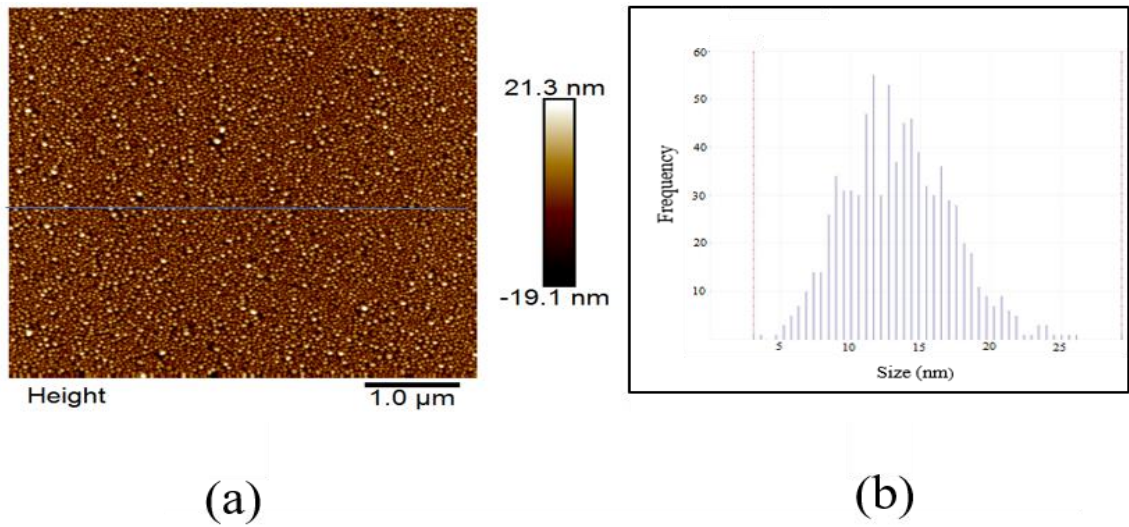


Figure 4.4 (a) AFM image of Cr 3nm/5nm gold nanostructure (b) histogram of height distribution of gold nano-islands

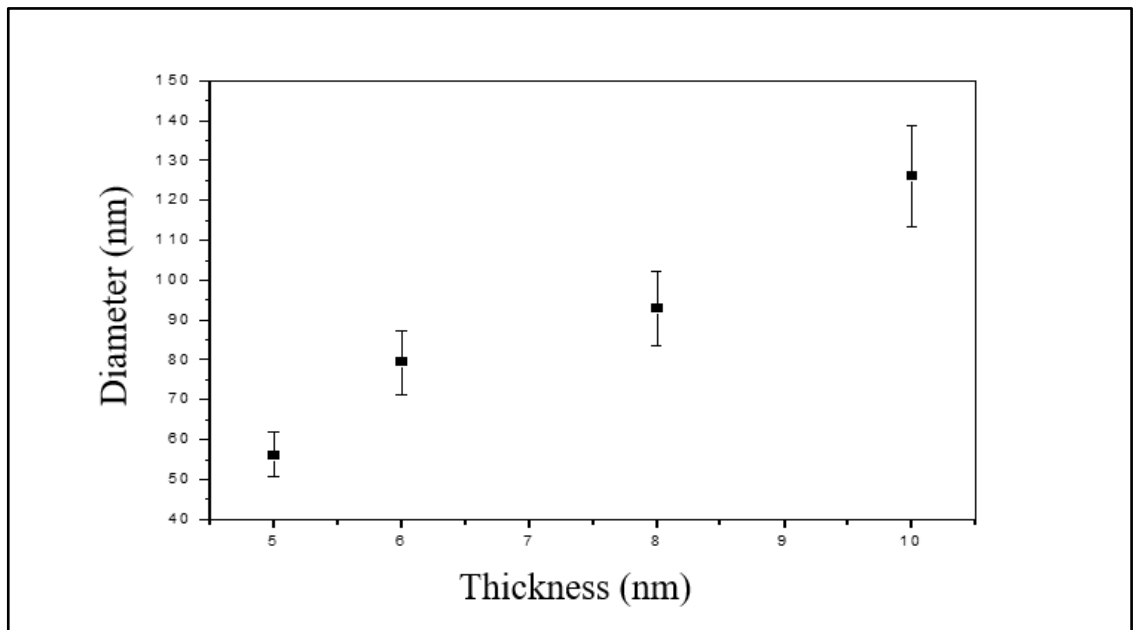


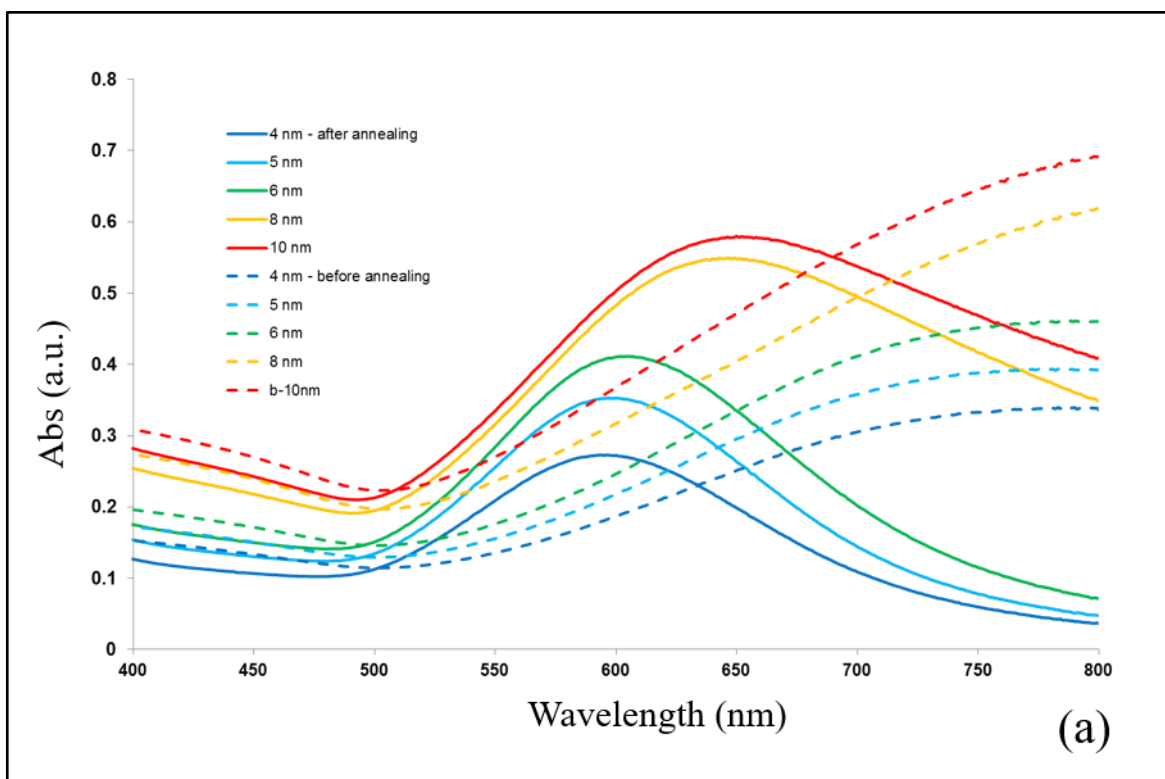
Figure 4.5 The dependence of Au islands diameter versus initial film thickness obtained by AFM data particle analysis (with Cr film of 3 nm thickness)

Figure 4.5 illustrate the dependence of the average diameter of Au nano-island on the initial film thickness. These data obtained by analysis of AFM images show the gradual increase of the diameter with thickness increase.

4.3 Optical study

4.3.1 UV-vis spectroscopy

UV-vis absorption spectra in Fig. 4.6. show a dramatic transition from classical Drude dispersion spectra for continuous (as deposited) gold films to distinctive LSPR band at around 600 nm for gold nano-islands as a result of thermal annealing. The position of LSPR band shifts to higher wavelength with the increase in the mean size of Au nano islands which correlate with nominal film thickness.



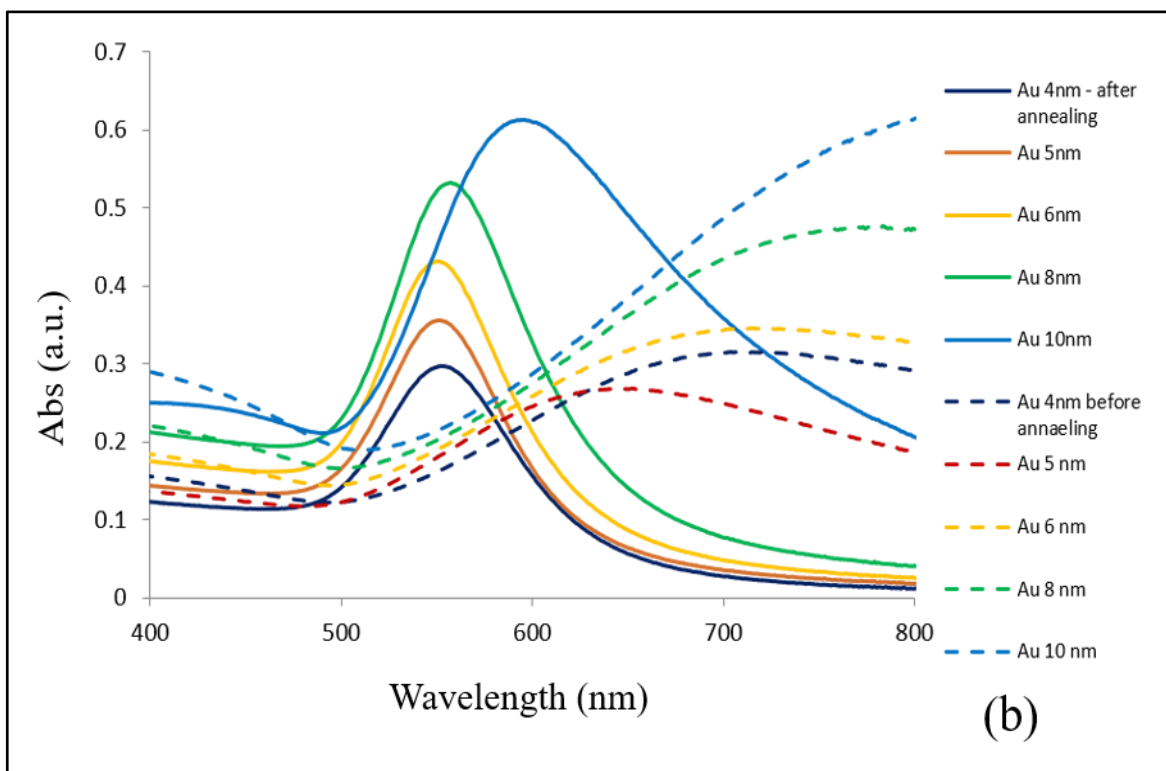


Figure 4.6. UV-vis absorption spectra of Au thin films of different thicknesses before (dotted lines) and after (solid lines) (a) thermal annealing (with Cr), (b) Microwave annealing

The UV-vis absorption spectra of annealed thin Au films showed a pronounced LSPR peak in the middle of visible spectral range position of which is gradually shifted to high wavelength upon increasing in the nominal film thickness. More detailed study of optical properties of nano-structured Au films was carried out using spectroscopic ellipsometry.

4.3.2 Spectroscopic ellipsometry

Typical ellipsometry spectra of gold nano-structures produced are shown in Figure 4.7. Ψ spectra resemble SPR curves with the minima corresponding to plasmon resonance, while Δ spectra have a characteristic drop of phase near plasmon resonance.

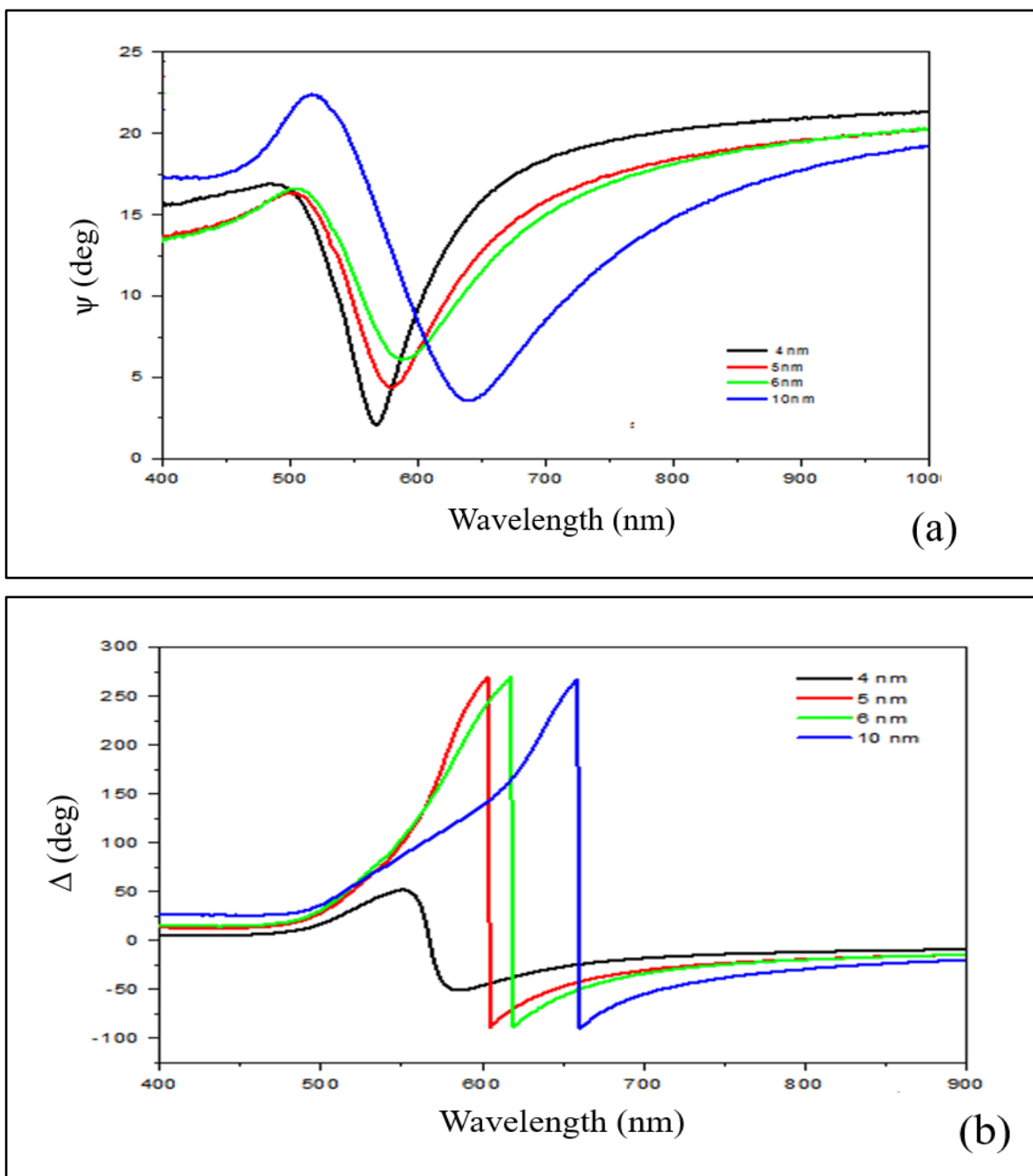


Figure 4.7. Spectroscopic ellipsometry spectra of a series of gold nano-structures made from different nominal films thicknesses (with Cr /annealed using oven): (a) Ψ spectra; (b) Δ spectra

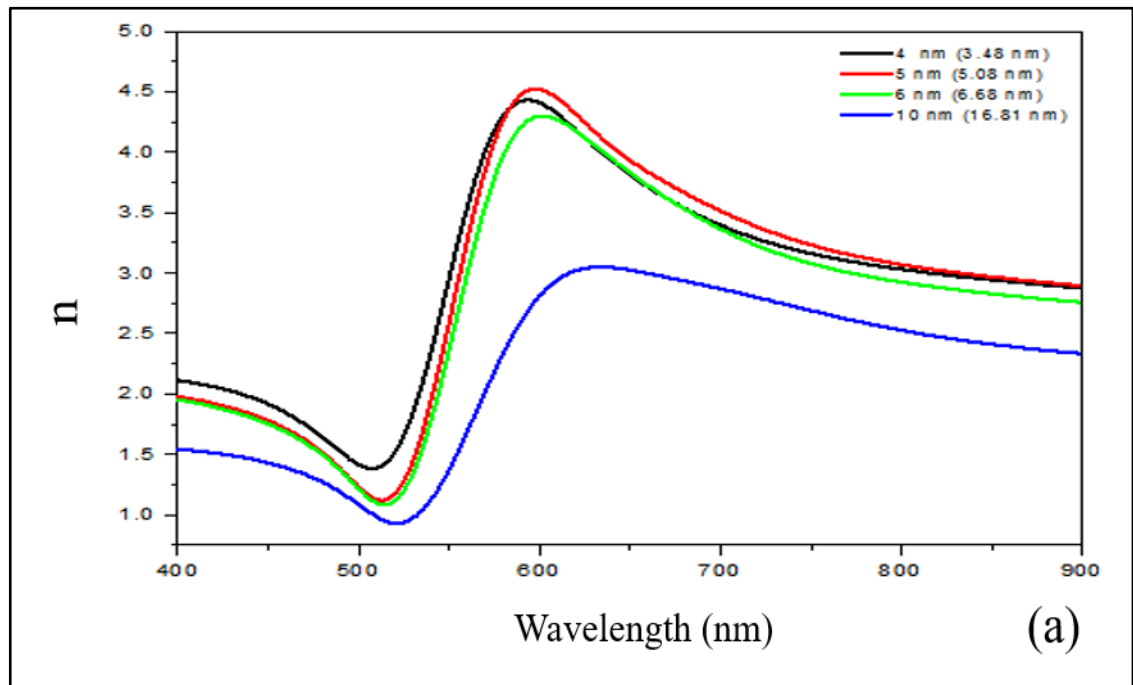
Ellipsometry data fitting was carried out using J.A. Woollam Complete Ease software. The nanostructured gold film was modelled by a combination of Drude dispersion function and three additional Gaussian oscillators, two of them were very close to each other in their energy around 2 eV and most likely correspond to quantization of plasmons in two lateral directions (x, y) of Au nano-island, while the third one around 5 eV may correspond to plasmon quantization in vertical direction (z).

Table 4.3. The results of ellipsometry data fitting

Nominal thickness	4 nm	5 nm	6 nm	10 nm
Fitted thickness	3.48 nm	5.18 nm	6.87 nm	16.34 nm
Amp2	13.398	19.07	16.22	7.38
Br2(eV)	0.216	0.222	0.225	0.263
En2 (eV)	2.197	2.179	2.175	2.121
Amp3	7.615	8.305	8.215	6.004
Br3(eV)	7.183	11.908	13.968	10.443
En3(eV)	5.174	4.309	6.039	1.778
Amp4	6.999	4.762	5.093	3.818
Br4(eV)	0.362	0.333	0.307	0.397
En4(eV)	2.145	2.032	2.034	1.960

The resulted values of the nanostructured gold films as well as the parameters of oscillators for different nominal films thicknesses of Au films are also given in Table 4.3. The values of actual film thickness, which is the average of the thickness of nano-islands and the empty space between them, correlate reasonably well to the nominal thickness of Au films.

Here Amp is the amplitude, E_n is the energy or position of Gaussian peak, and Br is the broadening. The dispersion characteristics of refractive index (n) and extinction coefficient (k) obtained values by ellipsometry data fitting are given in Figure 4.8. The resulted spectra of n and k are Kramers - Kronig consistent, e.g. peaks on k -spectra, which correspond to LSPR, coincide with the largest gradient on n -spectra. The inset in Fig. 4.8b shows linear increase in the LSPR position against the actual gold film thickness. The LSPR peak positions are very close to those found with UV-vis absorption spectroscopy.



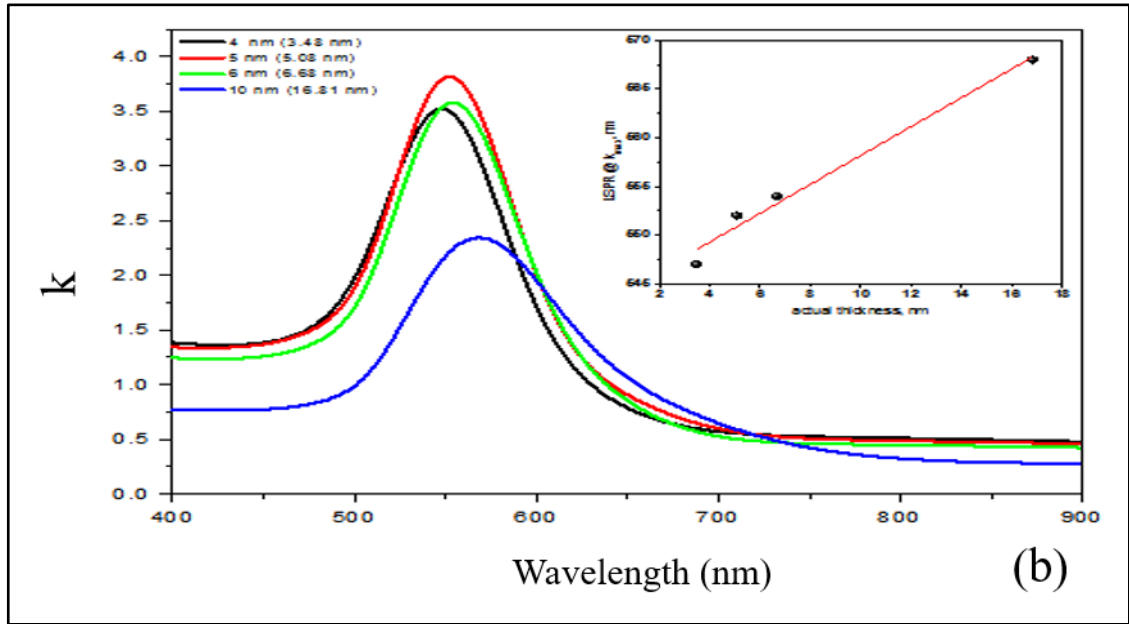


Figure 4.8. Dispersion characteristics of n (a) and k (b) obtained by ellipsometry data fitting. Inset shows the dependence of the position of LSPR peak on the actual gold film thickness. Both UV-vis absorption spectroscopy and spectroscopic ellipsometry show features associated with LSPR.

4.4 Comparison between thermal and microwave annealing

Instead of traditional technology of thermal annealing of thin gold films for making nano-islands by de-wetting process (Karakouz et al., 2008), we attempted using microwave traditional oven for annealing gold film. This is a great alternative to a long (10 hours) thermal annealing, since the microwave annealing gives similar results in just few minutes (Tsuji et al., 2005; Hsu et al., 2009; Zhang et al., 2010; Panagiotopoulou et al., 2015). Comparison of the structural and optical properties of gold nano-islands formed by both thermal and microwave annealing was carried out using AFM, SEM, XRD, UV-vis absorption spectroscopy and ellipsometry.

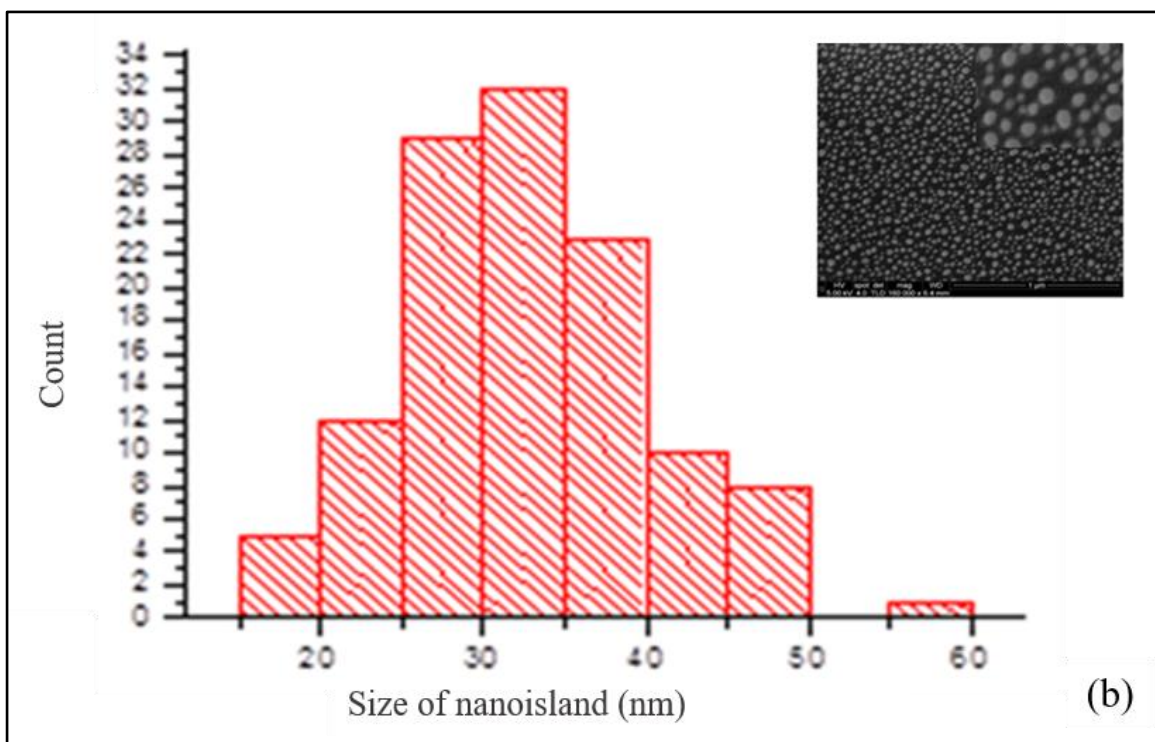
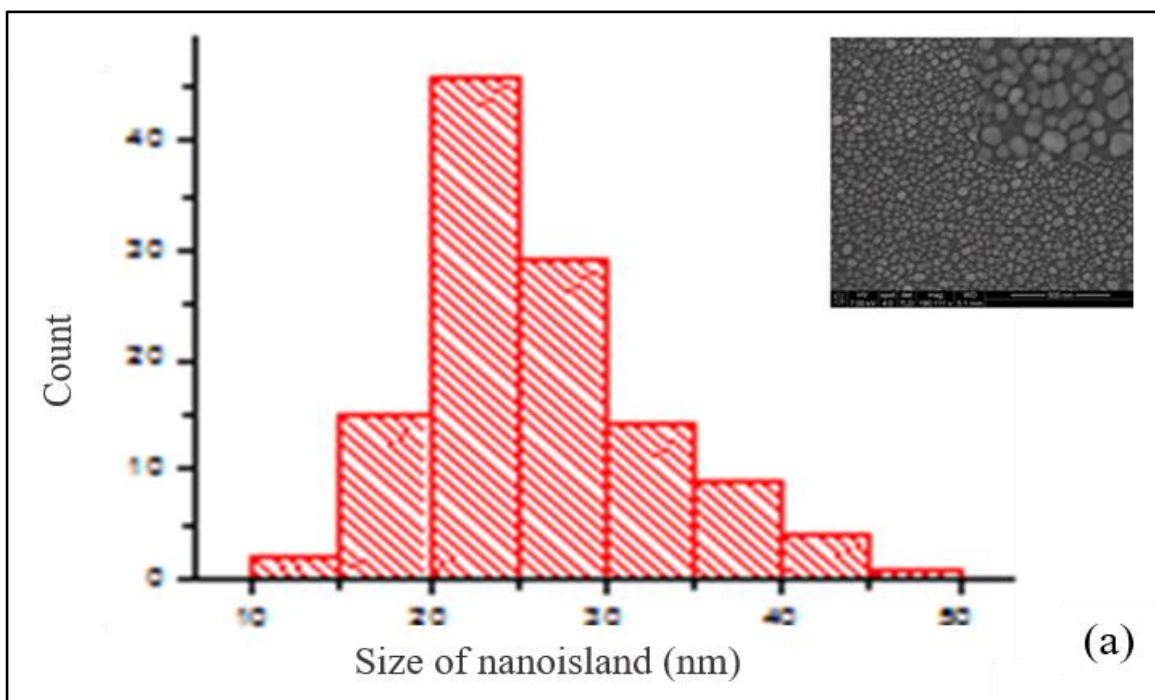


Figure 4.9 SEM images and their analysis for gold films: annealed using microwave (a) and oven (b)

Figure 4.9 shows typical SEM images along with statistical analysis of nano-islands produced by annealing of 5 nm thick gold film in microwave (Figure 4.9(a)) and in

conventional oven (Figure 4.9(b)). Au nano-islands obtained in microwave appeared to have slightly larger size (such as 5nm thick) and more narrow size-dispersion as compared to those produced in the oven. Also, the islands made in microwave are slightly faceted which indicate their better crystallographic ordering.

4.4.1 XRD study of gold nanostructures

Crystallography of gold nano-islands prepared by microwave annealing of evaporated thin gold films was studied with XRD. Figure 4.10 shows XRD pattern with characteristics peaks corresponding to Au (111). The size of Au nano-crystals evaluated by analysis of XRD data are summarized in Table 4.4, which confirm the larger crystallite sizes for microwave annealed Au films.

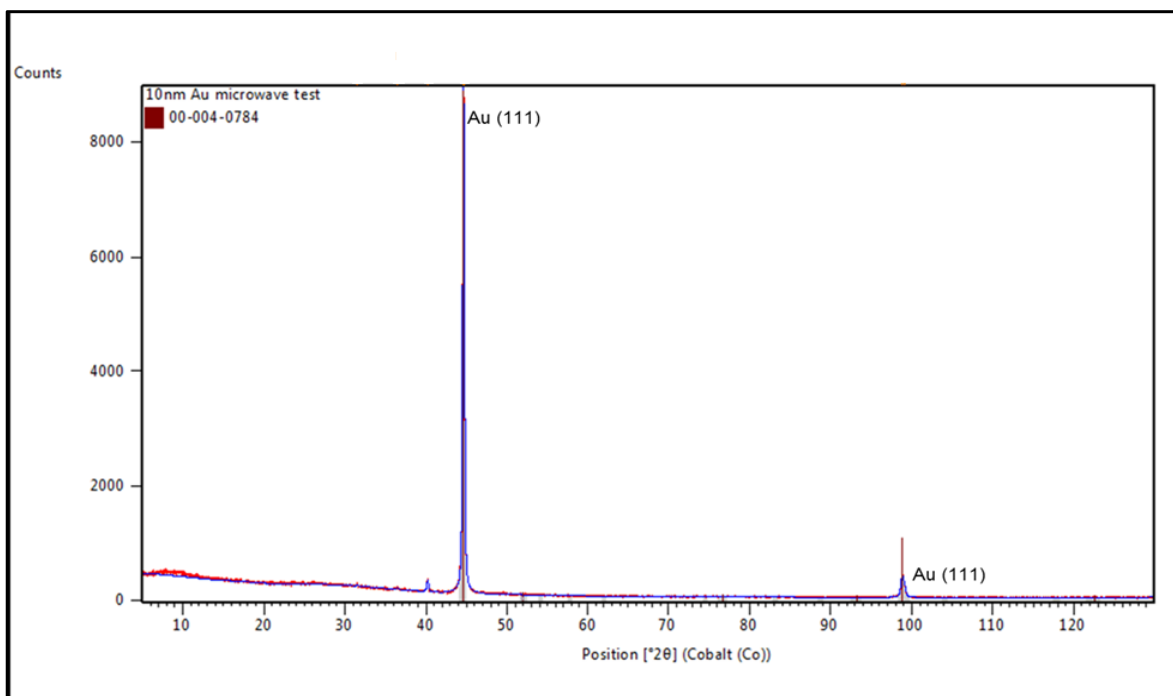


Figure 4.10. XRD pattern of Au 10 nm film annealed in microwave

Table 4.4 XRD data of the size of Au nan -crystals evaluated by XRD analysis

Nominal Au film thickness	Peak pos. [$^{\circ}2\theta$]	B obs. [$^{\circ}2\theta$] $\beta = \text{FUHM}$	Crystallite size [nm]
10nm Au microwave	44.596	0.162	61.4725
10nm Au oven	44.581	0.192	51.9017
8nm Au microwave	44.459	0.285	34.9928
8nm Au oven	44.565	0.358	27.8718
6nm Au microwave	44.589	0.387	25.7971
6nm Au oven	44.574	0.384	25.9908
5nm Au microwave	44.581	0.440	22.6855
5nm Au oven	44.584	0.473	21.0702
4nm Au microwave	44.532	0.526	18.9408
4nm Au oven	44.540	0.682	14.6192

4.4.2 UV-vis absorption spectroscopy

UV-vis spectra of gold nanostructures were recorded using UV-vis absorption spectrophotometer (Cary 50, Varian). Typical spectra in Figure 4.11(a) exhibit an LSPR absorption band in the visible spectral range after annealing. The microwave annealing gives red-shifted LSPR bands similar to thermal annealing with larger crystallite size in some thicknesses, the position of LSPR is gradually shifted to high wavelengths upon increasing the Au crystallite size from 18.9 nm to 61.4 nm (see data in Table 4.3) as clearly illustrated in Figure 4.11(b). The nanostructures formed by microwave annealing were also studied with spectroscopic ellipsometry and proved to be suitable for LSPR biosensing see Figure 4.12.

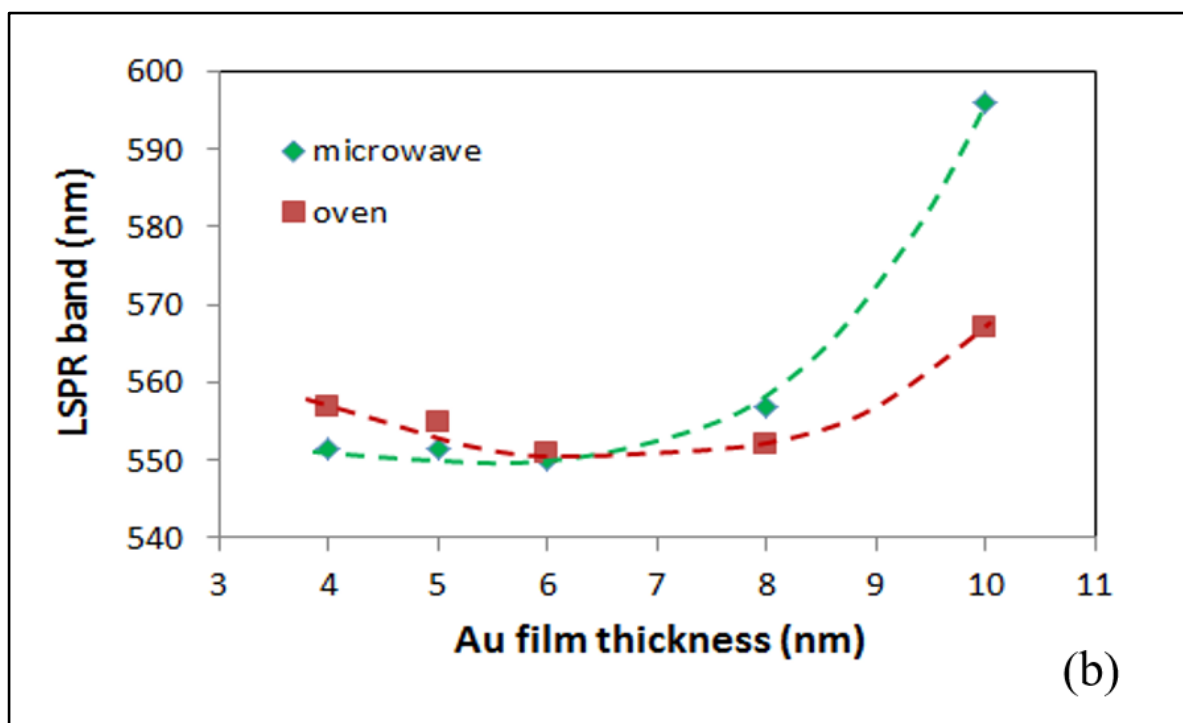
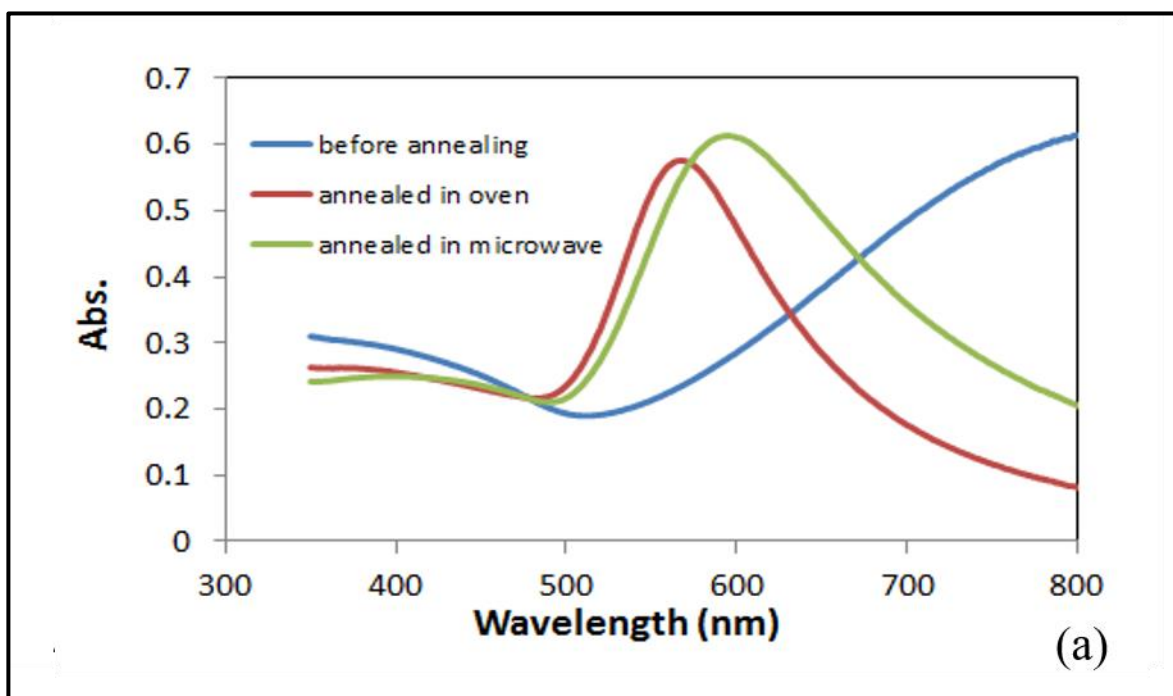


Figure 4.11 (a) UV-vis spectra of 10nm Au film before and after annealing (b) position of LSPR is gradually shifted to high wavelengths depend upon initial film thickness

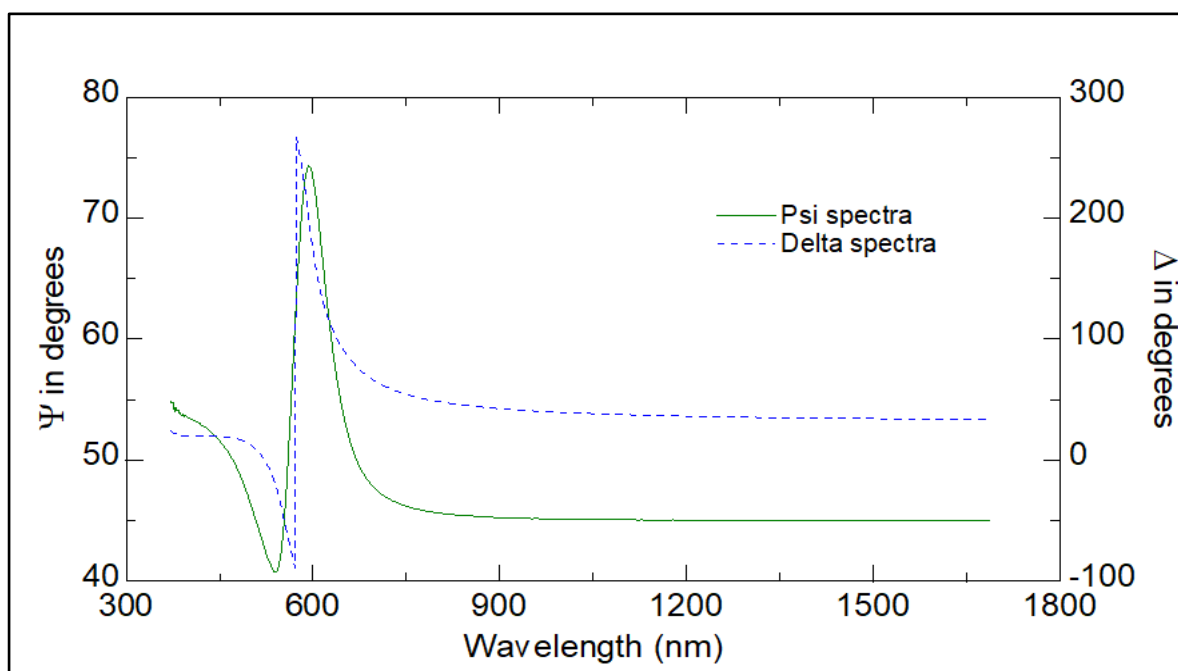


Figure 4.12 Spectroscopic ellipsometry spectra (ψ and Δ) of 5nm Au film annealed using microwave

The results showed the advantages of microwave technology (in addition to a short time of treatment) which gave larger, less dispersed and more ordered nano-islands which exhibit an LSPR absorption band in the visible spectral range, as shown in Figure 4.6 (a and b). The gold-nanostructures formed by microwave annealing were successfully used in LSPR/TIRE biosensing.

4.5 Evaluation of refractive index sensitivity (RIS)

The refractive index sensitivities (RIS) of Uv.vis absorption spectroscopy and spectroscopic ellipsometry were compared by carrying out measurements in media of different refractive indices of air (1.00), water (1.33), ethanol (1.36), chloroform (1.45), and Dimethyl sulfoxide (DMSO) (1.48). The method of external ellipsometry is not very popular in sensing because the light beam travels through the medium which does affect the

measurements; for this reason the cell have been designed to measure different refractive indices, which causes progressive red shift of LSPR band. The cell was designed to be suitable for using different solution by coupling the light into the surface of thin gold film, as shown in Figure 4.13

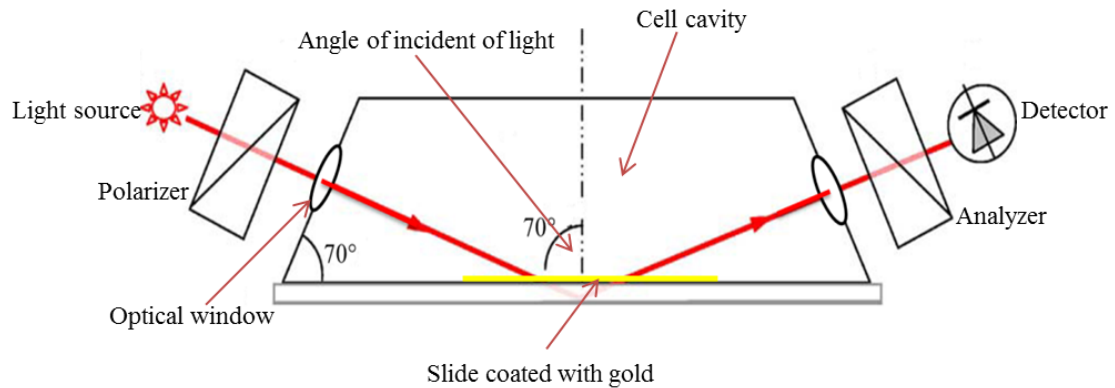
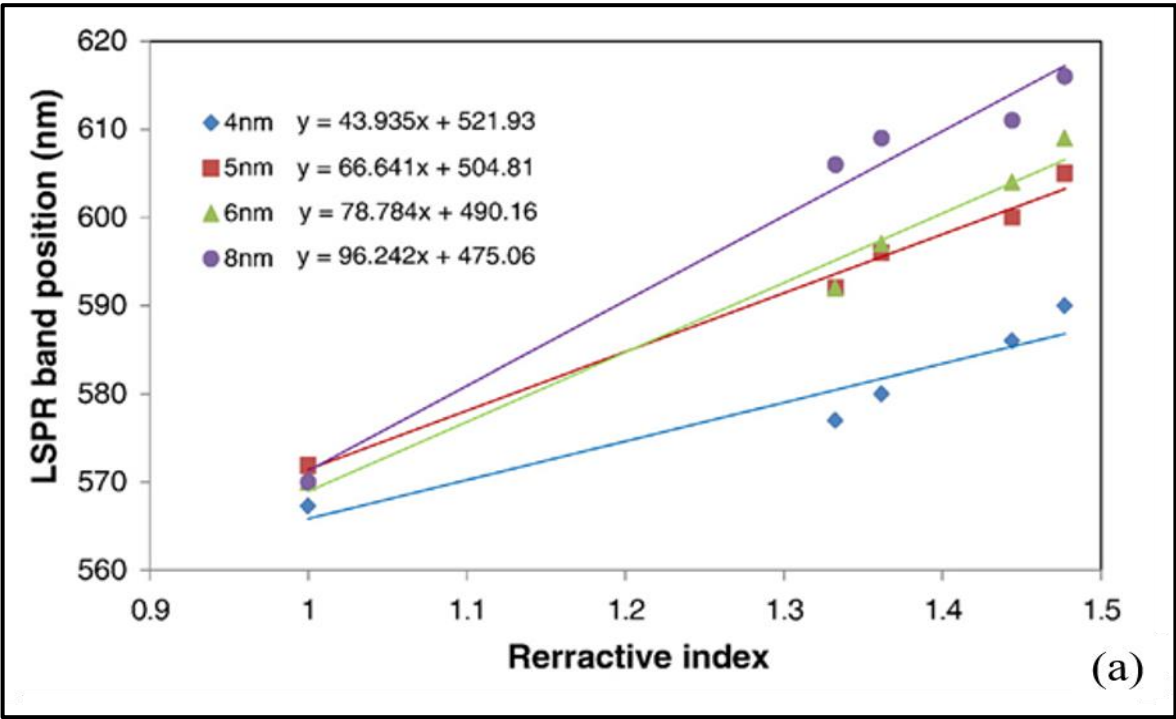


Figure 4.13. Cell designed of the measurement of different solution using external ellipsometry

The main principle of LSPR sensing lies in the dependence of LSP peak position on the refractive index of the surrounding medium. The obtained plot is possible to conclude that if the refractive index increases, the resonance dips will be shifted in the direction of the higher wavelengths, and the amplitude of the dips will decrease too. If the position of the dips is registered, it is possible to trace a new plot of the variation of the resonance wavelengths with the resonance dips. Because the position of the dips varies linearly with the refractive index, a linear regression could be calculated. The slope of the linear regression gives the sensitivity of the device. Therefore, using Microsoft Excel, it was possible to obtain the results which are presented in Figure 4.14(a and b for our samples) 4.14 (a and b for samples from our collaborates). as dependencies of LSPR band position vs. refractive index. All dependencies are linear, and their gradients gave an important parameter of refractive index sensitivity (RIS). The obtained values of RIS are summarized

in (Table 4.5 for our samples) and (Table 4.6 for samples from our collaborates). There are two important findings to be highlighted: (i) RIS increases with the increase in the nominal thickness and thus the size of Au nano-islands, (ii) SE measurements gave higher RIS values as compared to that obtained by absorption spectroscopy (see the RIS_{ES}/RIS_{Abs} ratio in Tables 4.5 and 4.6). The latter fact is surprising because the RIS must be related to physical parameters of Au nano-structured, not the methods of their analysis. This fact could be understood if we take into account multiple reflections (three reflections are essential) of light in ellipsometry measurements as compared to a single interaction in absorption spectroscopy. According to Fresnel's theory the number of reflections of light in ellipsometry of thin films is infinite, though only the first three reflections can be considered as significant (Azzam and Bashara, 1977); that is perhaps why RIS in ellipsometry experiments is two to three times higher than that obtained from uv. vis measurements. Therefore, the reflected electromagnetic wave can probe several nano-islands, which explains the dependence on the island size.



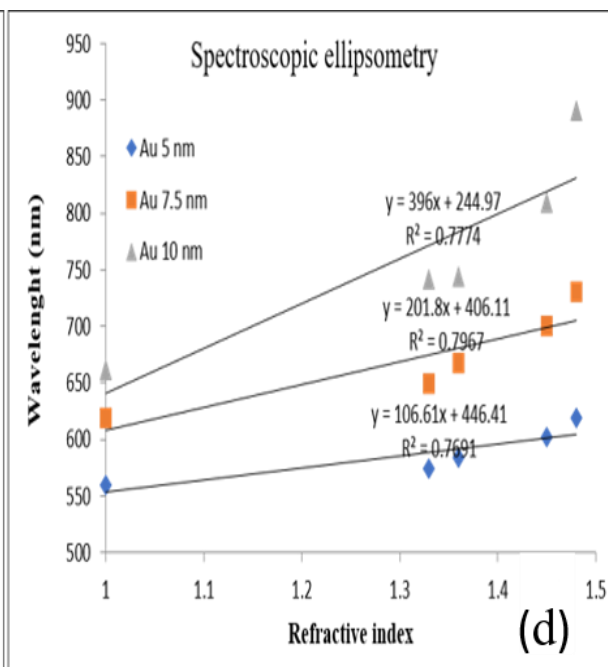
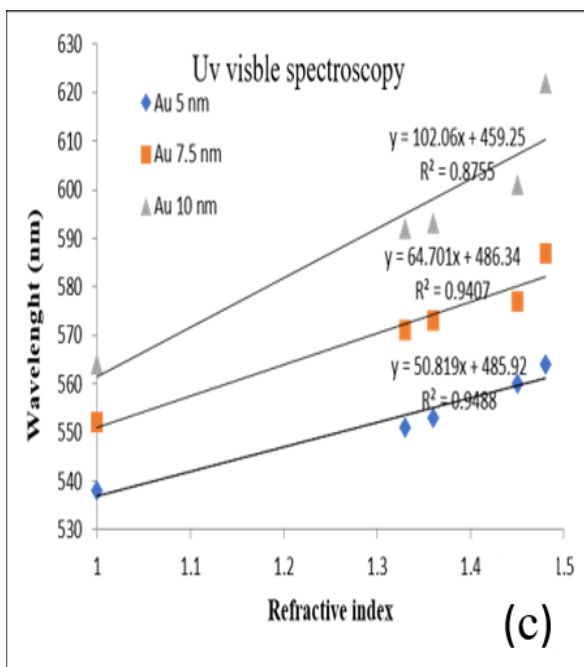
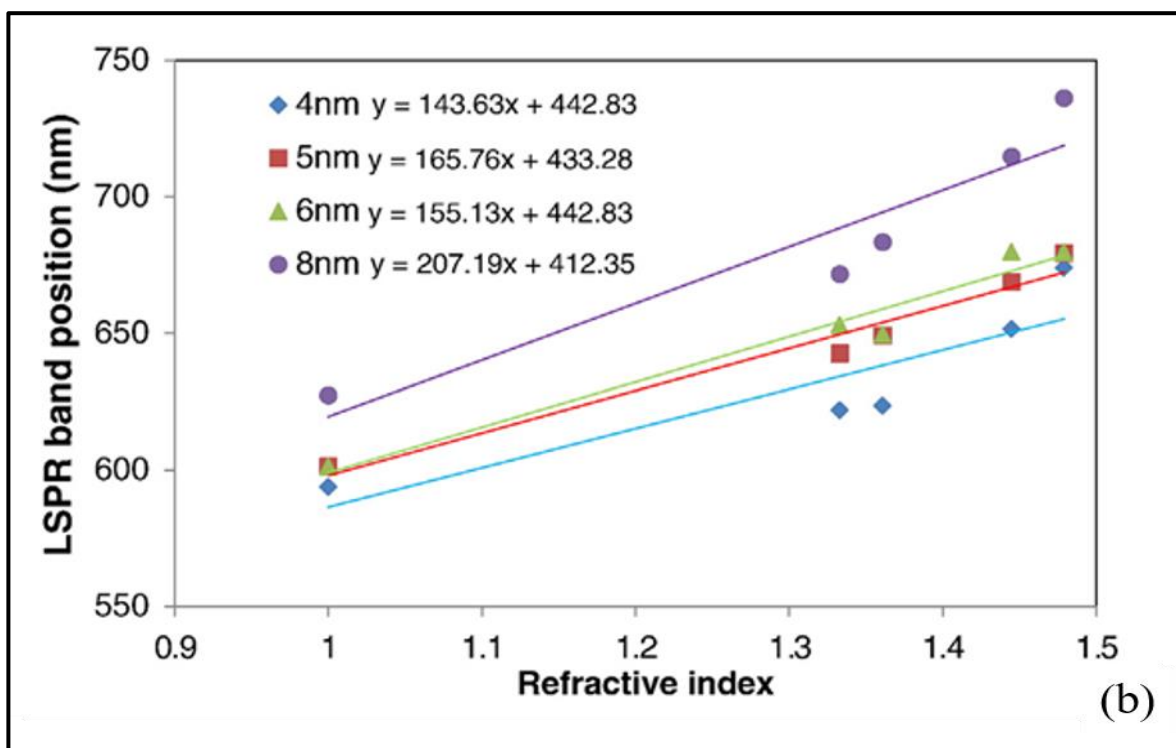


Figure 4.14 Dependencies of LSPR band position vs. refractive index obtained from (a) absorption spectra and (b) ellipsometry measurements (our samples Au 4,5,6,8 and 10nm) (c) absorption spectra and (d) ellipsometry measurements (samples from our collaborates au 5,7.5 and 10nm)

Figure 4.14a shows UV. visible spectra: Position of the resonance maximum versus the refractive index, with the equation of the linear regression. The refractive index sensitivity was 50.8, 64.7 and 102nm/RIU (Refractive Index Unit) for Au thicknesses 5, 7.5 and 10nm respectively. Figure 4.14b shows spectroscopic ellipsometry (psi spectra): Position of the resonance dip versus the refractive index, with the equation of the linear regression. The refractive index bulk sensitivity was 106.6, 210.8 and 396 nm / RIU (Refractive Index Unit) of the Au 5, 7.5 and 10 nm respectively which are a good sensitivity, proving that this kind of devices is very sensitive to small changes of surrounding medium (The graphics were plotted with the auxiliary of Microsoft Excel).

Table 4.5 Evaluation of refractive index sensitivity using UV. Visible absorption and spectroscopic ellipsometry for sample prepared in our laboratory. The gold layer was coated on typical glass slide on Cr 3nm as intermediate layer to improve adhesion of gold on glass surface annealed at 480 °C for 2 hours

Nominal thickness of Au films (nm)	RIS (nm/RIU) (abs. spectra)	RIS (nm/RIU) (ellipsometry)	RIS _{SE} /RIS _{Abs}
4	43.9	143.6	3.27
5	66.6	165.7	2.49
6	78.8	155.1	1.97
8	96.2	207.2	2.15

Table 4.6 Evaluation of refractive index sensitivity using UV. Visible absorption and spectroscopic ellipsometry for samples from our collaboration. Gold coated on cover slide without Cr intermediate layer annealing for 10 hours at 550 °C (samples from collaborates)

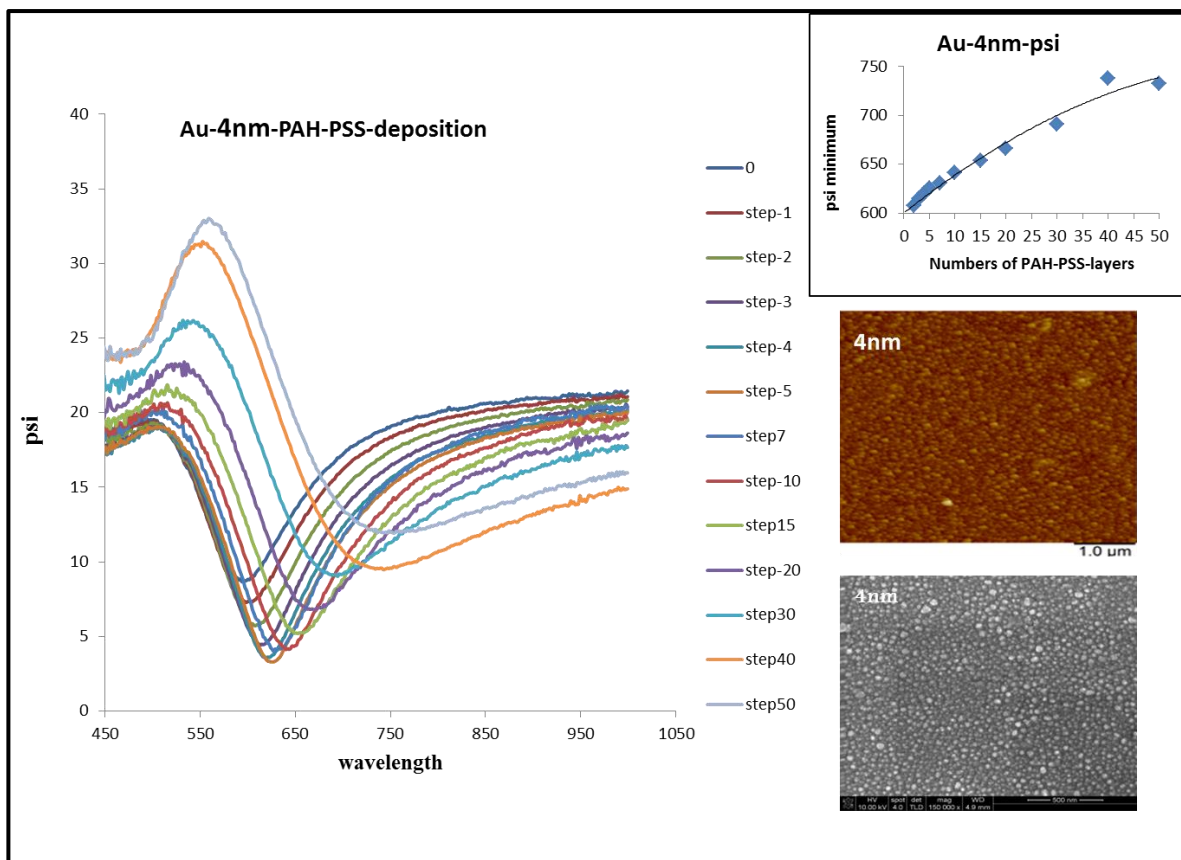
Nominal thickness of Au films(nm)	RIS (nm/RIU) (abs. spectra)	RIS (nm/RIU) (ellipsometry)	RIS _{SE} /RIS _{Abs}
5	50.8	106.6	2.09
7.5	64.7	201.8	4.3
10	102	396	3.9

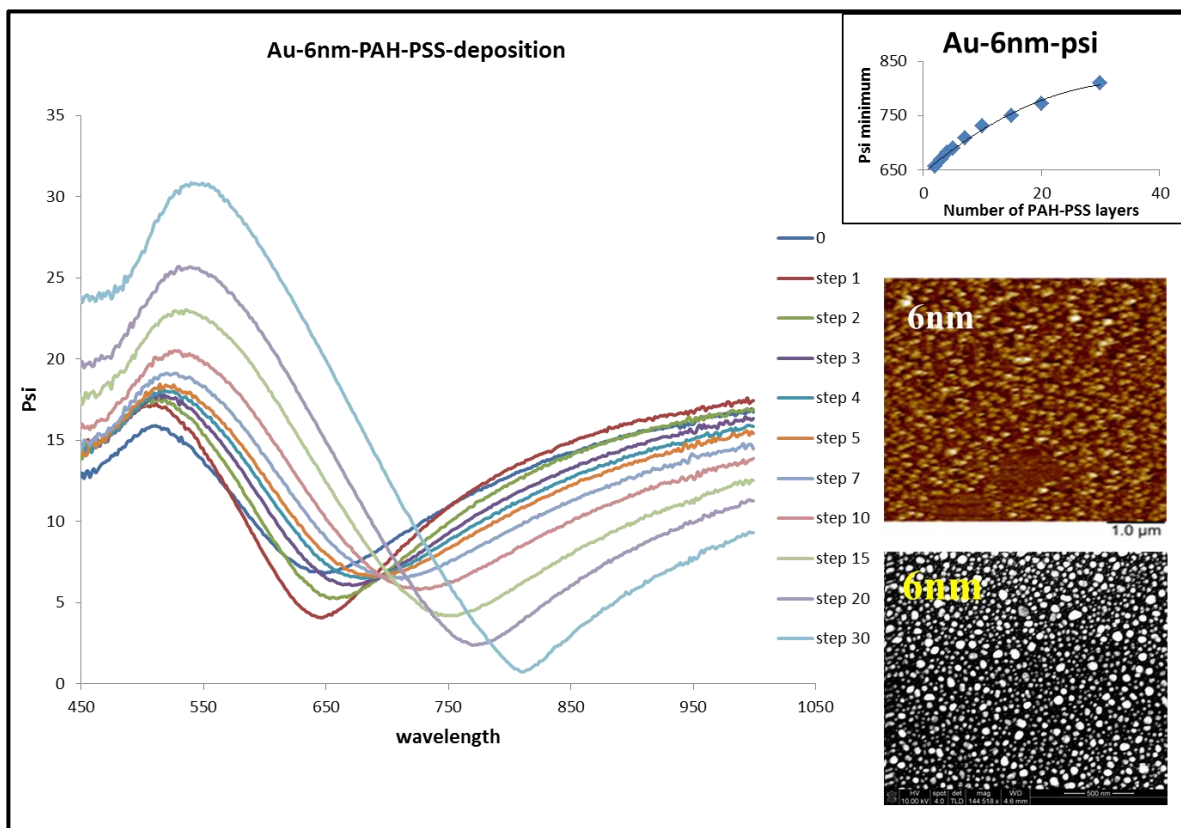
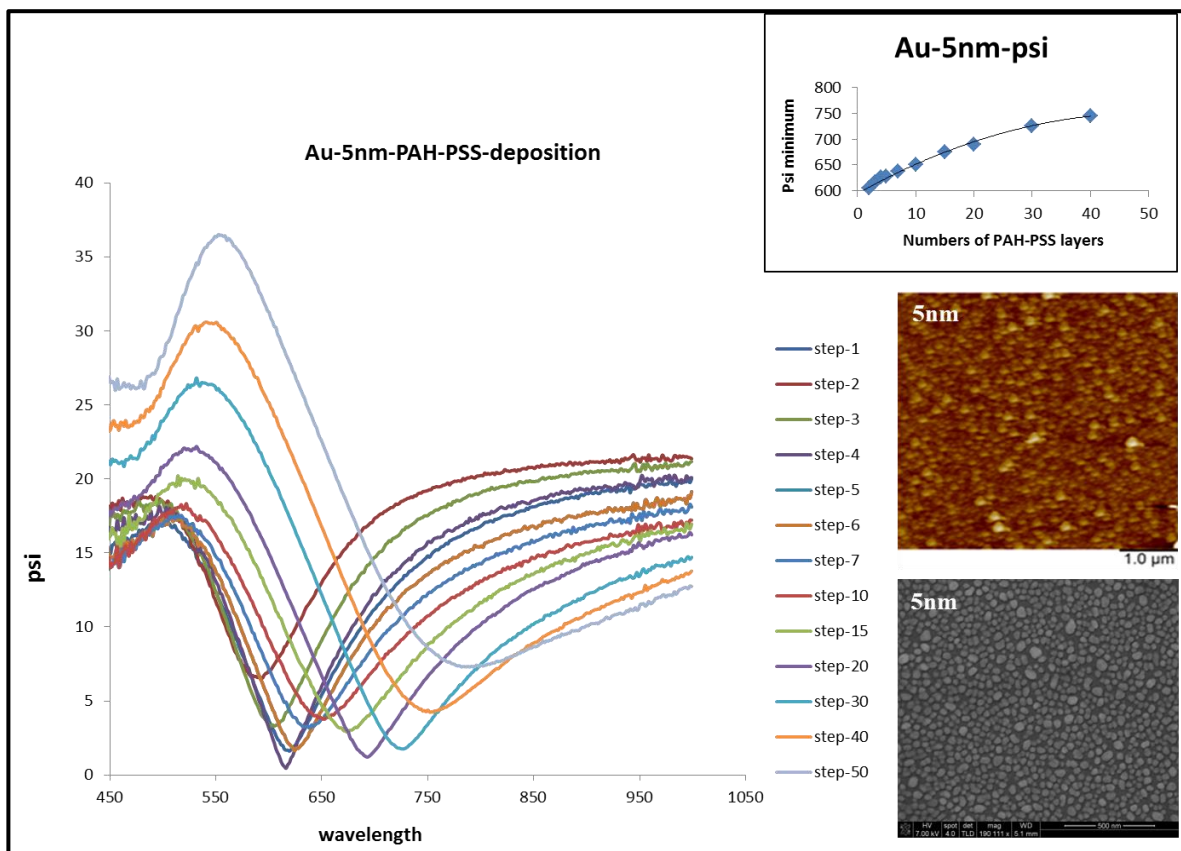
From the RIS data presented in table 4.5 and 4.4 it's clear that RIS is higher for ellipsometry.

4.6 Limitations of LSPR

Another characteristic property of metal nano-structures which should be considered is the much shorter evanescent field decay length as compared to that in total internal reflection geometry (Kedem et al., 2014). The experimental study of this effect was carried out by monitoring the LSPR spectral shift of the deposition of polyelectrolyte layers, i.e. PAH and PSS. Ellopsometric measurements of poly (allyamine hydrochloride) PAH / poly-steryl sulfonate sodium salt (PSS) deposition is, presented in Figure 4.15 (a, d, c, d and f) for different thicknesses (4, 5, 6, 8 and 10 respectively). The graphs show refractive index dispersion and saturation with sample 4, 5, 6, 8 and 10nm after 30-50 times deposition. The

spectral shift is however saturated upon deposition of layers of PAH and PSS, which demonstrate the effect of evanescent field decay.





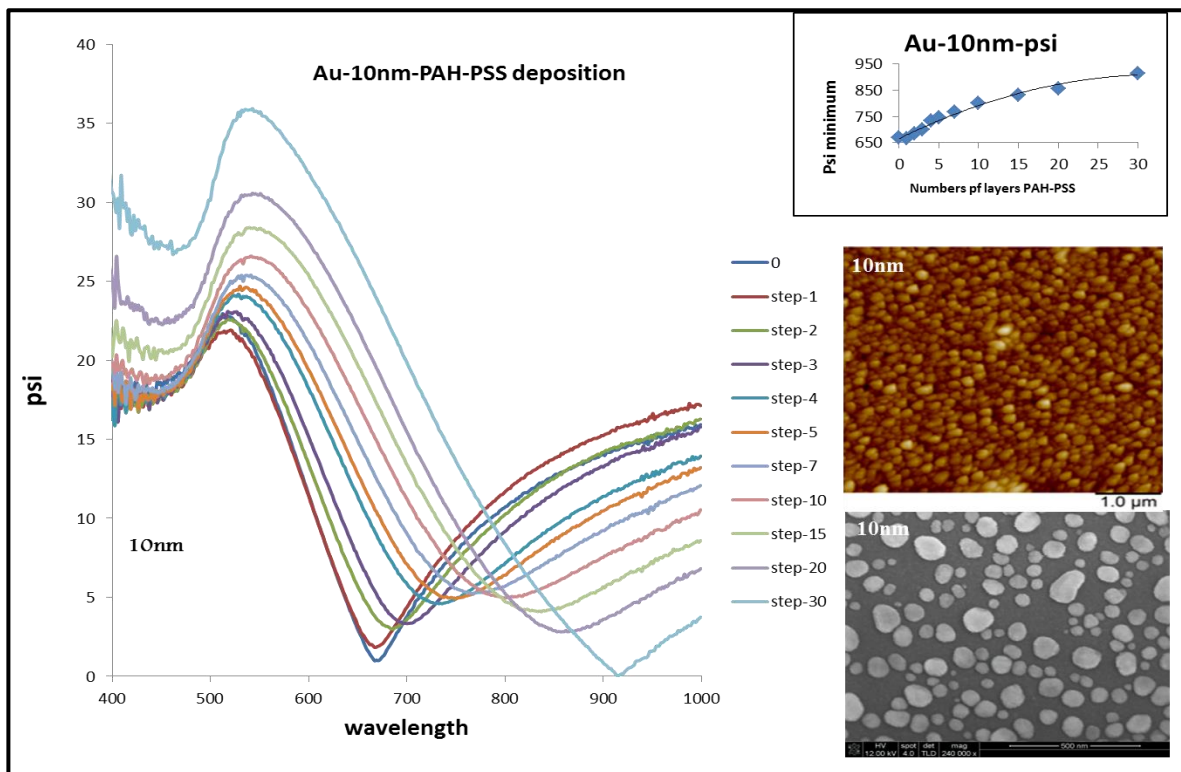
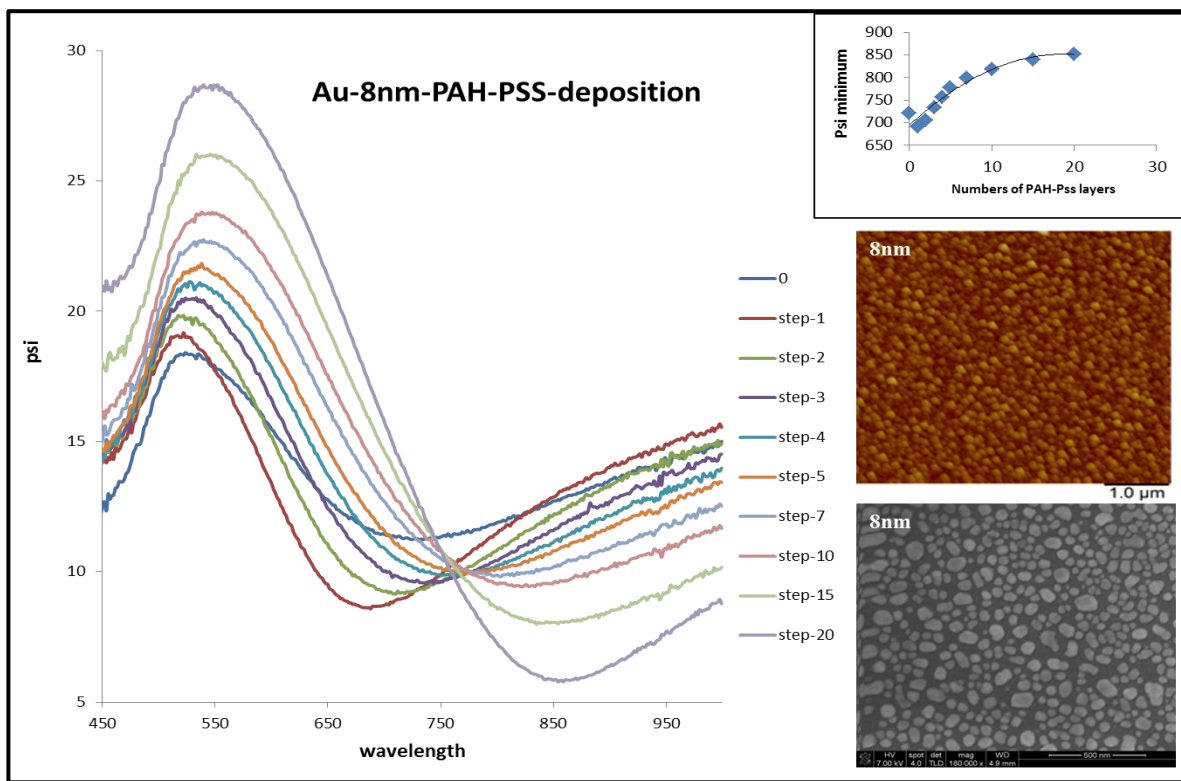


Figure 4.15 Spectroscopic ellipsometry ψ spectra of Cr/Au nanostructures of different thicknesses (4, 5, 6, 8 and 10nm) on deposition of PAH – PSS layers; inset shows

saturation of deposition of PAH and PSS layers and SEM and AFM images of gold thin film

The saturation of the spectral shift observed experimentally fits into rising exponential function, by using the following equations, we calculated decay length of the LSPR (Kim et al., 2017):

$$R = m \cdot \Delta n [1 - \exp(-d/l)] \quad (4.1) \text{ (Petryayeva and Krull, 2011)}$$

$$l = -\frac{d}{\ln(1-R/m \cdot \Delta n)} \quad (4.2)$$

where R is the transducer response (wavelength shift, intensity change, etc.), m is refractive index sensitivity (RIS), Δn is the change in refractive index of the surrounding medium effected by adsorbate, d is the dielectric (adsorbate) layer thickness, and l is the plasmon effective decay length. This allows the evaluation of the decaying length as presented in Figure 4.16(a) for our samples and Figure 4.16 (b) for samples from our collaborates. It appears that the evanescent field decay length varies (for our samples) from 16 nm for small Au-nano-islands (4nm nominal thickness) up to 31nm for large Au nano-islands (10nm nominal thickness). For samples from our collaborates the variation of decay length was from 17 nm for small Au-nano-islands (3nm nominal thickness) up to 61nm for large Au nano-islands (10 nm nominal thickness); such values are much smaller than evanescent decay length in traditional SPR experiments (Li et al., 2015). This fact has serious implications on LSPR biosensing, particularly on the dimensions of bio-receptors used.

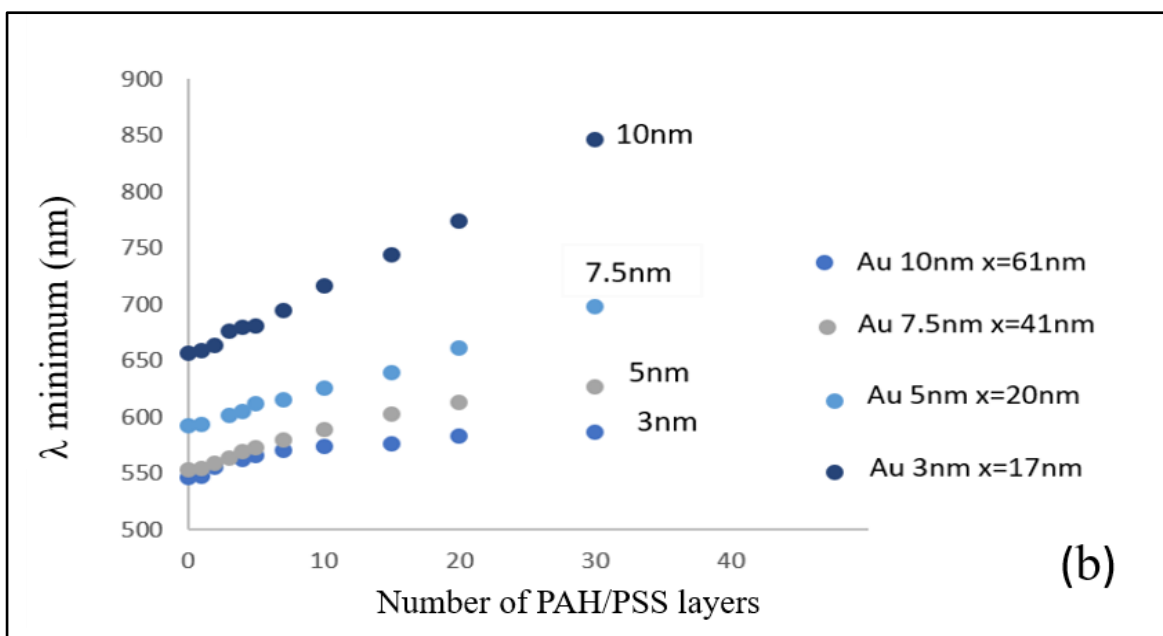
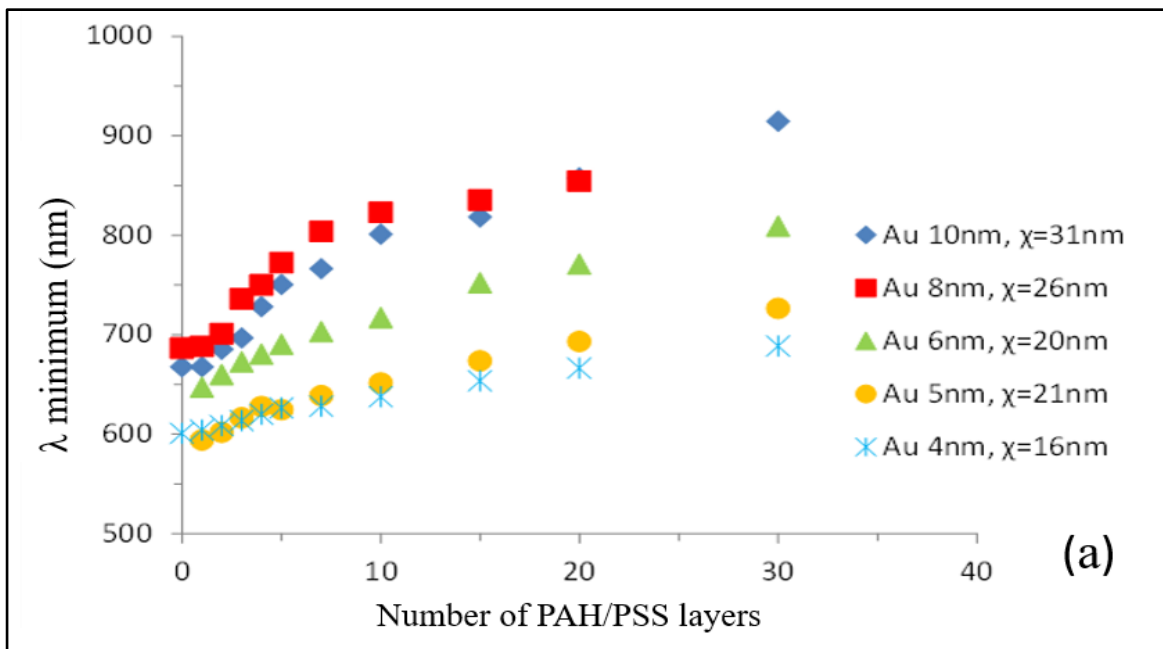


Figure 4.16. Dependence of the position of LSPR band (ψ degree) vs the number of PAH/PSS layers deposited on (a) Au of our samples (b) Au from collaborators. The values of evanescent field decay length are shown near respective curves.

Summary

SEM and AFM images provided important information on correlation between the optical properties and morphology of nano-structured Au films; the data obtained correlated well with the traditional UV-vis absorption spectra as well as with the morphology of Au nano-islands.

Several annealing options were used and compared. It appeared that microwave annealing is the best procedure for Au films annealing. Spectroscopic ellipsometry measurements of nano-structured gold films provided additional information for studying the LSPR phenomenon. The refractive index sensitivity appeared to depend on the size of Au nano-islands. Also, spectroscopic ellipsometry showed two to three times higher refractive index sensitivity than that of absorption spectroscopy which is most-likely related to multiple reflections of light in ellipsometry measurements according to Fresnel equation. It was found that Au nanostructures have quite short evanescent field decay length (in tens of nanometers). Therefore, the use of whole antibodies electrostatically immobilized on gold film via PAH and protein A which demonstrates low sensitivity of LSPR/TIRE detection.

Reference list

Arwin, H., Poksinski, M., & Johansen, K. (2004). Total internal reflection ellipsometry: principles and applications. *Applied optics*, 43(15), 3028-3036.

A.V. Nabok, A. Tsargorodskaya, A.K. Hassan, N.F. Starodub. (2005). Total internal reflection ellipsometry and SPR detection of low molecular weight environmental toxins, *Appl. Surf. Sci.* 246, 381–386 0169-4332.

Karakouz, T., Tesler, A. B., Bendikov, T. A., Vaskevich, A., & Rubinstein, I. (2008a). Highly stable localized plasmon transducers obtained by thermal embedding of gold island films on glass. *Advanced Materials*, 20(20), 3893-3899.

Karakouz, T., Tesler, A.B, Bendikov, T.A., Vaskevich, A., Rubinstein, I. (2008b), Highly stable localized plasmon transducers obtained by thermal embedding of gold island films on glass, *Advanced Materials*, 20, 3893-3899.

Kedem, O., Vaskevich A., Rubinstein, I. (2014), Critical issues in localized plasmon sensing, *J. Phys. Chem. C*, 118 (16), 8227–8244.

Kim, S. W., Lee, J. S., Lee, S. W., Kang, B. H., Kwon, J. B., Kim, O. S., ... & Kang, S. W. (2017). Easy-to-fabricate and high-sensitivity LSPR type specific protein detection sensor using AAO nano-pore size control. *Sensors*, 17(4), 856.

Li, M., Cushing, S. K., & Wu, N. (2015). Plasmon-enhanced optical sensors: a review. *Analyst*, 140(2), 386-406.

Nabok, A., Tsargorodskaya, A., Mustafa, M. K., Szekacs, I., Starodub, N. F., & Szekacs, A. (2011b). Detection of low molecular weight toxins using an optical phase method of ellipsometry. *Sensors and Actuators B: Chemical*, 154(2), 232-237.

Nabok, A. V., Tsargorodskaya, A., Hassan, A. K., & Starodub, N. F. (2005). Total internal reflection ellipsometry and SPR detection of low molecular weight environmental toxins. *Applied Surface Science*, 246(4), 381-386.

Petryayeva, E., & Krull, U. J. (2011). Localized surface plasmon resonance: nanostructures, bioassays and biosensing—a review. *Analytica chimica acta*, 706(1), 8-24.

Tesler, A. B., Maoz, B. M., Feldman, Y., Vaskevich, A., & Rubinstein, I. (2013). Solid-state thermal dewetting of just-percolated gold films evaporated on glass: development of the morphology and optical properties. *The Journal of Physical Chemistry C*, 117(21), 11337-11346.

Chapter 5: Detection of mycotoxins using antibodies

5.1 Introduction

As has been shown in previous chapter the sensitivity of LSPR measurements is limited by a finite evanescent decay length in gold nano-islands which is typically in the range of tens of nanometers. In order to achieve the best results, the bio-receptors must be small and placed as close to the gold surface as possible. One solution to this problem was the use of halved antibodies immobilized covalently on the surface of gold (Iwata et al., 2008; Lee et al., 2005; Bonroy et al., 2006). In this work we used the technology of splitting antibodies by the S-S bridge in the main domain in 2-Mercaptoethylamine with subsequent immobilization of halved antibodies on the surface of gold via native thiol groups (Karyakin et al., 2000; Balevicius et al., 2011; Vikholm-Lundin, 2005) which was described in detail in (chapter 2, Figure 2.21); as a result the sensitive Fab-fragments appeared to be much closer to the gold surface.

In this chapter a series of bio-sensing LSPR/TIRE experiments on detection of mycotoxins, i. e. aflatoxin B1 and zearalenone, were carried out in direct assay with their respective half-Ab immobilized on the surface of gold nanostructure.

5.2 Aflatoxin detection using TIRE method: Preliminary results using whole antibodies as bio-receptors

Preliminary biosensing tests on the detection of aflatoxin B1 was carried out using TIRE measurements on nanostructured gold films. A series of TIRE spectra recorded on nanostructured Au films are shown in Figure 5.1. The LSPR features, i.e. minima on Ψ spectra and phase drop in Δ spectra, are quite obvious. The increase in the size of Au nano-islands (or nominal Au film thickness) causes the shift of LSPR to large wavelengths. The results of biosensing tests on detection of aflatoxin B1 in direct immunoassay with specific antibodies are shown in Figure 5.2. The samples of 5 nm Au annealed at high temperature of 550 °C appeared to be more stable than those annealed at lower temperature and therefore they were used in these measurements. As one can see a noticeable spectral shift upon absorption of layers of PAH, antibodies, and aflatoxin B1 was observed. These results are similar to those obtained earlier on continuous gold films (Nabook et al., 2011a). The spectral shift of nearly 20 nm caused by binding aflatoxin B1 from its stock solution (1 μ g/ml in water) is particularly impressive. However, the detection of small concentrations of aflatoxin B1 was problematic. Typical results shown in Figure 5.3 demonstrates detection of aflatoxin B1 from 1ng/ml which is much higher than 0.1ng/ml achieved on 25 nm thick continuous gold film.

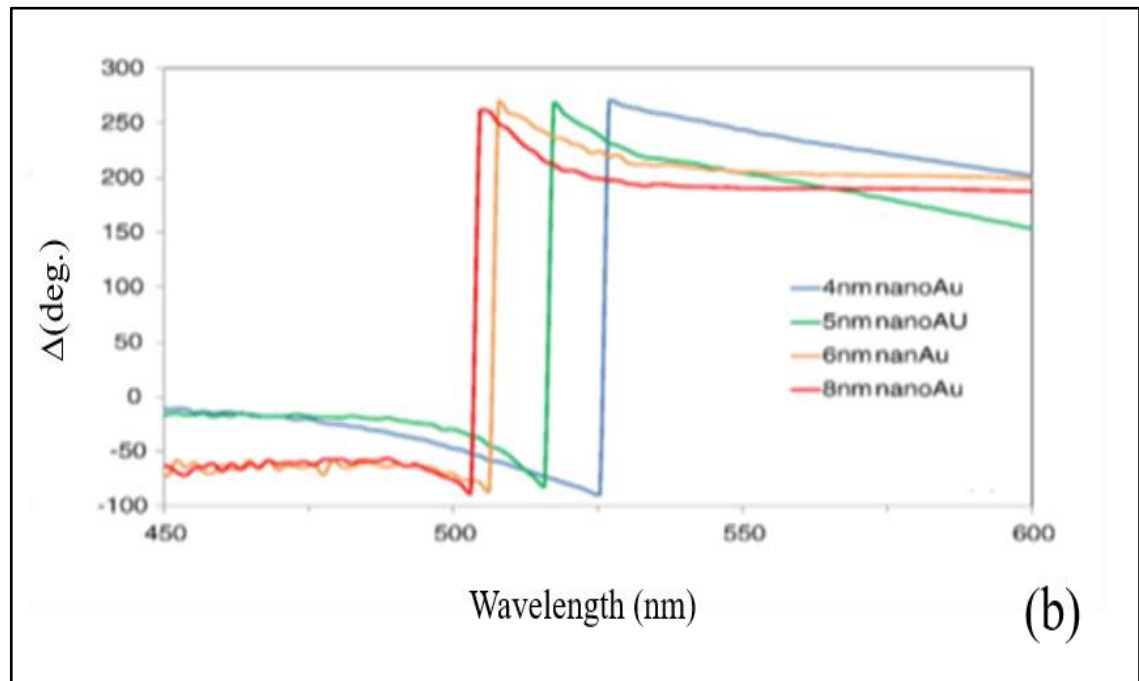
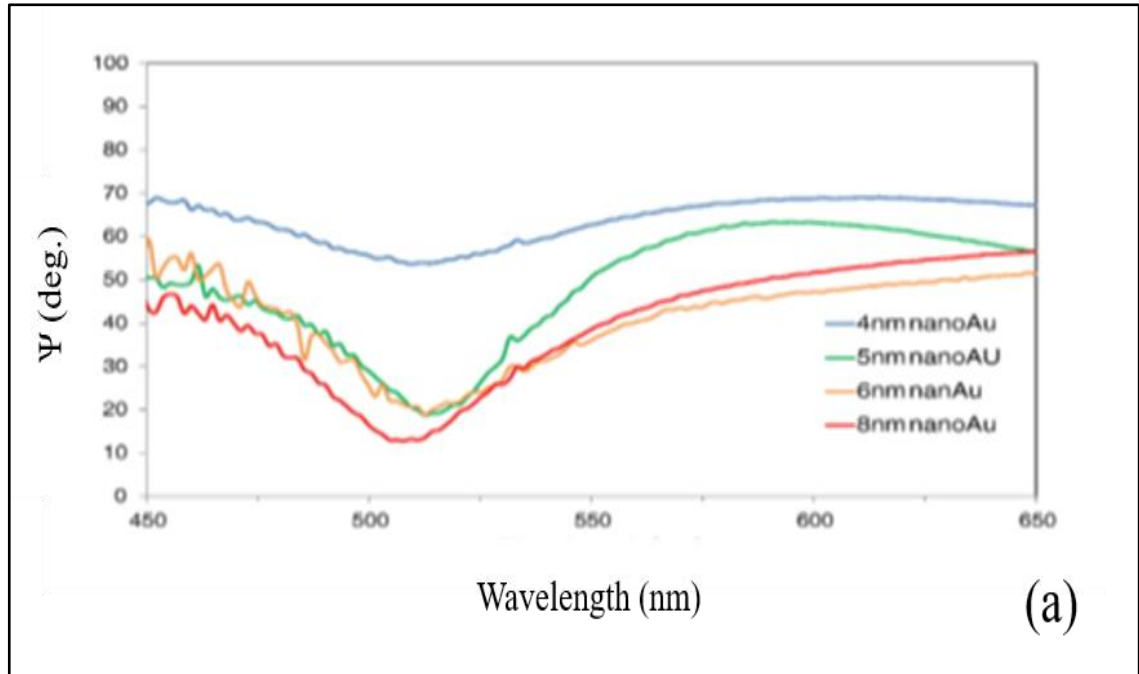


Figure 5.1. TIRE spectra Ψ (a) and Δ (b) for Au nano-structures of different nominal thicknesses

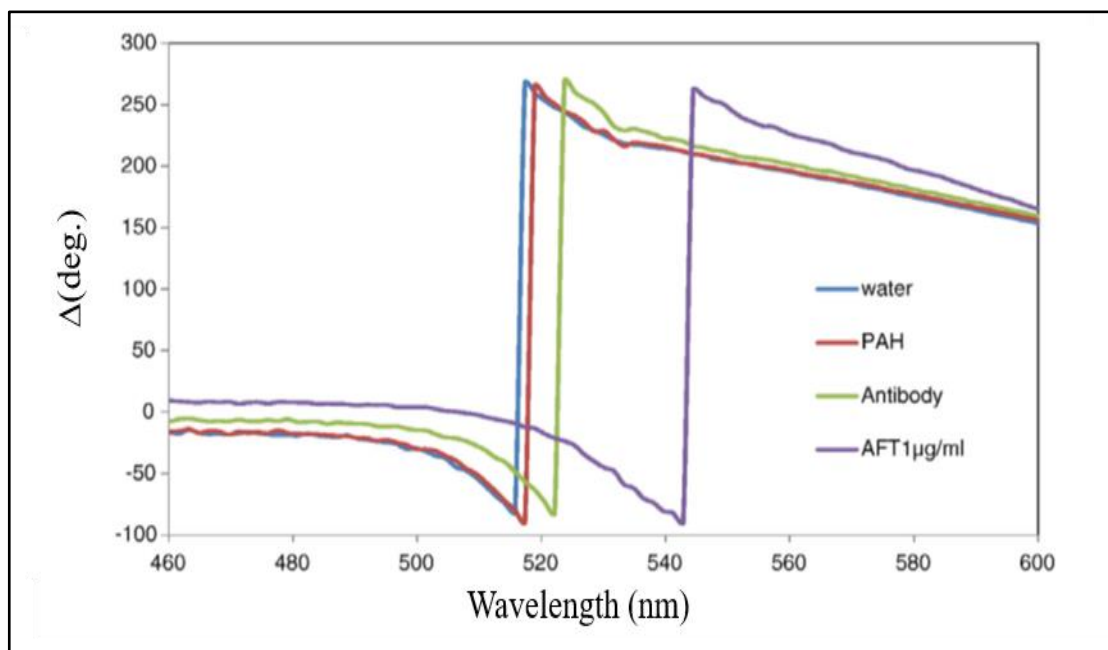


Figure 5.2. The series of TIRE (Δ) spectra corresponding to deposition of layers of PAH, antibodies, and aflatoxin B1 on nanostructured Au film of 5 nm of nominal thickness annealed at higher temperature 550 °C for 10 h

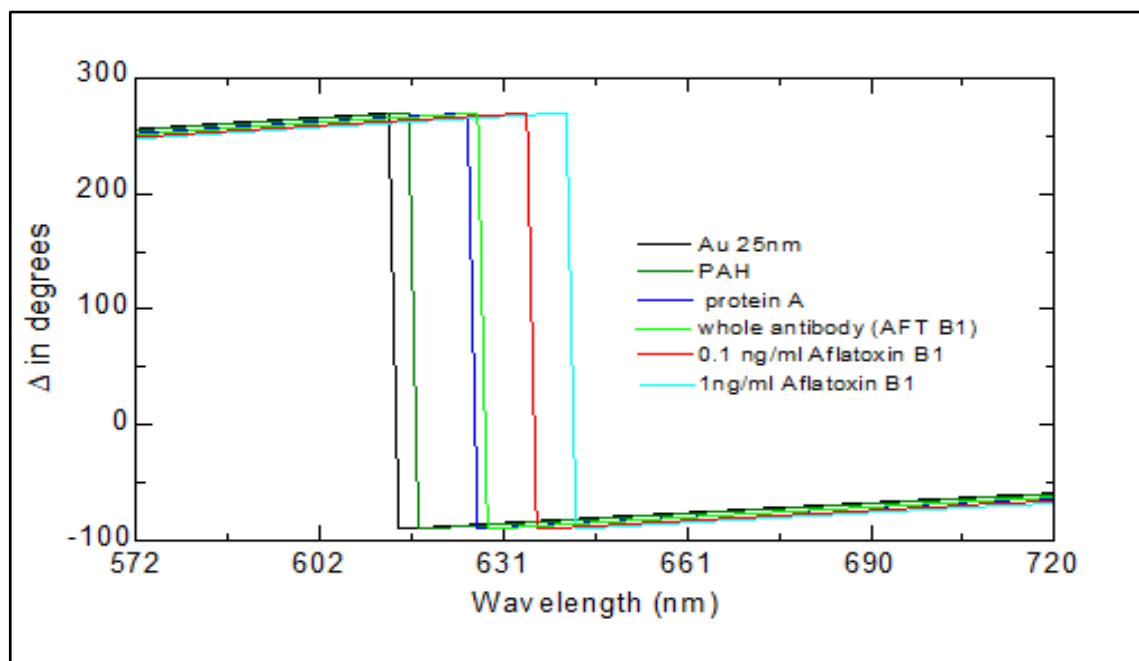


Figure 5.3. The series of TIRE Δ spectra corresponding to deposition of layers of PAH, antibodies, and aflatoxin B1 on continuous Au film of 25 nm deposited on glass slide and 3nm Cr as intermediate layers

The initial disappointing results on LSPR/TIRE detection of AFT B1 is most likely due to the large size of bioreceptors used e.g. whole antibodies. The sensitivity was compromised because of the short evanescent field decay length.

5.3 Electrophoresis study

Electrophoresis experiments were carried out in order to prove the splitting of antibodies. The results of these tests illustrated in Figure 5.4 proved the presence of one 50 KDa band corresponding to split heavy chain of antibodies in contrast to two 50 KDa bands in the original antibodies.

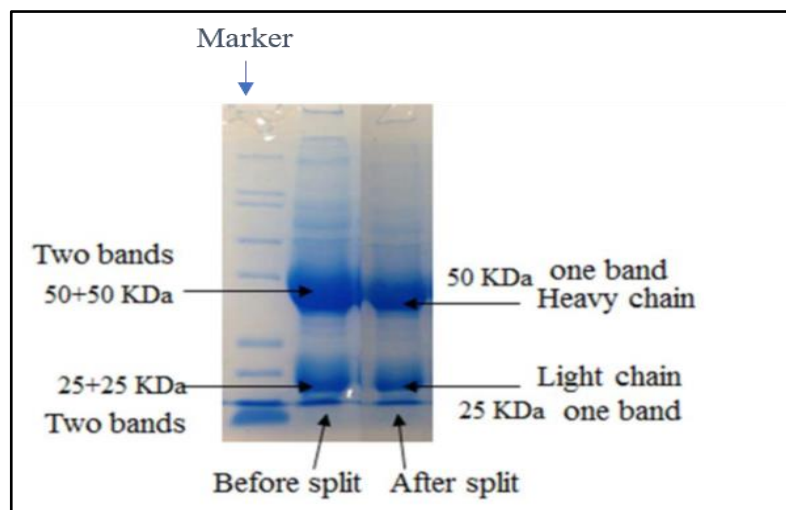


Figure 5.4. SDS – PAG electrophoresis of antibodies before and after splitting

The graph shows the bands after the split of antibody by adding 2-Mercaptoethylamine; these bands after split Ab become half molecular weight than before split Ab i.e. before antibody split it was two bands each band has 100 KD and 50 KD molecular weight as one can see in first well of gel of electrophoresis and after antibody split (second well) become 50KD and 25KD according to the reference of antibody in first well of gel electrophoreses.

5.4 Detection of aflatoxin B1 and Zearalenone using small size of bioreceptors: split antibodies

TIRE biosensing experiments were carried out on the LSPR structures using the set-up built on the basis of M-2000 J.A. Woollam spectroscopic ellipsometer and the methodology described in detail in chapter 3 (Nabok et al., 2005; Nabok et al., 2009).

The nanostructured gold substrates for these measurements were produced by thermal annealing of 5nm thick gold film deposited on glass. Immobilization of split antibodies on to these substrates was carried out using the procedure described in chapter 3.

Solutions of mycotoxins (aflatoxin B1 and zearalenone) of different concentrations in phosphate buffer solution (PBS) in the increasing order (0.01, 0.1, 1, 10, 100, and 1000 ng/ml) were injected into the cell with the intermediate rinsing with buffer. The incubation time was 10 min. Dynamic spectra were recorded during binding reaction, while single spectroscopic scans were recorded in a standard PBS (100 mM, pH 7) after completion of each binding steps. A series of Δ spectra was recorded after binding aflatoxin B1 to split antibodies immobilized on gold nano-islands, as shown in Figure 5.5.

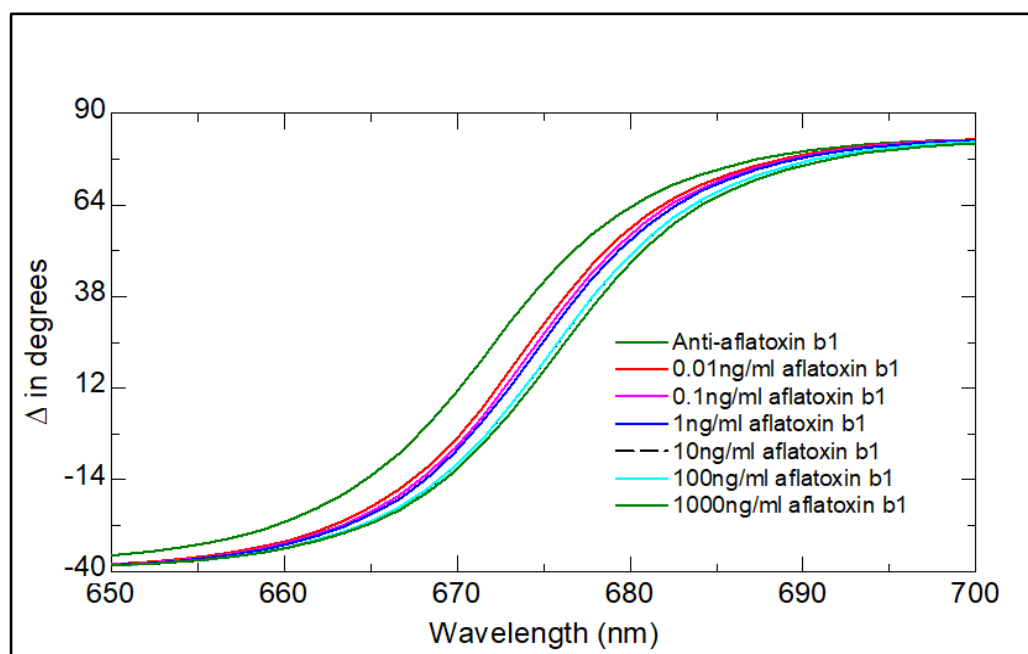


Figure 5.5. Ellipsometric Δ spectra recorded after binding of aflatoxin B1 of different concentrations to split antibodies immobilized on 5nm nano-Au layer

As one can see, binding of aflatoxin results in a progressive red shift of Δ spectra. The values of a spectral shift against the concentration of aflatoxin B1 are summarized in Figure 5.6. A surprisingly large spectral shift of about 2.4 nm was found as a result of binding the minimal concentration of Aflatoxin B1, e.g. 0.01ng/ml. The sensor response tends to saturate at high concentrations of the analytes due to saturation of binding sites. This means that the detection limit could be much lower, most-likely in sub-ppt level.

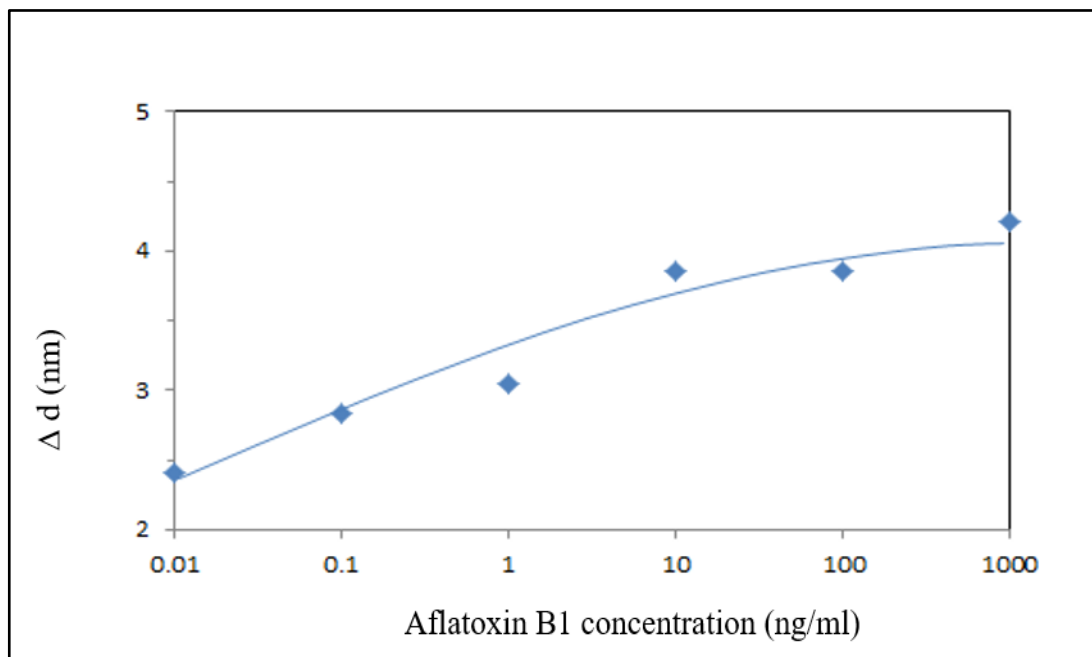


Figure 5.6. The spectral shift of Δ vs the concentration of aflatoxin B1

Similar results were obtained for another mycotoxin zearalenone. Substantial red spectral shifts of 4.78 nm and 6.34 nm were observed when binding, respectively, 0.01ng/ml and 0.1ng/ml of zearalenone. However, further increase in concentration resulted in a blue spectral shift (to shorter wavelengths), which is typically associated with peeling off the molecular layer. This might have been caused by the use of serum with polyclonal antibodies, which were not split properly and therefore not strongly bound to the surface, their concentration may not be high enough resulting in a quick saturation of the sensor response as demonstrated in Figure 5.7.

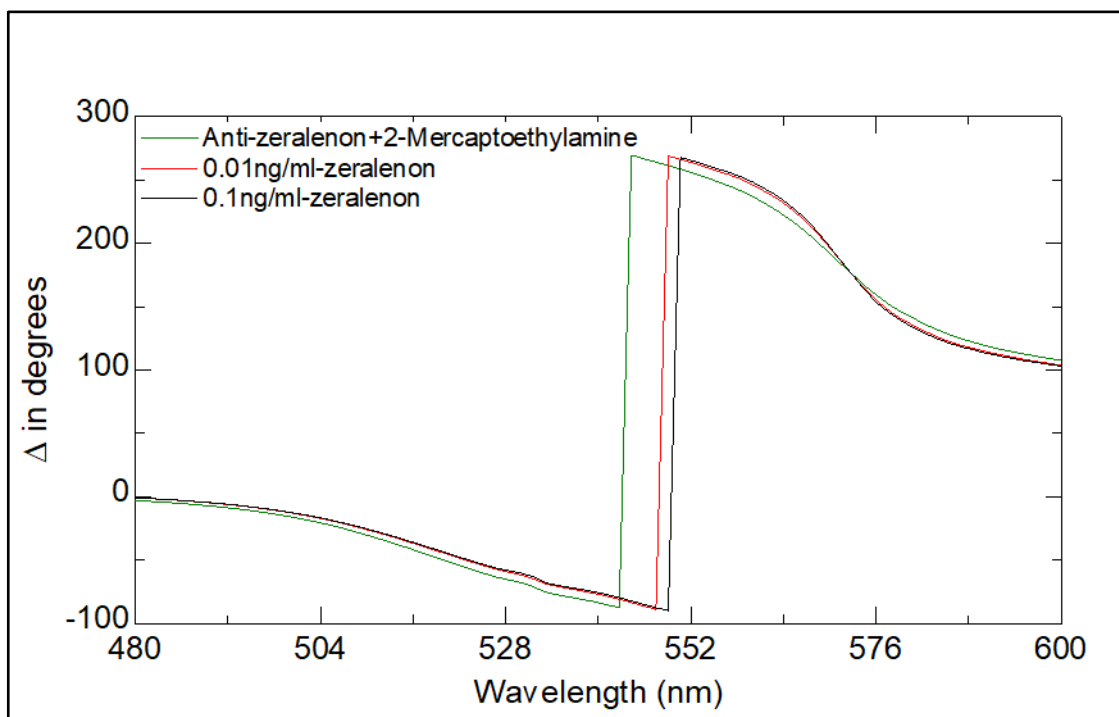


Figure 5.7. TIRE spectra of binding zearalenone 0.1- 0.01 ng/ml to split antibodies

Summary

The limitations of sensitivity of LSPR associated with a short evanescent field decay length has been overcome using split antibodies covalently immobilized and positioned flat on the surface of gold nano-islands with Fab-fragments very close to the surface. Our attempts of detecting mycotoxins were successful. The lowest detected concentrations of 10 part per trillion (ppt) for both aflatoxin B1 and zearalenone with a very likely possibility of having much lower detection limit in sub-ppt concentration is an amazing achievement for direct immunoassay analysis.

Reference list

- Balevicius, Z., Ramanaviciene, A., Baleviciute, I., Makaraviciute, A., Mikoliunaite, L., & Ramanavicius, A. (2011). Evaluation of intact-and fragmented-antibody based immunosensors by total internal reflection ellipsometry. *Sensors and Actuators B: chemical*, *160*(1), 555-562.
- Bonroy, K., Frederix, F., Reekmans, G., Dewolf, E., De Palma, R., Borghs, G., ... & Goddeeris, B. (2006). Comparison of random and oriented immobilisation of antibody fragments on mixed self-assembled monolayers. *Journal of immunological methods*, *312*(1-2), 167-181.
- Iwata, R., Satoh, R., Iwasaki, Y., & Akiyoshi, K. (2008). Covalent immobilization of antibody fragments on well-defined polymer brushes via site-directed method. *Colloids and Surfaces B: Biointerfaces*, *62*(2), 288-298.
- Karyakin, A. A., Presnova, G. V., Rubtsova, M. Y., & Egorov, A. M. (2000). Oriented immobilization of antibodies onto the gold surfaces via their native thiol groups. *Analytical chemistry*, *72*(16), 3805-3811.
- Lee, W., Oh, B. K., Lee, W. H., & Choi, J. W. (2005). Immobilization of antibody fragment for immunosensor application based on surface plasmon resonance. *Colloids and Surfaces B: Biointerfaces*, *40*(3-4), 143-148.
- Nabok, A. V., Tsargorodskaya, A., Hassan, A. K., & Starodub, N. F. (2005). Total internal reflection ellipsometry and SPR detection of low molecular weight environmental toxins. *Applied Surface Science*, *246*(4), 381-386.
- Nabok, A., Tsargorodskaya, A., Mustafa, M. K., Székács, A., Székács, I., & Starodub, N. F. (2009). Detection of low molecular weight toxins using optical phase detection techniques. *Procedia Chemistry*, *1*(1), 1491-1494.
- Nabok, A. V., Mustafa, M. K., Tsargorodskaya, A., & Starodub, N. F. (2011). Detection of aflatoxin B1 with a label-free ellipsometry immunosensor. *BioNanoScience*, *1*(1-2), 38-45.
- Vikholm-Lundin, I. (2005). Immunosensing based on site-directed immobilization of antibody fragments and polymers that reduce nonspecific binding. *Langmuir*, *21*(14), 6473-6477.

Chapter 6: Small size bio-receptors: Aptamers for the detection of mycotoxins

6.1 Introduction

In this chapter, we used another type of bio-receptors commonly used these days where instead of antibodies; these are aptamers, which are utilized in bio-sensing tests to detect several mycotoxins, e.g. ochartoxin A and aflatoxin B1, M1. The aptamers change their conformation (in simple terms, wrapped around the target molecules) upon binding. We used anti- OTA aptamers, though without label, in combination with the TIRE method, and achieved the detection of OTA down to 0.01 ng/ml concentrations. We also used non-labelled aptamers (from Microsynth, Switzerland) for AFT B1 having the following nucleotide sequence: SH-5'-GTTGGGCACGTGTTGTCTCTCTGTGTCTC-GTGCCCTTCGCTA GGCCCACA-3'

with SH group at 5' (or C5) terminal and label-free terminal 3' (orC3). The presence of a thiol group at one end allowed simple immobilization of aptamers on gold, the other end could be either label-free or may contain functional groups suitable for electrochemical study.

6.2 Results and discussion

6.2.1 OTA detection using 25 nm continuous Au film

6.2.1.1 Sample preparation and immobilization of aptamers

Standard microscopic glass slides were cleaned in hot piranha solution (3:1 mixture of H₂SO₄ and H₂O₂) for 1 h followed by rinsing with deionized Milli-Q water and drying under a stream of nitrogen gas. A thin (2–3 nm) layer of chromium was first evaporated to improve the adhesion of gold layer to glass. Gold layers of about 25 nm in thickness were evaporated on glass slides using Edwards E306A metal evaporator unit. Such two-stage evaporation was carried out without breaking the vacuum of no less than 10⁻⁶ Torr.

DNA-based aptamers specific to OTA acquired from M/s Microsynth (Schutzenstrasse, Balgach, Switzerland) have the following oligonucleotides sequence: 5-SH-GATCGGGTGTGGGTGGCGTAAAGGGAGCATCGGACA-3. The aptamer was functionalized with the thiol group (C3-SH) on the 5-terminal position to obtain strong and oriented binding to gold. The immobilization of aptamers on the gold surface was carried out by mixing the original 100 mM aptamer solution with 2 mM of 1,4-Dithiothreitol (DTT) diluted in 100 mM HEPES buffer (pH 7.4) supplemented with 2 mM of MgCl₂ in order to remove the protecting group and subsequently release aptamers with the SH end-groups which then bind to gold (Tombelli et al., 2005). Before immobilization, the liquid aptamer samples were activated by quick (5 min) heating up to 90°C followed by 5 min cooling to 4°C using thermo-cycling PCR unit (Master cyclerpersonal Eppendorf VWR, Leuven, Belgium). Immobilization was carried out by casting aptamer solution onto gold coated slides; the immobilization

time was 10–12 h at room temperature in moist atmosphere. The unreacted oligonucleotide was removed from the gold slides by several rinsing stages with HEPES/MgCl₂ buffer. Then, gold coated glass slides with immobilized aptamers were kept in HEPES/MgCl₂ to prevent aptamers from coiling. Interestingly, the samples prepared were quite stable and kept their functionality for few a weeks.

6.2.1.2 TIRE measurements

The method of total internal reflection ellipsometry (TIRE) and its application for detection of mycotoxins has been described previously in detail in chapters 2 and 3. Ellipsometry data in ψ and Δ are recorded where the more sensitive Δ -spectra are typically exploited in TIRE biosensing and thus used in this work. Gold coated glass slides with continuous films and immobilized aptamers were used in these experiments. The injected solution was ochratoxin A (OTA) acquired from Microsynth (Switzerland); the original stock solution (10 $\mu\text{g/ml}$) of OTA in acetonitrile was multiply diluted with PBS buffer to obtain the required concentrations of 0.01, 0.1, 1, 10, 100, and 1000 ng/ml. Two types of ellipsometric measurements were carried out: (i) single spectroscopic scans carried out in a standard buffer solution after completion of the adsorption (or binding) stage and (ii) dynamic measurements, i.e, a large number of spectroscopic scans taken during the binding of analytes to receptors which provide information related to the reaction kinetics. The latter measurements were used for sensing. The shift of Δ spectra (a phase related ellipsometric parameter), constitutes the TIRE sensor response. A typical series of TIRE Δ -spectra recorded after injecting OTA of different concentrations is shown in Figure 6.1. As one can see, a progressive blue

spectral shift has developed upon OTA binding. This is observation which can be interpreted by decreasing in the molecular layer thickness (or refractive index).

The ellipsometry data fitting using a four-layer model (glass-gold-molecular layer-water) allows evaluating the thickness of the immobilized aptamer layers (the data fitting procedure was described in detail previously (Nabok and Tsargorodskaya, 2008; Nabok et al., 2011)). Similar to our earlier works, it was assumed that the refractive index of the molecular layer was not much affected during binding OTA, and thus the effect was associated entirely with changes in the aptamer layer thickness.

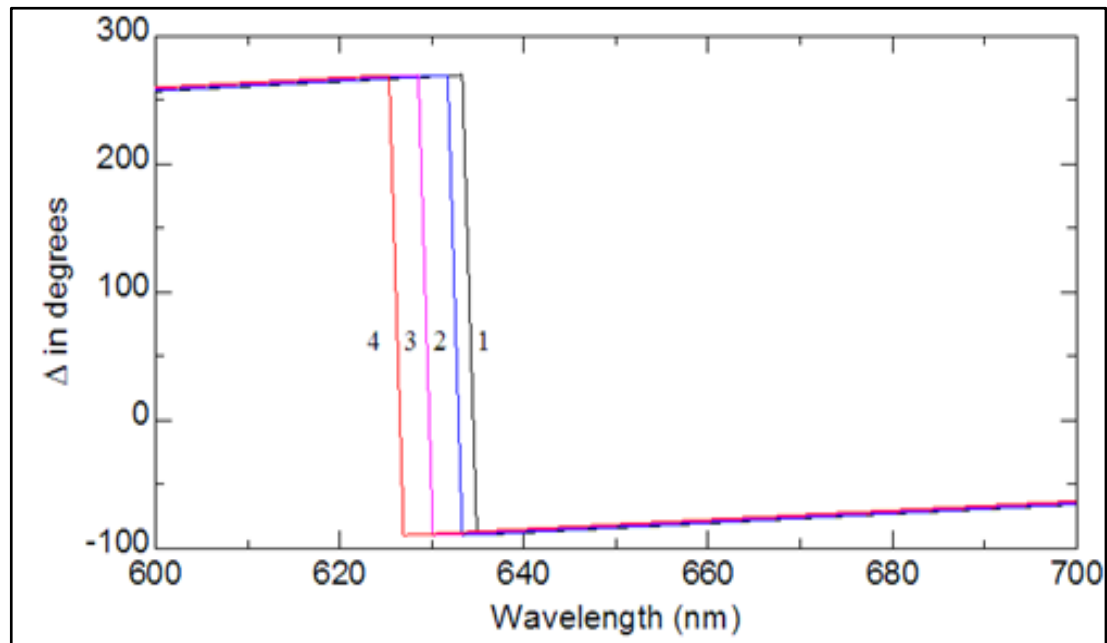


Figure 6.1. TIRE spectra recorded on aptamer layer (1), and after binding OTA of 0.01ng/ml (2), 1ng/ml (3), and 10ng/ml (4)

The results of TIRE data fitting are shown in Figure 6.2 as the dependence of thickness against the concentration of OTA. As one can see, the thickness increment appeared to be negative thus corresponding to decrease in the aptamer layer thickness upon binding

of OTA. Such process is well-understood assuming that aptamers are coiling around the OTA target molecule by forming G-quadruplex as illustrated on inset in Figure 6.2. The minimal detected concentration of OTA in these experiments was 0.01ng/ml.

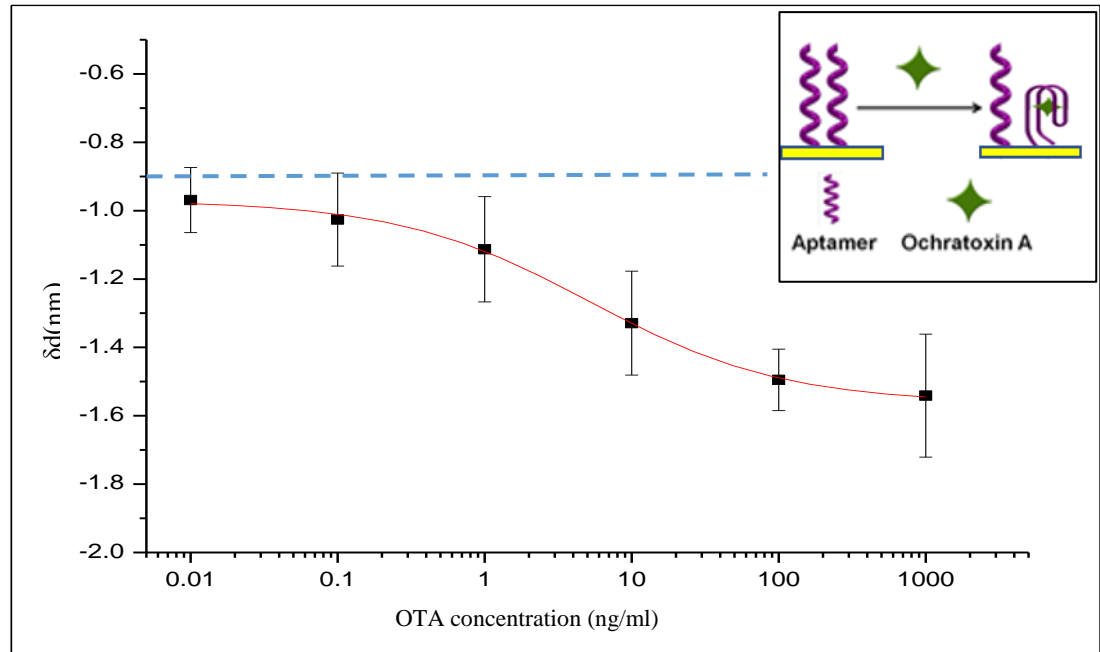


Figure 6.2. Dependence of the thickness decrease of the aptamer layer vs OTA concentration

Negative control experiments were carried out by injecting pure PBS buffer solution (with no OTA) into the cell. The results of such measurements are shown in Figure 6.3. There is no noticeable spectral shift recorded.

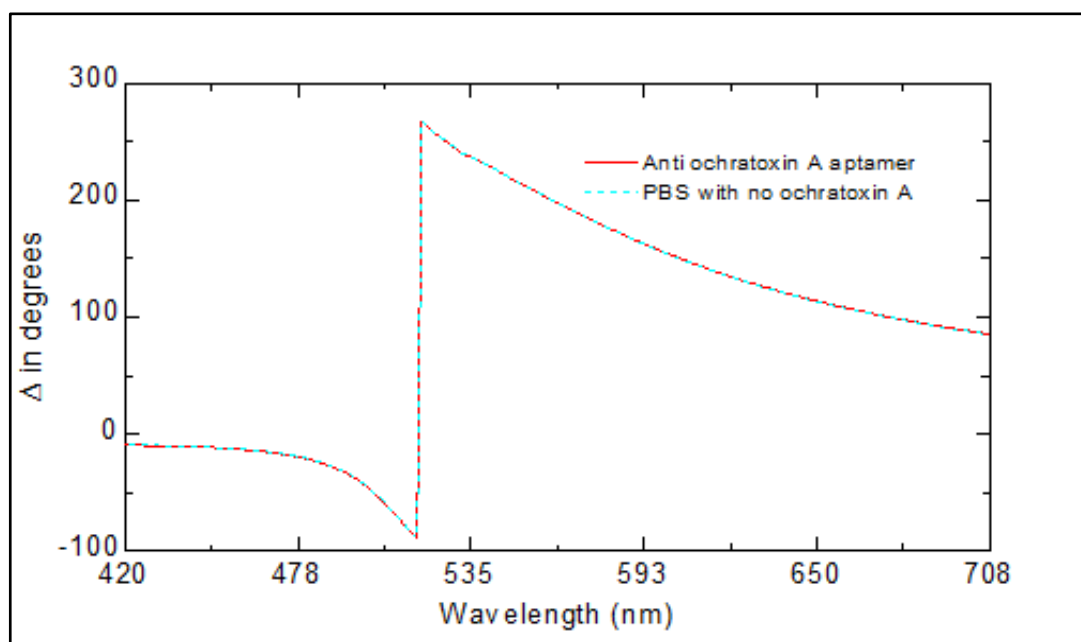
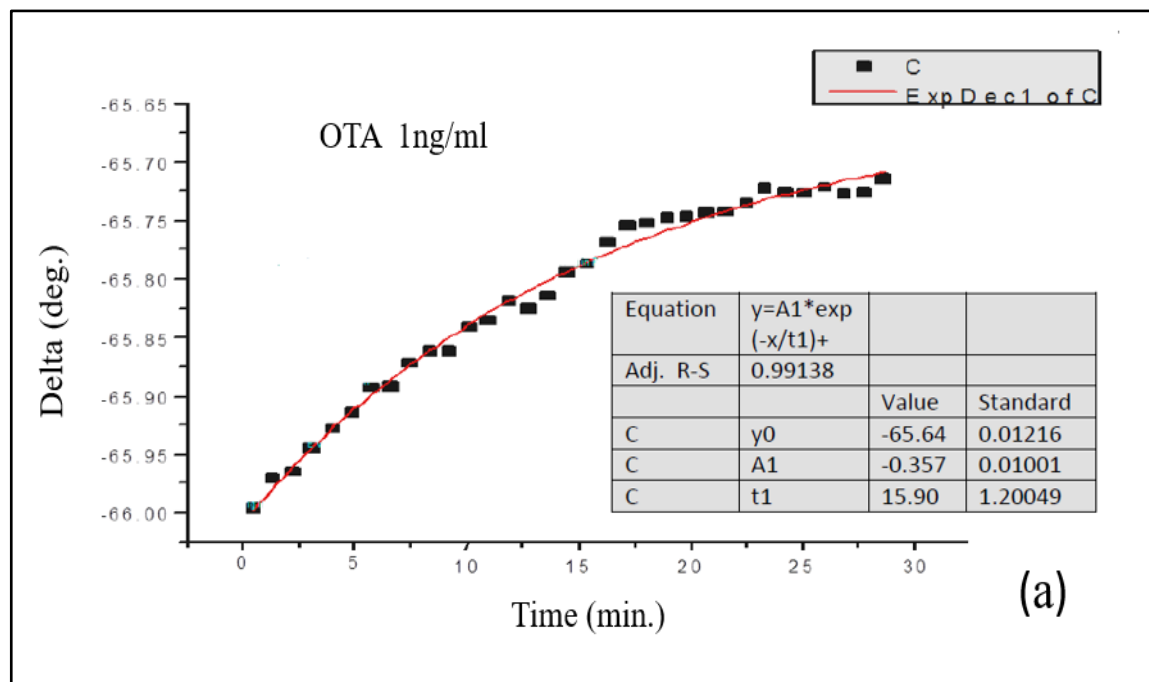


Figure 6.3. TIRE spectra of aptamer layer show no shift after injecting pure PBS buffer solution with no ochratoxin A into the cell

The data fitting gives actually a small “blue” spectral shift corresponding to a thickness decrease of about 0.9 nm. This can be explained by spontaneous self-coiling of aptamers in BPS buffer (aptamers are usually kept in HEPES buffer containing $MgCl_2$ salt in order to prevent self-coiling). Such 0.9 nm thickness decrease can be considered as a baseline for detection (shown as a dotted line in Figure 6.2). The thickness increment of about 1 nm corresponding to 0.01 ng/ml concentration of OTA is just above the baseline. The achieved detection limit of 0.01 ng/ml for OTA is remarkable for direct assay format, an order of magnitude lower than it was reported earlier for TIRE detection of mycotoxins in direct immunoassay with antibodies (Nabok and Tsargorodskaya, 2008; Nabok et al., 2011).

6.2.1.3 OTA-aptamer binding kinetics

The kinetics of OTA binding to aptamers was studied using the data analysis protocol developed earlier for immune binding reaction and successfully applied for detection of mycotoxins in direct immunoassay with specific antibodies (Nabok et al., 2007; Nabok et al., 2011). This approach is based on Langmuir adsorption model of binding analytes of concentration C to molecular receptors with concentration N on the surface as was mentioned in detail in chapter 2. The binding kinetics was therefore studied by recording a number of TIRE spectra during binding of OTA to aptamers and plotting the resulted time dependences of Δ (or Ψ) at particular wavelength, e.g. 600nm, as shown in Figure 6.4(a) and (b). The time constant (τ) was then extracted by fitting the data to the rising exponential function.



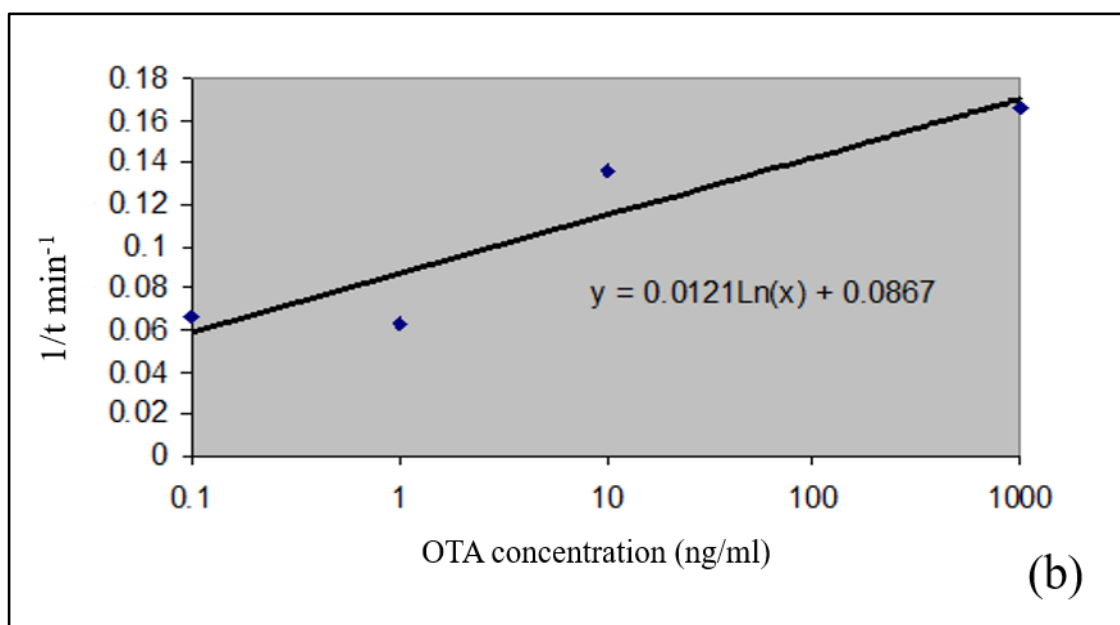


Figure 6.4. Typical time dependence of Δ during binding of OTA of 1ng/ml to aptamers (a); evaluation of K_A (b)

Such procedure was repeated for all dynamic scans taken during binding OTA of different concentrations, and the results were presented in a graph $1/\tau$ against the OTA concentration in Figure 6.4c. The values of k_a and k_d can be found as the gradient and intercept, respectively, of the linear dependence $1/\tau = k_a C + k_d$ in Figure 2.6. Then both the association constant (K_A) and affinity constant (K_D) can be found as $K_A = k_a/k_d$ and $K_D = 1/K_A$. The obtained values of $K_A = 5.63 \cdot 10^7$ (mol^{-1}) and $K_D = 1.77 \cdot 10^{-8}$ (mol) for aptamers-OTA binding are typical for high affinity reactions and similar to those of antibody-antigen binding (Nabok et al., 2007; Nabok et al., 2011).

6.2.2 Detection of AFT B1 and M1 using aptamers immobilized on 5 nm nano-structured Au film

6.2.2.1 Samples preparation

The fabrication of nanostructured gold films for LSPR experiments is schematically outlined in Figure 6.5. Standard microscopic glass slides are cleaned with hot "piranha"

solution, then rinsed with deionized water and dried under a stream of nitrogen gas. A layer of gold was thermally evaporated on clean glass slides in 10^{-7} Torr vacuum using Edwards 360 metal evaporation unit. The thickness of Au layers was in the range from 5 nm to 10 nm and controlled by QCM sensor during evaporation. The gold coated slides were then annealed in air at 550-580 C° for 10 hours as described in (Karakouz et al., 2008) which transforms the continuous gold films into nanostructures consisting of randomly distributed gold islands with the average lateral dimensions of 25 to 150 nm and exhibiting a distinctive LSPR band in the visible spectral range.

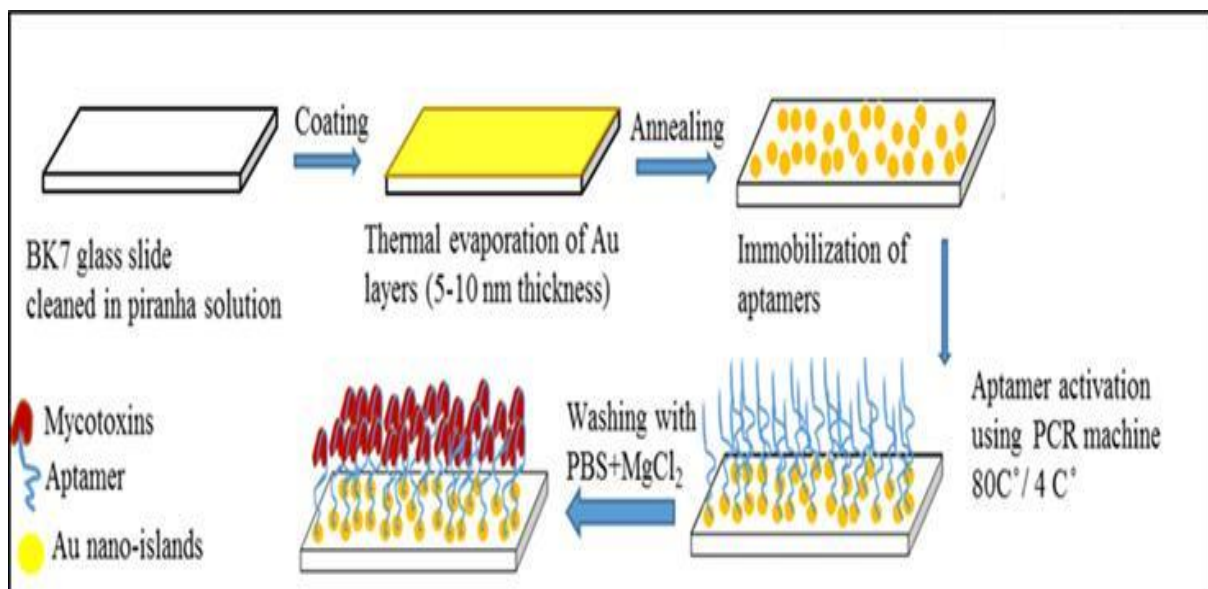


Figure 6.5 The sequence of steps of samples preparation and immobilization of aptamer on gold nanostructures

6.2.2.2 Aptamers for AFT B1 and M1

The aptamers used in our work were synthesized and purified by Microsynth (Schutzenstrasse, Balgach, Switzerland). The sequence of nucleotides for anti-aflatoxin B1 (AFT B1) and anti-aflatoxin M1 (AFT M1) aptamers which were established previously in (Xiaoyuan et al., 2014) and (Malhotra et al., 2014) are shown below:

5'SH-GTTGGGCACGTGTTGTCTCTCTGTGTCTCGTGCCCTTCGCTAGGCCACACA-3'
for AFT B1, and 5'SH -ACTGCTAGAGATTTTCCACAT-3' for AFT M1.

For our purpose we used aptamers with no labels on 3' termini, but only SH groups at 5' termini for immobilization on the surface of gold. Aflatoxin B1 and M1 were purchased from Sigma-Aldrich. The other chemicals used were magnesium chloride (MgCl_2), (Dithiothreitol (DTT) an excellent reagent for maintaining SH groups) also purchased from Sigma-Aldrich. All reagents were of analytical grade. Deionized Milli-Q water was used for preparation of reagents throughout the experiments. Hepes binding buffer solution (HBB, 50 mM) was prepared by dissolving 50 mM Hepes sodium salt (3 mM MgCl_2 , 120 mM NaCl, and 5 mM KCl) in deionized Milli-Q water. The pH of the buffer was adjusted to 7.4. Similarly, phosphate binding buffer (PBB, 100 mM) was prepared by dissolving 10 mM Na_2HPO_4 , 1.76 mM KH_2PO_4 , 3 mM MgCl_2 , 2.7 mM KCl, and 137 mM NaCl in deionized water. The pH of the buffer was adjusted to 7.4. The presence of MgCl_2 in both HBB and PBB solutions is crucial for preventing self-coiling of aptamers.

The aptamers are delivered in lyophilized form. Therefore, aptamer stock solution is prepared at 100 μM by adding an appropriate volume of de-ionized water. For long-term storage, as-received aptamers were prepared in small 100 μM aliquots in deionized water and stored frozen. The stock solution of aptamer was diluted at desired concentration with HBB or PBB supplemented with 1 mM of DTT and then subjected to heating at 90 °C for 5 min and cooling at 4 °C for 5 min cycle in PCR machine before use. Aflatoxin B1 and M1 stock solutions (1 mg mL^{-1}) were prepared in acetonitrile. In addition, further diluted solutions were prepared in HBB or PBS. We maintained the percentage of acetonitrile at less than 2% in the final assay throughout

the experimental procedure. All of the working solutions were prepared freshly before use and stored at 4 °C when not in use.

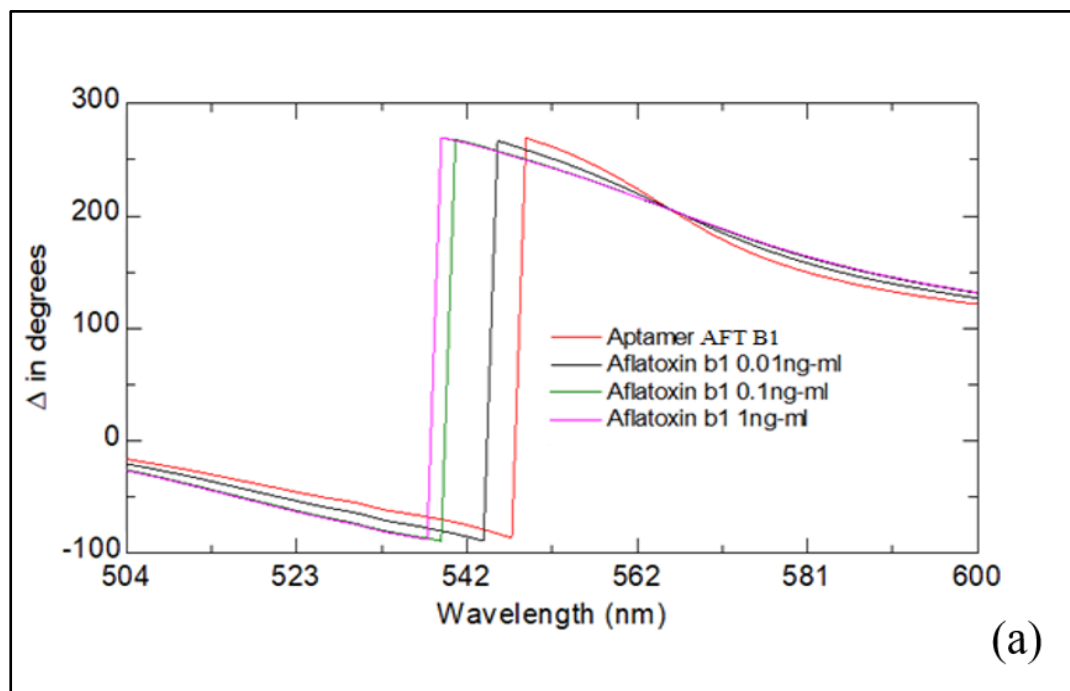
6.2.2.3 Immobilization of aptamers on gold

Immobilization of anti-AFT B1 and anti-AFT M1 aptamers on nanostructured gold films was carried out following the protocols described in detail in (Rhouati, et al., 2013; Balamurugan et al., 2008). As shown in Figure 6.5, a 100 μ l of respective aptamer solution of optimized concentration of 5 μ M or 2 μ M in PBB or HBB buffer supplemented with 1mM of DTT was pipetted onto prepared glass slides with nano-structured gold. After incubation for 4 h in a humidity chamber, the slides were rinsed with PBB to remove unbound aptamers. The resultant aptamer modified slides were either used directly as aptasensor or stored in binding buffer at 4°C for several days without any noticeable decrease in their functionality.

6.2.2.4 TIRE experimental of detection AFTB1 and M1

A 0.2 mL PTFE cell is attached to the sample which allows the injection of different solutions into the cell to study different concentration of Aflatoxin B1 and M1. The TIRE method has an advantage of recoding two ellipsometric parameters Ψ and Δ , which represent, respectively, the amplitude ratio and phase shift between p- and s-components of polarized light. Figure 6.6a shows a set of Δ spectra recorded on our LSPR transducers functionalized with anti- aflatoxin (anti-AFT) B1 after consecutive binding steps of aflatoxin B1 starting from small concentrations. A progressive “blue” (to shorter wavelength) spectral shift was observed, which is typically associated with

the reduction in the aptamer layer thickness due to aptamers coiling around the target molecules. Similar results were obtained for binding aflatoxin M1 to its specific aptamer (see Figure 6.6b), however the saturation of the response was observed at much smaller concentrations of AFT M1 of 1 ng/mL, which could be caused by a smaller concentration of active aptamers immobilized on the surface. In addition, the cross-sensitivity of the two aptamers was tested, and no spectral shift was recorded when attempting bind AFT B1 to an aptamer specific to AFT M1, and vice versa. Also, both the anti-AFT B1 and anti-AFT M1 aptamers do not bind OTA (ochratoxin A), and no spectral shift was recorded when attempted binding AFT B1 to an aptamer specific to AFT M1, and vice versa.



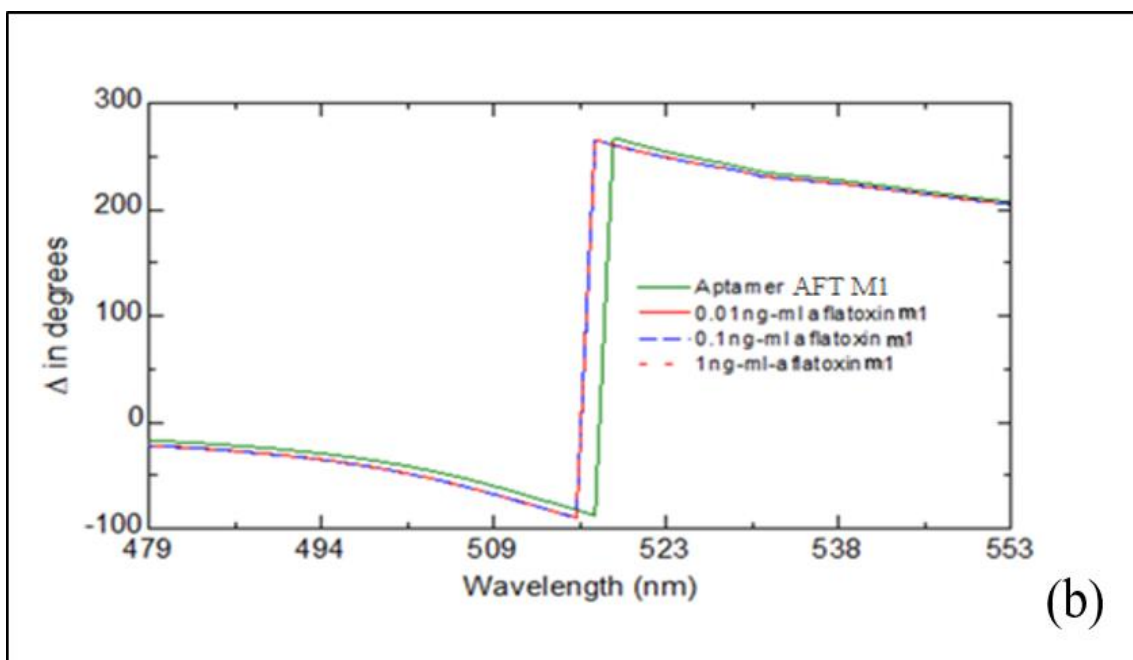


Figure 6.6. A series of TIRE Δ spectra recorded upon binding of AFT B1 (a) and AFT M1 (b) to respective specific aptamers

The fitting of the TIRE spectra to a three-layer model, allowed the evaluation of the aptamer layer thickness that is shown in Figure 6.7. The absolute values of the aptamer layer thickness, which depends on several factors, i.e., aptamer chain length, concentration of aptamers, concentration of $MgCl_2$ in the buffer. The main interest was in the changes of aptamer layer thickness upon binding the target molecules. The decrease in the anti-AFT B1 aptamer layer thickness by 14.2%, upon increasing the concentration of AFT B1, is much more noticeable in Figure 6.7a than the 2.6% for the layer of anti-AFT M1 binding to the respective target in Figure 6.7b.

Negative tests were performed and resulted in no spectral shift for attempted binding AFT B1 to anti-AFT M1 aptamer, and vice versa. Also, both the anti-AFT B1 and anti-AFT M1 aptamers do not bind OTA (Ochratoxin A).

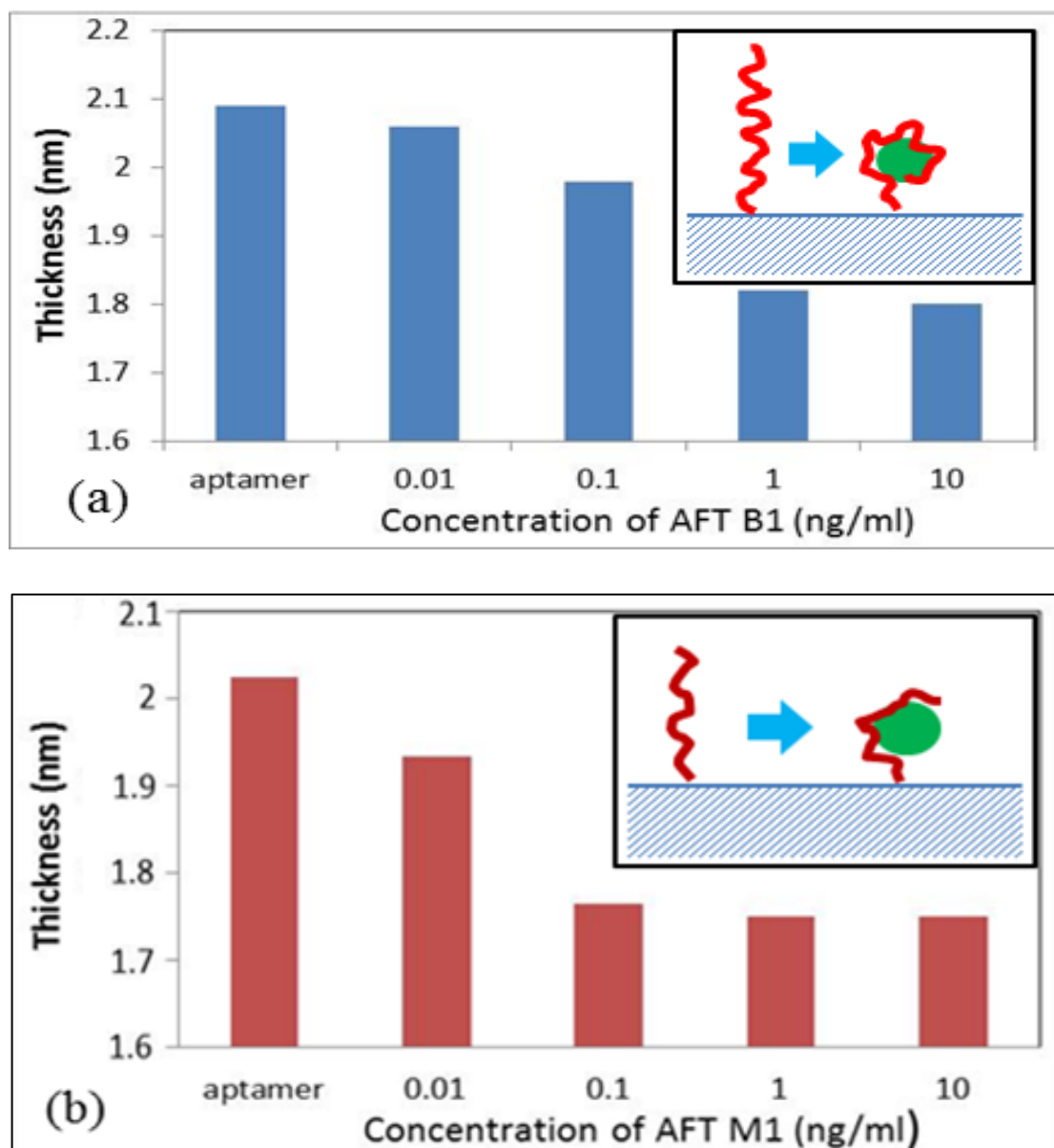


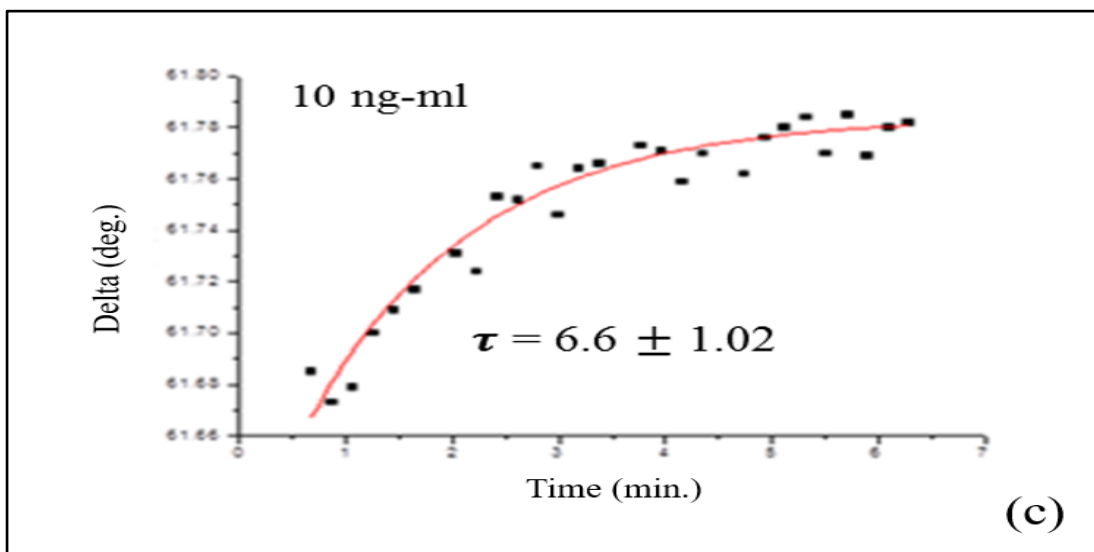
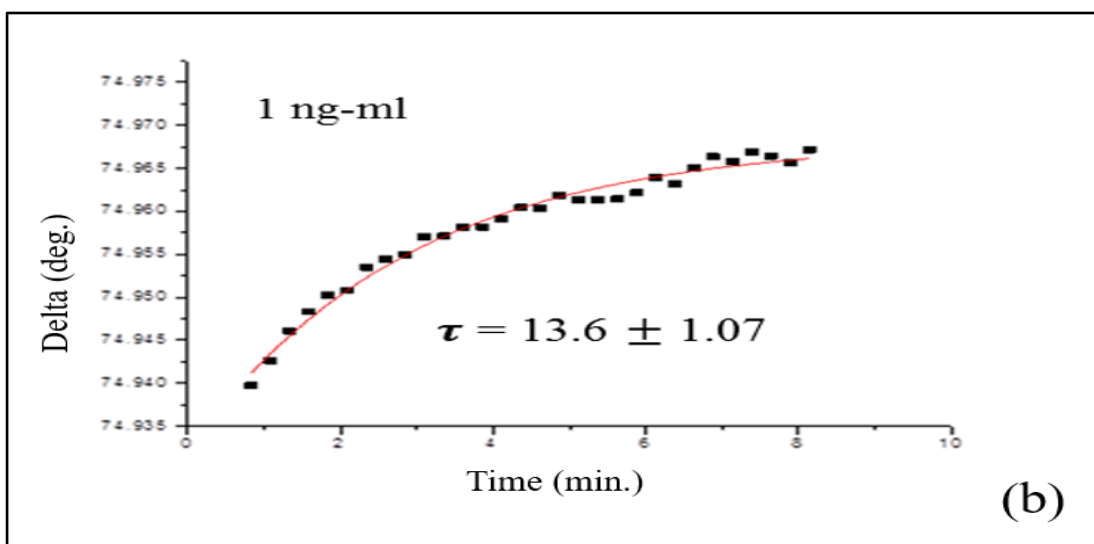
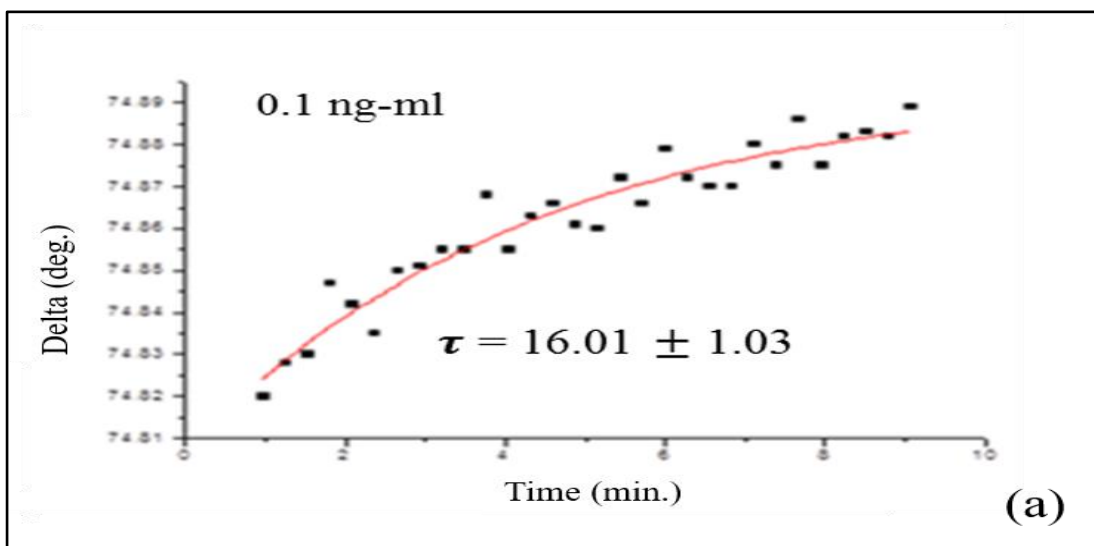
Figure 6.7. Dependences of the aptamer layer thickness vs concentration of AFT B1 (a) and AFT M1 (b)

The processes of aptamer/target binding are illustrated by the corresponding insets. As was suggested, the decrease in the aptamer layer thickness upon binding aflatoxins is caused by coiling aptamers around the target molecules, and this process is schematically illustrated on inset in Figure 6.7(a). The differences in the binding abilities of anti-AFT B1 and anti-AFT M1 are most-likely related to their oligonucleotides chain length (50 and 21,

respectively). The much shorter aptamer to AFT M1 may not fully engulf the target molecule, but rather have a small bend in the chain as illustrated in the inset in Figure 6.5(b), which is still detectable using a sensitive ellipsometry instrument. The spectral resolution of our ellipsometry instrument did not allow the detection of aflatoxins below 0.01 ng/mL. Nevertheless, the minimal detected concentration of 0.01 ng/mL for both aflatoxins corresponding to 10 part per billion (ppb) is a remarkable result for direct aptamer assay format.

6.2.2.5 Study of Aflatoxin-Aptamer Binding Kinetics

Following the procedure described earlier (Nabok et al., 2007; Nabok et al., 2011;), the study of the kinetics of binding AFT B1 to a specific aptamer was carried out by recording a number of TIRE spectra during binding reaction, and then plotting the time dependences of the values of Ψ or Δ at a particular wavelength. Figure 6.8 (a-d) shows a typical time dependence of Δ at 600 nm during binding of 0.1, 1, 10 and 100 ng/mL of AFT B1 to specific aptamer. The time constant τ was evaluated by fitting the data to the rising exponential function. The same procedure was repeated for different concentrations of AFT B1, and the obtained values of τ were plotted as $1/\tau$ against AFT B1 concentration (C) in Figure 6.8



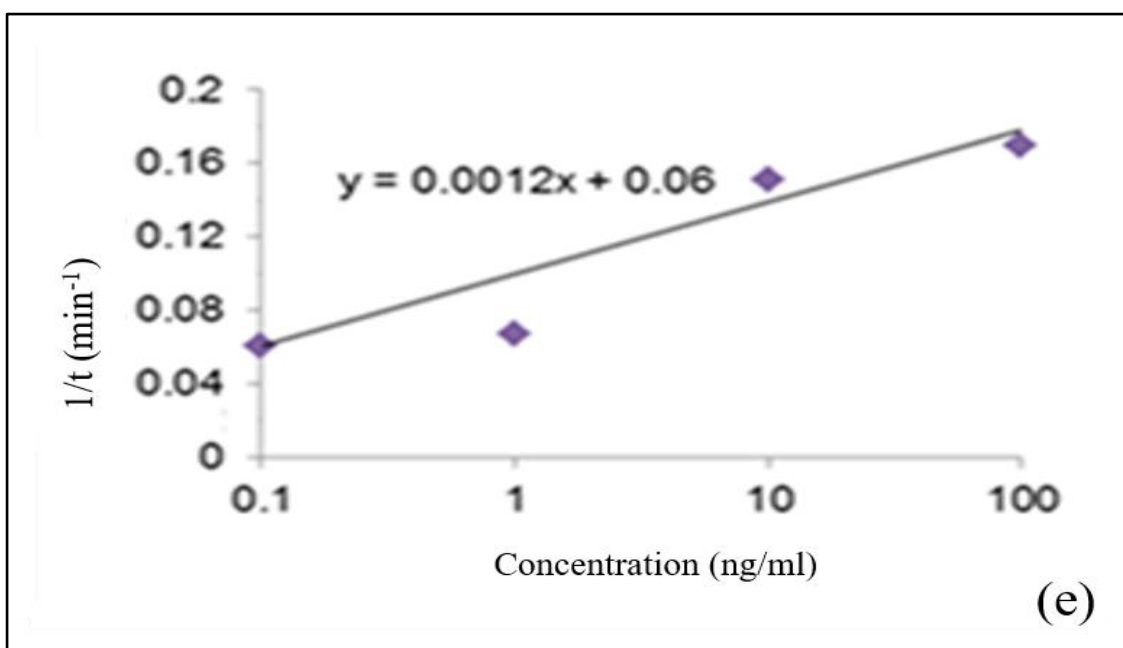
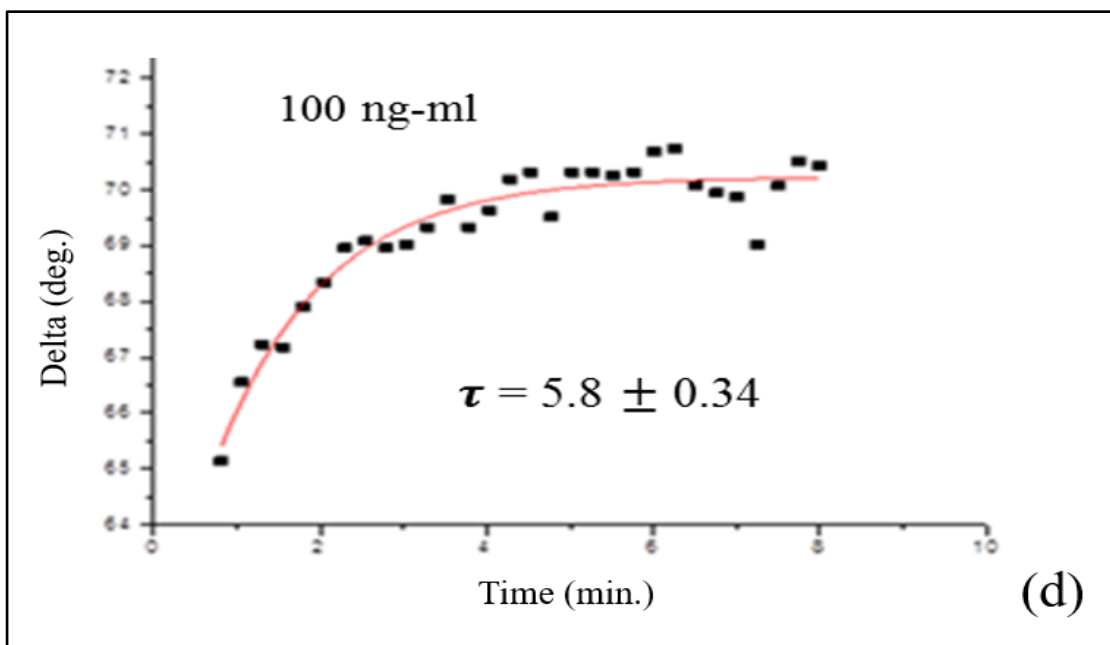


Figure 6.8 Typical time dependences of Δ at 600 nm during binding of AFT B1 of different concentrations (a) 0.1 ng/ml, (b) 1 ng/ml, (c) 10 ng/ml and (d) 100 ng/mL to specific aptamer (e) $1/\tau$ against AFT B1 concentration.

The absorption rate (k_a) and desorption rate (k_d) were found, respectively, from the gradient and intercept of the linear graph $1/\tau = k_a C + k_d$ then the association and affinity constants were found as $K_A = k_a / k_d$ and $K_D = 1 / K_A$. The obtained values of $K_A = 3.12 \cdot 10^7$ (mol^{-1}) and $K_D = 3.2 \cdot 10^{-8}$ (mol) shows high specificity of AFT B1/aptamer interaction, similar to that of monoclonal antibodies to AFT B1 (Nabok et al., 2011). Similar analysis was carried out for binding kinetics of AFT M1 to respective aptamer and yielded the values of $K_A = 4.64 \cdot 10^6$ (mol^{-1}) and $K_D = 2.1 \cdot 10^{-7}$ (mol). The affinity of a shorter anti-AFT M1 aptamer appeared to be much smaller than that of anti-AFT B1 having longer chain. This proved our initial suggestion of the effect of the aptamer nucleotide chain length on its affinity. The minimum concentration of AFT B1 detected was also 0.01ng/ml, though potentially the LDL could be an order of magnitude lower. The saturation of the response was observed at much smaller concentrations of AFT B1 of about 10ng/ml. This situation could be improved, and the dynamic range of detection extended if we use higher concentration of aptamers.

Summary

The combination of a simple LSPR transducer based on nanostructured gold films and the optical method of total internal reflection ellipsometry (TIRE) allowed for label-free detection of small molecules of aflatoxin in direct assay with specific aptamers immobilized on the surface of gold. The observed decrease in the aptamer layer thickness upon the binding of their specific target molecules is consistent with the model of aptamers wrapping round the target. The concentration range for aflatoxin B1 detection stretches from 0.01 ng/mL to 100 ng/mL, where the minimal detected concentration of aflatoxins and

OTA corresponding to 0.01 ppb is remarkably low for LSPR-based biosensors, especially considering the small molecular weight of aflatoxin molecules and direct aptamer assay format. Such sensitivity, although it may not be as good as that for advanced methods of HPLC or mass spectroscopy, is suitable for the detection of mycotoxins in concentrations close to the legislated limits (Romerlabs, 2016). The study of binding kinetics of AFT B1 and AFT M1 to specific aptamers confirmed the high specificity of the aptamer/target reaction with the affinity constants found to be in tens of nano-moles, which are similar to the values reported earlier (Ma et al., 2014; Malhotra et al., 2014) and similar to those of antigen/antibody reactions (Nabok et al., 2008; Nabok et al 2007; Nabok et al., 2011).

Aptamer to AFT M1 appeared to be less specific as compared to longer-chain aptamer to AFT B1. To our knowledge, this is the first report on the experimental evaluation of aptamers affinity. The association constant $K_A = 5.63 \cdot 10^7 \text{ mol}^{-1}$ and the affinity constant $K_D = 1.77 \cdot 10^{-8} \text{ mol}$ found from the binding kinetics study are characteristic for highly specific aptamer-OTA binding. The other advantages of the proposed method are label-free detection and the use of a simple, quick and cost-effective direct assay format.

Reference list

Balamurugan, S., Obubuafo, A., Soper, S. A., & Spivak, D. A. (2008). Surface immobilization methods for aptamer diagnostic applications. *Analytical and bioanalytical chemistry*, 390(4), 1009-1021.

Bueno, D., Mishra, R. K., Hayat, A., Catanante, G., Sharma, V., Muñoz, R., & Marty, J. L. (2016). Portable and lowcost fluorescence set-up for in-situ screening of Ochratoxin A. *Talanta*, 159, 395-400.

Karakouz, T.; Tesler, AB.; Bendikov, TA.; Vaskevich, A.; Rubinstein, I. (2008). Highly stable localized plasmon transducers obtained by thermal embedding of gold island films on glass. *Adv. Mater*, 20, 3893-3899.

Ma, X., Wang, W., Chen, X., Yu, X.; Wu, S., Duan, N., Wang, Z. (2014) Selection, identification, and application of Aflatoxin B1 aptamer. *Eur. Food Res. Technol*, 238, 919–925.

Malhotra, S., Pandey, A.K., Rajput, Y.S., Sharma, R.J. (2014). Selection of aptamers for aflatoxin M1 and their characterization. *J. Mol. Recognit*, 27, 493–500.

Nabok, A.; Tsargorodskaya, A.; Mustafa, M.K.; Szekacs, I.; Starodub, N.F.; Szekacs, A. (2009). Detection of low molecular weight toxins using optical phase detection techniques. *Procedia Chem*, 1, 1491–1494.

Nabok, A. V., Tsargorodskaya, A., Holloway, A., Starodub, N. F., & Gojster, O. (2007). Registration of T-2 mycotoxin with total internal reflection ellipsometry and QCM impedance methods. *Biosensors and Bioelectronics*, 22(6), 885-890.

Nabok, A. V., Mustafa, M. K., Tsargorodskaya, A., & Starodub, N. F. (2011). Detection of aflatoxin B1 with a label-free ellipsometry immunosensor. *BioNanoScience*, 1(1-2), 38-45.

Nabok, A., & Tsargorodskaya, A. (2008). The method of total internal reflection ellipsometry for thin film characterisation and sensing. *Thin Solid Films*, 516(24), 8993-9001.

Rhouati, A.; Yang, C.; Hayat, A.; Marty, J-L. (2013). Aptamers: A promising tool for Ochratoxin A detection in food analysis. *Toxins*. 2013, 5, 1988-2008.

Tombelli, S.; Minunni, M.; Mascini, M. (2005). Analytical applications of aptamers. *Biosens & Bioelectron*, 20, 2424–2434.

Worldwide Mycotoxin Regulations—Romer Labs. (2016). Available online:<https://www.romerlabs.com/en/knowledgecenter/knowledgelibrary/articles/news/worldwide-mycotoxin-regulations/> (accessed on 16 June 2016).

Xiaoyuan Ma; Wenfeng Wang; Xiujuan Chen; Yu Xia; Shijia Wu; Nuo Duan; Zhouping Wang. (2014)., Selection, identification, and application of Aflatoxin B1 aptamer, *Eur. Food Res.& Technol*, 238 (6), 919–925.

Chapter 7: Development of nano-structured Au platform for SERS biosensing

7.1 Introduction

In this chapter we attempted to use Au nanostructures as platform for SERS biosensing. Two types of samples were prepared: (i) random gold nano-islands formed by dewetting, (ii) regular pointed nano-islands formed by nano-sphere lithography. The characterization was carried out using SEM, AFM, and UV-vis absorption spectroscopy. Raman spectra measurements were carried out on both continuous and nano-structured gold substrates, and the results were compared .

7.2 Formation of Au nano-structures using nano-sphere lithography

The effect of LSPR appeared to be more or less the same in both regular and random metal nanostructures. The advantages of ordered nano-structures are in the effect of SERS, which was observed in particular types of nanostructures. SERS-based sensors which are capable of detecting single molecules is the main direction in sensing research nowadays (Zhang et al., 2005; Haynes et al., 2005; Le Ru and Etchegoin, 2008).

One of the simplest methods of the formation of ordered metal nano-structures is nano-sphere lithography (Zhang et al., 2005) which was described briefly in chapter 2.

Polystyrene nano-spheres of 200 nm in diameter (from Fisher Scientific) were deposited on glass slides using a method of slow lifting as described in (Haynes et al., 2005; Zhang et al., 2005). Glass slides were thoroughly cleaned in pirahana solution and rinsed in deionised water prior to deposition.

A special care have to be taken to prevent incorporation of dust particles in the nano-sphere monolayer, therefore the deposition was carried out in a clean cabinet.

As shown in the diagram in Figure 7.1 colloid solution of polystyrene nano-spheres was dispensed on the surface of clean glass slide.

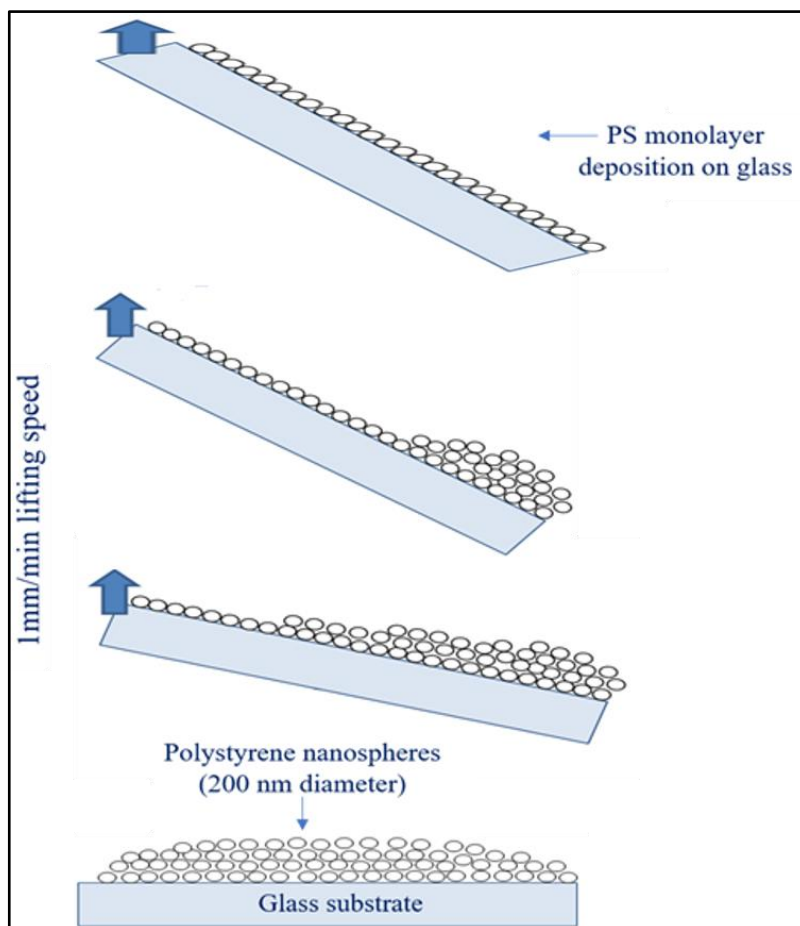


Figure 7.1. Deposition of close-packed spheres by slow lifting method

The slide was slowly (1mm/min) lifted at one end causing the liquid to roll down and leaving a monolayer of closely-packed spheres on the surface of glass slide. This process is illustrated by photographs in Figure 7.2.



Figure 7.2. Deposition of polystyrene nano-spheres monolayer on glass slide by slow lifting method

Then a layer of gold of about 20 nm in thickness was evaporated on top of PS monolayer using Edwards 306 metal evaporation system. A thin (3nm) layer of Cr was used to improve adhesion of gold to glass. After deposition of gold the polystyrene nano-spheres were removed by dissolving in tetra-hydrofuran (THF) which leave a regular pointed gold nano-island structure on the surface of glass. The process of nano-sphere lithography is illustrated in Figure 7.3.

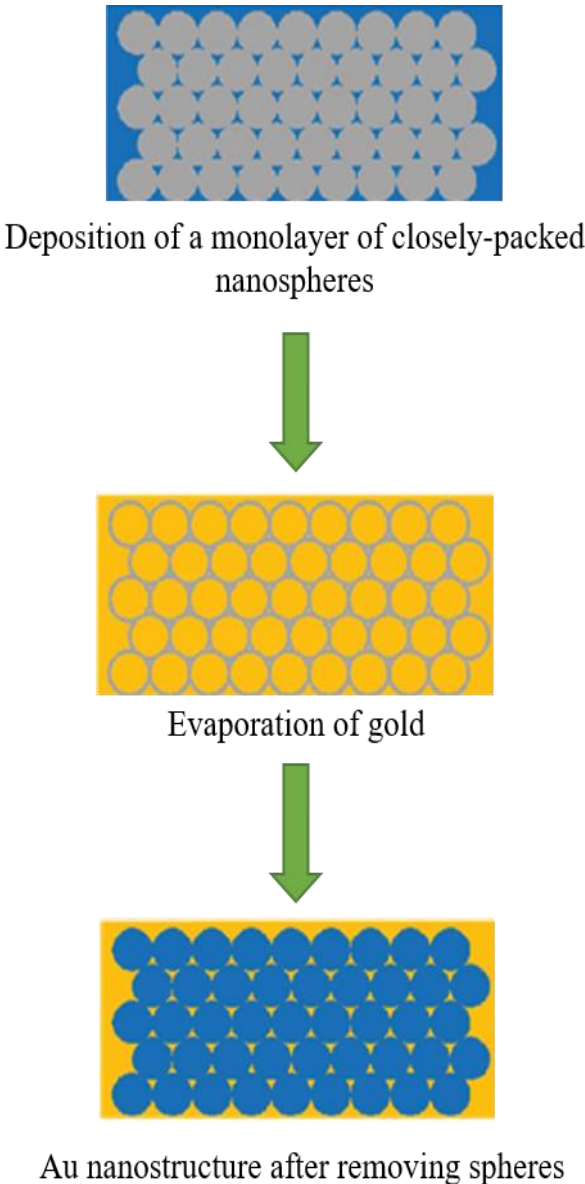
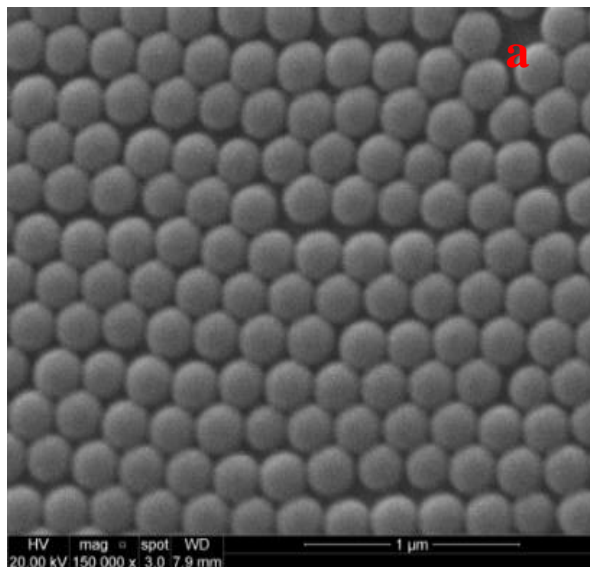


Figure 7.3. Formation of gold nano-structure by nano-sphere lithography

7.3 Characterization of Au nano-structures produced by nano-sphere lithography

The gold nano-structures produced by nano-sphere lithography were characterized using SEM, AFM and optical methods of UV-vis spectroscopy and SERS.

SEM image in Figure 7.4a shows a monolayer of polystyrene nano-spheres (200 nm in diameter) coated with gold. After removal of nano-spheres in THF (Bantzet al., 2011), SEM image in Figure 7.4b shows the remaining gold layer in a form of triangular nano-islands. The obtained Au nano-structure is not perfect because of defects in the closely-packed monolayer, but the regularity of the structure is apparent. AFM image in Figure 7.5 shows a monolayer of polystyrene nano-spheres coated with gold.



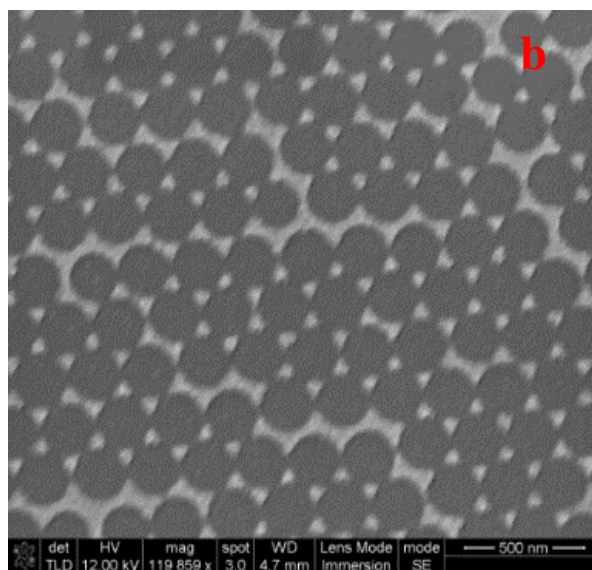


Figure 7.4. SEM images of closely-packed monolayer of polystyrene nanosphere coated by gold (a) and gold-nano-structures obtained after removing polystyrene sphere (b)

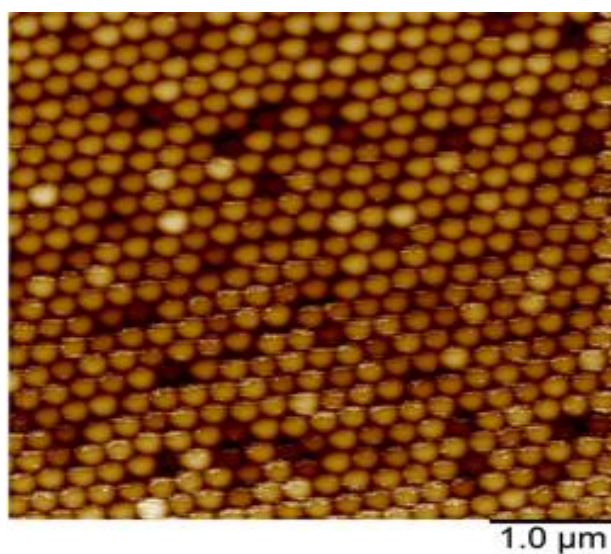


Figure 7.5. AEM image of closely-packed monolayer of polystyrene nano-sphere coated by gold

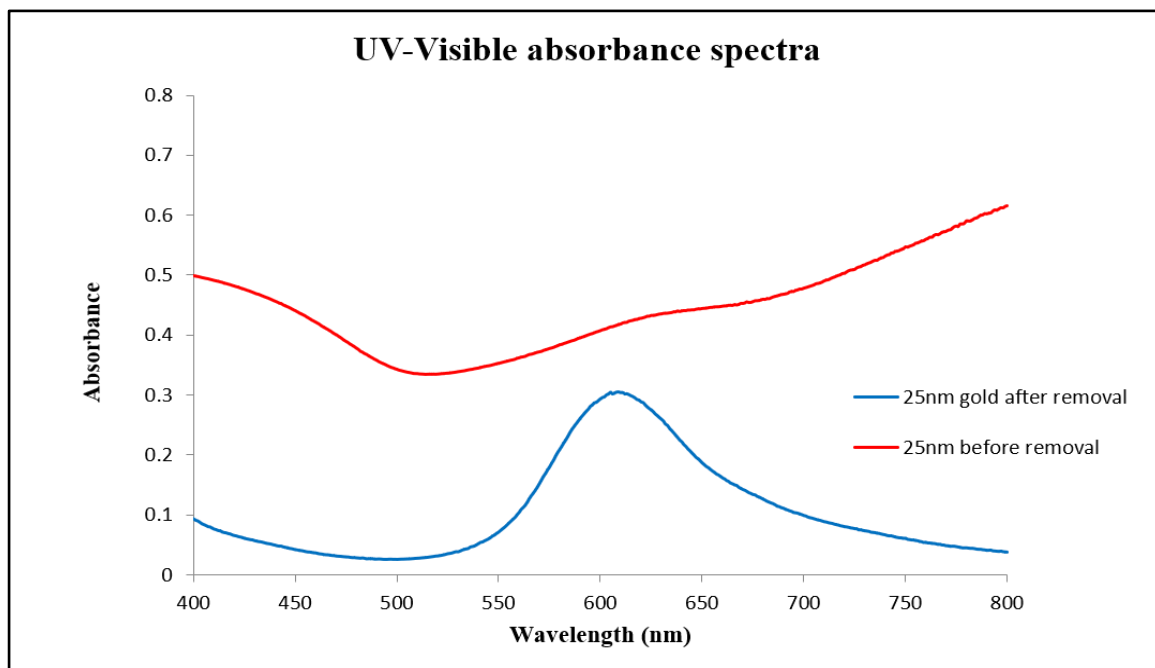


Figure 7.6. UV-Visible absorbance spectra of gold layer before and after removal of polystyrene nano-spheres

UV-visible spectra in Figure 7.6 shows the transformation of spectra after removal of polystyrene nano-sphere. The appearance of an LSPR band around 600nm corresponds to the formation of gold nano-islands.

7.4 SERS measurements of gold-nano-structures

Raman spectra measurements were performed on gold nano-structures using Thermo Fisher Scientific DXR2 Raman Microscope and employing 532 nm excitation a laser.

For Raman spectra measurements, the gold nanostructures were spin-coated with a layer of tetra-tertbutyl metal-free phthalocyanine (ttb-H₂P_c) (Bumrah and Sharma, 2016; Tsargorodska et al., 2014); this is a molecule with very strong characteristic absorption spectrum in visible range. The selection of this organic dye for Raman spectroscopy study

could help the observation of the effect of SERS as enhancement of characteristic vibration spectral lines by gold nano-structures. The SERS phenomenon occurs with metal nanostructures (Stiles et al., 2008; Haynes, 2005).

For comparison purposes, ttb-H₂P_c molecules were also deposited on the surface of continuous 25 nm Au layer. The Raman spectra of these two samples shown in Figure 7.7 demonstrate substantial enhancement of Raman spectral bands on nano-structured support due to the SERS effect. Comparison of the two spectra yields Raman enhancement of about 30 times.

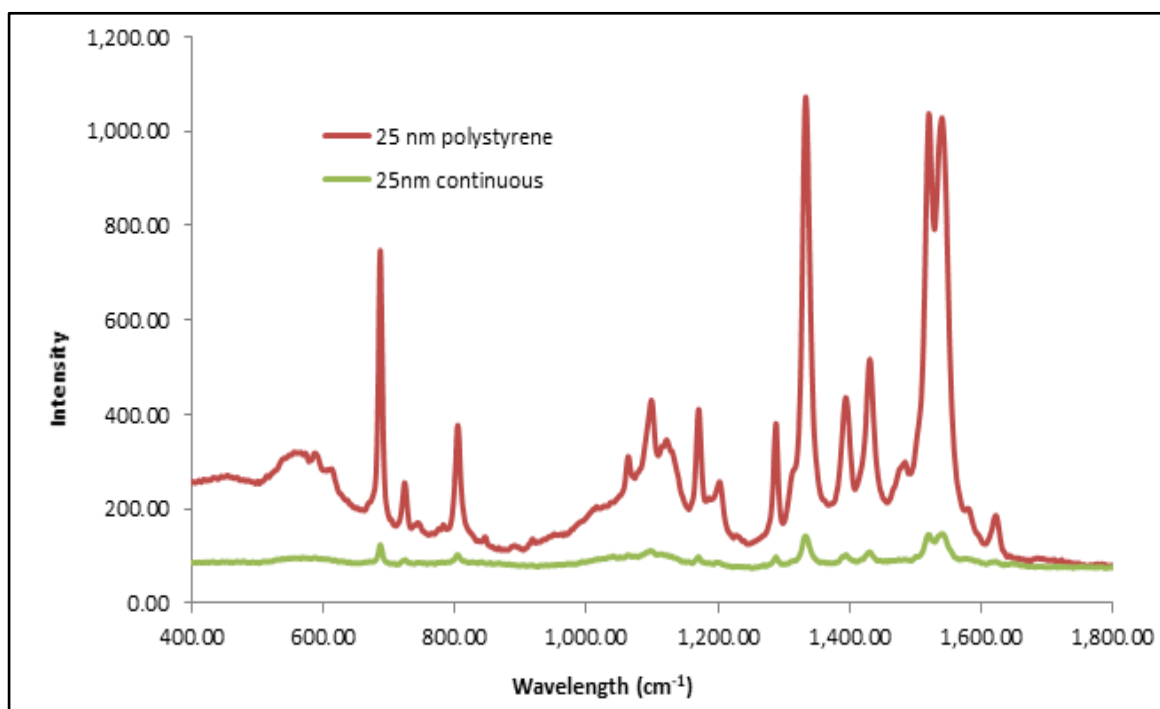


Figure 7.7 Raman spectra of ttb-H₂P_c deposited on 25nm thick continuous Au film (green line) and Au nano-structures formed by nano-sphere lithography (red line)

Similar experiments were carried out on irregular gold nano-structures obtained by thermal and microwave annealing. The Raman spectra of Au nano-structures made by both thermal

and microwave annealing given in Figure 7.8 show much smaller Raman enhancement of about 8 times as compared to control samples of $\text{ttb-H}_2\text{P}_c$ depended on continuous gold film and $\text{ttb-H}_2\text{P}_c$ powder.

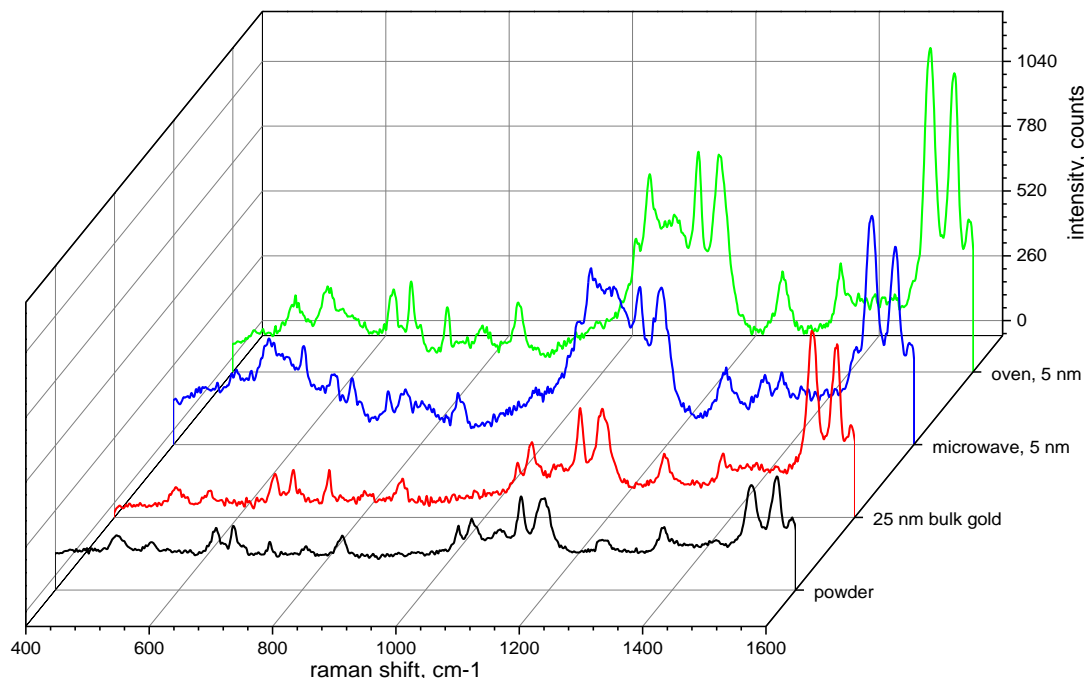


Figure 7.8. Raman spectra of $\text{ttb-H}_2\text{P}_c$ in a powder form (black) and thin films deposited on 25 nm thick continuous Au film (red), 5nm Au annealed film in a standard microwave (blue) and in oven (green)

Summary

The method of nano-sphere lithography allowed the formation of pointed gold nano-structures which provide the SERS effect with the Raman enhancement of about 30 times, higher than that of an irregular gold nano-structures produced by either thermal or microwave annealing. Such enhancement, however, was not sufficient to perform the

measurements on mycotoxins. On a positive note, the enhancement is relatively homogenous in a wide spectral range from 600 cm^{-1} to 1700 cm^{-1} which could be useful for biosensing. Further work is required to improve the SERS effect which could be achieved using nano-spheres of different diameters, different metals (for example Ag), and perhaps different types of nano-structures including a classical electrochemically roughened Ag.

Reference list

Aouani, H., Rahmani, M., Sipova, H., Torres, V., Hegnerová, K., Beruete, M., ... & Maier, S. A. (2013). Plasmonic nanoantennas for multispectral surface-enhanced spectroscopies. *The Journal of Physical Chemistry C*, 117(36), 18620-18626.

Bantz, K. C., Meyer, A. F., Wittenberg, N. J., Im, H., Kurtuluş, Ö., Lee, S. H., ... & Haynes, C. L. (2011). Recent progress in SERS biosensing. *Physical Chemistry Chemical Physics*, 13(24), 11551-11567.

Bumbrah, G. S., & Sharma, R. M. (2016). Raman spectroscopy—Basic principle, instrumentation and selected applications for the characterization of drugs of abuse. *Egyptian Journal of Forensic Sciences*, 6(3), 209-215.

Haynes, C. L., McFarland, A. D., & Duyne, R. P. V. (2005). Surface-enhanced Raman spectroscopy.

Le Ru, E., & Etchegoin, P. (2008). *Principles of Surface-Enhanced Raman Spectroscopy: and related plasmonic effects*. Elsevier.

Stiles, P. L., Dieringer, J. A., Shah, N. C., & Van Duyne, R. P. (2008). Surface-enhanced Raman spectroscopy. *Annu. Rev. Anal. Chem.*, 1, 601-626.

Tsargorodska, A., El Zubir, O., Darroch, B., Cartron, M. L., Basova, T., Hunter, C. N., ... & Leggett, G. J. (2014). Fast, simple, combinatorial routes to the fabrication of reusable, plasmonically active gold nanostructures by interferometric lithography of self-assembled monolayers. *ACS nano*, 8(8), 7858-7869.

Zhang, X., Yonzon, C. R., Young, M. A., Stuart, D. A., & Van Duyne, R. P. (2005, December). Surface-enhanced Raman spectroscopy biosensors: excitation spectroscopy for optimisation of substrates fabricated by nanosphere lithography. In *IEE Proceedings-Nanobiotechnology* (Vol. 152, No. 6, pp. 195-206).

Chapter 8: Conclusion and Future work

8.1 Conclusion

The main aim of this research was the development of novel optical biosensing technologies for detection of environmental pollutants toxins, and mycotoxins in particular. The particular interest in mycotoxins detection was simulated by their toxicity, carcinogenic and endocrine disrupting properties as well as their common presence in different agriculture products, mainly grains, nuts, spices, coffee beans, dry fruits, and associated food and animal feed.

The choice of LSPR as the main optical detection technique was due to the great scientific interest to this biosensing technology which is capable of single-molecule detection. Another attraction of LSPR lies in its relative experimental realization simplicity which combines the standard optical instrumentation with simple technologies of metal nanostructures formation such as de-wetting of thin metal films during annealing.

The starting point of the research was the exploration of different technological possibilities for the formation of gold nanostructures. Gold nanostructures were produced by either thermal or microwave annealing of thin gold films evaporated on glass slides. The morphology of gold nanostructures produced was characterized with SEM, AFM, and XRD methods which revealed the formation of gold nano-islands by de-wetting mechanism. Both horizontal (diameter) and vertical (thickness) dimensions of the gold nano-islands formed

correlated with the initial thickness of gold films. The study of optical properties of gold nano-structures produced using UV-vis absorption spectroscopy and spectroscopic ellipsometry revealed the formation of LSPR band in the middle of the visible spectral range which depends on the initial gold thickness. The structural and optical characterization of nano-structured gold films allows the optimization of the technology of their formation. The optimal technological parameters achieved were in the use of 5nm thick Au films annealed in the oven at 550 °C for 10 h which allowed the formation of stable gold nano-islands partially embedded in glass. Later in the project, similar or even slightly better gold nano-structures were produced by microwave annealing for a much shorter time of 10-15 min.

The main outcome of the optical study of gold nano-structures was the evaluation of refractive index sensitivity (RIS) of the gold nanostructures produced. It appeared that spectroscopic ellipsometry in TIRE configuration yields 3-4 times higher RIS values as compared to traditional UV-vis absorption spectroscopy. This fact inspired us using a combination of TIRE transducing method with gold nanostructures exhibiting LSPR effect in biosensing. The novel biosensing method of LSPR/TIRE was therefore established as a versatile analytical tool for a wide range of biosensing applications, particularly useful for detection of low molecular weight analytes such as mycotoxins.

The limitations of the LSPR biosensing are due to the short evanescent field decay length. The ellipsometry measurements of the PAH/PSS multilayers deposited on gold nanostructures allowed the evaluation of the evanescent field decay length which appeared to be in the range from 15 to 30 nm depending on the dimensions of gold nano-islands, which is much shorter than that for traditional total internal reflection conditions. This means that gold nanostructures can be sensitive to changes in the medium refractive index

only in close vicinity of the nano-island. This condition sets a limitation on the size of bioreceptors immobilized on the surface of metal nano-islands.

The detection of several mycotoxins, i.e. aflatoxin B1 and M1, ochratoxin A, and zearalenone was carried out using a combination of LSPR and TIRE methods in direct assay with their specific bio-receptors immobilized on the surface of nano-structured gold. Different types of bio-receptors were used in this project including (i) whole monoclonal and polyclonal antibodies electrostatically immobilized on the surface of gold via PAH and Protein A (or G) layers, (ii) half-antibodies obtained by splitting the whole antibodies along the constant domain and subsequently immobilized on gold surface via native SH groups, and (iii) aptamers immobilized via SH groups attached at C3 termini.

As was expected, the LSPR/TIRE detection of mycotoxins using large size whole antibodies immobilized on gold nanostructures via PAH and protein A (G) was not successful, because the dimensions of bio-receptors were comparable or even larger than the evanescent field decay length. The minimal detected concentration of aflatoxin B1 was 1 ng/ml which is 100 times higher than that achieved with traditional TIRE detection on continuous 25 nm gold films.

At the same time the use of small-size bio-receptors such as half-antibodies or aptamers was a success; all mycotoxins were detected in concentrations down to 0.01 ng/ml (or 10 ppt) which is a remarkable achievement for direct assay format. The use of other assay formats (i.e. competitive or sandwich assay) or amplification of LSPR using gold nanoparticles functionalized with antibodies may increase the sensitivity even further.

Similar achievements were demonstrated with the use of aptamers as bio-receptors in LSPR/TIRE biosensing, which has been done for the first time. The detection limit was

similar to that obtained for antibody receptor in 0.01 ng/ml range. The study of kinetics of aptamer-analyte binding, also carried out for the first time, which allowed the evaluation of the association constant which appeared to be in the range of 10^7 Mol^{-1} for all aptamers used. These pioneering experiments proved the high specificity of aptamers which is comparable with antibodies. In addition to the low cost of aptamers and the absence of ethical restriction of their synthesis, aptamers have advantages over traditional antibodies in their stability, simple immobilization protocol, and reusability (by simple heating/cooling PCR cycling). All these factors contribute to high popularity of aptamers which nowadays have substituted traditional antibodies in majority of applications.

Several attempts were made to produce regular gold nanostructures using nano-sphere lithography, which, according to the literature, is capable of formation of pointed metal nanostructures causing local enhancement of the electric field and thus enhancement of Raman scattering. This phenomenon, called SERS, is particularly attractive for bio-detection. Such nanostructures were produced by deposition of a monolayer of closely packed polystyrene nano-spheres (200 nm in diameter) on glass slides followed by evaporation of gold on top. After removal of nano-spheres by dissolving them in THF, the pointed gold nanostructures were left on the surface. These nano-structures were characterized with SEM, AFM and optical methods of UV-vis absorption spectroscopy and Raman spectroscopy. In addition, the LSPR band appearance, these structures caused enhancement of Raman signal, e.g. SERS. These preliminary experiments yielded Raman enhancement of about 30 times in a wide spectral range from 650 to 1700 cm^{-1} which was not suitable so far for biosensing applications; further work is required to achieve SERS effect suitable for detection of mycotoxins.

As an overall assessment of the project, it could be concluded that the main objectives of the research were achieved and a novel biosensing technology of LSPR/TIRE combined with small size bio-receptors (half-antibodies and aptamers) was developed and successfully applied for detection of mycotoxins in concentrations down to ppt level.

8.2 Future work

The future work could involve the expansion of the mycotoxins range, by including for example patulin, as well as general expansion of the types of analytes by including different environmental pollutants such as pesticides and organic chemicals.

The use of microwave annealing for the formation of metal nanostructures could be explored further. Some other metals, for example silver or copper could be used as well.

Design of portable LSPR sensors by combining the planar waveguides coated with gold nanostructures exhibiting LSPR effect.

Development of SERS-based biosensors using different types of metal nanostructures could be of great interest. In addition to regular nanostructures produced by nano-sphere lithography, the use of random nanostructures, such as the original electrochemically roughened silver layers can be considered.